

Investigating the role of the P2X7 intracellular domains in coupling to downstream signalling

By

Ahmad Qaseem Jaradat

Supervisors

Dr Mark Young

Dr Peter Watson

Date of thesis submission 24th May 2021

DEDICATION

To who was the cause of my existence in this life and always try to give me what I want and encourage me to be distinguished and support me with everything they have

My Dear and Great Father

My Dear and Great Mother

To my beloved wife and daughter, **Heba & Sara**

To my beloved brothers, **Safwan, Asem and Mohammad**

To my beloved sisters **Reema, Rasha and Rama**

To who make me happy just by seeing them and playing with them

To who are always proud of being one of them

My Family

And

To who was always asking about me and my study and research

My Friends and Colleagues

ACKNOWLEDGMENTS

A unique, great and infinity thank **ALLAH** who created me and provided me with the mind, thinking, capabilities, and skills to complete this research and make it possible.

I want to thank Dr Mark Young, my advisor and Dr Peter Watson, for my co-advisor, for their supervision, guidance and help.

I also want to thank my friends and colleagues in the PhD program to support and help during my study and research.

A great thank to my friends, colleagues, and everyone who was continuously asking about my study and research and for everyone taught and helped me even a little to reach this moment.

Finally, to the dearest people on my heart, my Great father and mother, my brothers and sisters and my family, I present a great and special thank for their generous support during my life, study and research.

Contents

DEDICATION	II
ACKNOWLEDGMENTS	III
Contents	IV
List of Figures	VIII
List of Tables	IX
List of Abbreviations	X
Abstract	XIV
Chapter 1: General Introduction	1
1.1. Purinergic signalling	2
1.2. P2 receptors	3
1.2.1. P2Y receptors.....	3
1.2.2. P2X receptors- an overview	4
1.3. P2X7 receptors- an overview.....	10
1.3.1. P2X7 splice variants and single nucleotide polymorphisms.....	10
1.3.2. P2X7 intracellular motifs and interacting proteins	15
1.3.3. The role of P2X7 in disease	18
1.3.4. P2X7 signalling pathways.....	22
1.3.5. 3D-structure of the full-length rat P2X7 (P2X7A)	34
1.4. Aims and objectives	37
Chapter 2: Materials and Methods	39
2.1. rP2X7-GFP-(His) ₈ mutant construction, cell culture and transfection	40
2.1.1. rP2X7-GFP-(His) ₈ mutant construction.....	40
2.1.2. Cell culture and transfection	44
2.2. Cell lysis, Bradford protein and Cholesterol assays	45
2.2.1. Cell lysis.....	45
2.2.2. Bradford protein assay	45
2.2.3. Cholesterol measurement assay	46
2.3. Western blotting.....	47

2.4. Functional assays	49
2.4.1. Imaging of cell blebbing	49
2.4.2. Cell surface expression assay (Biotinylation)	50
2.4.3. YO-PRO-1 dye uptake assay	51
2.4.4. Calcium influx assay	52
2.4.5. Extracellular Regulated Kinases ERK1/2 phosphorylation assay	53
2.5. rP2X7 wild-type vs rP2X7-GFP-(His) ₈ comparison assays	53
2.6. rP2X7-GFP-(His) ₈ , NMMHC-IIA interaction assays	54
2.6.1. Proximity Ligation Assay (PLA)	54
2.6.2. Pull-down assay	56
2.7. Statistical analysis	57
Chapter 3: Investigating the role of P2X7 intracellular domains in ATP-mediated cell blebbing	58
3.1. Introduction	59
3.2. Rationale for the mutant used in this study	61
3.2.1. Truncation mutants	61
3.2.2. C-Cys Anchor domain	62
3.2.3. Internal deletions	64
3.3. Results	66
3.3.1. Functional comparison of non-tagged and GFP-(His) ₈ -tagged rat P2X7 receptors	66
3.3.2. rP2X7-mediated cell blebbing in HEK-293 and Hela cells	73
3.3.3. Blebbing in the absence of the extracellular calcium	77
3.3.4. P2X7-dependent cell blebbing is reversible	81
3.3.5. Quantification of wild-type and mutant cell-surface expression using biotinylation	82
3.4. Discussion	87
3.4.1. rP2X7 fusion with GFP-(His) ₈ does not affect receptor activity	87
3.4.2. The N-terminal domain of rP2X7-GFP-(His) ₈ receptor is required for cell-surface protein expression	87
3.4.3. rP2X7-GFP-(His) ₈ induces a reversible cell blebbing independently of cell type and extracellular calcium	88

3.4.4. Disruption of rP2X7 intracellular domains impair cell-surface expression...	88
3.4.5. The C-Cys anchor and ballast domains may not be required for cell blebbing	89
Chapter 4: The effect of deletion of P2X7 intracellular domains on ATP-stimulated calcium influx, pore formation and ERK1/2 phosphorylation.....	90
4.1. Introduction.....	91
4.2. Results.....	92
4.2.1. ATP-stimulated calcium influx of wild-type rP2X7-GFP-(His) ₈ and mutant constructs	92
4.2.2. ATP-stimulated YO-PRO 1 dye uptake of wild-type rP2X7-GFP-(His) ₈ and mutant constructs	96
4.2.3. ATP-stimulated ERK1/2 phosphorylation of wild-type rP2X7-GFP-(His) ₈ and mutant constructs	100
4.3. Discussion.....	119
4.3.1. P2X7 intracellular domains are essential for protein function and trafficking	119
4.3.2. Cell blebbing and pore formation are intrinsically coupled.....	119
4.3.3. P2X7 receptor intracellular domains are essential for ERK1/2 phosphorylation.....	120
4.3.4. How might the intracellular domains of P2X7 couple to the ERK1/2 phosphorylation cascade?	121
Chapter 5: Investigating the mechanisms of ATP-induced cell blebbing via P2X7 receptor activation.....	123
5.1. Introduction.....	124
5.1.1. The proposed molecular mechanism for P2X7-dependent cell blebbing - disruption of the interaction between P2X7 and the cytoskeleton <i>via</i> NMMHC-AII	124
5.1.2. The role of cholesterol in P2X7 signalling	126
5.2. Results.....	128
5.2.1. NMMHC-IIA expression in HEK-293 and Hela cells.....	128
5.2.2. Proximity Ligation Assay (PLA) indicates a potential interaction between P2X7 and NMMHC-IIA	129
5.2.3. No interaction between P2X7 and NMMHC-IIA is observed in pull-down assay	134

5.2.4. Cell blebbing and pore formation in Cholesterol-depleted cells	136
5.3. Discussion	140
5.3.1. P2X7-NMMHC-AII dissociation and its role in cell blebbing	140
5.3.2. P2X7 induced cell blebbing and pore formation are uncoupled by membrane cholesterol depletion	141
Chapter 6: General Discussion.....	142
6.1. The C-terminal GFP-(His) ₈ tag does not affect receptor function	145
6.2. P2X7 intracellular domains are important for cell-surface protein expression	145
6.3. Cell blebbing and pore formation may not require the intracellular domains, but are regulated by them.....	146
6.4. Cell blebbing and pore formation in the light of recent cryoEM rat P2X7 structure-N-terminal domain, C-Cys anchor and ballast	147
6.5. P2X7 lies in close proximity to NMMHC-IIA, but does not necessarily dissociate from it on activation	148
6.6. Cell blebbing and pore formation are uncoupled by depletion of membrane cholesterol	149
6.7. The ‘hidden’ region in the recent P2X7 structure; D2: Δ (441-460)	150
6.8. The P2X7 intracellular domains may mediate ERK1/2 phosphorylation.....	151
Recommendations and future work	153
References	154
Appendix 1: PCR Conditions	183
Appendix 2: Oligonucleotide sequences.....	184
Appendix 3: Cell blebbing of truncation mutants in HeLa cells.....	185
Appendix 4: Cell blebbing of C-cys anchor mutants in HeLa cells.....	186
Appendix 5: Cell blebbing of the internal deletions in HeLa cells	187
Appendix 6: Cell surface expression blots.....	188
Appendix 7: ERK1/2 phosphorylation blots.....	192
Appendix 8: ERK(1/2) and P-ERK(1/2) levels	197
Appendix 9: P-ERK1 and P-ERK2 inductions	199
Appendix 10: ERK (1+2) and P-ERK (1+2) levels	200
Appendix 11: P-ERK (1+2) inductions.....	202
Appendix 12: Cell blebbing of truncation mutants in MCD-treated cells	203

Appendix 13: Cell blebbing of C-cys anchor mutants in MCD-treated cells	204
Appendix 14: Cell blebbing of internal deletions in MCD-treated cells	205

List of Figures

Figure 1: Cartoon view of the rat P2X7 full-length single subunit cryoEM structure	35
Figure 2: Cartoon representation of the intracellular domains of rat P2X7	36
Figure 3: rP2X7-GFP-(His) ₈ expression vector map	41
Figure 4: rP2X7-GFP-(His) ₈ protein sequence	42
Figure 5: Diagrammatic overview of the Duolink proximity ligation assay	55
Figure 6: Schematic structure of truncations mutants	62
Figure 7: Schematic structure of C-Cys anchor mutants	63
Figure 8: Schematic structure of internal deletions	65
Figure 9: Comparison of ATP induced calcium influx between rP2X7-GFP-(His) ₈ and rP2X7 WT	67
Figure 10: Comparison of ATP induced YO-PRO uptake between rP2X7-GFP-(His) ₈ and rP2X7 WT	69
Figure 11: ATP concentration-response curves for rP2X7-GFP-(His) ₈ and rP2X7 WT YO-PRO uptake	70
Figure 12: rP2X7-GFP-(His) ₈ and rP2X7 WT ERK (1/2) phosphorylation	71
Figure 13: Comparison of ATP induced P-ERK1/2 between rP2X7-GFP-(His) ₈ and rP2X7 WT	72
Figure 14: Cell blebbing of truncation mutants in HEK-293 cells	74
Figure 15: Cell blebbing of C-Cys anchor mutants in HEK-293 cells	75
Figure 16: Cell blebbing of the internal deletions in HEK-293 cells	76
Figure 17: Cell blebbing of truncation mutants in the absence of extracellular calcium ..	78
Figure 18: Cell blebbing of the C-Cys anchor mutants in the absence of extracellular calcium	79
Figure 19: Cell blebbing of the internal deletions in the absence of extracellular calcium	80
Figure 20: Reversible cell blebbing	81
Figure 21: rP2X7-GFP-(His) ₈ expression	82
Figure 22: rP2X7-GFP-(His) ₈ full-length and mutants total and cell-surface expression ..	83
Figure 23: Total band intensities of rP2X7-GFP-(His) ₈ full-length and mutants	85
Figure 24: Cell-surface band intensities of rP2X7-GFP-(His) ₈ full-length and mutants ..	86
Figure 25: Effect of truncation and C-Cys anchor mutants on calcium influx	93
Figure 26: Effect of mutants with an internal deletions on calcium influx and calcium gradient uptake	95

Figure 27: Effect of truncations and C-Cys anchor mutants on YO-PRO dye uptake	97
Figure 28: Effect of mutants with an internal deletions on YO-PRO dye uptake and gradient dye uptake	99
Figure 29: rP2X7-GFP-(His) ₈ and truncation mutants ERK (1/2) phosphorylation.....	102
Figure 30: Internal deletions and C-Cys anchor mutants ERK (1/2) phosphorylation...	103
Figure 31: Effect of truncation and internal deletion mutants on basal and ATP-stimulated ERK (1/2) levels	107
Figure 32: Effect of truncation and internal deletion mutants on P-ERK1 and P-ERK2 inductions	109
Figure 33: Effect of truncation and internal deletion mutants on basal and ATP-stimulated ERK (1+2) levels	113
Figure 34: Effect of truncation and internal deletion mutants on P-ERK (1+2) inductions	116
Figure 35: Non-Muscle Myosin (NMMHC-IIA) expression.....	128
Figure 36: Proximity ligation assay to measure the rP2X7-GFP-(His) ₈ -NMMHC-IIA interaction	130
Figure 37: rP2X7-GFP-(His) ₈ -NMMHC-IIA interaction after ATP application.....	131
Figure 38: rP2X7-GFP-(His) ₈ -NMMHC-IIA interaction intensity.....	133
Figure 39: No interaction between rP2X7-GFP-(His) ₈ and NMMHC-IIA was observed using pull-down assay	135
Figure 40: Quantification of cholesterol depletion in HEK-293 cells	137
Figure 41: Cell blebbing in MCD-treated cells.....	138
Figure 42: YO-PRO-1 dye uptake in MCD pre-treated and untreated HEK-293 cells ..	139

List of Tables

Table 1: Cell/tissue expression and physiological functions of P2X receptors	5
Table 2: Human P2X7 splice variants	12
Table 3: Murine P2X7 splice variants	13
Table 4: Human P2X7 single nucleotide polymorphism.....	14
Table 5: Types of cell blebbing	23
Table 6: Summary of cellular MAPK pathways.....	29
Table 7: Mutant constructs used in this study.....	43
Table 8: Polyacrylamide gel recipes	47
Table 9: Summary of calcium influx, cell blebbing, P-ERK1/2, and pore formation results obtained for all mutants studied.....	117
Table 10: Results summary.....	143

List of Abbreviations

Abbreviations	Description
ACP	Acid phosphatases
ADP	Adenosine diphosphate
AKT	Protein Kinase B
ALP	Alkaline phosphatases
ALL	Acute lymphocytic leukaemia
AML	Acute myeloid leukaemia
ANO6	Anoctamin-6/TMEM16F
ATP	Adenosine triphosphate
BBG	Brilliant Blue G
2-BP	2-bromopalmitate
BzATP	2',3'-O-(4-benzoyl-benzoyl) ATP
Ca ⁺	Calcium ion
cAMP	Cyclic adenosine monophosphate
CCR5	Chemokine receptor type 5
CDK	Cyclin-dependent kinase

CLL	Chronic lymphocytic leukaemia
CML	Chronic myeloid leukaemia
CRR	Cysteine-rich region
CXCR4	Chemokine receptor type 4
Cys	Cystine
DAPI	4',6-diamidino-2-phenylindole
DNA	Deoxyribonucleic acid
EMP	Epithelial Membrane Protein
ER	Endoplasmic Reticulum
ERK	Extracellular Regulated Kinases
FRET	Fluorescence Resonance Energy Transfer
GABA _A receptors	γ -Aminobutyric acid type A receptors
GPCR	G-protein coupled receptor
HEK-293	Human Embryonic Kidney cells
HIF-1 α	Hypoxia-inducible factor 1-alpha
HSP90	Heat-Shock Protein 90
IFN- γ	Interferon- γ
JNKs	Jun amino-terminal kinases
K ⁺	Potassium ion
LPS	Lipopolysaccharide
MAPK	Mitogen-Activated Protein Kinase

MCD	Methyl- β -Cyclodextrin
miRNA	Micro- Ribonucleic acid
MMP-3	Matrix Metalloproteinase-3
MVs/MPs	Microvesicles/Microparticles
MYD88	Myeloid differentiation primary response 88
Na ⁺	Sodium-ion
NADPH	Nicotinamide adenine dinucleotide phosphate
NFATc1	Nuclear factor of activated T-cells, cytoplasmic 1
NF- κ B	Nuclear factor kappa-light-chain-enhancer of activated B cell
NMDG	N-methyl-D-glutamine
NMMHC	Non-muscle myosin heavy chain
NTPDases	Nucleoside Triphosphate diphosphohydrolases
NPPs	Nucleotide Pyrophosphatases / Phosphodiesterase
p38/SAPKs	p38/stress-activated protein kinases
Panx1	Pannexin-1
PC	Phosphatidylcholine
PC9 lung	Human lung adenocarcinoma cell line
PE	Phosphatidylethanolamine
PMP-22	Peripheral myelin protein-22
PS	Phosphatidylserine
ROS	Reactive Oxygen Species

SM	Sphingomyelin
SNP	Single Nucleotide Polymorphisms
T47D	Human breast cancer cell line
TGN	Trans-Golgi network
THP-1	Human monocytic cells
TMD2	Second trans-membrane domain
TME	Tumor microenvironment
TLR4	Toll-Like Receptor 4
TNFR1	Tumor necrosis factor receptor 1
UDP	Uridine diphosphate
UTP	Uridine triphosphate
VEGF	Vascular Endothelial Growth Factor
VILIP-1	Visinin-like protein-1
Xkr8	XK-related protein 8

Abstract

The P2X7 receptor is a trimeric ATP-gated cation channel expressed in many mammalian cells, including immune and cancer cells. The wild-type receptor monomer is 595 amino acids in length, comprised of two transmembrane domains, a large extracellular loop, a short intracellular N-terminal domain and a 250 amino-acid long intracellular C-terminal domain. P2X7 receptor activation by extracellular ATP leads to the passage of small cations, such as Ca^{++} , K^{+} , and Na^{+} across the plasma membrane. It also initiates cell-dependent signalling pathways including cell blebbing, pore formation, cell proliferation and death, and ERK1/2 phosphorylation. Intracellular signalling *via* P2X7 activation is thought to be dependent on both the N- and C-terminal domains, but the specific sub-domains involved in distinct pathways are not known.

In this study, we set out to identify which intracellular domains are important for P2X7-mediated downstream signalling and whether distinct intracellular sub-domains govern different signalling phenomena. Using whole plasmid PCR, we constructed 17 truncation and deletion mutations in a C-terminally GFP-tagged rat P2X7 receptor construct; one within the N-terminal domain and 16 within the C-terminal domain. We analysed the effects of these mutations on ATP-induced cell blebbing, calcium influx, pore formation (through the uptake of YoPro1 dye) and ERK1/2 phosphorylation in transfected mammalian cells.

We found that a receptor construct lacking almost the entire ballast domain (1-380) was still capable of cell blebbing as was a construct lacking the C-Cys anchor (362-379), suggesting that these domains may not be necessary for P2X7-dependent cell blebbing. Deletion of the N-terminal domain (2-23) and many sub-regions within the ballast domain abolished cell blebbing, calcium influx, and pore formation, likely due to impaired receptor cell surface expression. The exceptions to this were receptor constructs lacking amino acids 441-460 or 583-595 in the ballast domain, which were capable of cell blebbing, and pore formation. However, combining the two deletions into one construct gave rise to a non-functional receptor with no detectable cell-surface expression. Strikingly, depletion of cholesterol from the plasma membrane abolished cell blebbing in all constructs including wild-type, but potentiated pore formation in the mutant lacking the ballast domain (1-380).

Investigation of the molecular mechanism for cell blebbing focused on the proposed role for dissociation of P2X7 from the actin-myosin cytoskeleton following receptor activation. However, we were unable to detect an interaction between P2X7 and non-muscle myosin (NMMHC-IIA) using pull-down assay from cell lysates, and while we were able to demonstrate that P2X7 receptors lie in close proximity to NMMHC-IIA in Hela cells using the DuolinkTM proximity ligation assay, we did not observe a change in proximity upon P2X7 activation with ATP.

Wild-type P2X7 was capable of ATP-induced ERK1/2 phosphorylation, but nearly all mutants abolished it, although issues with data collection and analysis prevented a full statistical comparison. Strikingly, for the N-terminal deletion mutant, which displayed undetectable levels of cell-surface expression, both ERK1 and ERK2 were phosphorylated in non-treated cells, and phosphorylation was significantly reduced by ATP treatment. This suggests that some receptor may be at the cell surface, responding to ATP, but how this may lead to a reduction in phosphorylation is entirely unclear.

In conclusion, our data suggests that P2X7-dependent cell blebbing and YoPro uptake do not require the intracellular C-terminal domain of the receptor. Cell blebbing has an absolute requirement for plasma membrane cholesterol, whereas cholesterol inhibits pore formation in mutants lacking the ballast domain. Finally, ERK1/2 phosphorylation may require the intracellular domains of the receptor; both the N-terminal domain and C-terminal domain may be important, but it is not possible to draw firm conclusions about their specific roles.

Chapter 1: General Introduction

1.1. Purinergic signalling

The purinergic signalling system has three main components which are responsible for the release, reception and inactivation of extracellular messengers such as ATP (Zimmermann 2016; Dou et al. 2018).

(i) The energy molecule, ATP is synthesised by glycolysis and oxidative phosphorylation inside cells and released by several mechanisms including transmembrane diffusion via ATP permeable channels like hemichannels (connexins and pannexins), organelle mediated exocytosis and active transport, cell damage or lysis, and in addition to basal or constitutive release from resting cells (Verkhratsky and Burnstock 2014; Zimmermann 2016).

(ii) Purinergic receptors that mediate purinergic transmission are divided into ionotropic P2X ATP-gated cation channels and metabotropic G-protein coupled receptors. G-protein coupled receptors are divided into P1 receptors activated by adenosine, and P2Y receptors stimulated by nucleotides like ATP, ADP, UTP, UDP, and UDP-sugars (Ralevic and Burnstock 1998; Verkhratsky and Burnstock 2014).

(iii) Nucleotide metabolising enzymes are specific plasma membrane enzymes which control the termination of purinergic signalling and include nucleoside triphosphate diphosphohydrolases (NTPDases), nucleotide pyrophosphatases/phosphodiesterase (NPPs), alkaline and acid phosphatases (ALP and ACP, respectively), and ecto-5' nucleosidase (CD73) (Millan 2006; Zimmermann 2006; Yegutkin 2008; Kukulski et al. 2011). These enzymes degrade ATP to ADP, AMP, and adenosine (Zimmermann 2016).

Purinergic signalling contributes to numerous physiological processes including biological defence, neurotransmission, cell proliferation and differentiation because most cells secrete ATP and express purinergic receptors; (Verkhratsky and Burnstock 2014).

1.2. P2 receptors

Purinergic P2 receptors can be subdivided into two families based on their signal transduction mechanism: metabotropic P2Y receptors and ionotropic P2X receptors (Cieslak et al. 2017).

1.2.1. P2Y receptors

P2Y receptors belong to a family of heptahelical receptors which activate intracellular mechanisms by coupling to G- proteins. There are eight subtypes of P2Y receptors (P2Y1, P2Y2, P2Y4, P2Y6, P2Y11, P2Y12, P2Y13, and P2Y14), which activate signalling cascades to regulate a number of cellular processes including proliferation, differentiation, phagocytosis, secretion, cell adhesion and migration (Erb and Weisman 2012).

The structure of P2Y receptors includes an extracellular N-terminus which contains several potential N-linked glycosylation sites, seven-transmembrane spanning domains that assist in forming the ligand-binding pocket, three extracellular loops, three intracellular loops that participate in G protein coupling, and an intracellular C-terminus that contains several consensus binding/phosphorylation sites for protein kinases (Erb et al. 2006; Alves et al. 2018).

The main agonists recognised by P2Y receptors are adenine and uridine nucleotides (ATP, ADP, UTP, and UDP) and nucleotide sugars (UDP-glucose). These agonists are released from many types of cells especially in response to mechanical stress, oxygen deprivation, viral infection, or apoptotic stimuli through pannexin 1 channels (Bao et al. 2004; Chekeni et al. 2010; Bargiotas et al. 2011; Seror et al. 2011).

G-proteins are heterotrimeric proteins that consist of a $G\alpha$ subunit associated $G\beta\gamma$ subunits and bind to P2Y receptors at the inner surface of the cell; as a result of P2Y receptor activation G-proteins dissociate from the receptors into the $G\alpha$ and $G\beta\gamma$ subunits (Erb and Weisman 2012). These separated G-protein subunits interact with various effector proteins, causing them to activate or deactivate (Neves et al. 2002).

1.2.2. P2X receptors- an overview

P2X receptors are ATP-gated ion channels which allow the passage of small cations, such as Ca^+ , K^+ , and Na^+ across the plasma membrane (Shiozaki et al. 2017). They are distributed in all mammalian tissues and mediate a wide variety of physiological processes including synaptic transmission, smooth muscle cell contraction, platelet aggregation, cell proliferation, cell differentiation and cell death (Burnstock et al. 2010). Seven mammalian P2X receptors (P2X1-P2X7) are known; they display differing tissue distribution and play distinct physiological roles (Table 1) (Burnstock 2013), and they differ in their subcellular distribution (some retained within the endoplasmic reticulum (ER), other at the cell surface or within endosomes and lysosomes) because of their different trafficking properties (Brake et al. 1994; Valera et al. 1994; North 2002; Robinson and Murrell-Lagnado 2013).

P2X receptors have a large glycosylated extracellular ligand-binding loop connecting the two transmembrane domains and intercellular N and C terminal domains. An important feature is the presence of ten conserved cysteine residues in the vertebrate receptors' extracellular domain which form five disulfide bridges (Schwarz et al. 2009; Kaczmarek-Hájek et al. 2012). These disulfide bridges were assigned in zfP2X4 (Cys119–Cys168, Cys129–Cys152, Cys135–Cys162, Cys220–Cys230, Cys264–Cys273) (Young 2010).

P2X receptors share (40-50)% identity at the amino-acid sequence level and their N-termini are similar in length (20-30 amino-acids), whereas their C-termini differ in length between 26 (P2X6) and 240 (P2X7) amino-acids; indicating that they might serve receptor-specific functions (Surprenant and North 2009; Murrell-Lagnado 2017).

Table 1: Cell/tissue expression and physiological functions of P2X receptors

Receptor	Cell and tissue expression	Physiological function
P2X1	Blood cells, smooth muscles	Platelet aggregation, muscle contraction.
P2X2	Sperm, cartilage, skeletal muscles, central nervous system (CNS)	Physiological reflex responses
P2X3	Sensory neurons, cardiac muscle	Physiological reflex responses, nociception.
P2X4	Endothelial cells, microglial cells, immune cells, and CNS	Cytokines release, neuropathic pain.
P2X5	Epithelial cells, skeletal muscle, skin	Cellular- differentiation in the granular layer.
P2X6	Epithelial cells, skeletal muscles, CNS	Heterotrimer only; neurotransmission and neuromodulation.
P2X7	Immune cells, microglial cells, fibroblasts, CNS	Cytokine release, inflammatory response.

Table reference: (Burnstock 2013).

In 2009, the first P2X receptor three-dimensional structure (3D), zebrafish (zf) P2X4.1 in the closed (*apo*-) state was published (Kawate et al. 2009). This was followed by a series of crystal structures of zfP2X4 bound to ATP (Hattori and Gouaux 2012), *Amblyomma maculatum* P2X (Kasuya et al. 2016), human P2X3 in the apo-, ATP- and antagonist-bound states (Mansoor et al. 2016), zfP2X4 bound to the low-affinity agonist cytidine triphosphate (CTP) (Kasuya et al. 2017a), and recently determined structures of giant panda P2X7 (Karasawa and Kawate 2016) and chicken P2X7 (Kasuya et al. 2017b).

P2X receptors interact in the form of homomeric and heteromeric channels. Heteromer formation alters receptor signalling, pharmacology and trafficking properties of the receptors. Heteromeric receptors comprised of P2X1/2, P2X1/4, P2X1/5, P2X2/3, P2X2/6, P2X4/5, P2X4/6 and P2X4/7 have been identified (Murrell-Lagnado and Qureshi 2008).

1.2.2.1. P2X receptors targeting and trafficking

P2X receptor targeting and trafficking depend on sequence motifs which determine receptor mobility within the plasma membrane and between the plasma membrane and intracellular membranes, and on interactions with other proteins and plasma membrane microdomains (lipid rafts) (Robinson and Murrell-Lagnado 2013). P2X receptors are synthesised core-glycosylated within the endoplasmic reticulum (ER) and then move to the plasma membrane *via* the trans-Golgi network, with the exception of the P2X6 receptor, which is retained in ER and can only exit as a heterotrimer with P2X2 or P2X4 (Bobanovic et al. 2002; Barrera et al. 2005; Ormond et al. 2006), and the human P2X5 receptor, because the predominant allele gives rise to an exon 10-deleted variant retained in the ER (Bo et al. 2003; Kotnis et al. 2010; Compan et al. 2012).

Because of relatively slow trafficking through the secretory pathway to appear at the plasma membrane; P2X2 and P2X7 receptors often appear to have a predominantly ER distribution (Robinson and Murrell-Lagnado 2013). The relatively slow trafficking of P2X2 may facilitate its interactions with other proteins such as GABA_A receptors, beta-amyloid precursor protein-binding protein Fe65 and visinin-like protein-1 (VILIP-1) (Bobanovic et al. 2002; Masin et al. 2006; Chaumont et al. 2008; Shrivastava et al. 2011).

P2X7 receptor trafficking is species and cell-type dependent. In human monocytes and lymphocytes, the P2X7 receptor is found to have predominantly intracellular localisation; however, it is expressed at the plasma membrane of macrophages differentiated from monocytes (Hickman et al. 1994; Gu et al. 2000; Gudipaty et al. 2001; Boumechache et al. 2009). The mechanism that regulates P2X7 trafficking from the ER to the cell membrane remains unclear even though it is thought to depend on the P2X7 C-terminal domain (Denlinger et al. 2003; Smart et al. 2003; Robinson and Murrell-Lagnado 2013).

P2X1, P2X3, and P2X4 receptors undergo rapid internalisation from the plasma membrane. While P2X1 is predominantly at the cell surface, both P2X3 and P2X4 are predominantly localised to late endosomes and lysosomes (Bobanovic et al. 2002; Qureshi et al. 2007; Vacca et al. 2009; Lalo et al. 2010; Lalo et al. 2012).

The C-terminal domain of all P2X receptors contains a cell surface regulator motif (YXXXXK) situated eight residues downstream of the second transmembrane domain (TMD2) and after an additional 18 amino acid cysteine-rich region (CRR) in the P2X7 receptor. Mutations around this motif in P2X2 or within it in other P2X receptors reduce cell membrane expression and increase internalisation (Chaumont et al. 2004). P2X receptor activation regulates their trafficking from and to the cell membrane by stimulating receptor' internalisation and recycling back to the plasma membrane in a calcium-dependent manner (Ennion and Evans 2001; Vacca et al. 2009; Lalo et al. 2010).

1.2.2.2. P2X receptors in lipid rafts

Lipid rafts are a plasma membrane microdomain rich in cholesterol, sphingolipids, and saturated phospholipids. The nature and the stability of the lipid rafts within the plasma membrane differs depending on their proteins and lipids composition (Pike 2004).

Within the P2X receptor family, only P2X5 and P2X6 are not detected in lipid rafts (Murrell-Lagnado 2017). The other P2X receptors (P2X1-4 and P2X7) are associated with lipid rafts and their distribution between raft, and non-raft fractions depend on the cell type in which they are expressed and the raft preparation method (Vacca et al. 2004; Vial and Evans 2005; Vial et al. 2006; Barth et al. 2007; Barth et al. 2008; Gonnord et al. 2009; Allsopp et al. 2010; Gnanasekaran et al. 2011).

Using a detergent-free method; P2X1-4 receptors expressed in HEK-293 cells associate with the raft fraction. However, using Triton-X 100 detergent in raft preparation, the receptors shift to a non-raft fraction (Allsopp et al. 2010). P2X7 receptors heterologously-expressed in HEK-293 and natively -expressed in rat submandibular gland, peritoneal macrophages and mouse lung alveolar cells have been shown to associate to lipid rafts and this association is caveolin-1 and palmitoylation dependent (Garcia-Marcos et al. 2006a; Garcia-Marcos et al. 2006b; Barth et al. 2007; Barth et al. 2008; Gonnord et al. 2009).

P2X7 receptors and caveolin-1 were detected and co-immunoprecipitated from mouse lung alveolar epithelial cells (Weinhold et al. 2010). Also, epithelial cells from caveolin-1 knock-out mice showed reduced P2X7 plasma membrane expression. In direct contrast to these findings, an interaction between P2X7 receptor and caveolin-1 was not detected in mouse osteoblast cells by co-immunoprecipitation, and caveolin-1 knockdown in the same cells led to an increase P2X7 receptor currents (Gangadharan et al. 2015).

Palmitoylation is a reversible process in which palmitate (16-carbon fatty acid) couples to cysteine residues *via* a thioester bond (Murrell-Lagnado 2017). Treatment of cells with radiolabeled palmitate, followed by detection of P2X7, demonstrated that labelled P2X7 was found mainly in lipid raft and disruption of P2X7 palmitoylation using the palmitic acid analogue 2-bromopalmitate (2-BP) reduced P2X7 targeting to lipid rafts (Barth et al. 2007; Barth et al. 2008; Gonnord et al. 2009). P2X7 has 16 conserved intracellular cysteines, two of them within the N-terminal domain (amino-acid residue numbers 4 and 5), six within the C-cys anchor (362, 363, 371, 373, 374, and 377 residues) and eight residues which contribute to the Zn^{+2} coordination site (477, 479, 482, 498, 499, 506, 572, and 573). At least five cysteine residues (4, 362, 363, 374, and 377) and one serine residue (360) are known to be palmitoylated. Substitution of C-terminal cysteines by alanine significantly reduces both P2X7 palmitoylation and cell surface expression (Gonnord et al. 2009; McCarthy et al. 2019a).

Several studies show the regulation of P2X receptors by association with lipid raft. Cholesterol depletion by methyl β -cyclodextrin (MCD) inhibited P2X1 receptor-mediated currents, contraction, and calcium responses in HEK-293 cells, rat tail artery and platelets respectively (Vial and Evans 2005; Vial et al. 2006; Allsopp et al. 2010). P2X3 and P2X4 receptor currents are insensitive to cholesterol depletion (Vacca et al. 2004; Allsopp et al. 2010; Gnanasekaran et al. 2011). In THP-1 monocytes, calcium influx-mediated by P2X4 receptor was reduced by cholesterol depletion with MCD or fluvastatin (Li and Fountain 2012).

1.3. P2X7 receptors- an overview

The P2X7 receptor is expressed in various mammalian cells including hematopoietic cells, osteoblasts, fibroblasts, endothelial cells, immune cells, epithelial cells, central and peripheral nervous cells (Burnstock and Knight 2004; Sperlagh et al. 2006; Lenertz et al. 2011; Wiley et al. 2011). Within the P2X receptors family, P2X7 is the largest monomeric subunit with a length of 595 amino acids (Bartlett et al. 2014). The C- terminal domain of the P2X7 is 240 amino acids in length, 120-200 amino acids longer than other P2X subtypes (Smart et al. 2003; Becker et al. 2008).

1.3.1. P2X7 splice variants and single nucleotide polymorphisms

1.3.1.1. P2X7 splice variants

Alternative splicing is a mechanism that enables a messenger RNA (mRNA) to synthesise different protein variants or isoforms that may have other cellular functions, protein-protein interaction and subcellular localisation (Benzaquen et al. 2019). Several factors control this scission process, allowing a precise pattern rearrangement of intron and exon elements to alter the mRNA coding sequence including cis-regulatory elements and ribonuclear-protein complexes (RNP) (Chow et al. 1977; Tazi et al. 2009; Bessonov et al. 2010).

Cis-regulatory elements are sequences localised within the exon (exonic splicing silencer (ESS) or exonic splicing enhancer (ESE)) or intron (intronic splicing silencer (ISS) or intronic splicing enhancer (ISE)). The silencer elements inhibit pre-mRNA splicing, while, the enhancer elements mediate mRNA splicing (Benzaquen et al. 2019). RNP is divided into two families, the heterogeneous nuclear RNP (hnRNPs) which bind to RNA and serine- arginine-rich protein family (SR proteins) that recognise proteins. Both of them regulate pre-mRNA splicing through binding enhancers or silencers elements (Buratti et al. 2006; Tazi et al. 2009; Keren et al. 2010; Chabot and Shkreta 2016).

The human P2X7 receptor is located on chromosome 12q24 and consists of 13 exons that encode P2X7-A mRNA and translate to the full-length protein 595 amino acids (Buell et al. 1998; Cheewatrakoolpong et al. 2005). Table 2 shows a summary of eight human P2X7 receptor splice variants.

Table 2: Human P2X7 splice variants

hP2X7 splice variants	Missing part	Function	Reference
P2X7-A	-	Functional	(Rassendren et al. 1997)
P2X7-B	Δ C-terminal	Functional channel, no pore formation	(Cheewatrakoolpong et al. 2005; Adinolfi et al. 2010)
P2X7-C	Very short. Lack part of the extracellular domain, TMD2, and C-termini	Nonfunctional	(Cheewatrakoolpong et al. 2005)
P2X7-D	Lack of N-termini, TMD1, and part of the extracellular domain	-	(Cheewatrakoolpong et al. 2005)
P2X7-E	Very short. Lack part of the extracellular domain, TMD2, and C-termini	Nonfunctional	(Cheewatrakoolpong et al. 2005)
P2X7-F	Very short. Lack part of the extracellular domain, TMD2, and C-termini	Nonfunctional	(Cheewatrakoolpong et al. 2005)
P2X7-G	Very short. Lack of N-termini, TMD1, part of the extracellular domain, TMD2, and C-termini	Nonfunctional	(Cheewatrakoolpong et al. 2005)
P2X7-H	Δ TMD1	-	(Cheewatrakoolpong et al. 2005)
P2X7-J	Lack part of the extracellular domain, TMD2, and C-termini	Nonfunctional alone. Reduced ligand binding ability and channel function when co-expressed with P2X7-A	(Feng et al. 2006; Guzman-Aranguez et al. 2017)

Murine P2X7 receptor has four splice variants (P2X7-B, P2X7-C, P2X7-D, and P2X7-K), with the full functional length (595 residues) subunits known as P2X7-A (Table 3).

Table 3: Murine P2X7 splice variants

Murine P2X7 splice variants	Receptor length	function	Reference
P2X7-A	Full length, 595 residues	Functional	(Sluyter 2017)
P2X7-B	Truncated C-terminal, 431 residues length	Negatively modulate the basal activity of full-length P2X7 receptor	(Haanes et al. 2012; Masin et al. 2012; Kido et al. 2014)
P2X7-C	Truncated C-terminal, 442 residues length	Low channel activity	(Haanes et al. 2012; Masin et al. 2012; Kido et al. 2014)
P2X7-D	Truncated C-terminal, 153 residues length	Negatively modulate the basal activity of full-length P2X7 receptor	(Kido et al. 2014)
P2X7-K	592 residues	Increased receptor activity and sensitivity to agonists compared to P2X7-A	(Nicke et al. 2009; Schwarz et al. 2012)

1.3.1.2. P2X7 single nucleotide polymorphisms

Over 1500 single nucleotide polymorphisms (SNPs) have been reported in human P2X7 receptors associated with musculoskeletal, inflammatory, cardiovascular diseases, and cancer; (Table 4) (Bartlett et al. 2014). Clinical investigations of P2X7 demonstrates that some of these polymorphisms are related to several diseases such as; E496A associated with loss of receptor function and the appearance of chronic lymphocytic leukaemia (CLL) in patients harbouring this polymorphism (Gu et al. 2001), E496A-linked to a reduced risk of ischemic stroke and ischemic heart diseases (Gidlof et al. 2012), and A348T which prevent *Toxoplasma gondii* infection, and increased recurrence with rheumatoid arthritis patients and with people suffering from major depressive disorders (Lucae et al. 2006; Jamieson et al. 2010; Al-Shukaili et al. 2011).

Table 4: Human P2X7 single nucleotide polymorphism

SNPs type	Location	Mechanism of loss or gain function
Loss of receptor function	V76A	Not clear
	R117W	Not clear
	G150R	Not clear
	E186K	Not clear
	L191P	Not clear
	R276H	Not clear
	R307Q	Contribute to ATP binding
	T357S	Not clear
	I568N	Lies within the trafficking motif, do not traffic to the cell surface.
The gain of receptor function	H155Y	Not clear, thought to increase cell surface expression.
	H270R	Not clear
	A348T	Not clear

Nonsynonymous SNPs alter human P2X7 function (Bartlett et al. 2014).

1.3.2. P2X7 intracellular motifs and interacting proteins

The P2X7 receptor C-terminal domain contains multiple protein and lipid interaction motifs that directly suggest the C-terminal domain's importance in regulating P2X7 receptor signalling pathways (Denlinger et al. 2001; Kopp et al. 2019a). In terms of protein interaction motifs, P2X7 receptor contains a PXXP motif located within (441-460) residues; this motif enables P2X7 receptor to bind proteins containing Src homology 3 (SH3) domains like protein tyrosine kinases (PTKs) of the Src-family, myosin, cortactin, amphiphysin and spectrin (Denlinger et al. 2001; Kurochkina and Guha 2013). A motif with similarity to a tumour necrosis factor receptor 1 (TNFR 1) domain is present within (436-531) residues of P2X7 receptor that overlaps its death domain, suggesting a potential role for P2X7 in caspase activation and apoptosis (Feinstein et al. 1995; Ferrari et al. 1999; Bang et al. 2000; Humphreys et al. 2000; Denlinger et al. 2001).

Additionally, two regions of the C-terminal domain (389-405 and 494-508) of P2X7 are homologous to domains within high molecular weight protein 3 (HMW3) from *Mycoplasma genitalium* and the hypothetical *Caenorhabditis elegans* protein C18H2.1 respectively (Denlinger et al. 2001). While HMW3 is involved in the localisation of adhesion proteins to the attachment organelle of *Mycoplasma*, C18H2.1 contains two Ankyrin repeats, domains that are involved in the cytoskeletal organisation (Krause 1998; Sedgwick and Smerdon 1999). The distal end of P2X7 (amino-acids 573-590) contains a conserved (approximately 90%) potential binding site for bacterial lipopolysaccharide (LPS) (Lamping et al. 1996; Schumann et al. 1997; Denlinger et al. 2001).

P2X7 receptor has been demonstrated to interact with more than 50 proteins that may be involved in regulation of receptor function and signalling. 22 of these proteins are involved in the immune response, underlining the role of the P2X7 receptor in the inflammatory and immune system (Kopp et al. 2019a). Co-precipitation experiments demonstrate an interaction of P2X7 pannexin-1 (Poornima et al. 2012; Kanjanamekanant et al. 2014; Boyce and Swayne 2017), and this association may mediate pore formation and interleukin-1 β release by P2X7 receptors (Pelegrin and Surprenant 2006). Rat P2X7 receptors contain a calmodulin-binding motif in the ballast domain (amino-acids 540-595) as shown by co-immunoprecipitation and mutagenesis studies; P2X7calmodulin-binding has been shown to facilitate Ca²⁺ cell entry and play a role in cell blebbing and cytoskeletal rearrangement (Roger et al. 2008).

Yeast two-hybrid experiments using the isolated C-terminal domain of rat P2X7 as bait, and subsequent immunoprecipitation experiments using whole proteins identified epithelial membrane proteins (EMP-1, EMP-2, EMP-3, and PMP-22), as C-terminal domain interacting proteins, and showed that these proteins were involved in cell blebbing (Wilson et al. 2002). In *IFN- γ* and *LPS*-stimulated THP-1 cells, P2X7 receptors associated with cytoskeletal protein Non-Muscle Myosin Heavy Chain (NMMHC-IIA), protein-tyrosine phosphatase, Ro 52, β -actin, and myosin regulatory light chain 2. (Gu et al. 2009).

P2X7 receptors interact with several proteins involved in the immune response including CD14 and Myeloid differentiation primary response 88 (MYD88) (Kopp et al. 2019a). Binding of pathogen-associated molecular patterns (PAMPS) such as LPS to Toll-like receptor 4 (TLR4) activates the immune response and recruits adaptor proteins (Luo et al. 2019). CD14 serves as a co-receptor with TLR4 and P2X7 to facilitate innate immune responses and interleukin secretion for TLR4 and enable LPS internalisation and binding for P2X7 (Zanoni and Granucci 2013; Dagvadorj et al. 2015). Coimmunoprecipitation and confocal microscopy experiments demonstrate physical interaction between P2X7 and CD14 and co-localisation in LPS-stimulated HEK-293 cells (Dagvadorj et al. 2015).

MYD88 is an adaptor protein, connecting to Toll receptors, which receives signals from outside the cell to induce pro-inflammatory cytokines synthesis via NF- κ B signalling (Kopp et al. 2019a). It is reported that P2X7 interacts with MYD88 in transfected HEK-293 cells and that P2X7 mediates MYD88-dependent NF- κ B activation. This interaction is dependent on the P2X7 C-terminal domain because the mutation G586A impaired the interaction in both HEK-293 and RAW264.7 cells (Liu et al. 2011).

Co-immunoprecipitation of protein complexes from rat P2X7-transfected HEK-293 cells followed by mass spectrometry was used to identify Heat Shock Protein 90 (HSP90) as a potential interactor with P2X7 (Kim et al. 2001; Gu et al. 2009). HSP90 is a molecular chaperone and ATPase (Kopp et al. 2019a). It is involved in several pathological conditions including neurodegenerative disease, inflammation and cancer (Schopf et al. 2017). HSP90 phosphorylation was shown to decrease P2X7 currents and cell membrane blebbing in HEK-293 and rat peritoneal macrophages (Adinolfi et al. 2003). HSP90 nitration was demonstrated to increase P2X7-dependent activation of the Fas (CD95; member of the tumour necrosis factor receptor) pathway and subsequent apoptosis in PC12 cells (Franco et al. 2013). In addition, HSP90 has been demonstrated to be involved in P2X7-dependent pore formation, autophagic death of dystrophic muscles, and activation of NLRP3 inflammasome pathways (Young et al. 2015; Zuo et al. 2018).

1.3.3. The role of P2X7 in disease

1.3.3.1. Cancer

Cancer is a term for a disease in which abnormal cells divide without control and invade nearby tissues. Cancer cells can also spread to other parts of the body through the blood and lymph systems. Six major features of cancers enable its growth and metastatic dissemination; sustaining proliferative signalling, evading growth suppressors, resisting cell death, promoting replicative immortality, inducing angiogenesis, and activating invasion and metastasis (Hanahan and Weinberg 2011).

Tumour cells interact with the host cells through the tumour microenvironment (TME) which supports cancer growth and progression, acting on cancer cells and interactions with immune, endothelial and nervous cells (Adinolfi et al. 2015). TME contains a high (hundred-micromolar) ATP concentration that accumulates through spontaneous release, tumour necrosis or chemotherapy, and this high concentration of ATP exerts a trophic activity on cancer cells and surrounding tissue (Adinolfi et al. 2015; Di Virgilio et al. 2016).

P2X7 receptors are highly expressed in many cancers, including acute myelogenous leukaemia (AML), acute lymphoblastic leukaemia (ALL), chronic myelogenous leukaemia (CML) and thyroid papillary cancer (Zhang et al. 2004; Solini et al. 2008). P2X7 is known to behave as a bifunctional receptor according to its level of activation, and given cell types can either lead to cell death following activation with high ATP concentrations (likely to build up in the microenvironment of tissue injury and inflammation), or support proliferation under conditions of low ATP production such as tonic autocrine or paracrine stimulation (Di Virgilio et al. 1989; Baricordi et al. 1996; Surprenant et al. 1996; Di Virgilio et al. 1998; Adinolfi et al. 2002).

Despite the high concentration of ATP in the tumour microenvironment; P2X7 receptor activation does not have a cytotoxic effect (Raffaghello et al. 2006; Bianchi et al. 2014; Di Virgilio et al. 2016). Conversely, it has been reported that P2X7 affects energy metabolism *via* increasing the efficiency of oxidative phosphorylation and aerobic glycolysis which leads to elevated total cellular ATP levels and biosynthetic intermediates for the synthesis of nucleic acids, phospholipids, non-essential amino acids, and reducing molecules in the form of NADPH (Adinolfi et al. 2005; Amoroso et al. 2012; Pavlova and Thompson 2016). In addition, P2X7 signalling activates many key intracellular growth-promoting pathways such as NFATc1, ERK, Akt and HIF-1 α (Jacques-Silva et al. 2004; Adinolfi et al. 2009; Tafani et al. 2011; Amoroso et al. 2012; Amoroso et al. 2015).

Tumour growth and metastasis are angiogenesis processes dependent on enabling cancer cells to exchange oxygen, nutrients and waste products with blood vessels (Adinolfi et al. 2015). Angiogenesis is a process of endothelial cell proliferation and migration, degradation of the extracellular matrix and morphogenesis tube formation of endothelial cells (Folkman and Shing 1992; Risau 1997). P2X7 mediates the release of vital angiogenic molecules including Vascular Endothelial Growth Factor (VEGF) from a number of cancer cell lines (Wei et al. 2008; Chong et al. 2010; Adinolfi et al. 2012). However, pharmacological blockage or silencing of P2X7 reduced VEGF secretion and vessel formation (Adinolfi et al. 2012), which confirms the role of the P2X7 receptor in tumour-associated angiogenesis.

P2X7 receptor-stimulated microvesicles/microparticles (MVs/MPs) are released from the cancer cells into extracellular space and blood (Rak 2010). MVs/MPs contain bioactive factors such as miRNA, DNA, tissue factor, cysteine cathepsins and metalloproteinases that digest the extracellular matrix and promote tissue infiltration, contributing to cell cancer invasion and migration (Gu and Wiley 2006; Di Virgilio et al. 2016).

It is reported that P2X7 receptor activation promotes migration and invasion of PC9 lung carcinoma and T47D breast cancer cells (Takai et al. 2014; Xia et al. 2015). P2X7 receptor silencing inhibits prostate cancer cell migration by down-modulating the expression of genes involved in the epithelial/ mesenchymal transition including Snail, E-cadherin, and Claudin-1, IL-8, and MMP-3 (Qiu et al. 2014).

1.3.3.2. Inflammatory diseases

Inflammation is an innate immune response to protect the body against exogenous pathogens including parasites, bacteria, and viruses, or endogenous sources of danger (Adinolfi et al. 2018). Immune responses are carried out by specialised cells which express the P2X7 receptor including monocytes/macrophages, neutrophils, mast cells, and lymphocytes (Di Virgilio 2015). During the immune response, activated pattern recognition receptors such as Toll-like receptors induce ATP release which activates P2X7, modulating cellular immune responses in several inflammatory diseases (Burnstock 2017).

In the respiratory tract, stimulation of P2X7 receptors increase surfactant secretion from alveolar epithelial cells, highlighting its physiological role in lung homeostasis (Mishra et al. 2011). However, P2X7 hyperactivation is implicated in pulmonary hypertension, asthma, chronic obstructive pulmonary disease and pulmonary fibrosis by increasing the secretion of IL-1 β , IL-1 α , and tissue fibrosis markers such as lung collagen, matrix metalloproteinase-1 inhibitor and neutrophil recruitment (Gentile et al. 2015; Savio et al. 2018).

P2X7 is involved in oxidative, fibrogenesis, and inflammatory mechanisms in liver disease by activating Kupffer and hepatic stellate cells (Vaughn et al. 2012). It is reported that P2X7 blockade with A438079 reduced mouse CCl₄-induced liver fibrosis (Huang et al. 2014), and P2X7 receptor blockade with brilliant blue G (BBG) attenuated the inflammatory response, cytokines production and liver fibrosis in mice (Savio et al. 2017).

P2X7 is weakly expressed in healthy kidney cells including podocytes, endothelial, mesangial, and tubular epithelial cells, but its expression is upregulated after kidney injury, suggesting a significant role for P2X7 receptor in the inflammatory reactions that occur in renal diseases (Goncalves et al. 2006; Burnstock et al. 2014; Franco et al. 2015). Besides promoting the stimulation of the NLPR3 inflammasome and consequent release of IL-1 β and IL-18 cytokines, activated P2X7 receptors participate in renal fibrosis through interstitial collagen production (Solini et al. 2013; Rodrigues et al. 2014; Koo et al. 2017).

1.3.4. P2X7 signalling pathways

Activation of P2X7 receptors by extracellular ATP leads to the initiation of several cell-specific downstream signalling pathways such as membrane blebbing, pore formation, ERK1/2 phosphorylation, cytokine release, reactive oxygen species, phosphatidylserine exposure, and gene transcription (Wilson et al. 2002; Becker et al. 2008; Bartlett et al. 2014).

1.3.4.1. Cell blebbing

Blebs are cellular membrane protrusions resulting from cytoskeletal rearrangement; either actomyosin contractions of the cytoskeletal cortex, transient detachment of the cell membrane from the actin cortex or rupture in the actin cortex. The changes in the cytoskeletal arrangement or tethering lead to the 'flow' of the cytosol away from the cell body leading to the formation of circular plasma membrane extensions 2-15 μm in diameter (Charras 2008). The life cycle of a bleb is subdivided into three phases; rapid bleb expansion, a short static phase, and retraction of the bleb to the exact cell membrane position where it originated. During the expansion phase of bleb formation, which lasts approximately 30s, blebs are devoid of actin. The bleb area's surface increases through further tearing of membrane from the cortex, and convective flows of lipids in the membrane's plane through the bleb neck (Cunningham 1995; Charras et al. 2005; Tournaviti et al. 2007). These cytoskeletal rearrangements are controlled by the Rho family of small GTPases, resulting in distinct types of actin-rich protrusions such as filopodia and lamellipodia invadopodia, podosomes, phagocytic cups, and uropods that serve physiological and biological functions (Chhabra and Higgs 2007).

Blebbing has been observed in different types of cells such as fibroblasts, endothelial and mesenchymal cells, cancer cells, immune cells, germ cells, amoeba, parasites and bacteria (Khajah and Luqmani 2016), and implicated in various physiological phenomenon including cytokinesis, cell spreading, virus infection, protective mechanisms against injury (Charras and Paluch 2008; Fackler and Grosse 2008; Babiychuk et al. 2011), and pathological conditions including lipid peroxidation, anoxia, cancer invasion and immunological disorders (Langridge and Kay 2006; Norman et al. 2010; Norman et al. 2011; Khajah and Luqmani 2016).

Blebbing can be either reversible (nonapoptotic) or irreversible (apoptotic), initiated by cellular insults such as lipid peroxidation, anoxia, and energy depletion or cell exposure to various chemicals like bradykinin, cAMP, and ATP. The cellular distribution of blebs can be either polarised on one side of the cells or uniform distribution. Commonly observed types of blebbing are listed in-Table 5 (Khajah and Luqmani 2016).

Table 5: Types of cell blebbing

Bleb types	Reversible (nonapoptotic)	Irreversible (apoptotic)
Stimuli	A chemical such as ATP, bradykinin, and cAMP	Cellular insults such as anoxia, and lipid peroxidation
Cellular process	Motility, invasion, cytokinesis, spreading, and mitosis	Cell lysis
Time of bleb formation	5 min to 4h	>4h
Bleb distribution over the cell membrane	Polarised in case of motility and invasion, whereas uniform in case of other processes	Uniform distribution

Table reference: (Khajah and Luqmani 2016)

P2X7 receptor activation is thought to mediate cell membrane blebbing by two distinct pathways, a reversible calcium-dependent pathway which triggers cytoskeletal disruption and membrane blebbing directly within seconds following receptor activation, and irreversible cell blebbing *via* a calcium-independent, ROCK-1 dependent pathway following prolonged P2X7 receptor activation for more than 30 min which eventually causes cell death (Mackenzie et al. 2005). While P2X7-dependent blebbing has been widely studied, the precise molecular mechanisms coupling receptor activation to blebbing and the receptor subdomains involved in this process are not well understood; fluorescence experiments observed the localization of the co-transfected P2X7-AcGFP and NMMHC-AII-DsRed in the plasma membrane of HEK-293 cells and cell blebbing following BzATP application (Gu et al. 2009). Further investigations using Fluorescence Resonance Energy Transfer (FRET) demonstrated the interaction of the P2X7-DsRed monomer and the NMMHC-IIA-AcGFP in HEK-293 cells, and fluorescence intensity was decreased following incubation of co-transfected cells with BzATP for 15 minutes (Gu et al. 2009), suggesting that cell blebbing occurs as a result of P2X7-NMMHC-AII dissociation.

1.3.4.2. Pore formation

P2X7 receptor stimulation by extracellular ATP leads to the formation of a cell membrane pore that allows molecules up to 900 Da to permeate the cells (Steinberg et al. 1987; Di Virgilio 1995; Surprenant et al. 1996; Alves et al. 2014). Evidence from multiple studies has demonstrated P2X7- dependent pore formation in heterologously expressed P2X7 receptors in various cells, measuring the uptake of organic cations such as ethidium bromide and YO-PRO-1 (Surprenant et al. 1996; Chessell et al. 1997; Rassendren et al. 1997). Furthermore, macrophages derived from P2X7 receptor knockout mice fail to take up large dye molecules following ATP addition (Solle et al. 2001).

The mechanisms of pore formation are poorly understood. However, there are two hypotheses. The P2X7-Pannexin-1 (Panx1) complex theory states that ATP-release Panx1 channel constitutes the pore that opens in response to P2X7 activation, supported by the facts of that (i) activation of P2X7 receptors open two distinct pores for small and large ions (Nuttall and Dubyak 1994; Virginio et al. 1997; Faria et al. 2005; Jiang et al. 2005), (ii) expression of P2X7 in the absence of Panx1 does not give rise to functional dye-permeable pores (Pelegrin and Surprenant 2006), (iii) Panx1 antagonists, but not P2X7 inhibitor, block dye uptake (Locovei et al. 2007), and (iv) both P2X7 and Panx1 are co-immunoprecipitated from different cell lines (Silverman et al. 2009; Li et al. 2011; Poornima et al. 2012).

However, this theory has been challenged by other studies showing that Panx1 knockout mouse macrophages normally take up YO-PRO 1 dye (Qu et al. 2011), Panx1 antagonists do not block dye uptake (Xu et al. 2012; Alberto et al. 2013), and ATP is acting as an antagonist for Panx1 channel activity (Qiu and Dahl 2009).

The second theory holds that the P2X7 transmembrane domains themselves form the large pore, which starts by dilating a small cation permeable pore upon prolonged or repeated activation by ATP. The observation supports this theory that the large cation N-methyl-D-glucamine (NMDG), becomes more permeable over the time of ATP application in whole-cell patch-clamp experiments (Virginio et al. 1999). However, the ‘pore dilation’ hypothesis has recently been challenged by a study showing that the time-dependent NMDG permeability is due to a consequence of unintended ion accumulation in whole-cell patch-clamp experiment, and that P2X7 receptors are already fully NMDG-permeable when activated by ATP (Li et al. 2015).

The significance of the C- terminal domain of P2X7 in pore formation is clear. However, Smart *et al.* demonstrated that truncation of the C- terminal domain to yield P2X7-(1-380, 1- 400, 1-418, 1-460, 1-500, 1-540, 1-550) prevented pore formation without altering ion channel properties, and receptors truncated at residue 581 displayed negligible ethidium ion uptake, whereas those truncated at position 582 showed normal ethidium ion uptake, suggesting that pore formation requires greater than 95% of the C terminal domain (Smart et al. 2003). More recently, Karasawa *et al.* have proposed, using in vitro studies of reconstituted truncated panda P2X7 receptors, that the pore-forming activity of P2X7 receptor depends only on lipid composition, and that the pore opens independent of its N- and C-terminal domains, although the C-terminal domain plays a vital role in lipid regulation of pore activity (Karasawa et al. 2017).

From these data, our current view is that pore formation may be intrinsic to P2X7, at least in some cell types, but that the C-terminal domain plays an important role in regulation of pore formation. It is currently unknown whether pore formation is coupled to other P2X7-dependent signalling events (i.e. if the same domains in P2X7 govern all signalling phenomena, or if discrete portions of the receptor are involved in discrete signalling events).

1.3.4.3. Phosphorylation of extracellular signal- Regulated Kinases (ERK1/2)

Cells respond to extracellular signals by sending intracellular instructions to regulate suitable actions (Robinson and Cobb 1997). Protein kinases are enzymes that covalently bind phosphate to the side chain of either tyrosine, serine or threonine of specific protein substrates (including other protein kinase, phospholipases, transcription factors, and cytoskeletal proteins) inside the cells (Johnson and Lapadat 2002). Phosphorylation of proteins controls their enzymatic activity (switch on or off), interaction with other molecules, location in the cells, and the tendency for degradation by protease enzymes (Johnson and Lapadat 2002; Serber and Ferrell 2007; Holt et al. 2009).

The Mitogen-Activated Protein Kinase (MAPK) family regulates vital signal transductions in eukaryotes such as cell proliferation, cell differentiation, and cell death (Qi and Elion 2005; Raman et al. 2007; Keshet and Seger 2010). The MAPK family is subdivided into three kinase subfamilies; Jun amino-terminal kinases (JNKs), stress-activated protein kinases (p38/SAPKs), and extracellular signal-regulated kinases (ERK) (Morrison 2012). All MAPKs have a Thr-X-Tyr motif within their activation loop, and the phosphorylation of threonine and tyrosine is essential for kinases activation (Zhang and Dong 2007). Kinases of the JNK family contain a Thr-Pro-Tyr activation motif, and are activated by environmental stresses (such as ionising radiation, heat, oxidative stress, and DNA damage), growth factors and inflammatory cytokines (Johnson and Nakamura 2007). The JNK family include JNK1, JNK2, and JNK3, which play a vital role in apoptosis, inflammation, cytokine release and metabolism (Huang et al. 2009; Rincón and Davis 2009); JNK1 and JNK2 have a ubiquitous expression while JNK3 is brain-specific (Zhang and Dong 2007). Like JNK, the p38 family is activated by environmental stresses and inflammatory cytokines. It has a Thr-Gly-Tyr activation motif and contributes to inflammation, apoptosis, cell differentiation, and cell cycle regulation (Cuenda and Rousseau 2007; Cuadrado and Nebreda 2010). The p38 family include p38 α , p38 β , p38 γ , and p38 δ (Zhang and Dong 2007).

The ERK subfamily contains a Thr-Glu-Tyr activation motif and is subdivided into the classic ERKs that consists mainly of the kinase domain such as ERK1 and ERK2, with molecular masses of 44 and 42 kDa respectively; and the large ERKs such as ERK3, ERK5, ERK7, and ERK8 which consist of both a kinase and a C-terminal domain, their size ranging from 60 kDa to a greater than 100 kDa (Kuo et al. 2004; Zhang and Dong 2007).

A specific extracellular signal such as stress, growth factor binding, or inflammatory cytokines binding, lead to the activation of a particular MAPK following activation of the specific MAPK kinase kinase (MAPKKK) and MAPK kinase (MAPKK) (Morrison 2012); Table 6. The MAPKKK is activated by interactions with small GTPases and /or phosphorylation by a protein kinase downstream from cell membrane receptor (Cuevas et al. 2007). The MAPKKK directly activates MAPKK, which activates the MAPK by dual phosphorylation of a conserved activation motif Thr-X-Tyr (Tanoue and Nishida 2003; Morrison 2012). The MAPKs contain docking sites for MAPKKs and substrates to allow high-affinity protein-protein interactions to confirm the specificity of the activated upstream MAPKK and the recognition of the downstream targets (Bardwell and Thorner 1996; Tanoue and Nishida 2003).

The magnitude, duration, and inactivation of MAPKs are pivotal for an appropriate physiological response (Zhang and Dong 2007). The MAPK phosphatases (MKPs) have been identified as a negative regulator of MAPKs, which have common structural features of the C-terminal catalytic domain containing the conserved HCXXXXXR motif and two Cdc25-like domains. The MKPs inactivate MAPKs through dephosphorylation of threonine and/or tyrosine residues within the Thr-X-Tyr motif (Camps et al. 2000; Theodosiou and Ashworth 2002; Farooq and Zhou 2004).

Table 6: Summary of cellular MAPK pathways

MAPKs	ERK1/2	JNKs	p38 MAPKs	ERK5
Extracellular signals	Growth factors, GPCR agonists	Stress, GPCR agonists, inflammatory cytokines and growth factors	Stress, GPCR agonists, inflammatory cytokines and growth factors	Stress, GPCR agonists, and growth factors
MAPKKK	A-Raf, B-Raf, Raf1, Mos, Tpl2	MEKK1/4, MLK2/3, DLK, Tpl2, ASK1, TAK1	MEKK1-4, Tpl2, MLK2/3, ASK1/2, DLK, TAK1, TAO1/2	MEK2/3, Tpl2
MAPKK	MEK1/2	MKK4/7	MKK3/6	MEK5
Biological response	Growth, survival, differentiation and development	Inflammation, apoptosis, growth, differentiation	Inflammation, apoptosis, growth, differentiation	Growth, differentiation, development
MKPs negative regulators	VHR, MKP (2-4/6)	VH5, Pac-I, MKP-5, MKP-7	MKP-1, DSP2	VHR, MKP (2-4/6)

* Table reference: (Zhang and Dong 2007; Morrison 2012).

*GPCR: G-protein coupled receptor.

The ERK1/2 kinase proteins are widely expressed and involved in the control of cell division, cell differentiation, transformation, and cell senescence (Johnson and Lapadat 2002; Deschenes-Simard et al. 2014). In vertebrates, ERK2 gene is larger than ERK1 gene, however at the protein level two isoforms are 84% identical with human ERK1 (44 kDa) being larger than ERK2 (42 kDa) due to an extension of 17 amino-acids at its N-terminal and 2 amino-acids at its C-terminal (Buscà et al. 2016). The docking domain in ERK1 and ERK2 is nearly identical, indicating the same substrate specificities (Yoon and Seger 2006), and both isoforms are activated by the same upstream kinases and display the same activation kinetics (Lefloch et al. 2008).

Activation of ERK1/2 promotes human cancers progressions (Schubbert et al. 2007; Sebolt-Leopold 2008), consistent with the fact that ERK kinases control the cell cycle by increasing the building blocks for cell growth (Ying et al. 2012), by activation of the cyclin-dependent kinase (CDK)- cyclin complexes required for cell cycle progression (Chambard et al. 2007), and by preventing cell death (Rasola et al. 2010).

Several studies show that the stimulation of P2X7 mediates the activation of ERK1/2 in numerous cell lines (Bradford and Soltoff 2002; Budagian et al. 2003; Gendron et al. 2003). Using C- and N-terminal P2X7 receptor deletion mutants Amstrup and Novak were able to demonstrate that a P2X7 mutant lacking the N-terminal domain (amino-acids 1-25) was unable to mediate activation of ERK1/2. In contrast, deleting the final 230 amino-acids in the C-terminal did not impair ERK1/2 activation (Amstrup and Novak 2003).

The molecular mechanism by which P2X7 activation induces ERK1/2 phosphorylation is unknown. However, Gendron *et al.* demonstrate the importance of proline-rich/ Ca^{2+} - activated tyrosine kinase (Pyk2), c-Src, and phosphatidylinositol 3'kinase (PI-3K) phosphorylation in P2X7-mediated ERK1/2 phosphorylation in astrocytes (Gendron et al. 2003). Activation of P2X7 by BzATP mediates the phosphorylation of Pyk2 on tyrosine residues (402 and 881) in the presence of calcium, and the phosphorylated Pyk2 in turn; serve as kinase and docking site for phosphorylated c-Src and PI-3K and subsequently activation of ERK1/2. In addition, calcium chelation or the application of inhibitors of c-Src or PI 3K significantly reduced P2X7-mediated ERK1/2 activation (Lev et al. 1995; Sabri et al. 1998; Blaukat et al. 1999; Gendron et al. 2003).

1.3.4.4. IL-1 β secretion

IL-1 β is a member of the pro-inflammatory interleukin-1 cytokine family which includes IL-1 (IL-1 α , IL-1 β , IL-33, IL-1Ra), IL-18 (IL-18, IL-37), and IL-36 (IL-36Ra, IL-36 α , β , γ , IL-38) (Dinarello 2018). Binding of pathogen-associated molecular patterns (PAMPs) such as LPS to TLR4 leads to activation of the transcription factor NF-kB which induces the synthesis of Pro-IL-1 β . Inflammasome assembly and activation of caspase-1 by danger-associated molecular patterns (DAMPs) including ATP induces IL-1 β maturation and secretion (Mariathasan et al. 2006). Again, the molecular processes underpinning the involvement of P2X7 in this process are poorly understood. However, K⁺ efflux following P2X7 receptor activation by extracellular ATP has been demonstrated to drive recruitment and activation of NLRP3 inflammasome assembly, which cleaves pro-caspase-1 to produce activated caspase-1, which then cleaves the pro-IL-1 β to produce mature IL-1 β cytokines (Giuliani et al. 2017).

Four mechanisms describe IL-1 β secretion from the activated immune cells; exocytosis of IL-1 β containing secretory lysosomes, shedding of IL-1 β containing plasma membrane micro-vesicles, exocytosis of IL-1 β containing exosomes, and IL-1 β release following plasma membrane damage and cell death (Giuliani et al. 2017).

1.3.4.5. Reactive Oxygen Species (ROS) formation

ROS are produced by normal physiological processes such as the electron transport chain in mitochondria, and the activation of NADPH oxidases in pathological conditions such as the immune response to kill phagocytosed microorganisms. However, over-production of ROS or low levels of anti-oxidant secretion leads to protein and lipid damage and DNA modification (Kopp et al. 2019a). NADPH oxidases are activated by several receptors and regulated by Ca^{2+} -signalling and phosphorylation of protein kinase C, p38, ERK1/2 or phosphoinositide-3 kinase (Spooner and Yilmaz 2011; Haslund-Vinding et al. 2017; Belambri et al. 2018). It is reported that P2X7 receptor activation leads to activate the NADPH oxidases and ROS production in microglia, macrophages, and erythroid cells (Parvathenani et al. 2003; Moore and MacKenzie 2009; Wang and Sluyter 2013). Both Ca^{2+} influx through P2X7 and kinase activity (ERK1/2 and c-Src/Pyk) are essential for ROS production (Martel-Gallegos et al. 2013).

1.3.4.6. Phosphatidylserine exposure

The plasma membranes of animal cells are primarily composed of four major phospholipids; phosphatidylcholine, phosphatidylethanolamine, phosphatidylserine, and sphingomyelin, asymmetrically distributed between the two halves of the membrane bilayer. Phosphatidylcholine and sphingomyelin are mainly present in the cell membrane's outer leaflet, whereas phosphatidylserine and phosphatidylethanolamine are primarily found in the inner leaflet (Marino and Kroemer 2013).

During apoptosis (programmed cell death that occurs in multicellular organisms), biochemical events lead to characteristic cell changes to be cleared by macrophages (Segawa and Nagata 2015b). phosphatidylserine exposure on the cell membrane's external leaflet is a common feature of apoptotic cell death; this externalisation contributes to recognising and then removing dead cells by phagocytes (Lee et al. 2013; Segawa and Nagata 2015b).

phosphatidylserine is thought to be translocated to the cell surface by Anoctamin-6/TMEM16F (ANO6) and XK-related protein 8 (Xkr8) (Suzuki et al. 2010; Suzuki et al. 2013; Segawa and Nagata 2015a). It is reported that activation of the P2X7 receptor leads to increased phosphatidylserine exposure in different cells (Constantinescu et al. 2010; Bartlett et al. 2013). Also, it is reported that P2X7 receptor activates and physically interacts with ANO6 and this is the suggested molecular mechanism for phosphatidylserine flipping (Ousingsawat et al. 2015).

1.3.4.7. The role of P2X7 in gene transcription

P2X7 mediates the activation of several transcription factors including NF- κ B, Nuclear factor of activated T cells (NFAT), and Hypoxia-inducible factor (HIF) (Kopp et al. 2019a).

NF- κ B is a protein complex acting as transcription factor through binding to κ B- motifs on DNA and control cell survival and cytokines release (Zhang et al. 2017). It is found in all animal cells and activated by pro-inflammatory and stressful stimuli like cytokines, bacteria, and viral antigens via cell surface receptors (Christian et al. 2016). P2X7 activation mediates κ B inhibitor degradation, NF- κ B phosphorylation, nuclear translocation and DNA transcription in mechanisms including ROS production and caspase activation, ERK1/2 and Akt, MAP kinases and MyD88 (Ferrari et al. 1997; Aga et al. 2004; Genetos et al. 2011; Liu et al. 2011; Tafani et al. 2011; Kim et al. 2013).

NFAT is a family of five (NFAT1-NFAT5) transcription factors expressed in most immune cells, which regulate their response (Serfling et al. 2012). In T cells, P2X7 activation leads to NFAT induction and IL-2 secretion (Yip et al. 2009). However, in stimulated B cells, NFAT nuclear translocation was shown to be decreased by P2X7-mediated cell membrane depolarisation (Pippel et al. 2015).

HIFs are upregulated in low oxygen or hypoxia conditions and implicated in tumour growth (Kopp et al. 2019a). P2X7 up- or down-modulation has been shown to lead to up-or down-regulation of HIF, respectively (Amoroso et al. 2015; Hirayama et al. 2015; Hirayama and Koizumi 2017).

1.3.5. 3D-structure of the full-length rat P2X7 (P2X7A)

In 2019, as the experimental work in this thesis neared completion, the first full-length cryo-EM structures of rat P2X7 receptor in *apo* (closed) and ATP-bound (open) states was published (Figure 1) (McCarthy et al. 2019a). These structures reveal two important intracellular domains which provide the first insight into P2X7 cytoplasmic domain architecture and function; firstly the C-Cys anchor which corresponds to the 18 amino-acid residue “cysteine-rich region (CRR)” (~360-377 in rP2X7) (Karasawa et al. 2017; McCarthy et al. 2019a). This domain begins as TMD2 leaves the cell membrane and enters the cytoplasm; It forms a loop that points away from TMD2 and then redirects the peptide backbone to the receptor's axis of symmetry. All the cysteines side-chains in this loop (C362, C363, C371, C373, and C377) point toward the TMD2. Palmitoylation of the cysteine residues in the C-Cys anchor and cysteine number 4 (C4) in the N terminus secures TMD2 to the plasma membrane and prevents desensitisation of P2X7 receptor (McCarthy et al. 2019a).

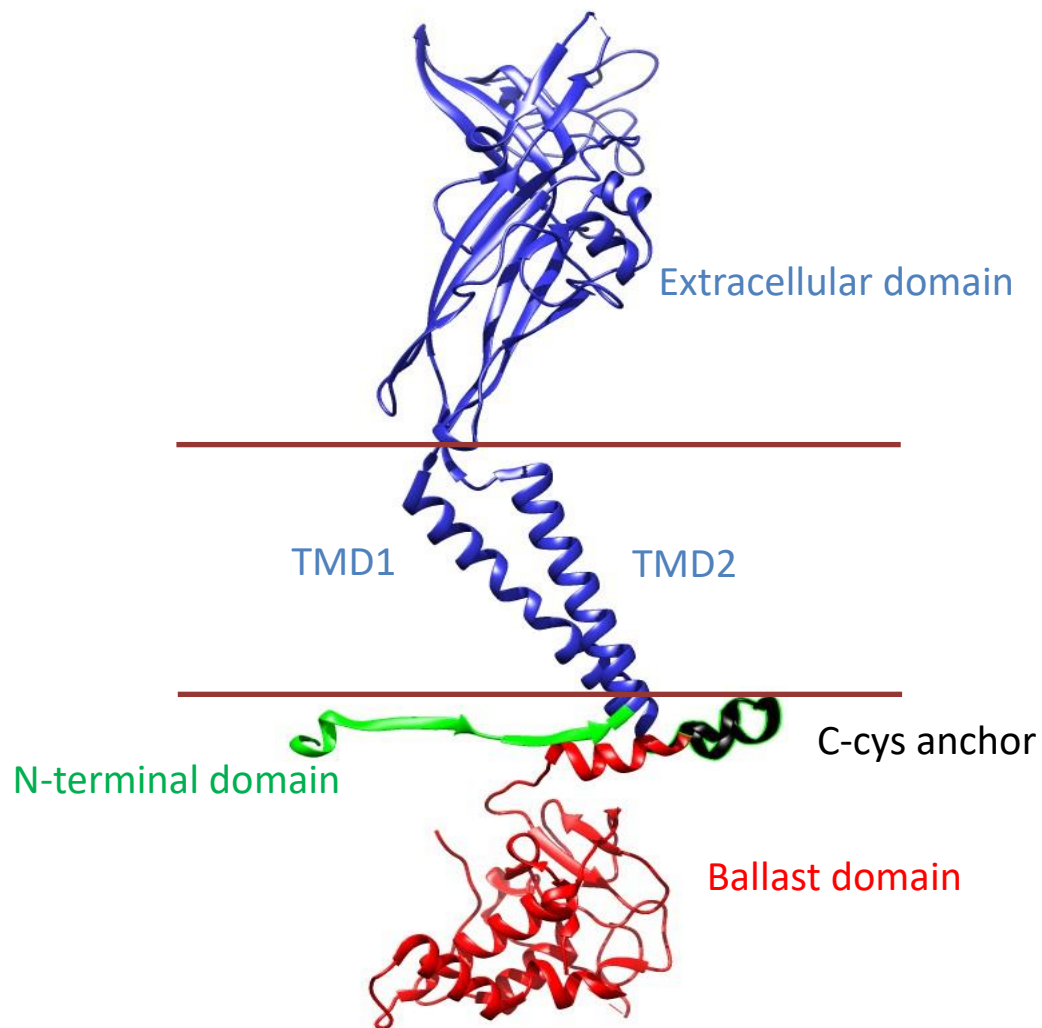


Figure 1: Cartoon view of the rat P2X7 full-length single subunit cryoEM structure

Extracellular and transmembrane domains (TMD1 and TMD2) are shown in blue; the N-terminal domain is shown in green; the C-Cys anchor domain is shown in black; and the ballast domain is shown in red (McCarthy et al. 2019a); PDB: 6U9V.

The second domain is termed the cytoplasmic ballast, and contains the final 200 amino acids in the P2X7 receptor (395-595 residues). Every P2X7 receptor has three cytoplasmic ballasts, and each ballast hangs under the TMD of the next subunit (McCarthy et al. 2019a). The rat P2X7 receptor's cytoplasmic domain contains a zinc ion complex and a guanosine nucleotide-binding site (Figure 2) (McCarthy et al. 2019a).

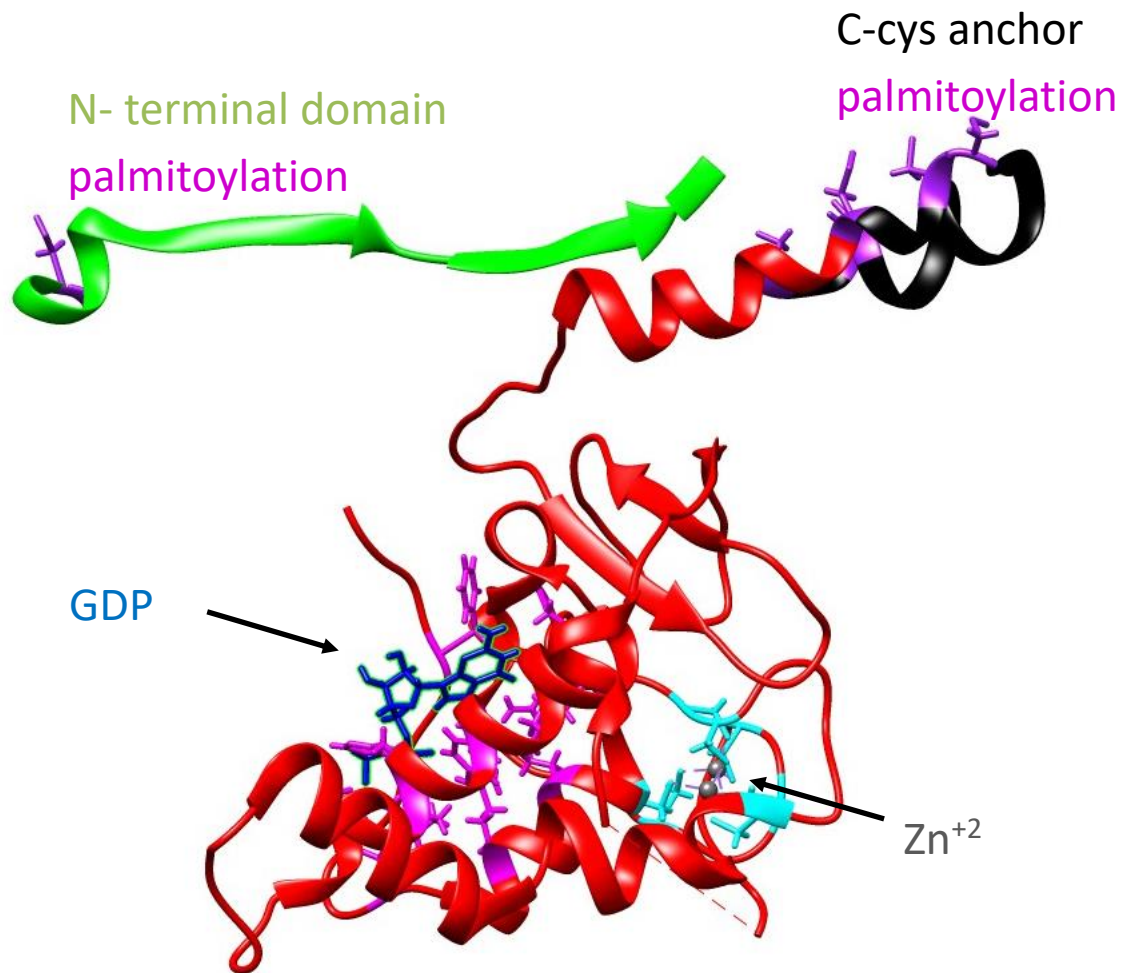


Figure 2: Cartoon representation of the intracellular domains of rat P2X7

The N-terminal domain is shown in green, the C-Cys anchor in black and the ballast domain in red. Palmitoylated residues are shown in purple within the N-terminal and C-Cys anchor domains; the dinuclear Zn complex is shown in gray with its binding residues in cyan and GDP is shown in blue with its binding residues in magenta (McCarthy et al. 2019a); PDB: 6U9V.

1.4. Aims and objectives

P2X7 receptors are involved in a variety of cellular signalling pathways, and their intracellular domains are thought to play key roles in modulating and coupling to these pathways. The C-terminal domain of P2X7 is 120 amino acids longer than any of other P2X receptors (Smart et al. 2003), and several mutagenesis studies demonstrate that the P2X7 intracellular domains modulate kinetic responses of the receptor to ATP, ion channel function, kinase activation and cell surface expression (Surprenant et al. 1996; Worthington et al. 2002; Amstrup and Novak 2003; Boldt et al. 2003). This evidence hints at roles for intracellular domains in mediating P2X7 signalling events, and potentially also that discrete regions of the intracellular domains may be involved in different signalling pathways.

The main aim of this study was to determine which roles the intracellular domains of P2X7 might play in three key signalling responses; cell blebbing, pore formation, and ERK1/2 phosphorylation. This study attempted to address the following questions: Is the intact (full-length) receptor required for all signalling responses? Are the same portions of the receptor intracellular domains involved in all signalling pathways? Do discrete regions of the intracellular domains participate in discrete signalling pathways?

In order to answer these questions, we required a system in which it would be easy to construct and express receptor mutants, visualize cellular responses and (in future) easily purify receptor-target protein complexes for further analysis. We chose at the outset to use a C-terminally GFP-(His)₈-tagged P2X7A (1-595) construct as our ‘wild-type’ receptor, transfected into mammalian cells (either HEK-293 or Hela cells) so that we could easily visualise P2X7-dependent cell blebbing. Our initial studies showed that receptor tagging did not affect the function of the receptor (Mark Young, personal communication; we also confirm these findings in Chapter 3). We chose to analyse two additional cellular responses; pore formation (YoPro1 dye uptake) and ERK1/2 phosphorylation (by Western blot), thought to be intrinsic to the receptor and governed by the N-terminal domain respectively (Amstrup and Novak 2003; Karasawa et al. 2017) .

We have made the assumption that any signalling pathways involved in these responses will be conserved in our system (i.e. that molecular mechanisms of blebbing, pore formation, and ERK1/2 phosphorylation are conserved across different cell types).

After selecting our assays and expression system, we constructed a series of intracellular domain truncations and deletion mutants of our tagged receptor and assayed their function in the 3 assays mentioned, as well as their total and cell-surface protein expression, and ATP-stimulated calcium uptake, in an attempt to identify the intracellular domains essential for P2X7 mediated channel activity, cell blebbing, pore formation and ERK phosphorylation and whether the same domains or distinct regions regulate them.

The thesis has three results chapters; **chapter three** describes the rationale for construction of our mutant constructs, and starts with comparison between our tagged rP2X7-GFP-(His)₈ construct and the wild-type untagged receptor, and ends with studying of mutant constructs effect on P2X7-mediated cell blebbing in HEK-293 in the presence and absence of extracellular calcium. It demonstrates that P2X7-mediated blebbing is reversible, and presents assays of both total and cell-surface protein expression for the mutants. **Chapter four** looks at calcium channel activity, pore formation and ERK1/2 phosphorylation of the mutants. **Chapter five** looks at the molecular mechanism of blebbing *via* testing the proposed P2X7-NMMHC-IIA interaction/dissociation, which is thought to be required for cell blebbing, and the effect of cholesterol depletion from the plasma membrane on both cell blebbing and pore formation.

Chapter 2: Materials and Methods

2.1. rP2X7-GFP-(His)₈ mutant construction, cell culture and transfection

2.1.1. rP2X7-GFP-(His)₈ mutant construction

The rat P2X7-GFP-(His)₈ construct used in this study (rP2X7-GFP-(His)₈) was generated by PCR amplification of the coding sequence for rat P2X7 from a pcDNA-based expression vector (Rassendren et al. 1997; Young et al. 2007), adding *XhoI* and *EcoRI* sites at the 5'- and 3'- ends respectively, followed by restriction digestion and ligation into a zebrafish P2X4-GFP expression vector based on pEGFP-C1 (kindly provided by Eric Gouaux) to replace the zebrafish P2X4 coding region with rP2X7 (Figure 3).

The rationale of using rP2X7 full-length or mutants with a C-terminal thrombin-cleavable eGFP-(His)₈ was to permit the easy visualisation in fluorescence microscopy (eGFP-tag), enable analysis of protein interactions using a pull-down assay ((His)₈-tag), and (for future experiments) purification and structural studies (hence the addition of a thrombin cleavage site to enable tag removal). Preliminary experiments demonstrated that this construct formed functional ion channels capable of cell blebbing, pore formation, and calcium influx (Mark Young, personal communication). Figure 4, shows the sequence of rP2X7-GFP-(His)₈.

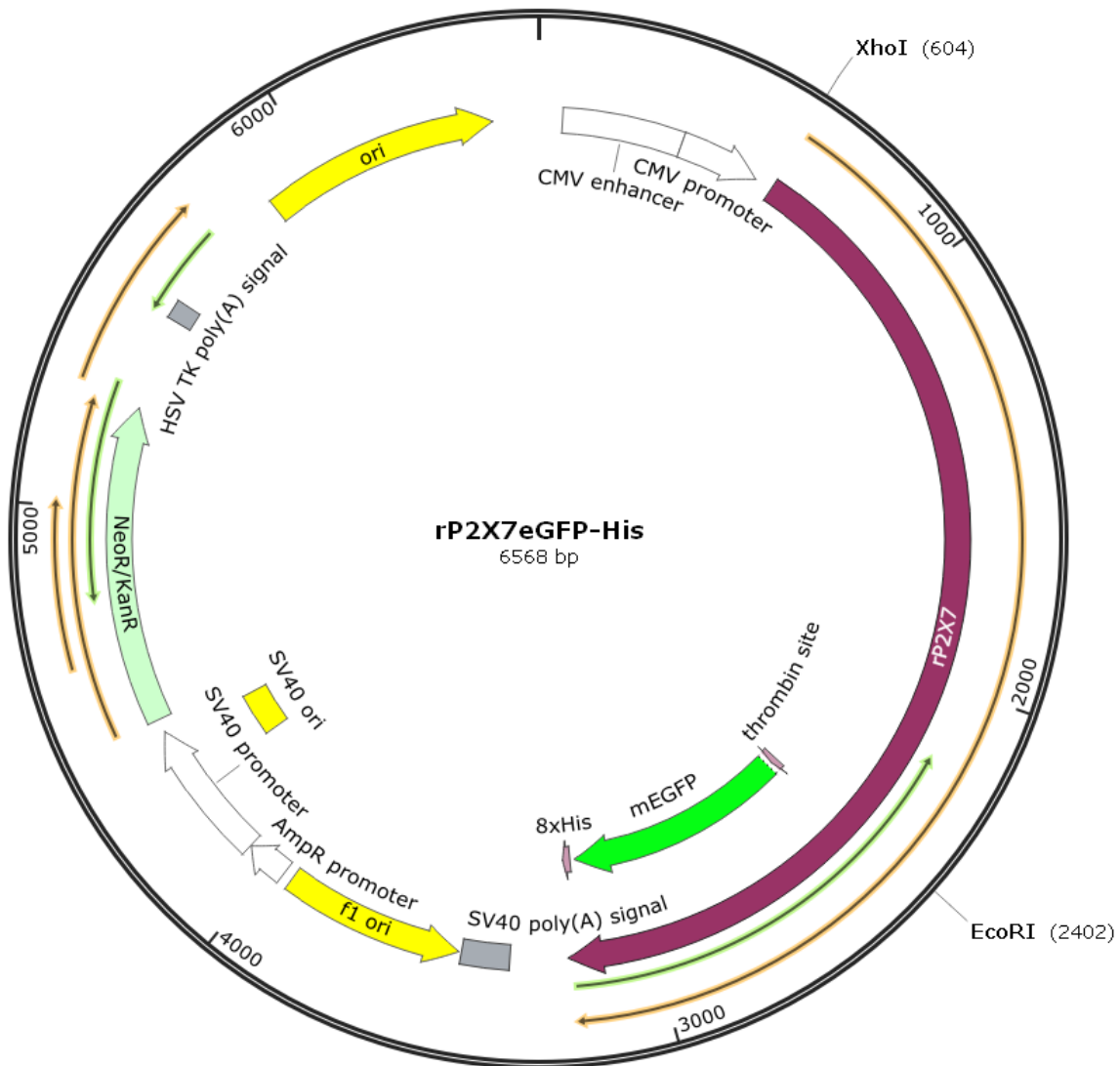


Figure 3: rP2X7-GFP-(His)₈ expression vector map

rP2X7 full-length with a C-terminal thrombin-cleavable eGFP-(His)₈ tag. The plasmid is Neomycin/Kanamycin resistance (NeoR/KanR), contains CMV, simian virus 40 (SV40) and ampicillin resistance (AmpR) promoters and three origin of replications (ori, SV40 ori, and f1 ori). In addition, it contains two poly(A) signal sites (SV40 and Herpes simplex virus thymidine kinase (HSV TK)) to process polyadenylation of mRNA.

1 MPACCSWNDV FQYETNKVTR IQSVNYGTIK WILHMTVFSY VSFALMSDKL YQRKEPLISS 60
 61 VHTKVKGVAE VTENVTEGGV TKLVHGIFDT ADYTLPLQGN SFFVMTNYLK SEGQEQKLCP 120
 121 EYPSRGKQCH SDQGCIGWM DPQSKGIQTG RCIPYDQKRK TCEIFAWCPA EEGKEAPRPA 180
 181 LLRSAENFTV LIKNNIDFPG HNYTTRNLP GMNISCTFHK TWPQCPIFR LGDIFQEIGE 240
 241 NFTEVAVQGG IMGIEIYDC NLDWSHRCQ PKYSFRRLLD KYTNESLFPG YNFRYAKYYK 300
 301 ENGMKERTLI KAFGVRFDIL VFGTGGKFDI IQLVVIYIGST LSYFGLATVC IDLIINTYAS 360
 361 TCCRSRVYPS CKCCEPCAVN EYYRKKCEP IVEPKPTLKY VSFVDEPHIW MVDQQLLGKS 420
 421 LQDVKGQEVN RPQTDLELS RLSLSLHHSP PIPGQPEEMQ LLQIEAVPRS RDSPDWCQCG 480
 481 NCLPSQLPEN RRALEELCCR RKPQCITTS ELFSKIVLSR EALQLLLLYQ EPLLALEGEA 540
 541 INSKLRHCAY RSYATWRFVS QDMADFAILP SCCRWKIRKE FPKTQGQYSG FKYPYANSAV 600
 601 DAGLVPRGSA AAVSKGEEL FTGVVPILVE LDGDVNGHKF SVSGELEGDA TYGKLTCLKFI 660
 661 CTTGKLPVPW PTLVTTLTYG VQCFSRYPDH MKQHDFFKSA MPEGYVQERT IFFKDDGNYK 720
 720 TRAEVKFEGD TLVNRIELKG IDFKEDGNIL GHKLEYNYS HNVYIMADKQ KNGIKVNFKI 780
 781 RHNIEDGSVQ LADHYQQNTP IGDGPVLLPD NHYLSTQSKL SKDPNEKRDH MVLLEFVTAA 840
 841 GITLGMDELY KSGLRSHHHH HHHH

Figure 4: rP2X7-GFP-(His)8 protein sequence

Rat P2X7 N-terminal domain is shown in dark yellow; the C-Cys anchor is shown in red; the ballast domain is shown in grey. The linker is shown in yellow; the GFP and (His)₈ tags are shown with green and blue respectively.

Mutant constructs were created by whole-plasmid PCR using primers (Integrated DNA Technologies; Appendix 1 and 2) designed to develop 17 mutant constructs grouped into five truncations, eight internal deletions and four mutants in the C-cys anchor domain (Table 7). Mutations were verified by sequencing the full coding region (MWG Eurofins).

Table 7: Mutant constructs used in this study

Construct type	Mutant constructs
Truncations	Δ N: Δ (2-23)
	380M: Δ (381-595)
	418M: Δ (419-595)
	581M: Δ (582-595)
	582M: Δ (583-595)
Internal deletions	D1: Δ (389-405)
	D2: Δ (441-460)
	D3: Δ (494-508)
	D4: Δ (389-531)
	D5: Δ (381-417)
	D6: Δ (441-493)
	D7: Δ (418-460)
	D8: Δ (441-460) & Δ (583-595)
C-cys anchor mutants	CRR: Δ (362-379)
	CRRa: Δ (362-370)
	CRRb: Δ (371-379)
	C(X)A: C371A, C373A, C374A, C377A

2.1.2. Cell culture and transfection

2.1.2.1. Cell culture

HEK-293 cells were cultured in Dulbecco's modified Eagle's medium (PAN-Biotech) supplemented with 10% fetal bovine serum (PAN-Biotech), 100X stock solution of 10,000 units/ml penicillin and 10,000 µg/ml streptomycin (The final concentration would be 100 U/ml penicillin and 100 µg/ml streptomycin; Life technologies) at 37°C in a 5% CO₂ enriched humidified atmosphere. Hela cells were cultured in Minimum Essential Medium (MEM) / glutamax (Life technologies) supplemented with 10% fetal bovine serum at 37°C in 5% CO₂ enriched humidified atmosphere.

2.1.2.2. Cell transfection

To transfect HEK-293 cells on plastic or glass-bottom dishes (35 mm diameter); 90-98 µl of Dulbecco's modified Eagle's medium (DMEM/F12) without supplement was added to sterile 1.5 ml tubes, then 1 µg of DNA of either GFP, rP2X7-GFP-(His)₈ or mutant construct was added and mixed in the appropriate 1.5 ml tube making the final volume 100 µl. Then, 3 µl of Fugene HD transfection reagent (Promega) was added and mixed to the medium in each 1.5 ml tube. The Fugene HD transfection reagent and DNA construct mixtures were incubated at room temperature for 15 minutes. Subsequently, the Fugene HD transfection and DNA construct mixture was added over the cells in the plastic or glass-bottom dishes and mixed with the culture media by pipetting. Transfected cells were returned to the cell incubator for 48 hours to allow full protein expression. Hela cells were transfected in the same process; however, the Minimum Essential Medium (MEM) / glutamax without supplement was used as a medium for Fugene HD transfection reagent and DNA mixture.

2.2. Cell lysis, Bradford protein and Cholesterol assays

2.2.1. Cell lysis

Cells in individual wells from a 6-well plate were washed once with 1 ml ice-cold phosphate-buffered saline ((PBS); PAN-Biotech). Then cells were collected by pipetting up and down in 1 ml ice-cold PBS, transferred to a 1.5 ml tube and centrifuged at 4000 rpm for 3 minutes in a benchtop microcentrifuge. Cells pellets were homogenized in 50 μ l lysis buffer (150 mM NaCl, 20 mM Tris-HCl pH 7.4, 1 mM MgCl₂, 1 mM CaCl₂, 1% (w/v) Fos-choline 12 detergent (FC-12), and 20 μ l/ml of one completeTM – EDTA protease inhibitor (Life Technologies) dissolved in 1 ml H₂O) and incubated for 30 minutes on ice before centrifugation 13,000 rpm for 2 minutes. Supernatants containing solubilized protein were transferred to fresh 1.5 ml tubes.

2.2.2. Bradford protein assay

A standard curve of known concentrations of bovine serum albumin (BSA; Fisher Scientific) (ranging from blank (0 μ g/ml) to 500 μ g/ml) was generated and used to determine the protein concentration in each sample (samples were diluted 1:50 in distilled water). 10 μ l of each standard and diluted sample (n=3) were transferred to individual wells in a 96-well plate, then 200 μ l of 1X protein assay reagent (prepared by diluting Bio-Rad 5X concentrated protein assay reagent in distilled water (1:5)) was added to each standard and diluted sample. The CLARIOstar plate reader was used to measure the absorbance at 595 nm. All readings (standards and diluted samples) were subtracted from blanks (readings from buffer alone), and sample concentrations were determined by cross-reference with the standard curve and multiplication by 50 (the dilution factor).

2.2.3. Cholesterol measurement assay

The amplexTM red cholesterol assay kit (contains cholesterol reference standard (2 mg/ml), reaction buffer, working solution (2 U/ml horseradish peroxidase (HRP), 2 U/ml cholesterol oxidase, and 0.2 U/ml cholesterol esterase) was used to measure the cholesterol concentration.

A standard cholesterol curve of known concentration was generated by dilution of the appropriate amount of 2 mg/ml cholesterol reference standard into reaction buffer to produce a range of cholesterol concentrations (from 0 µg/ml to 8.0 µg/ml) and used to determine the cholesterol concentration in each sample. Samples were diluted 1:5 in reaction buffer, then 50 µl of the diluted samples and standards were pipetted into separate wells of a 96- well plate (n=3). Subsequently, 50 µl working solution was added to each microplate well containing the diluted samples and standards and incubated for 30 minutes at 37°C, protected from light.

The fluorescence signal was measured by CLARIOstar using excitation in the range of 530–560 nm and emission detection at 590 nm. All readings (standards and samples) were subtracted from blank readings (reaction buffer alone) to correct for background fluorescence and sample concentrations were determined by cross-reference with the standard curve and multiplication by 5 (the dilution factor).

2.3. Western blotting

Polyacrylamide gels (10%) were prepared to run samples to detect either rP2X7-GFP-(His)₈ or NMMHC-IIA and 15% polyacrylamide gels to detect ERK1/2 and p-ERK1/2 according to (Table 8), allowing 20-25 minutes for polymerization of the separating gel before pouring the stacking gel (4.5% polyacrylamide). After the polymerization of stacking gel, 20 µl sample (25 µg protein lysate, 5 µl 4X LDS sample buffer (Life Technologies), and water) was loaded in an individual well of stacking gel and run in 1X TGS running buffer (25 mM Tris-HCl, 192 mM Glycine, and 0.1% Sodium dodecyl sulfate (w/v) in 1 L MilliQ water) for 10-15 minutes at 100 V to allow the proteins to align at the bottom of stacking gel followed by 60 -90 minutes running at 120 V in the separating gel.

Table 8: Polyacrylamide gel recipes

Polyacrylamide gel	Component	Volume to add
Stacking gel (5 ml)	H ₂ O	3.5 ml
	1 M Tris-HCl, pH 6.8	0.625 ml
	30% / 0.8% acrylamide/Bis-acrylamide (w/v)	0.75 ml
	20% Sodium dodecyl sulfate (w/v)	0.025 ml
	30% ammonium persulfate (w/v)	0.015 ml
	TEMED	0.005 ml
10% polyacrylamide separating gel (10 ml)	H ₂ O	4.1 ml
	1.5 M Tris-HCl, pH 8.8	2.5 ml
	30%/0.8% acrylamide/Bis-acrylamide (w/v)	3.4 ml
	20% Sodium dodecyl sulfate (w/v)	0.05 ml
	30% ammonium persulfate (w/v)	0.035 ml
	TEMED	0.01 ml
15% polyacrylamide separating gel (10 ml)	H ₂ O	2.5 ml
	1.5 M Tris-HCl, pH 8.8	2.5 ml

	30% / 0.8% acrylamide/Bis-acrylamide (w/v)	5 ml
	20% Sodium dodecyl sulfate (w/v)	0.05 ml
	30% ammonium persulfate (w/v)	0.035 ml
	TEMED	0.01 ml

Proteins were transferred from the separating gel to nitrocellulose membranes (Bio-Rad) using a trans-blot Turbo transfer system for 7 minutes (according to manufacturers' instructions). Membranes were blocked on a rocking platform with 10 ml Odyssey blocking buffer (LI-COR Biosciences UK Ltd) for 1 hour at room temperature. After that, membranes were incubated overnight at 4°C with either rabbit anti-GFP ((1:1000); from Life Technologies) to detect rP2X7-GFP-(His)₈, mouse anti- NMMHC-IIA ((1:1000); from Abcam) to detect NMMHC-IIA, rabbit anti- phospho-p44/42 MAPK (Erk1/2) ((1:1000); from Cell Signaling Technology) to detect phosphorylated ERK (1/2), or rabbit anti-p44/42 MAPK (ERK1/2) ((1:1000); from Cell Signaling Technology) to detect ERK (1/2). All these antibodies were diluted in 10 ml Odyssey blocking buffer.

Subsequently, membranes were washed in TBS-T washing buffer (25 mM Tris/HCl pH 7.4, 150 mM NaCl, and 0.02% Tween 20 in 1 L MilliQ water) three times; 5 minutes for each at room temperature, then membranes were incubated with either IR Dye 800 CW goat anti-mouse (1:15000) to detect anti- NMMHC-IIA or dye light 800 goat anti-rabbit (1:10000) to detect anti-GFP, anti-P-ERK and anti- ERK antibodies for 1 hour at room temperature (Secondary antibodies kindly provided by Dr Sonia Lopez de Quinto). Following secondary antibody incubation, membranes were washed in TBS-T (3 times; 5 minutes each, at room temperature). Finally, fluorescence was detected using the Odyssey CLx Infrared imaging system.

2.4. Functional assays

2.4.1. Imaging of cell blebbing

Fluorescence microscopy was performed on a spinning disk confocal microscope (Olympus IX71 motorized, inverted microscope) to image ATP-induced rP2X7-GFP-(His)₈ cell blebbing. Cells were seeded (confluency 70-85%) on glass-bottomed dishes for 24 hours, then transfected with either eGFP (negative control), rP2X7-GFP-(His)₈ full length or mutant constructs for 48 hours. On the day of the experiment, cells were incubated in pre-heated extra-cellular solution containing low divalent cations (ECS-LD; 147 mM NaCl, 10 mM HEPES, 13 mM Glucose, 0.2 mM CaCl₂, 2 mM KCl, pH: 7.4 in MilliQ water) for 15 minutes to reduce the inhibition caused by divalent cations at P2X7 (Young et al. 2007). Imaging was performed at 37°C in 5% CO₂ at 80% humidity.

To record cell blebbing in the absence of extracellular calcium; culture medium was replaced with pre-heated calcium-free ECS-LD (147 mM NaCl, 10 mM HEPES, 13 mM Glucose, 2 mM KCl, pH: 7.4 in MilliQ water). To record blebbing in cholesterol depleted cells; the culture medium was replaced and cells were incubated with ECS-LD-MCD (5 mM Methyl- β -cyclodextrin (MCD; Sigma-Aldrich), 147 mM NaCl, 10 mM HEPES, 13 mM Glucose, 0.2 mM CaCl₂, 2 mM KCl, pH: 7.4 in MilliQ water) for 1 hour at 37°C, Then ECS-LD-MCD was replaced with pre-heated ECS-LD for cell imaging.

Movies were recorded for each sample using time-lapse confocal microscopy. One frame was recorded every 2 seconds for two minutes, before stimulation of the cells by adding ATP to a final concentration of 1 mM ATP (Sigma-aldrich) and recording for five minutes after stimulation. eGFP was excited at 488 nm laser line. Image analysis was performed using the software package ImageJ.

2.4.2. Cell surface expression assay (Biotinylation)

HEK-293 cells were transfected with the cDNA of rP2X7-GFP-(His)₈ full length and constructs for 48 hours in 6-well plate. Transfected cells were washed three times with 1 ml ice-cold PBS (pH 8.0), then incubated with 1 ml of 0.5 mg/ml EZ-link Sulfo-LC-NHS Biotin (Thermo Fisher) dissolved in PBS (pH 8.0) on ice for 30 minutes. Subsequently, cells were washed twice with 1 ml cold 1X TG buffer; (10X TG: 1.21 g Tris base and 5.76 g glycine in 40 ml MilliQ water) to quench biotin and collected in 1 ml 1X TG buffer by pipetting up and down into 1.5 ml tube, then centrifuged at 4000 rpm for 3 minutes to pellet cells. Cell pellets were incubated with 50 µl solubilization buffer A (150 mM NaCl, 20 mM Tris-HCl pH 7.4, 1 mM MgCl₂, 1 mM CaCl₂, 2% (v/v) Triton X-100, 20 µl/ml Complete –EDTA protease inhibitors) for one hour on a rotating wheel at 4°C, centrifuged at 13000 rpm for 2 min to pellet debris and supernatants were transferred to fresh 1.5 ml tubes.

To capture biotinylated protein, 25 µl streptavidin agarose beads (Thermo Fisher) and 500 µl buffer A were added to fresh 1.5 ml tubes, then 200 µg of each protein lysate was added and incubated overnight at 4°C on a rotating wheel. Subsequently, samples were centrifuged at 5000 rpm for one minute to pellet beads. Beads were washed twice by adding 500 µl buffer A and inverting tubes 20 times and again centrifuged at 5000 rpm for one minute to pellet the beads. Finally, bead samples were prepared for SDS-PAGE by adding 25 µl of 4X LDS sample buffer and boiling at 100°C for 5 minutes. Total protein samples were prepared by adding 25 µg protein lysate, 5 µl 4X LDS sample buffer, and water to final volume 20 µl in clean 1.5 ml tube and boiling at 100°C for 2 minutes. Samples were separated on SDS-PAGE gels, transferred on to nitrocellulose membranes and blotted for rP2X7-GFP-(His)₈ using the anti-GFP.

2.4.3. YO-PRO-1 dye uptake assay

The ability of rP2X7-GFP-(His)₈ and the mutant constructs to mediate ATP-stimulated pore formation were measured using the cell-impermeant YO-PRO dye uptake assay. Cells were cultured on six-well plates for 24 hours and then transfected with either rP2X7-GFP-(His)₈ or mutant constructs for 48 hours. Negative control cells were not transfected. Subsequently, 50,000 cells/well were transferred to 96-well plates and incubated overnight. At the time of the experiment, the culture media over the cells in the 96-well plates was replaced with 99 μ l ECS-LD containing 5 μ M YO-PRO dye.

The CLARIOstar plate reader was used to record fluorescence (excitation wavelength 477 nm with a bandwidth of 14 nm; emission wavelength 525 nm with a bandwidth 30 nm; spiral mode reading; cycle time 86 seconds). The baseline signals were measured for ten cycles before the addition of 10 μ l ATP (final concentration 1 mM ATP in each well) by the CLARIOstar injector, and a further 50 cycles after ATP application.

For cholesterol depletion experiments, cells in 96-well plates were incubated with ECS-LD-MCD (5 mM MCD, 147 mM NaCl, 10 mM HEPES, 13 mM Glucose, 0.2 mM CaCl₂, 2 mM KCl, pH: 7.4 in MilliQ water) for 1 hour at 37°C. ECS-LD-MCD was replaced with 99 μ l ECS-LD containing 5 μ M YO-PRO dye and fluorescence readings were recorded as described above.

The YO-PRO uptake gradient was calculated by subtracting the reading of cycle number 11 after 1 mM ATP addition (cycle 21 in total) from the reading of cycle number 1 after 1 mM ATP application (cycle 11 in total) and dividing by the time taken (860 seconds).

2.4.4. Calcium influx assay

rP2X7-GFP-(His)₈ ATP-induced calcium influx was measured using a Fluo4-AM labelled calcium indicator molecule that exhibits an increase in fluorescence upon calcium binding. HEK-293 cells were transfected with either rP2X7-GFP-(His)₈ or mutant constructs for 48 hours, and negative control cells were not transfected. 50,000 cells/well were transferred to 96-well plate and incubated overnight. On the day of the experiment, culture medium was replaced with loading buffer (PBS containing 1% (w/v) BSA, 2.6 μ M Fluo4-AM and 20% Pluronic (non-ionic detergent that can assist in the dispersion of the nonpolar AM ester in aqueous media)), and cells were incubated for 30 minutes at 37°C. Subsequently, cells were washed once with PBS containing 1% (w/v) BSA. Cells were re-incubated with PBS containing 1% (w/v) BSA for 30 minutes at 37°C to allow complete de-esterification of intracellular acetoxymethyl (AM) esters. Subsequently, PBS containing 1% (w/v) BSA was replaced with 99 μ l working buffer (147 mM NaCl, 10 mM HEPES, 13 mM Glucose, 12 mM CaCl₂, 2 mM KCl; pH: 7.4 in MilliQ water).

The CLARIOstar plate reader was used for fluorescence recording (excitation wavelength 470 nm with a band width of 15 nm and the emission wavelength 515 nm with a band width of 20 nm; spiral mode reading; cycle time 23 seconds). The baseline signal was measured for five cycles before the addition of 10 μ l ATP (final concentration 1 mM ATP in each well) by the CLARIOstar injector, and a further 35 cycles after ATP application. Calcium influx for each sample was calculated by subtracting the reading of cycle number 11 after 1 mM ATP addition (cycle 16 in total) from the reading of cycle number 5 (last cycle before 1 mM ATP application), then divided by the reading of cycle number 5 ((final reading-initial reading)/initial reading).

2.4.5. Extracellular Regulated Kinases ERK1/2 phosphorylation assay

Cells used for ERK1/2 and phosphorylated ERK (P-ERK1/2) assay were incubated in pre-heated extra-cellular solution-low divalent ((ECS-LD); 147 mM NaCl, 10 mM HEPES, 13 mM glucose, 0.2 mM CaCl₂, 2 mM KCl, pH 7.4) for 15 minutes, and then only the cells used for p-ERK (1/2) assay were stimulated with 1 mM ATP final concentration for two minutes in ECS-LD. Cells were homogenized in the lysis buffer (same lysis buffer described in **section 2.2.1**) containing 20 μ l phosphatase inhibitor cocktail (Life Technologies); cell lysates were prepared as described in **section 2.2.1**. Samples were prepared for western blotting, as described in **section 2.3**.

2.5. rP2X7 wild-type vs rP2X7-GFP-(His)₈ comparison assays

To determine whether the GFP-(His)₈-tag affects the function of rP2X7 receptor or not; we performed a comparison assays between rP2X7 wild-type (pcDNA3 vector expressing untagged rat P2X7) and rP2X7-GFP-(His)₈. These assays include YO-PRO dye uptake, calcium influx, and ERK1/2 phosphorylation as described in **sections 2.4.3, 2.4.4, and 2.4.5**, respectively. Cell blebbing comparisons were not performed due to difficulties in determining untagged receptor expression levels on a cell-by-cell basis in transient transfections. Time constraints prevented us from developing a stably transfected HEK cell line expressing the untagged receptor.

Additionally, we estimated ATP EC₅₀ for YO-PRO dye uptake. This assay was performed in the same as for YO-PRO dye uptake (**section 2.4.3**); however, cells expressing the rP2X7 wild-type or rP2X7-GFP-(His)₈ were stimulated by different ATP concentrations (0.003 mM, 0.01 mM, 0.03mM, 0.1 mM, 0.3 mM, 1 mM, and 3 mM).

2.6. rP2X7-GFP-(His)₈, NMMHC-IIA interaction assays

2.6.1. Proximity Ligation Assay (PLA)

To test for proposed interaction between P2X7 receptor and NMMHC-IIA, which is thought to be important for cell blebbing (Gu et al. 2009), we used the Duolink *in situ* orange mouse/rabbit kit (Sigma-Aldrich) in conjunction with anti eGFP and anti NMMHC antibodies. 100,000 Hela cells were seeded on a coverslip in 12-well plates for 24 hours then cells (approx. 80% confluency) were transfected and allowed to express protein for 48 hours (as described in **section 2.1.2.2**). Subsequently, cells were washed twice with 1 ml PBS and fixed by adding 1 ml 4% paraformaldehyde for 15 minutes at room temperature; then cells were washed three times with 1 ml PBS. Subsequently, cells were permeabilized by incubating with 0.25% Triton X-100 (PBS-TX) for 5 minutes at room temperature and then washed three times with 1 ml PBS.

PLA was performed according to the kit's instructions (Figure 5). Fixed cells were imaged by confocal spinning disk microscopy; eGFP, 4',6-diamidino-2-phenylindole (DAPI) and orange signals (represent P2X7-NMMHC interaction) were excited at 488 nm, 405 nm, and 561 nm laser lines respectively. Imaging acquisition and counting of the number of puncta describing signal interaction (orange dots) were performed with the software package ImageJ.

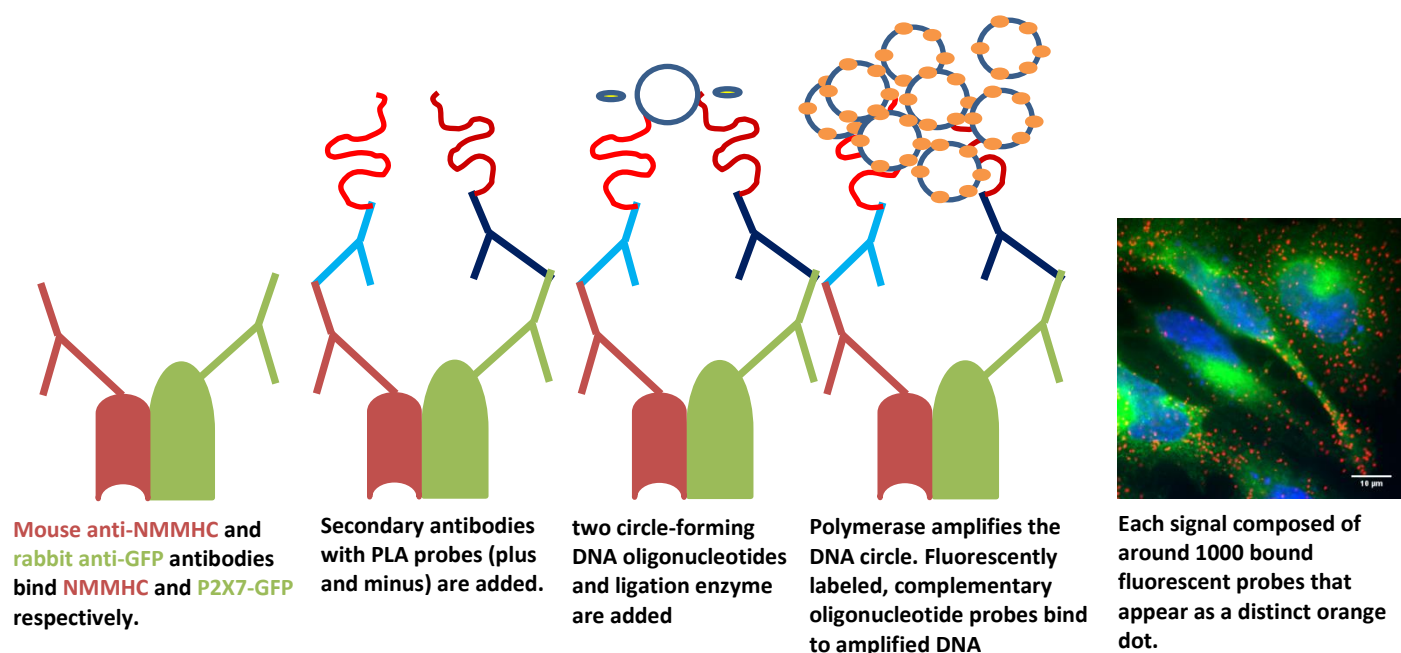


Figure 5: Diagrammatic overview of the Duolink proximity ligation assay

P2X7-GFP-(His)₈ and mutant transfected Hela cells were incubated with blocking buffer for 1 hour at room temperature; then cells were incubated with both (1:500 dilution) mouse anti-NMMHC and (1:500 dilution) rabbit anti-GFP antibodies for 1 hour at room temperature. After washing, diluted minus and plus probes were added to the Hela cells and incubated for 1 hour at 37°C. Subsequently, the ligation enzyme was added to Hela cells and incubated for 30 minutes at 37°C. Finally, Hela cells were incubated with polymerase for 100 minutes at 37°C. The slides were prepared for imaging using mounting media containing DAPI.

2.6.2. Pull-down assay

HEK-293 and rP2X7-GFP-(His)₈ stably transfected cells were cultured in 6-well plates for 48 hours. Subsequently, cells were collected in 1.5 ml microcentrifuge tubes, and cell lysates were prepared (as described in **section 2.2.1**). At this point, 10 µl of each lysate was taken as the total sample fraction. Subsequently, Ni-sepharose beads (Thermo Fisher) were resuspended, and 1 ml was pipetted (using a 1 ml pipette tip with the final ~5 mm cut off) into 1.5 ml tube and centrifuged at 5000 rpm in a benchtop microcentrifuge for 10 seconds, and the supernatant was removed. Then 500 µl of solubilisation buffer (20 mM Tris-HCl pH 7.4, 150 mM NaCl, 1 mM MgCl₂, 1 mM CaCl₂ containing 1% (w/v) dodecyl maltoside (DDM) and, 20 µL/mL of one completeTM – EDTA protease inhibitor) was added and mixed to beads for washing two times. Subsequently, 25 µl of beads were pipetted into fresh 1.5 ml tubes (1 per sample) containing 500 µl washing buffer (the solubilisation buffer containing 25 mM imidazole), then 500 µg solubilised protein sample was added and incubated overnight at 4°C on a rotating wheel to bind beads with the histidine tag of rP2X7-GFP-(His)₈. Subsequently, samples were centrifuged, and the supernatant was removed (10 µl of this supernatant were taken as a flow-through fraction). Subsequently, 500 µl washing buffer were added to beads for washing (repeated six times). Finally, 100 µl elution buffer (Solubilisation buffer containing 500 mM imidazole) was added to each tube and incubated for 5 minutes at room temperature, then centrifuged and the supernatant removed (10 µl of this supernatant were taken as elution fraction).

Bead fractions were prepared for western blotting by adding 25 μ l 4X LDS sample buffer to the beads fraction and boiling at 100°C for 5 minutes. Total protein, flow-through, and elution fractions were prepared by adding 5 μ l 4X LDS sample buffer and 5 μ l water to 10 μ l of each individually and boiling at 100°C for 2 minutes. Subsequently, sample fractions were centrifuged at 5000 rpm for 1 minute and loaded on SDS-PAGE for Western blot with anti-GFP and anti-NMMHC-AII antibodies (**section 2.3**).

2.7. Statistical analysis

Statistical analysis was performed using GraphPad. Experimental groups were compared using an analysis of variance (ANOVA). A P-value of less than 0.05 was indicative of the significant difference between the compared groups.

Chapter 3: Investigating the role of P2X7
intracellular domains in ATP-mediated cell
blebbing

3.1. Introduction

As previously discussed (**Section 1.3.4.1**), cell blebbing is a cell membrane protrusion that forms due to cytoskeletal rearrangement controlled by the Rho family of small GTPase (Chhabra and Higgs 2007; Charras 2008). Cell blebbing is implicated in a various physiological process such as cytokinesis and cell spreading (Charras and Paluch 2008; Fackler and Grosse 2008; Babiychuk et al. 2011), and pathological conditions including lipid peroxidation, cancer invasion and immunological disorders (Langridge and Kay 2006; Norman et al. 2010; Norman et al. 2011; Khajah and Luqmani 2016).

Two distinct pathways have been proposed to describe the role of P2X7 receptor in cell membrane blebbing; a reversible calcium-dependent pathway which triggers cytoskeletal disruption and membrane blebbing directly within seconds following the receptor activation, and an irreversible cell blebbing via a calcium-independent, ROCK-1 dependent pathway following prolonged P2X7 receptor activation for more than 30 min, which eventually causes cell death (Mackenzie et al. 2005).

Despite this, the molecular events that directly underpin P2X7 receptor activation to cell blebbing are poorly understood. It is not known, for example, whether blebbing is initiated by direct protein-protein interactions involving the intracellular domains of the receptor, or if it simply depends on receptor activation (i.e. a biophysical phenomenon due to ion flux). This part of the study aimed to identify if the intracellular domains of P2X7 were important for cell blebbing by imaging HEK-293 cells transiently transfected with rP2X7-GFP-(His)₈ and mutant constructs with truncations and deletions in the intracellular domains. It also looked to determine the effect of extracellular calcium on this signalling phenomenon.

GFP-tagged receptors were chosen for ease of visualization in fluorescence microscopy (for details of the construct used see **Chapter 2 section 2.1.1**). It is important to note the potential severe effects that tagging the receptor could have on channel function and downstream signalling. A small number of previous studies have demonstrated that P2X receptors with fluorescent protein tags are functional. Electrophysiological analysis of wild-type and C-terminally YFP- or CFP-tagged P2X receptors showed that both ion-channel function and the kinetics of activation, desensitization, and deactivation were not detectably affected for P2X1, P2X2, P2X3, P2X4, and P2X5 receptors (Young et al. 2008). C-terminally YFP- or CFP- tagged P2X7 receptors were also functional but they displayed a substantial degree of variability in their channel response (Young et al. 2008).

In *Xenopus* oocytes, P2X7 tagged with eGFP on either the N- or C-terminus displayed similar channel responses to wild-type (untagged) receptors, but the P2X7-eGFP receptor displayed a threefold reduction in ATP sensitivity (Smart et al. 2002). In HEK-293 cells, eGFP or triple hemagglutinin (3HA) tagging on the N-terminus of human P2X7 was shown to disrupt receptor-mediate pore formation and calcium influx, but C-terminally tagged receptors displayed similar function to wild-type (Dreisig et al. 2018).

Taken together, these observations suggest that the C-terminal tagging of P2X7 is unlikely to have a substantial effect on either channel function or downstream signalling pathways, and that our rP2X7-GFP-(His)₈ construct is suitable for our experiments.

3.2. Rationale for the mutant used in this study

The full-length rP2X7 cryoEM structure was published in 2019 (McCarthy et al. 2019a), two years after the start of this project. This structure (shown in Figure 1 and 2) showed that the C-terminal domain of the receptor was composed of a short cysteine-rich C-Cys anchor domain proximal to TM2 (360-377) and a globular ballast domain-containing bound GDP and dinuclear zinc (395-595). Initially, our mutants were constructed based on previous mutagenesis and sequence analysis studies, but we have used the cryoEM structure to show the locations of our mutants and place them in context in terms of which domains they disrupt. In this study, a series of 17 mutants were constructed, with all mutants retaining the GFP-(His)₈ tag. To explain rational for the construction of these mutants, we have grouped them into three main categories; truncations, internal deletions, and C-Cys anchor mutants.

3.2.1. Truncation mutants

This group includes four truncations in the ballast domain; 380M: Δ (381-595), 418M: Δ (419-595), 581M: Δ (582-595), 582M: Δ (583-595), and one truncation in the N-terminal domain; Δ N: Δ (2-23); Figure 6. These truncations were designed based on previous publications. The capability of ballast domain truncations of pore formation in terms of ethidium ion uptake was measured by Smart *et al*; 582M was demonstrated to be capable of pore formation, while 380M, 418M, and 581M were not (Smart et al. 2003). Δ N was designed based on work by Amstrup and Novak demonstrating that deletion of the N-terminal domain abolished ATP-stimulated ERK1/2 phosphorylation (Amstrup and Novak 2003).

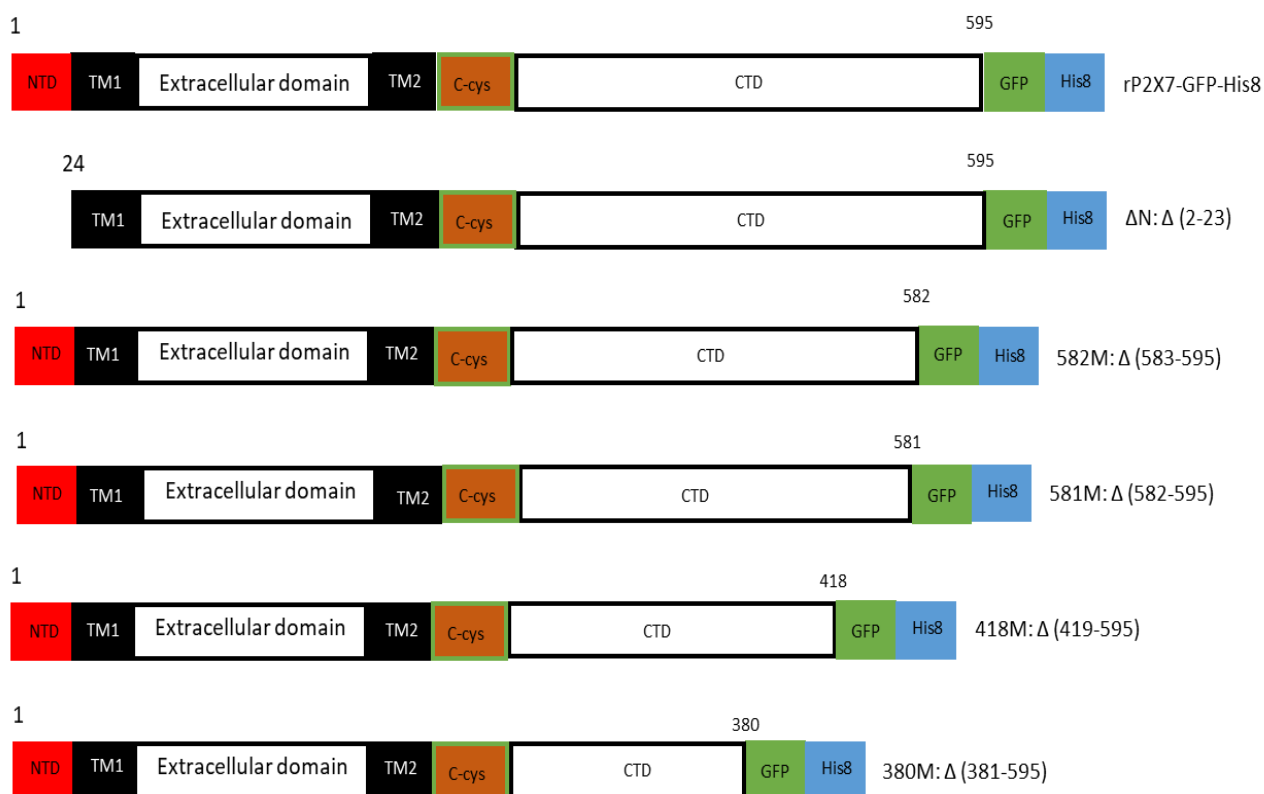


Figure 6: Schematic structure of truncations mutants

NTD: N-terminal domain, TM1 and TM2: transmembrane 1 and 2 domains respectively, C-Cys: C-Cys anchor domain, CTD: C-terminal domain representing the ballast domain, GFP: green fluorescence protein tag, His8: histidine 8 residues.

3.2.2. C-Cys Anchor domain

This group includes three deletion mutants in the heavily palmitoylated cysteine-rich region or newly named C-Cys anchor domain; CRR: Δ (362-379), CRRa: Δ (362-370), CRRb: Δ (371-379), and one point mutant C(X)A; where the four individual cysteine residues (C371, C373, C374, and C377) were mutated to alanine; Figure 7.

In studies using purified N- and C-terminally truncated *Ailuropoda melanoleuca* (Giant panda) P2X7 reconstituted into synthetic lipid vesicles, Karasawa *et al* demonstrated, by comparing constructs with or lacking the C-Cys anchor domain, that the C-Cys region counteract the inhibitory effect of membrane cholesterol on YO-PRO dye uptake

(Karasawa et al. 2017). They suggested that the C-Cys anchor domain was capable of interacting with cholesterol and preventing it from directly inhibiting pore formation (intrinsic to the P2X7 channel). To enable us to test their findings with rat P2X7, we constructed a deletion construct of CRR: Δ (362-379); (full-length rP2X7-GFP-(His)₈ lacking the CRR region). We next set out to identify the minimal region of CRR important for rP2X7-GFP-(His)₈ function by constructing half-deletions in the CRR region, CRRa: Δ (362-370) and CRRb: Δ (371-379). Subsequently, the C(X)A construct was created to study the importance of the cysteine residues in the CRRb region.

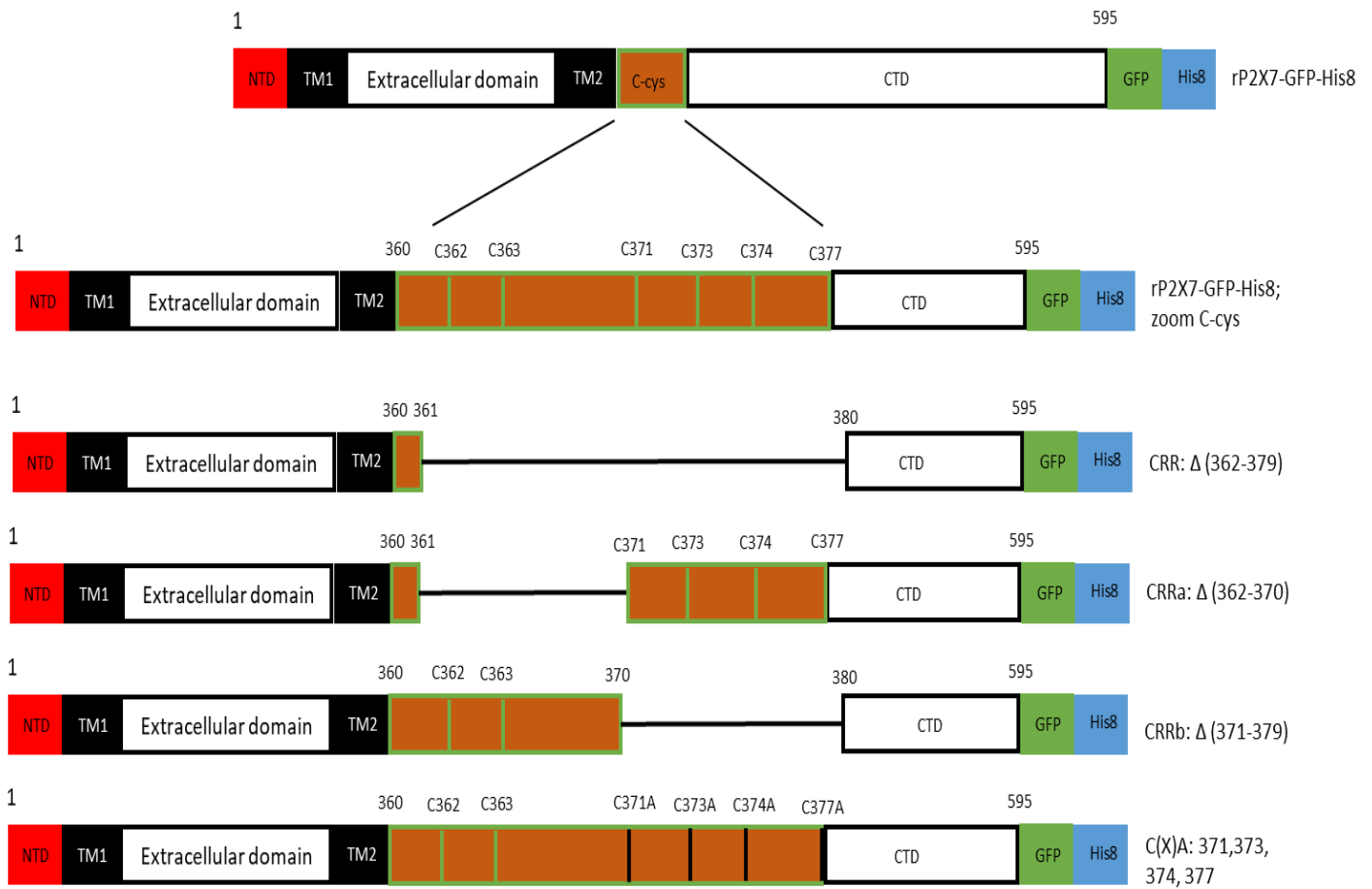


Figure 7: Schematic structure of C-Cys anchor mutants

NTD: N-terminal domain, TM1 and TM2: transmembrane 1 and 2 domains respectively, C-Cys: C-Cys anchor domain, CTD: C-terminal domain representing the ballast domain, GFP: green fluorescence protein tag, His8: histidine 8 residues.

3.2.3. Internal deletions

Before the cryoEM structure of rat P2X7 was published (McCarthy et al. 2019b), the 3D-structure and organization of the C-terminal domain was unknown; it does not display significant amino-acid sequence homology with any other protein, and the only information available was based on mutagenesis studies and analysis of potential domain conservation (Kopp et al. 2019b). We decided to use this information to generate a series of eight internal deletions within the ballast domains of rP2X7-GFP-(His)₈ (Figure 8). D1: $\Delta(389-405)$ and D3: $\Delta(494-508)$ are regions homologous to domains within high molecular weight protein 3 (HMW3) from *Mycoplasma genitalium* and the hypothetical *Caenorhabditis elegans* protein C18H2.1 respectively; which represent a potential interactions motifs with cytoskeletal proteins (Denlinger et al. 2001). D2: $\Delta(441-460)$ contains the PXXP motif suggesting that P2X7 C-terminal is able to bind proteins containing Src homology 3 (SH3) domains (Denlinger et al. 2001), and D4: $\Delta(389-531)$ is a large deletion encompassing D1, D2, and D3. D5: $\Delta(381-417)$, D6: $\Delta(441-493)$, D7: $\Delta(418-460)$, and D8: $\Delta((583-595) \& (441-460))$ are further deletions constructed based upon the data obtained from deletions D1-D4.

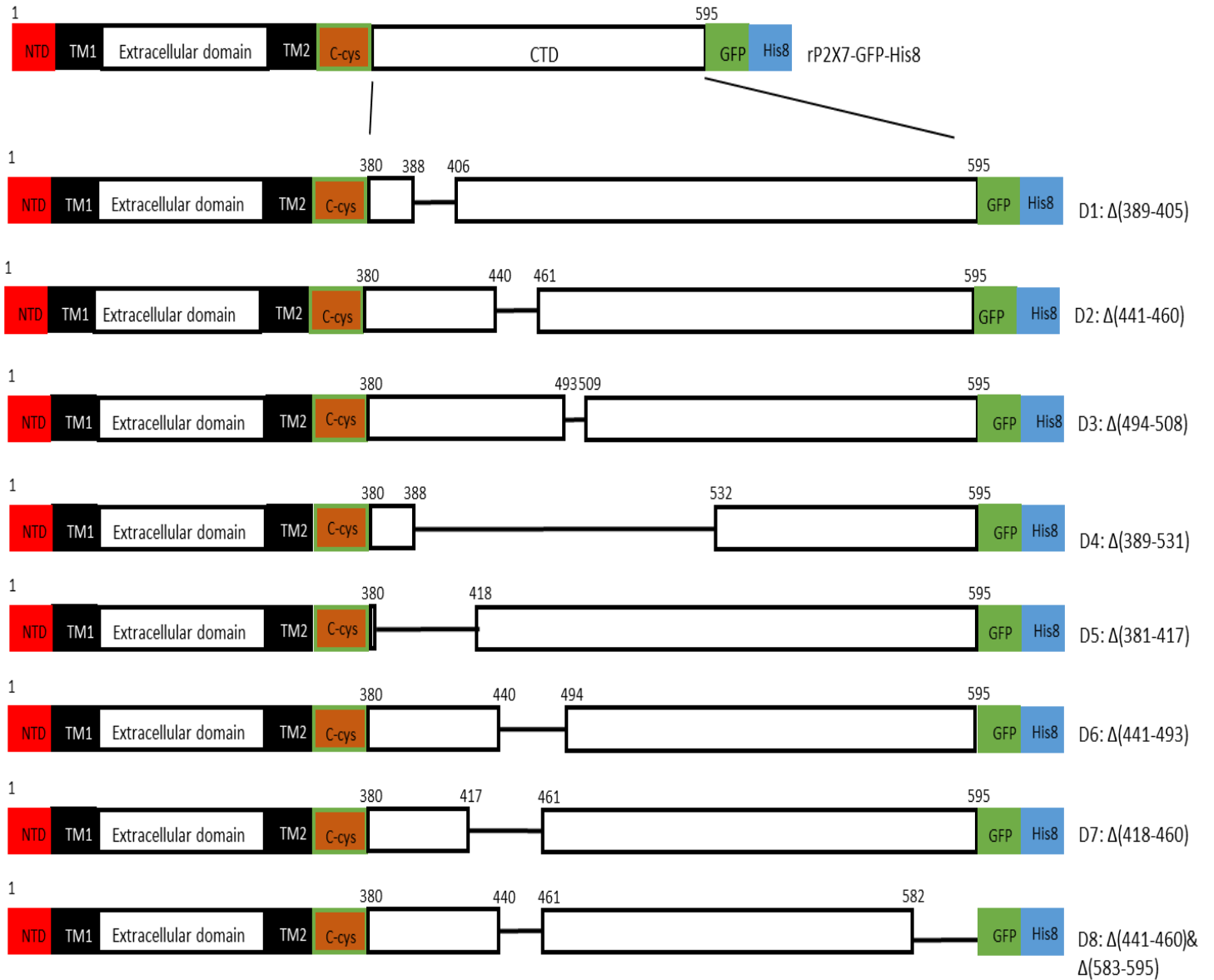


Figure 8: Schematic structure of internal deletions

NTD: N-terminal domain, TM1 and TM2: transmembrane 1 and 2 domains respectively, C-Cys: C-Cys anchor domain, CTD: C-terminal domain representing the ballast domain, GFP: green fluorescence protein tag, His8: histidine 8 residues.

3.3. Results

3.3.1. Functional comparison of non-tagged and GFP-(His)₈-tagged rat P2X7 receptors

All our constructs contain a C-terminal GFP-(His)₈ tag, which may have an effect on receptor function. We decided to compare calcium influx, pore formation, and ERK1/2 phosphorylation in both wild-type (untagged) receptor and our construct (rP2X7-GFP-(His)₈) to ensure that our observations were not compromised by our choice tag. Untagged and tagged receptors were transfected into HEK-293 cells and compared with non-transfected cells as a negative control. Cell blebbing was not performed because of the inability to visualize the rP2X7 wild-type (untagged) in confocal microscopy.

3.3.1.1. Calcium influx

Transfected cells in 96-well plates were loaded with Fluo4-AM and ATP-stimulated uptake was recorded by measuring an increase in fluorescent signal due to calcium getting inside cells and complexing with Fluo4 indicator molecule.

As expected, non-transfected cells (HEK) gave no response, whereas cells transfected with full-length rP2X7-GFP-(His)₈ and rP2X7 WT (untagged) showed ATP-stimulated calcium influx (Figure 9A). Initial gradients of calcium influx were calculated for each construct (Figure 9B); influx gradient for rP2X7-GFP-(His)₈ was not significantly different from rP2X7 WT, indicating that our GFP-(His)₈ tag does not affect rP2X7-mediate calcium influx.

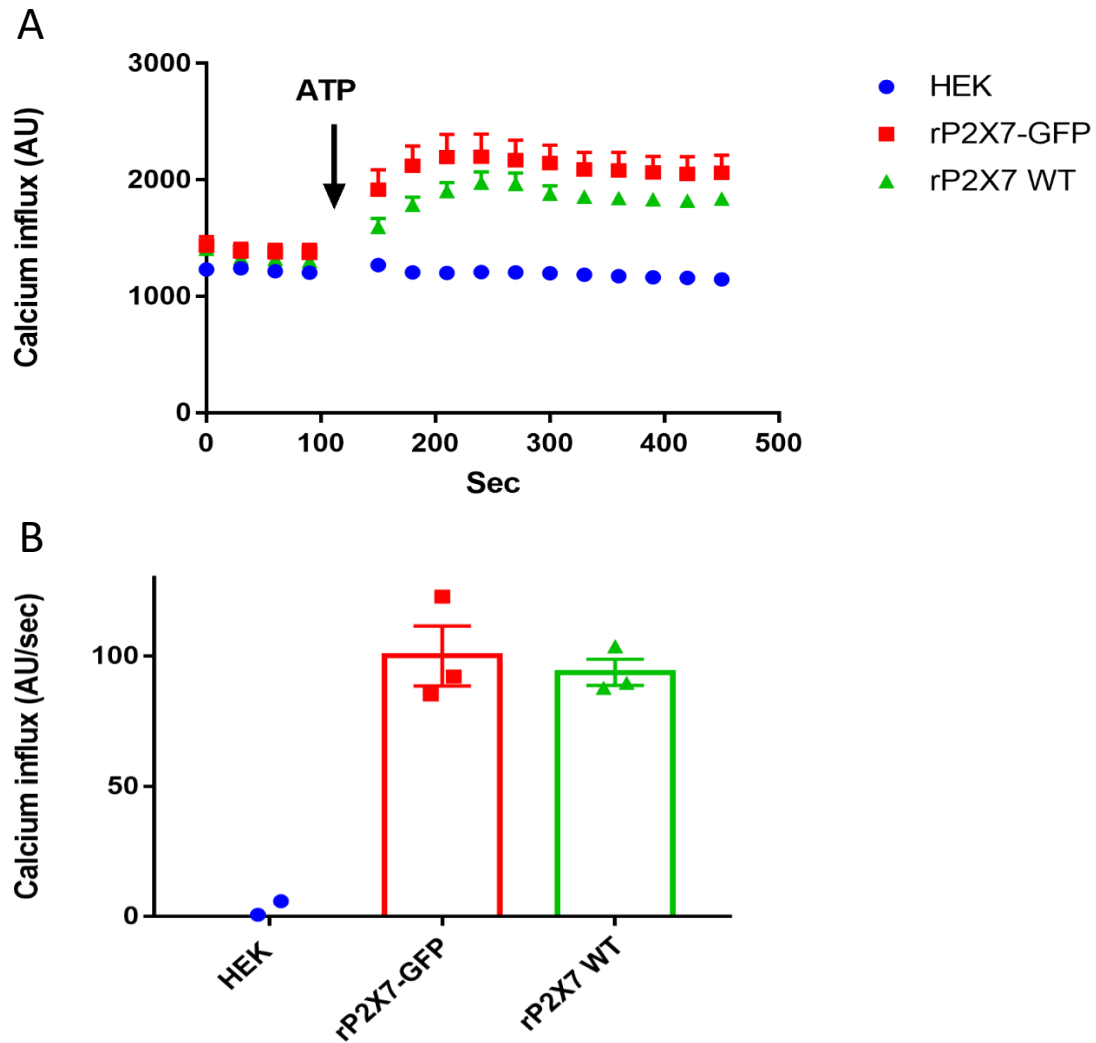


Figure 9: Comparison of ATP induced calcium influx between rP2X7-GFP-(His)₈ and rP2X7 WT

(A): line graph of calcium influx, representative mean \pm SEM from 1 experiment, (B): histogram shows calcium gradient influx. HEK: HEK-293 cells (un-transfected), rP2X7-GFP: rP2X7-GFP-(His)₈, rP2X7-WT: rP2X7 wild-type (untagged); no significant difference between rP2X7-GFP-(His)₈ and WT detected, representative mean \pm SEM from 3 independent experiments.

3.3.1.2. Pore formation

Transfected cells in 96-well plates were incubated with YO-PRO-1 dye and ATP-stimulated uptake was recorded by measuring an increase in fluorescent signal due to dye getting inside cells and complexing with nucleic acid.

As expected, non-transfected cells (HEK) gave no response, whereas cells transfected with full-length rP2X7-GFP-(His)₈ and rP2X7 WT (untagged) showed ATP-stimulated YO-PRO-1 uptake (Figure 10A). Initial gradients of YO-PRO-1 uptake were calculated for each construct (Figure 10B). Uptake gradient for rP2X7-GFP-(His)₈ was not significantly different from rP2X7 WT, indicating that our GFP-(His)₈ tag does not affect rP2X7-induced pore formation.

ATP EC₅₀ assay was performed in the same as for YO-PRO dye uptake. Negative control and cells expressing the rP2X7 wild-type or rP2X7-GFP-(His)₈ were stimulated across a range of ATP concentrations (0.003 mM, 0.01 mM, 0.03mM, 0.1 mM, 0.3 mM, 1 mM, and 3 mM).

Our results demonstrate no difference in YO-PRO dye uptake following receptor activation and ATP EC₅₀ values were 100 μ M for rP2X7-GFP-(His)₈ and 300 μ M for the wild type, (Figures 11; n=3).

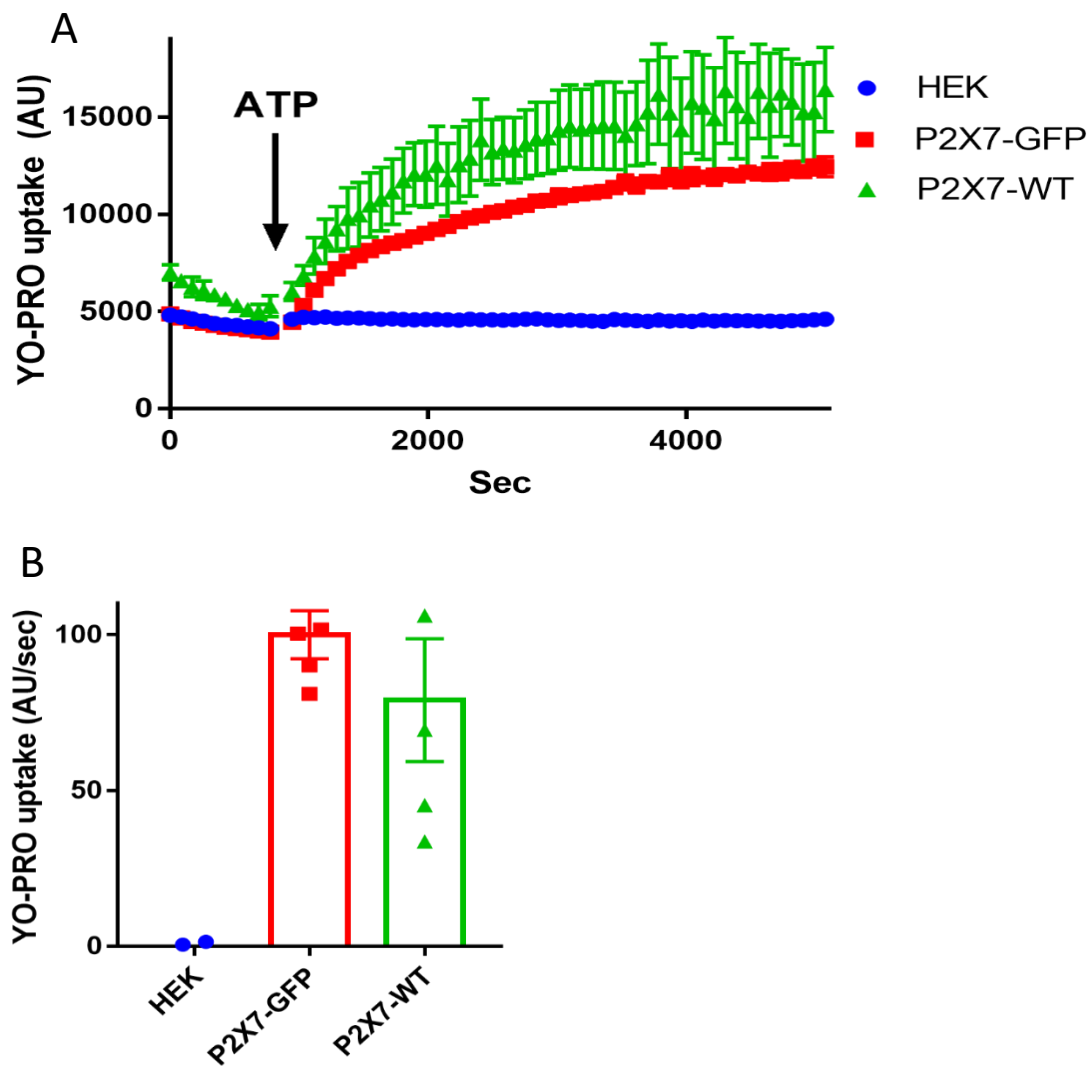


Figure 10: Comparison of ATP induced YO-PRO uptake between rP2X7-GFP-(His)₈ and rP2X7 WT

(A): line graph of YO-PRO dye uptake, representative mean \pm SEM from 1 experiment.

(B): histogram shows YO-PRO dye gradient uptake (\pm SEM). HEK: HEK-293 cells (untransfected), P2X7-GFP: rP2X7-GFP-(His)₈, P2X7-WT: rP2X7 wild-type (untagged); no significant difference between rP2X7-GFP-(His)₈ and WT detected, representative mean \pm SEM from 3 independent experiments.

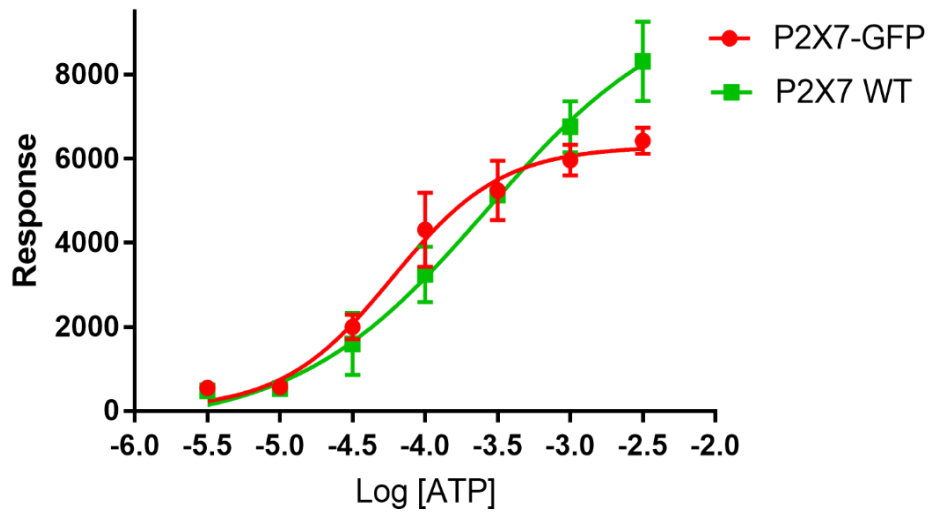


Figure 11: ATP concentration-response curves for rP2X7-GFP-(His)8 and rP2X7 WT YO-PRO uptake

P2X7-GFP: rP2X7-GFP-(His)₈; ATP EC₅₀ is 100 μ M. P2X7 WT: rP2X7 wild-type (untagged); ATP EC₅₀ is 300 μ M. Data analyzed using nonlinear regression (curve fit), agonist with four parameters.

3.3.1.3. ERK1/2 phosphorylation

As we described in **section 1.3.4.3**, stimulation of P2X7 mediates the activation of ERK1/2. We compared ERK1/2 phosphorylation in both rP2X7 wild-type (untagged) and our construct rP2X7-GFP-(His)₈ to test whether our tag compromised rP2X7-mediated ERK1/2 phosphorylation.

In all samples we observed bands for ERK1 and ERK2 (Figure 12; top panel); in non-transfected cells (HEK Figure 12; bottom panel) we did not observe bands for P-ERK1/2, and this did not change upon ATP-stimulation. For both full-length rP2X7-GFP-(His)₈ and rP2X7 WT (untagged), we did not observe bands for P-ERK1/2 (Figure 12; bottom panel) before stimulation but we did observe bands for P-ERK1/2 after ATP treatment, suggesting that our GFP-(His)₈ tag does not affect P2X7-mediate P-ERK1/2 phosphorylation.

We quantified the band intensities and measured the P-ERK(1+2) induction (P-ERK(1+2)/ERK(1+2)) (Figure 13), there is no significant difference between full-length rP2X7-GFP-(His)₈ and rP2X7 WT (untagged).

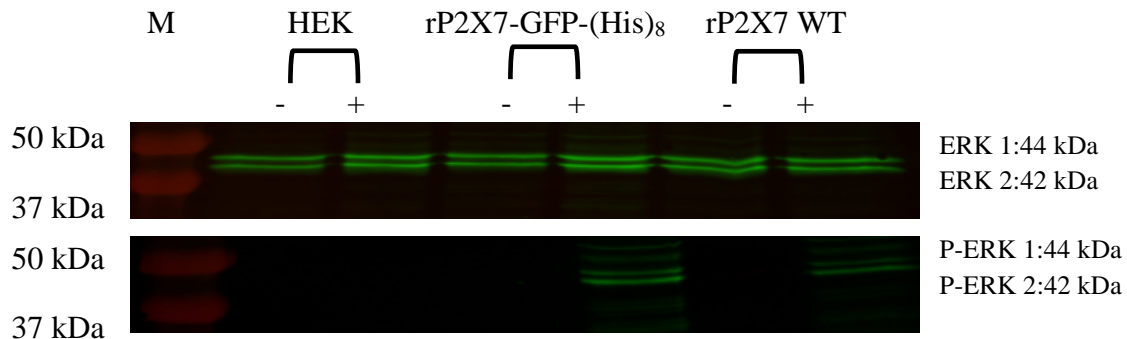


Figure 12: rP2X7-GFP-(His)₈ and rP2X7 WT ERK (1/2) phosphorylation

HEK: HEK-293 cells, rP2X7-GFP-(His)₈: rP2X7-GFP-(His)₈ full-length receptor transiently transfected, rP2X7 WT: rP2X7 wild-type (untagged) transiently transfected. Each sample has two groups, (+) cells were stimulated with 1 mM ATP for 2 minutes before cell lysis and (-) cells were not stimulated. ERK 1 is 44 kDa, and ERK 2 is 42 kDa.

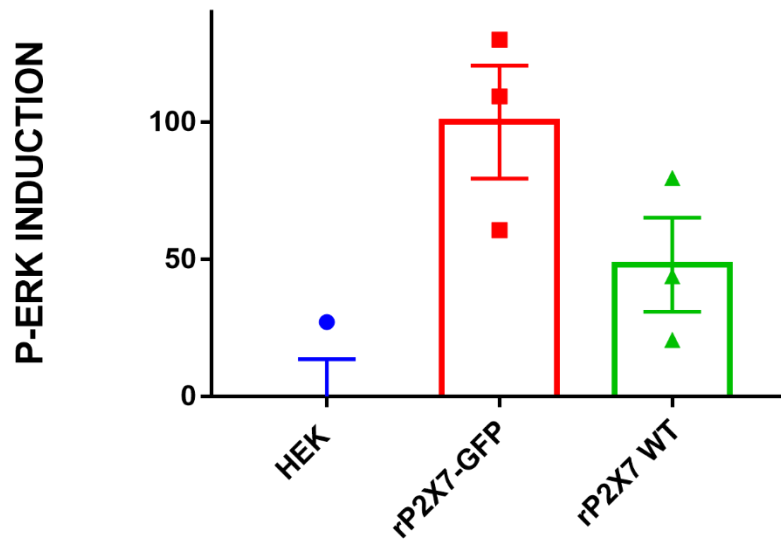


Figure 13: Comparison of ATP induced P-ERK1/2 between rP2X7-GFP-(His)₈ and rP2X7 WT

HEK: HEK-293 cells (un-transfected), rP2X7-GFP: rP2X7-GFP-(His)₈, rP2X7-WT: rP2X7 wild-type; no significant difference between rP2X7-GFP-(His)₈ and WT detected, representative mean \pm SEM from 3 independent experiments.

3.3.2. rP2X7-mediated cell blebbing in HEK-293 and Hela cells

We first decided to test the effect of mutations within the P2X7 intracellular domains on ATP-induced cell blebbing. Full-length rP2X7-GFP-(His)₈ receptors (termed wild-type) and mutant constructs were transiently transfected in HEK-293, and negative-control cells were transfected with eGFP alone. Samples were imaged using spinning-disk confocal microscopy, and movies were recorded (one frame taken every 2 seconds). After two minutes, ATP was applied to a final concentration of 1 mM, and imaging continued for a further five minutes. The number of cells analysed per experiment varied between (2-8) from 3 independent experiments.

We observed no cell blebbing in our negative-control cells (eGFP alone) either in the absence or presence of ATP (Figure 14), and no blebbing for any of our constructs in the absence of ATP (Figures 14, 15 and 16). As expected, ATP treatment of cells transfected with full-length rP2X7-GFP-(His)₈ induced robust and reproducible blebbing (Figure 14), with the fluorescent signal clearly present at the outside of the blebs, implying that P2X7 receptors are also present in the membranes of the blebs. For our truncation mutants, we observed ATP-stimulated blebbing in 380M and 582M, but not in 418M, 581M or Δ N (Figure 14).

For mutations within the C-Cys anchor domain, we observed cell blebbing CRR, CRRa, and C(X)A but not in CRRb (Figure 15). For the internal deletions, we only observed ATP-stimulated blebbing in D2: Δ (441-460), but not in D1, D3, D4, D5, D6, D7, and unexpectedly the combination construct D8: Δ (D2 & 582M) (Figure 16). The same results were obtained in Hela cells, demonstrating that rP2X7-GFP-(His)₈ mediates cell blebbing independently of cell type (appendix 3, 4, and 5).

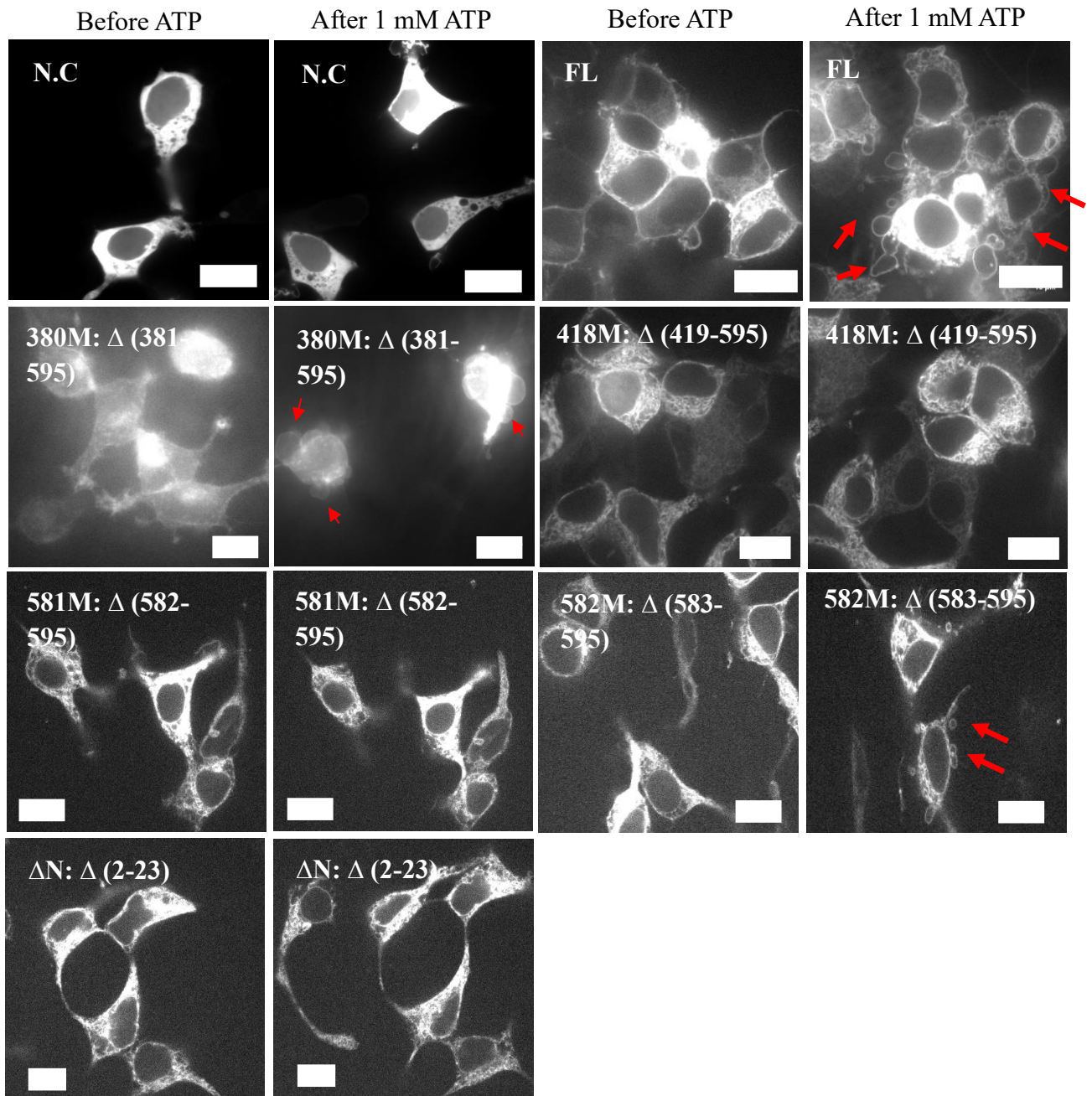


Figure 14: Cell blebbing of truncation mutants in HEK-293 cells

N.C: HEK-293 transfected with GFP, FL: rP2X7-GFP-(His)₈ full length. Red arrows show cell blebbing, scale bar represents 10 μm. The figure shows representative images, the number of cells analysed per experiment varied between (2-8) from 3 independent experiments.

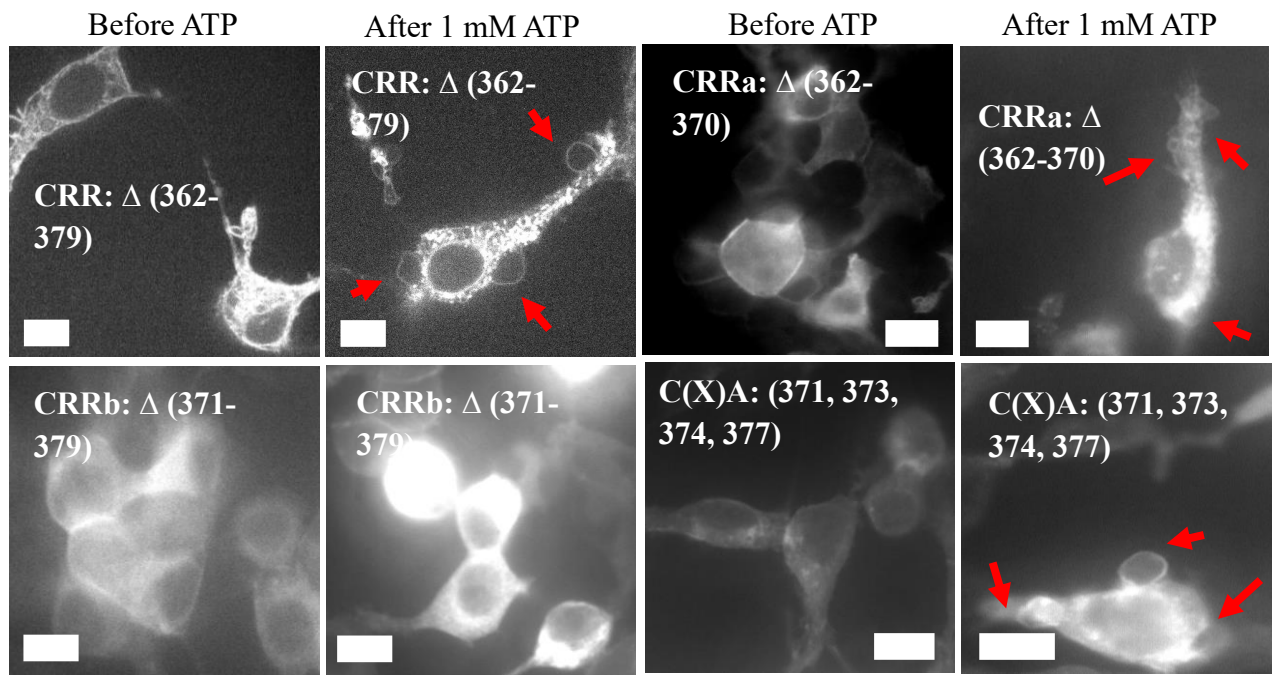


Figure 15: Cell blebbing of C-Cys anchor mutants in HEK-293 cells

Red arrows show cell blebbing; scale bar represents 10 μ m. The figure shows representative images, the number of cells analysed per experiment varied between (2-8) from 3 independent experiments.

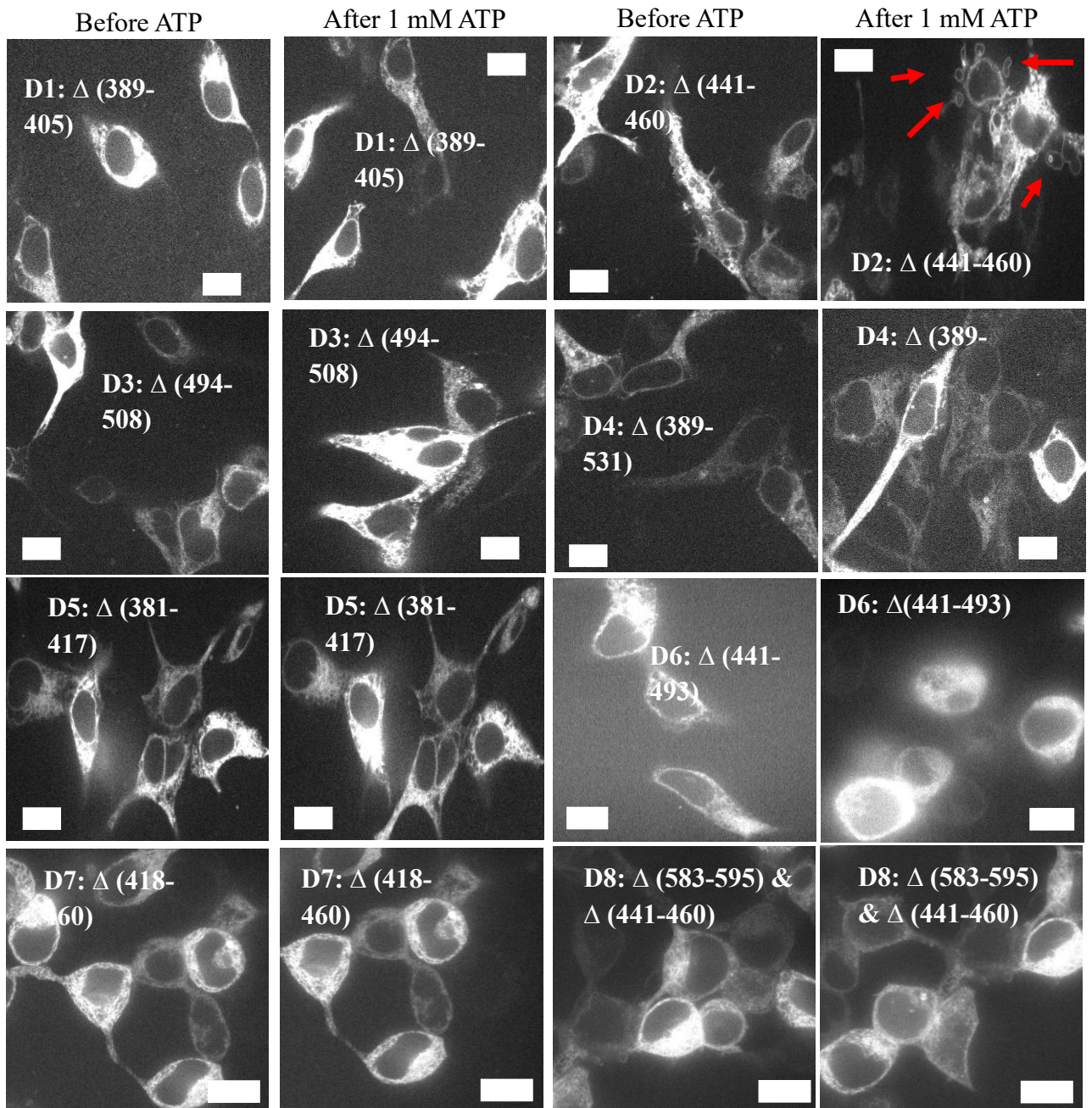


Figure 16: Cell blebbing of the internal deletions in HEK-293 cells

Red arrows show cell blebbing; scale bar represents 10 μm . The figure shows representative images, the number of cells analysed per experiment varied between (2-8) from 3 independent experiments.

3.3.3. Blebbing in the absence of the extracellular calcium

To determine the effect of extracellular calcium on blebbing, rP2X7-GFP-(His)₈ and mutant constructs were transfected in HEK-293 cells and imaged in calcium-free ECS-LD. We observed the same results as in ECS-LD, implying that extracellular calcium may not be required for cell blebbing (Figures 17, 18, and 19). However, it is important to note that residual calcium would still be present in this experiment, as we did not also use calcium chelators in our extracellular solution.

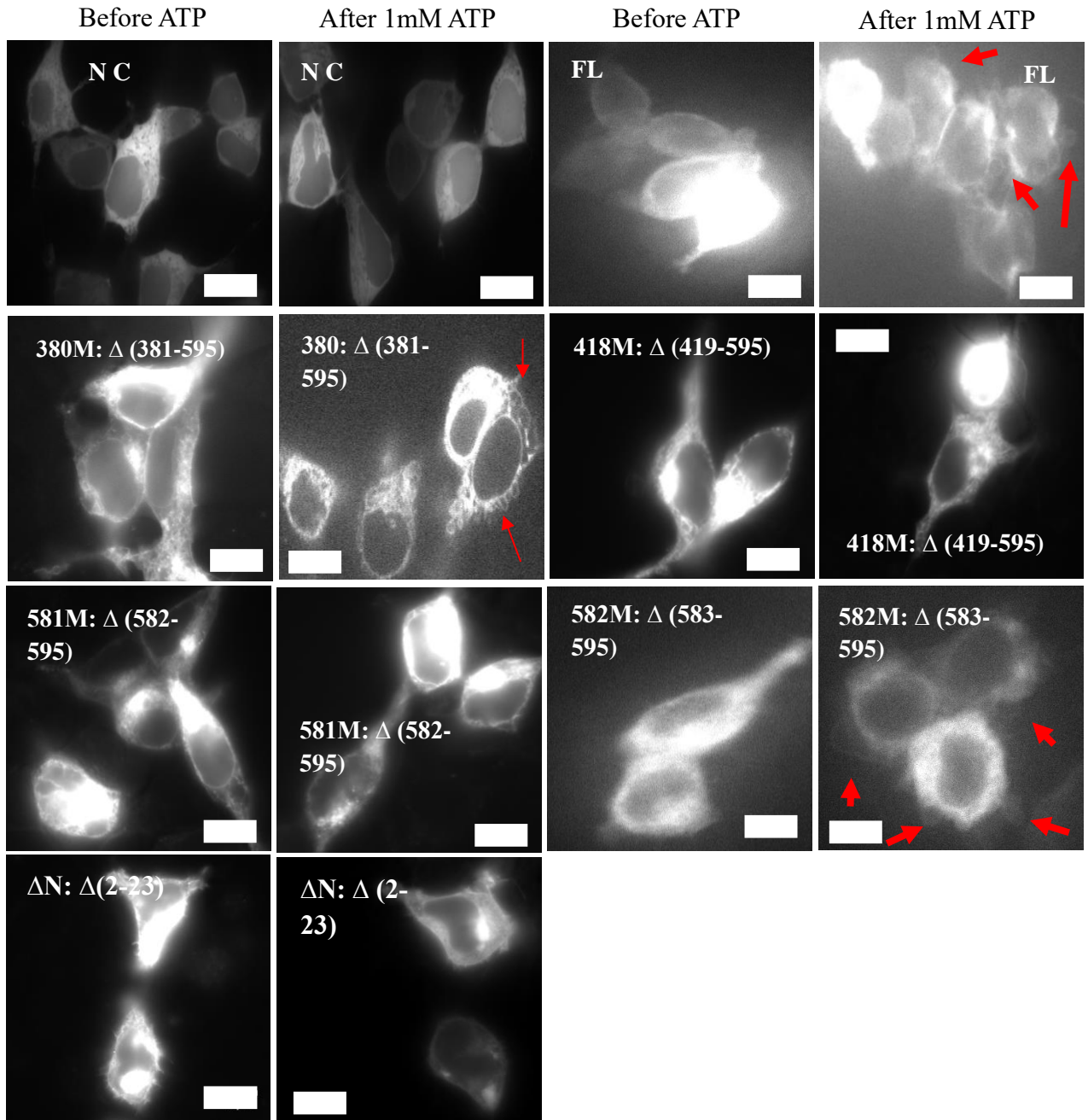


Figure 17: Cell blebbing of truncation mutants in the absence of extracellular calcium

N.C: HEK-293 cells transfected with GFP, FL: rP2X7-GFP-(His)₈ full-length. Red arrows show cell blebbing, scale bar represents 10 μm. The figure shows representative images, the number of cells analysed per experiment varied between (2-8) from 3 independent experiments.

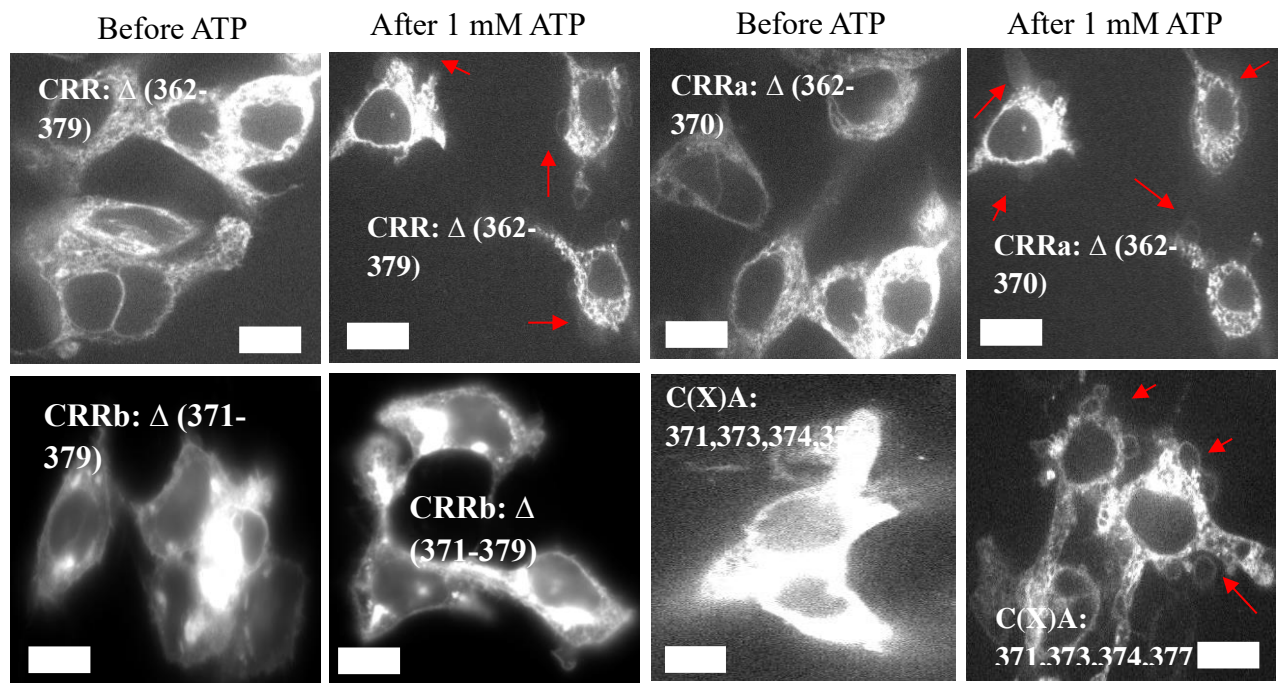


Figure 18: Cell blebbing of the C-Cys anchor mutants in the absence of extracellular calcium

Red arrows show cell blebbing; scale bar represents 10 μm . The figure shows representative images, the number of cells analysed per experiment varied between (2-8) from 3 independent experiments.

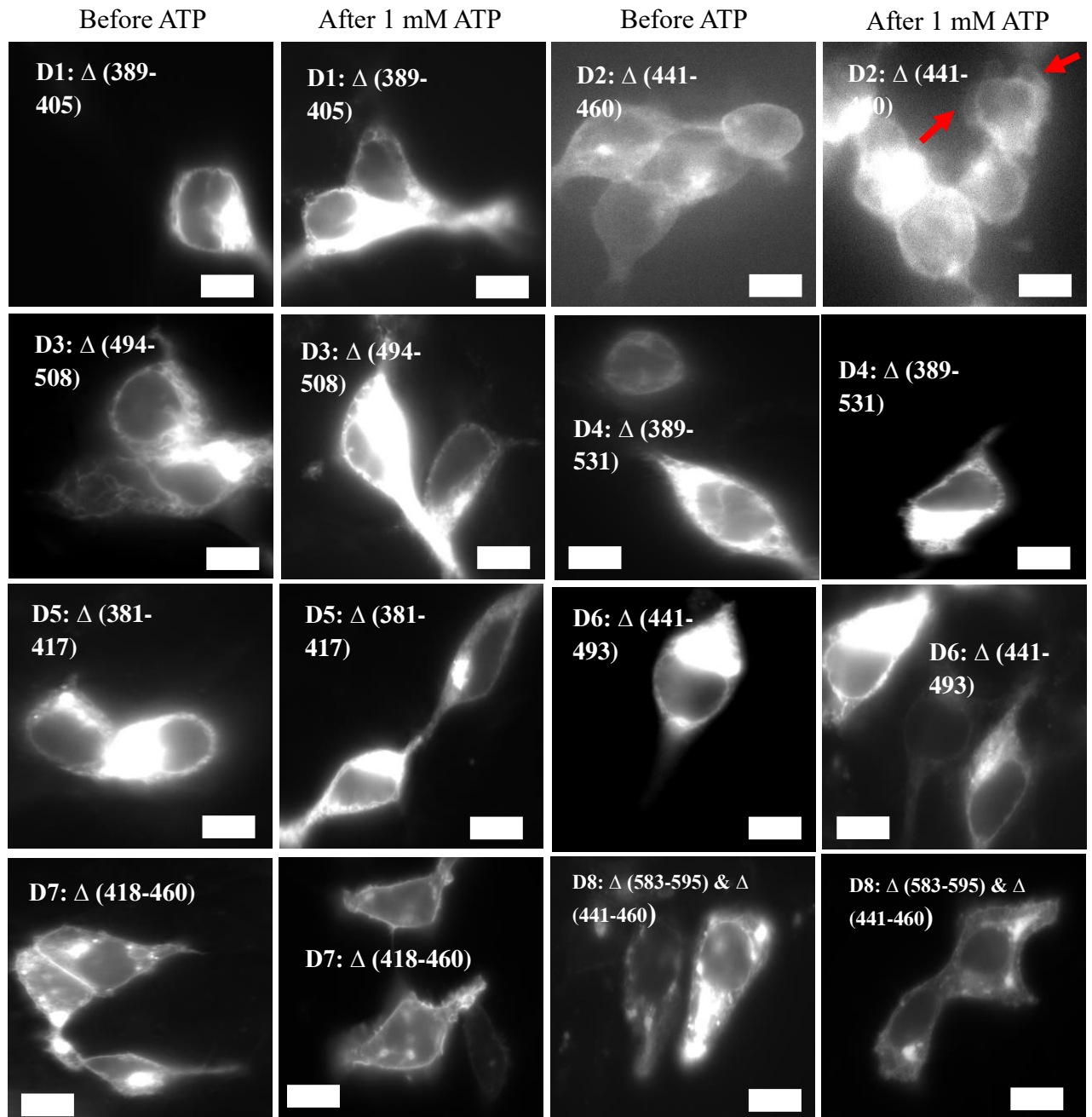


Figure 19: Cell blebbing of the internal deletions in the absence of extracellular calcium

Red arrows show cell blebbing; scale bar represents 10 μm . The figure shows representative images, the number of cells analysed per experiment varied between (2-8) from 3 independent experiments.

3.3.4. P2X7-dependent cell blebbing is reversible

HEK-293 stably expressed rP2X7-GFP-(His)₈ were tested for reversible cell blebbing. These cells were imaged for two minutes before ATP addition and five minutes after. Then cells were washed once with 1 mL pre-warmed ECS-LD and imaged for further five minutes. Upon removing ATP by washout with pre-warmed ECS-LD, blebbing stopped, and cell protrusions were seen to disappear (Figure 20).

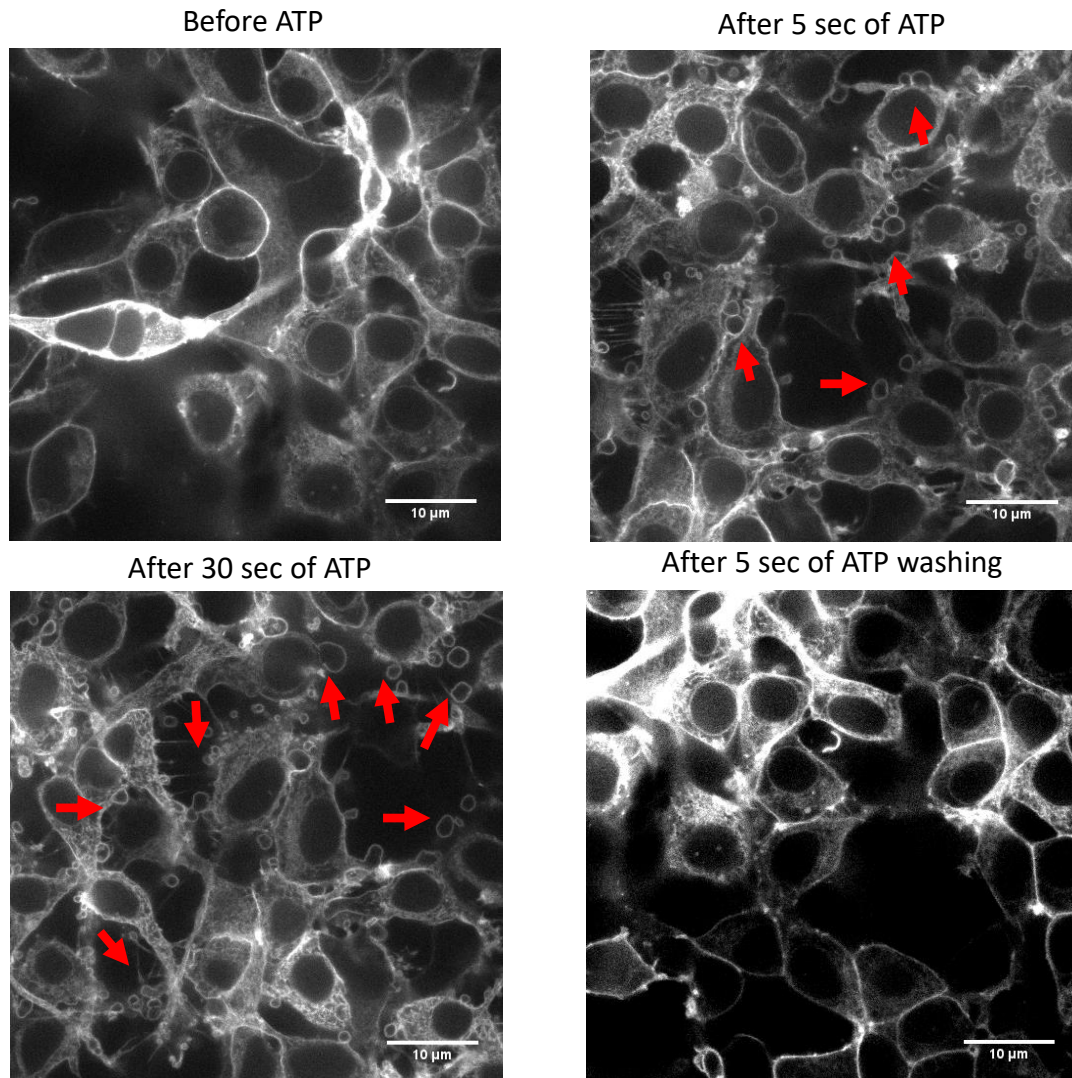


Figure 20: Reversible cell blebbing

ATP-induced cell blebbing is reversible. rP2X7-GFP-(His)₈-HEK-293 stably transfected cells were incubated in ECS-LD and treated with 1 mM ATP (blebbing after 5 and 30 seconds of ATP addition). After 5 minutes, the ATP- containing ECS-LD was replaced with fresh ECS-LD (after 5 seconds of ATP washing). Red arrows show cell blebbing.

3.3.5. Quantification of wild-type and mutant cell-surface expression using biotinylation

Our observations that constructs lacking either the C-Cys anchor domain (CRR) or ballast domain (380M) were still capable of cell blebbing, whereas the ΔN mutation was not, initially appear to suggest that it is the N-terminal domain that is important for cell blebbing. However, it is possible that a mutation simply prevents expression of the receptor at the cell-surface, rather than plays a direct role in regulating blebbing. To assess the impact of our mutant constructs on both total and cell-surface protein expression, we used the water-soluble and cell-impermeant crosslinker EZ-Link Sulfo-NHS-LC-Biotin to label cell surface protein *via* biotinylation of exposed amine groups, followed by capture using streptavidin resins and Western blotting. First, we showed that our rP2X7-GFP-(His)₈ construct gives a single band at slightly greater than 100 kDa, and that no signal is observed in non-transfected cells (Figure 21). Next, we measured both the total (top blot in each panel) and cell-surface (beads; bottom blot) expression in HEK-293 cells 48h following transient transfection (Figure 22; Appendix 6 (full blots)).

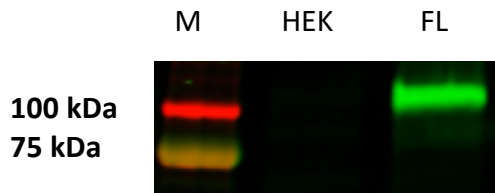


Figure 21: rP2X7-GFP-(His)₈ expression

HEK: HEK-293 wild type cells, FL: rP2X7-GFP-(His)₈ full-length transient transfection. rP2X7-GFP-(His)₈ is 102 kDa. Representative from 3 independent experiments.

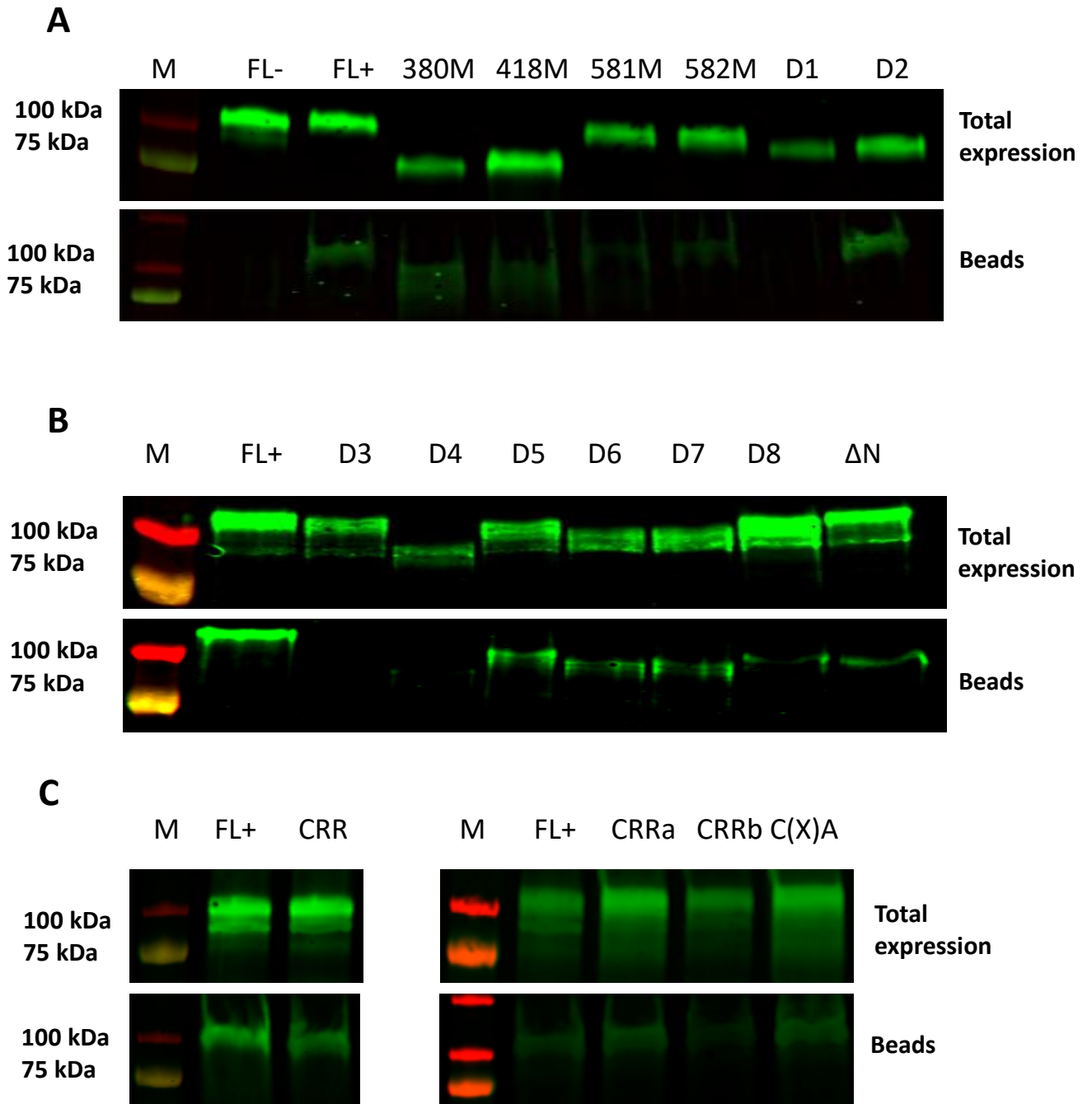


Figure 22: rP2X7-GFP-(His)₈ full-length and mutants total and cell-surface expression

FL-: rP2X7-GFP-(His)₈ transient transfected full-length (negative control, cells were not incubated with biotin, FL+: rP2X7-GFP-(His)₈ transient transfected full-length (positive control, cells were incubated with biotin. Representative from 3 independent experiments.

Data for total protein expression was quantified by measuring band density of mutants and normalizing to the full-length receptor rP2X7-GFP-(His)₈ total band density (Figure 23; n=3). Construct's cell-surface (beads) density was also quantified and normalized to the full-length rP2X7-GFP-(His)₈ cell-surface band density and the cell surface expression was calculated (Figure 24; n =3) according to the formula below:

$$\frac{\text{Mean normalized beads density}}{\text{Mean normalized total density}}$$

A one-way ANOVA test was performed to analyze the effect of our constructs on rP2X7-GFP-(His)₈ total expression and trafficking; only the mutants D3: Δ (494-508), D4: Δ (389-531), D5: Δ (381-417), and D7: Δ (418-460) led to a significant reduction in total protein expression. However, compared to the full-length receptor, all constructs exhibited a significant decrease cell-surface expression levels, perhaps underlining the importance of the intracellular domains for correct receptor trafficking to the cell surface. In particular, levels of cell-surface expression were virtually undetectable for 418M, D5, and ΔN and very low for 581M, D3, D4, D6, D7, and D8. This data suggests that the inability of these constructs to mediate ATP-induced cell blebbing likely to be due to lack of or low cell-surface protein expression rather than any direct effect on coupling to the signalling pathway.

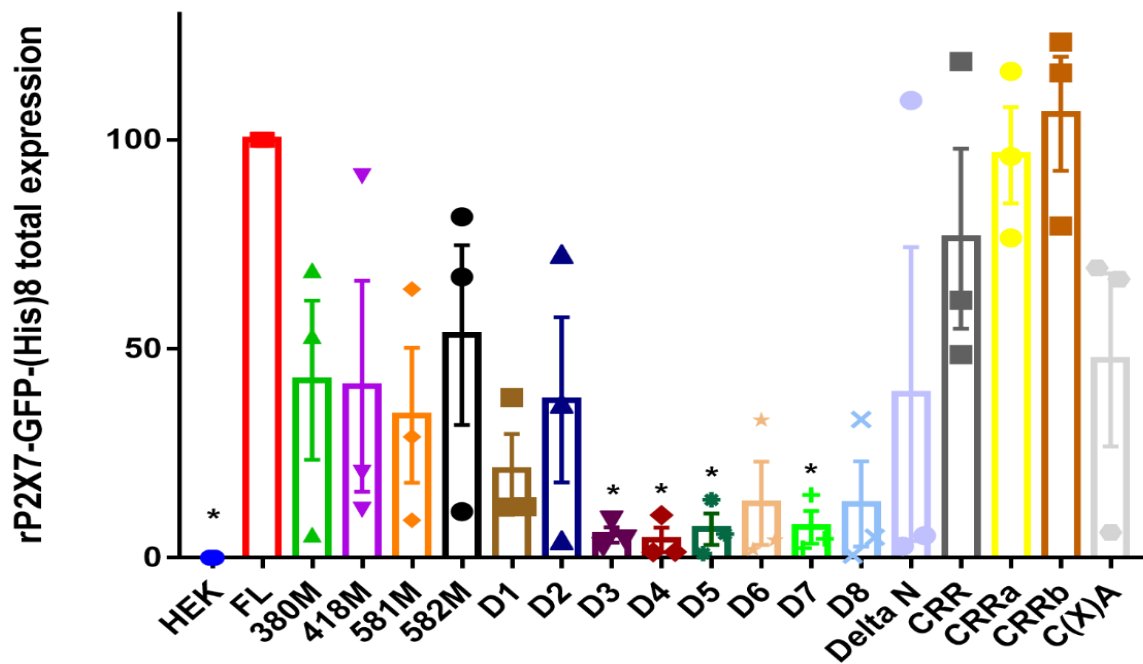


Figure 23: Total band intensities of rP2X7-GFP-(His)8 full-length and mutants

HEK: HEK-293 cells, FL: rP2X7-GFP-(His)₈ full-length transient transfected. *P-value ≤ 0.05. Representative mean ±SEM from 3 independent experiments.

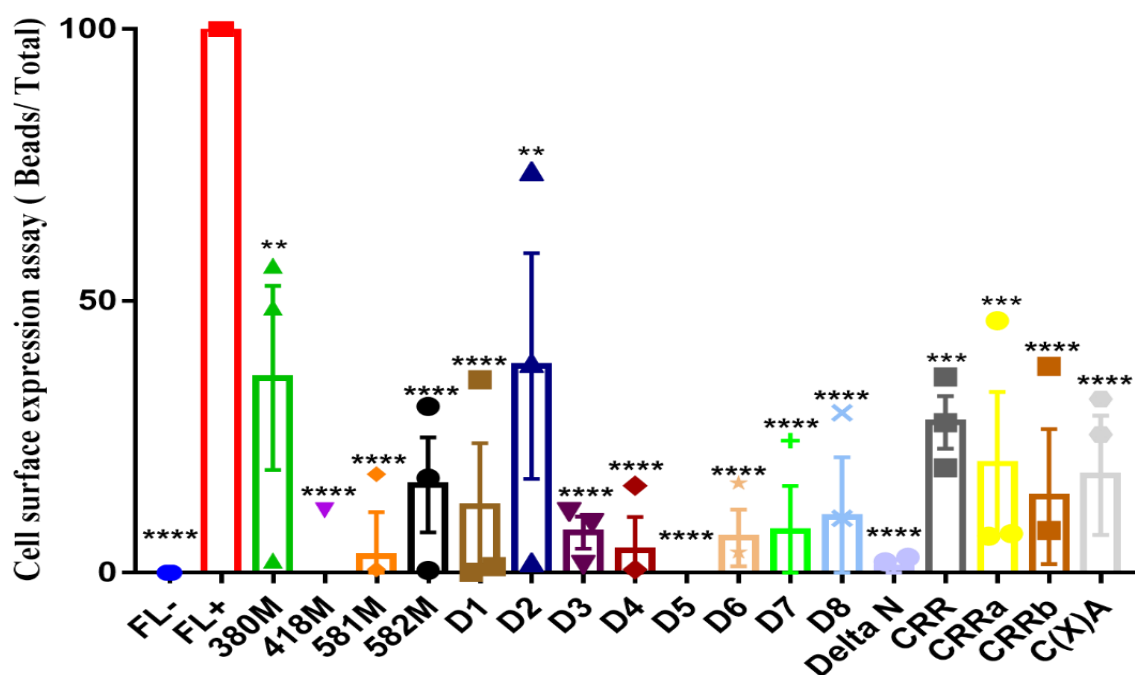


Figure 24: Cell-surface band intensities of rP2X7-GFP-(His)8 full-length and mutants

FL-: rP2X7-GFP-(His)₈ full-length transient transfected (cells were not incubated with biotin), FL+: rP2X7-GFP-(His)₈ full-length transient transfected (cells were incubated with biotin). **P-value ≤ 0.0021 , ***P value ≤ 0.0002 , ****P value ≤ 0.0001 . Representative mean \pm SEM from 3 independent experiments.

3.4. Discussion

3.4.1. rP2X7 fusion with GFP-(His)₈ does not affect receptor activity

To assess the GFP-(His)₈ tags effects on the rP2X7 plasmid used in this study, comparisons were performed between rP2X7-GFP-(His)₈ and rP2X7 WT in terms of pore formation and its ATP EC₅₀, calcium influx, and ERK phosphorylation. Similarly to the previous studies (Smart et al. 2002; Young et al. 2008; Dreisig et al. 2018), our observations demonstrated that GFP-(His)₈ tag on the C-terminal does not modulate the receptor activity.

3.4.2. The N-terminal domain of rP2X7-GFP-(His)₈ receptor is required for cell-surface protein expression

Our initial observations that deletion of the N-terminal domain abolished ATP-induced cell blebbing suggested a potential role for this domain (similar to what has previously been proposed for ERK (1/2) phosphorylation (Amstrup and Novak 2003). However, our finding that N-terminal deletion led to undetectable levels of cell-surface expression mean that we can only conclude that this domain is required for the receptor cell-surface expression. The N-terminal domain of P2X receptors contains a conserved protein kinase C site (TX(K/R)) (North 2002); several mutagenesis studies have demonstrated that phosphorylation of the conserved threonine residue in this region is necessary for the expression of functional channels (Boué-Grabot et al. 2000; North 2002).

3.4.3. rP2X7-GFP-(His)₈ induces a reversible cell blebbing independently of cell type and extracellular calcium

ATP-induced cell blebbing was rapid in its onset (several seconds) and fully reversible after washing the ATP out with ECS-LD (note that blebs persist if ATP is not removed), similar to what was previously observed for ‘zeiotic’ blebbing in the early phases P2X7 activation (Mackenzie et al. 2005). However, there was no similar delaying effect of extracellular calcium removal. This may be because residual calcium was still present in our solutions, as we did not control extracellular calcium levels tightly with EGTA. rP2X7-GFP-(His)₈ mediates cell blebbing independently of cell type because the same constructs capable of cell blebbing in HEK-293 cells were also capable of blebbing in Hela cells.

3.4.4. Disruption of rP2X7 intracellular domains impair cell-surface expression

Several mutagenesis studies demonstrate that mutations within the C-terminal domain of P2X7 receptor disrupts its trafficking to the plasma membrane, such as truncations within a region overlapping (551-581) (Smart et al. 2003), and single point mutations like C572G, R574G, or F581G (Kopp et al. 2019b). Indeed all P2X receptors share a YXXXXK motif in their C-termini (situated downstream of the C-Cys anchor domain in P2X7 receptor) which regulates their cell surface expression (Chaumont et al. 2004; Robinson and Murrell-Lagnado 2013).

Our truncation mutants in the C-terminal domain (380M, 418M, 581M, and 582M) were all impaired in terms of their cell-surface expression, confirming the importance of the C-terminal domain for correct cell-surface expression.

3.4.5. The C-Cys anchor and ballast domains may not be required for cell blebbing

rP2X7-GFP-(His)₈ constructs lacking either the C-Cys anchor domain (including CRR, CRRa, and C(X)A constructs) or the ballast domain (1-380) were capable of ATP-induced cell blebbing; which potentially suggests that these domains are not required. This somewhat surprising finding mirrors that observed for pore formation in truncated panda P2X7 receptors (Karasawa et al. 2017) and may imply that blebbing is an intrinsic property of channel activation, rather than relying on protein-protein interactions mediated by the intracellular domains. Analysis of the effects of our mutations on calcium influx, pore formation and ERK1/2 phosphorylation was the next focus of our work, presented in Chapter 4.

Chapter 4: The effect of deletion of P2X7
intracellular domains on ATP-stimulated
calcium influx, pore formation and ERK1/2
phosphorylation

4.1. Introduction

As described in section 1.3.4, activation of P2X7 receptors by extracellular ATP leads to not only the opening of a cation channel but also the initiation of several cell-specific downstream signalling pathways including pore formation and ERK1/2 phosphorylation (Wilson et al. 2002; Becker et al. 2008; Bartlett et al. 2014).

In Chapter 3, we demonstrated that rP2X7-dependent cell blebbing did not appear to require either the C-Cys anchor region or ballast domain. We could not ascertain the role of the N-terminal domain because our ΔN mutant did not appear to be expressed at the cell-surface. Recent work from Kawate group, showing that a truncated panda P2X7 construct lacking the intracellular domains was capable of ATP-induced pore formation (Karasawa et al. 2017), suggests that pore formation is an intrinsic property of the ion channel, but that it is regulated by the C-terminal domain, which sequesters cholesterol and prevents it from inhibiting the pore. We also observed receptors truncated at residue 581 were unable to mediate cell blebbing but that receptors truncated at residue 582 were, which is similar to the pore formation data obtained by Smart *et al* (Smart et al. 2003). However, our 581M construct displayed very low levels of cell-surface expression, and we cannot conclude that there were any functional channels expressed at the cell surface. In order to be able to interpret our blebbing and cell-surface expression data, and determine whether or not blebbing and pore formation only require a functional ion channel (i.e. not the intracellular domains), or if, for some mutants that display very low cell-surface protein expression, there are some functional channels present, we decided to assay channel activity and pore formation. Furthermore, we decided to analyse ATP-stimulated ERK1/2 phosphorylation, a process that has been previously shown to require the N-terminal domain of the receptor (Amstrup and Novak 2003), in an attempt to expand our studies of downstream signalling effects and try to ascertain if this downstream signalling pathway has any requirement for the C-terminal domain.

4.2. Results

4.2.1. ATP-stimulated calcium influx of wild-type rP2X7-GFP-(His)₈ and mutant constructs

The labelled calcium indicator molecule (Fluo4-AM) was used to measure the channel activity of rP2X7-GFP-(His)₈ and mutant constructs in this study. Transfected cells in 96-well plates were loaded with Fluo4-AM and ATP-stimulated calcium influx was recorded by measuring an increase in fluorescent signal due to calcium getting inside cells and complexing with Fluo4 indicator molecule.

As expected, non-transfected cells gave no response, whereas cells transfected with full-length rP2X7-GFP-(His)₈ showed a robust ATP-stimulated calcium influx (HEK and FL respectively, Figure 25A). For our truncation mutants, only 418M was capable of ATP-induced calcium influx, 581M and Δ N were not capable of calcium influx following ATP application (Figure 25A). Unexpectedly, both 380M and 582M showed very low levels of calcium influx (not significantly different from our negative control; Figure 25A), contrary to previously published data (Smart et al. 2003) which demonstrated that both these truncations were capable of calcium influx.

For mutations within the C-Cys anchor domain, only CRRa showed ATP-stimulated calcium influx. CRR, CRRb, and C(X)A gave no response (Figure 25B). For the internal deletions, only the D2 was capable of ATP-induced calcium influx (it also induced cell blebbing), but that D1, D3, D4, D5, D6, D7 and D8 were not (Figure 26A).

For further investigation, we compared mutants together (not only with negative control); we observed that 418M significantly decreased calcium influx comparing with D2 and CRRa and was also observed for D2 when comparing with CRRa.

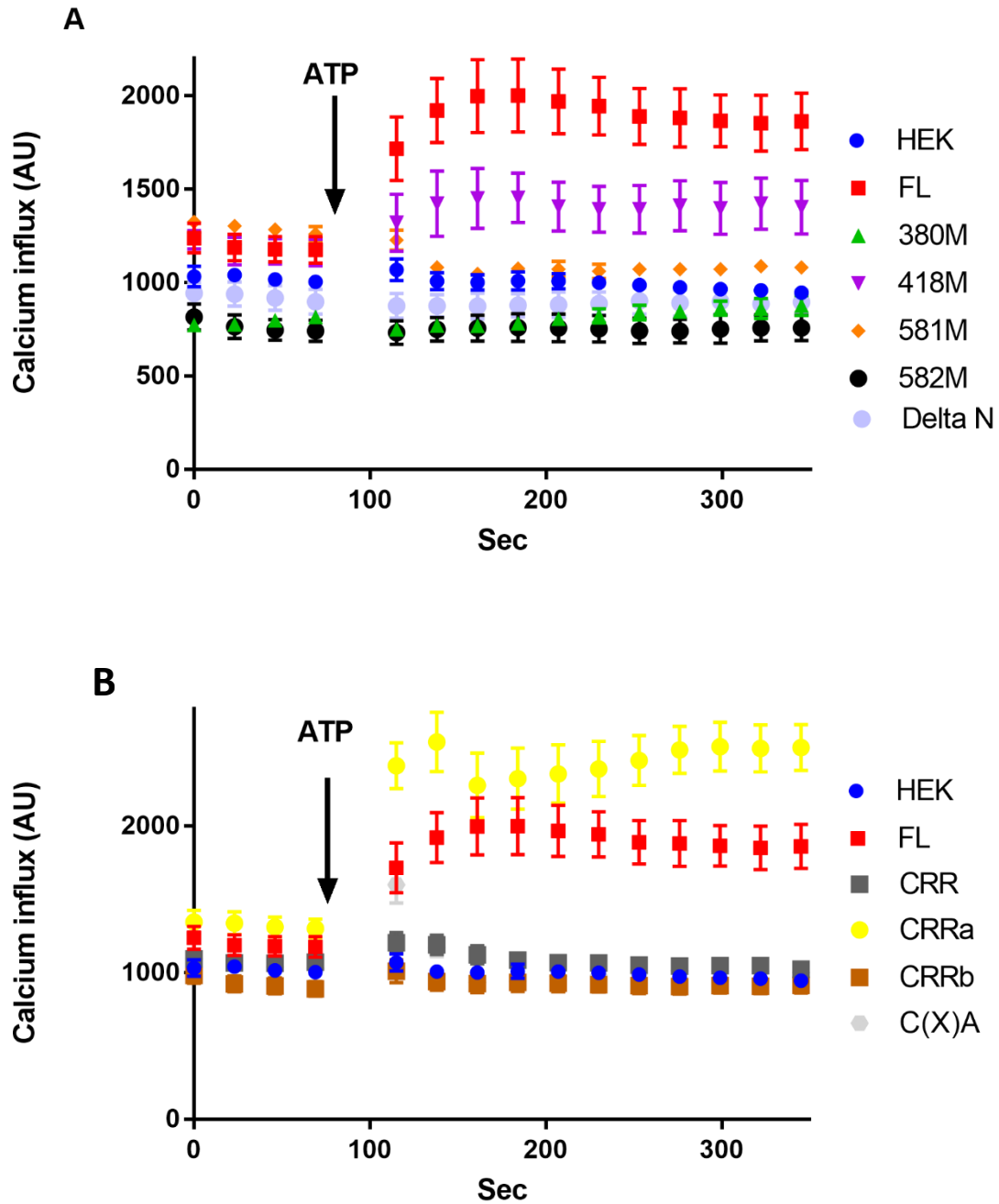


Figure 25: Effect of truncation and C-Cys anchor mutants on calcium influx

(A): A: Calcium influx measured in HEK-293 cells transfected with truncation mutants, B: Calcium influx measured in HEK-293 cells transfected with C-Cys anchor mutants; HEK: HEK-293 cells (un-transfected), FL: rP2X7-GFP-(His)₈ full-length. Representative mean \pm SEM from 1 experiment (technical number: 5 wells per plate).

Initial gradients of calcium influx were calculated for each construct and normalized to positive control (FL) values in each experiment (Figure 26B). Influx gradients for FL, 418M, D2, and CRRa were significantly different from the negative control, indicating that these constructs were capable of ATP-mediate calcium influx.

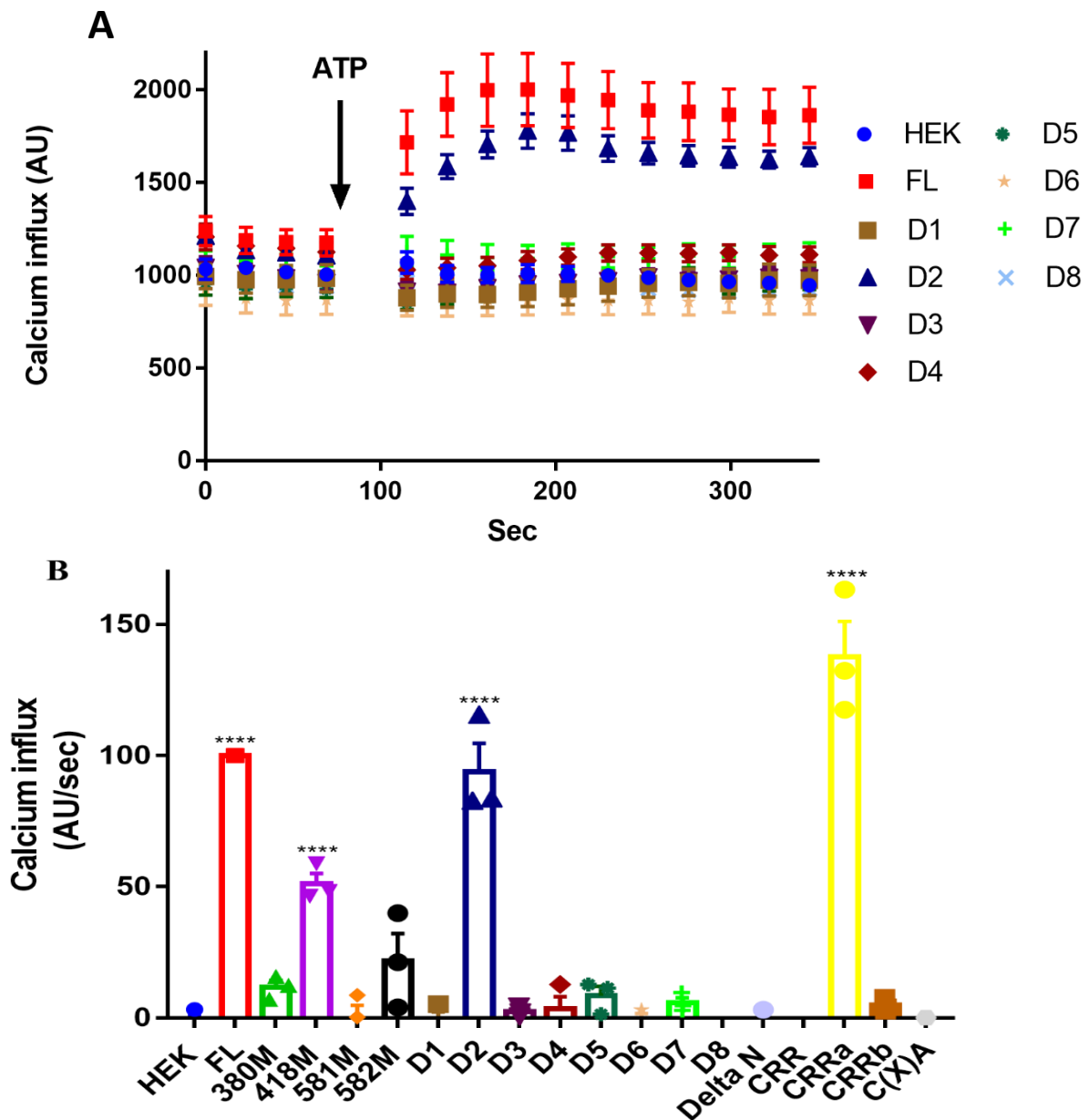


Figure 26: Effect of mutants with an internal deletions on calcium influx and calcium gradient uptake

A: Calcium influx measured in HEK-293 cells transfected with mutants with an internal deletions; representative mean \pm SEM from 1 experiment (technical number: 5 wells per plate) (B): calcium gradient uptake for rP2X7-GFP-(His)₈ full-length and mutants; ****P represent P-value ≤ 0.0001 . HEK: HEK-293 cells (un-transfected), FL: rP2X7-GFP-(His)₈ full-length. Representative mean \pm SEM from 3 independent experiments.

4.2.2. ATP-stimulated YO-PRO 1 dye uptake of wild-type rP2X7-GFP-(His)₈ and mutant constructs

YO-PRO-1 is a cell-impermeant dye normally used to identify apoptotic cells *via* staining of nucleic acid. YO-PRO-1 dye is used in this study to measure the ability of rP2X7-GFP-(His)₈ mutants to induce pore formation when expressed in HEK-293 cells. Transfected cells in 96-well plates were incubated with YO-PRO-1 dye and ATP-stimulated uptake was recorded by measuring an increase in fluorescent signal due to dye getting inside cells and complexing with nucleic acid.

As expected, non-transfected cells gave no response whereas cells transfected with full-length rP2X7-GFP-(His)₈ showed a robust ATP-stimulated dye uptake (HEK and FL respectively, Figure 27A). For our truncation mutants, both 380M (contrary to the previous study, (Smart et al. 2003)) and 582M showed YO-PRO-1 uptake following ATP whereas 418M, 581 and ΔN were not capable of pore formation (Figure 27A).

For mutations within the C-Cys anchor domain, CRRa showed a robust ATP-mediate YO-PRO-1 uptake, CRR, CRRb, and C(X)A showed a low level dye uptake but statistically significant when compared with the negative control (Figure 27B). For the internal deletions, only the D2 was capable of ATP-mediated YO-PRO-1 uptake (it also induced cell blebbing), but that D1, D3, D4, D5, D6, D7 and D8 were not (Figure 28A).

This data implies that the rP2X7 C terminus regulates the receptor pore formation. Also, both cell blebbing and pore formation signalling pathways are intrinsically linked; however, it is uncoupled by deletion of CRRb region. 380M construct represents the rP2X7 receptor lacking the ballast domain (ballast domain comprises the final 200 residues; (McCarthy et al. 2019b)). This construct is capable of cell blebbing and pore formation but not capable of calcium influx, suggesting that the rP2X7 ballast domain is not required for membrane blebbing and pore formation but is vital for receptor channel activity.

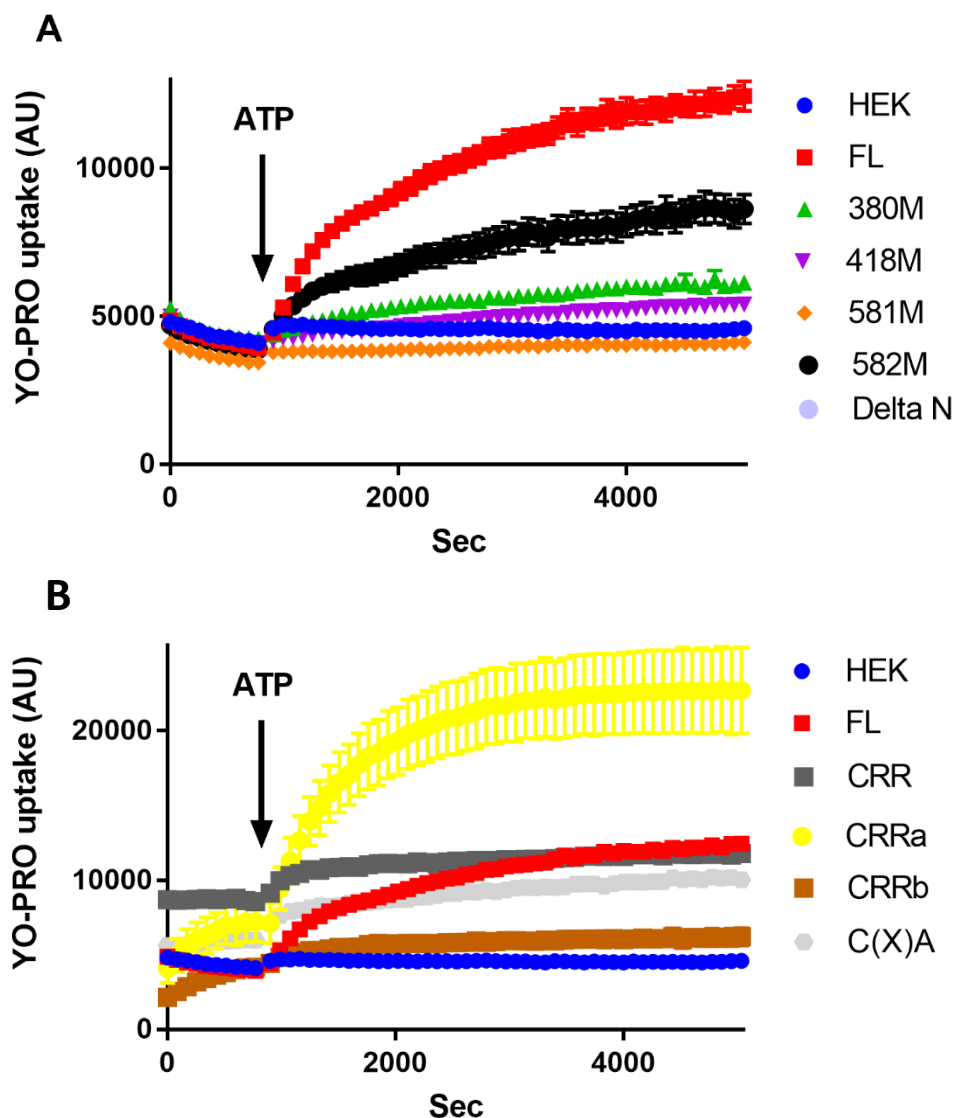


Figure 27: Effect of truncations and C-Cys anchor mutants on YO-PRO dye uptake

A: YO-PRO dye uptake measured in HEK-293 cells transfected with truncation mutants,
B: YO-PRO dye uptake measured in HEK-293 cells transfected with C-Cys anchor mutants; HEK: HEK-293 cells (un-transfected), FL: rP2X7-GFP-(His)₈ full-length. Representative mean \pm SEM from 1 experiment (technical number: 5 wells per plate).

Initial gradients of YO-PRO-1 uptake were calculated for each construct and normalized to positive control (FL) values in each experiment (Figure 28B). Uptake gradients for FL, 380M, 582M, D2, CRR, CRRa, CRRb, and C(X)A were significantly different from the negative control, indicating that these constructs were capable of ATP-induced pore formation.

We observed when compared mutants together that 380M, CRR, CRRb, and C(X)A significantly decreased dye uptake compare with D2 and CRRa but was still significant when compare with negative control.

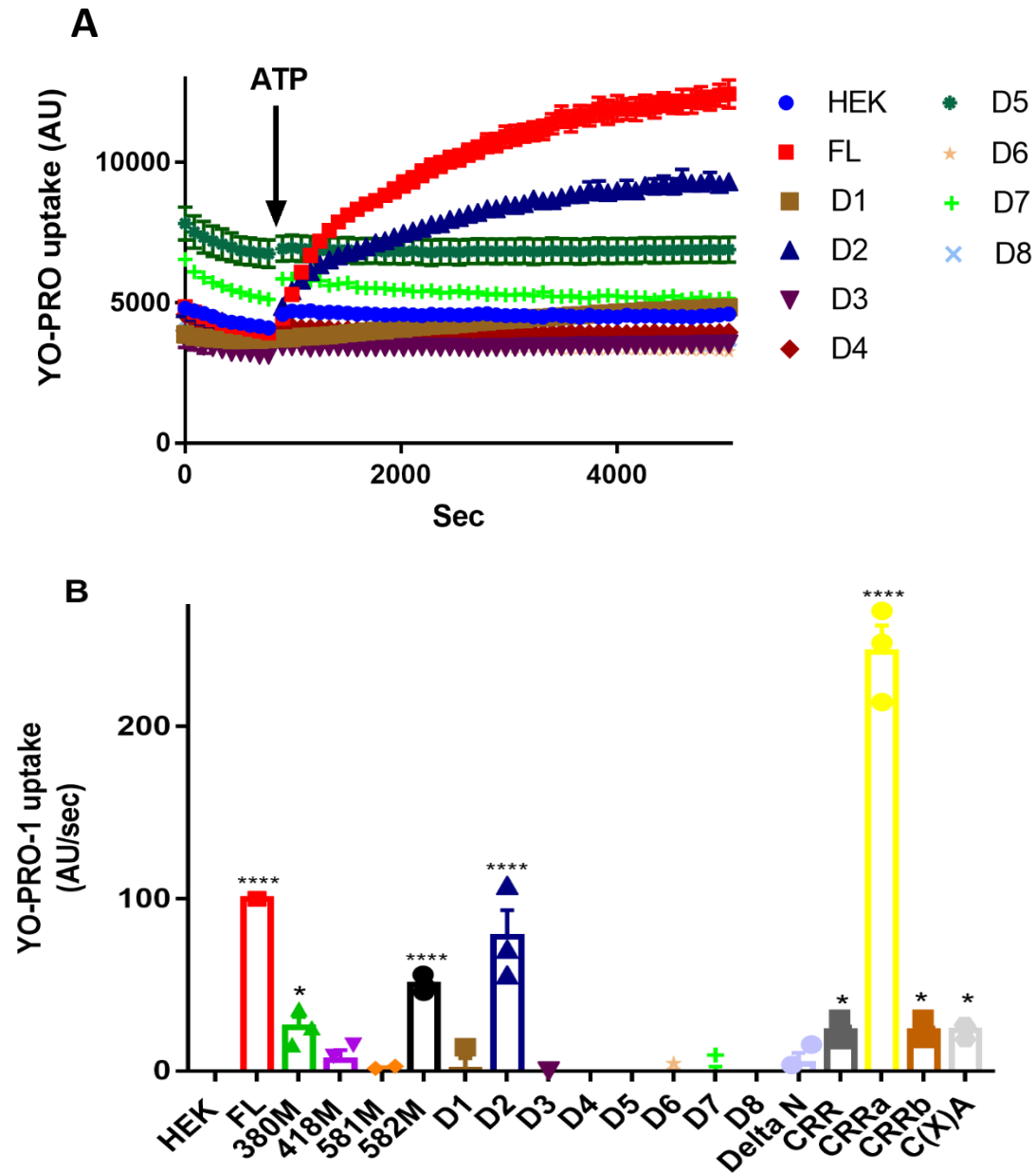


Figure 28: Effect of mutants with an internal deletions on YO-PRO dye uptake and gradient dye uptake

A: YO-PRO dye uptake measured in HEK-293 cells transfected with mutants with an internal deletions, representative mean \pm SEM from 1 experiment (technical number: 5 wells per plate). **B:** YO-PRO gradient uptake for rP2X7-GFP-(His)₈ full-length and mutants, *P, and ****P represent P-value ≤ 0.05 and ≤ 0.0001 respectively, HEK: HEK-293 cells (un-transfected), FL: rP2X7-GFP-(His)₈ full-length; representative mean \pm SEM from 3 independent experiments.

4.2.3. ATP-stimulated ERK1/2 phosphorylation of wild-type rP2X7-GFP-(His)₈ and mutant constructs

We wanted to expand our study to analyse other P2X7-dependent signalling pathways, and chose ERK1/2 phosphorylation, partly because it has previously been reported that the N-terminal domain of the P2X7 receptor is critical for this signalling phenomenon (Amstrup and Novak 2003). We measured ATP-induced ERK1/2 phosphorylation using quantitative Western blotting with infra-red labelled fluorescent secondary antibodies, using non-transfected HEK-293 cells as a negative control and rP2X7-GFP-(His)₈ full-length receptor stably transfected in HEK-293 cells as a positive control. All constructs (including a full-length control) were transiently transfected for quantitation.

Transfected cells, before and after 1 mM ATP stimulation, were compared side-by-side to facilitate the observation of ERK1/2 activation (representative Western blots shown in (Figures 29 and 30). In all samples we observed bands for ERK1 and ERK2; in non-transfected cells (HEK. Figure 29) we observed a very faint band for P-ERK2 that did not change upon ATP-stimulation. In our positive controls (both stably and transiently transfected cells with full-length rP2X7-GFP-(His)₈; FL-S and FL respectively, Figure 29) we observed faint bands for P-ERK2 before stimulation and strong bands for both P-ERK1 and P-ERK2 after ATP treatment, consistent with P2X7 receptor activation leading to P-ERK1/2 phosphorylation. Strikingly, in our Δ N mutant, strong bands for both P-ERK1 and P-ERK2 were observed before ATP stimulation, but these were not present in the stimulated sample (Figure 29). We obtained the same result in 3 biological replicates. Given that we previously showed that this mutant (i) cannot bleb, (ii) is not present at the cell surface, (iii) cannot mediate calcium influx and (iv) cannot mediate YO-PRO-1 uptake, this result is very surprising.

For the C-terminal truncation mutants (Figure 29 bottom blots), we observed that 380M and 418M were similar to our negative control (no change on ATP stimulation), that 581M appeared similar to full-length P2X7 (increase in P-ERK1 and P-ERK2 on ATP stimulation) and that 582M appeared similar to Δ N (decrease in P-ERK1 and P-ERK2 on ATP stimulation).

For the ballast domain internal deletions, D2 and D3 showed a small degree of ATP-stimulated P-ERK2 phosphorylation (Figure 30), but D4 appeared similar to ΔN . For our C-Cys anchor mutants we did not observe substantial changes in P-ERK1 levels on ATP stimulation.

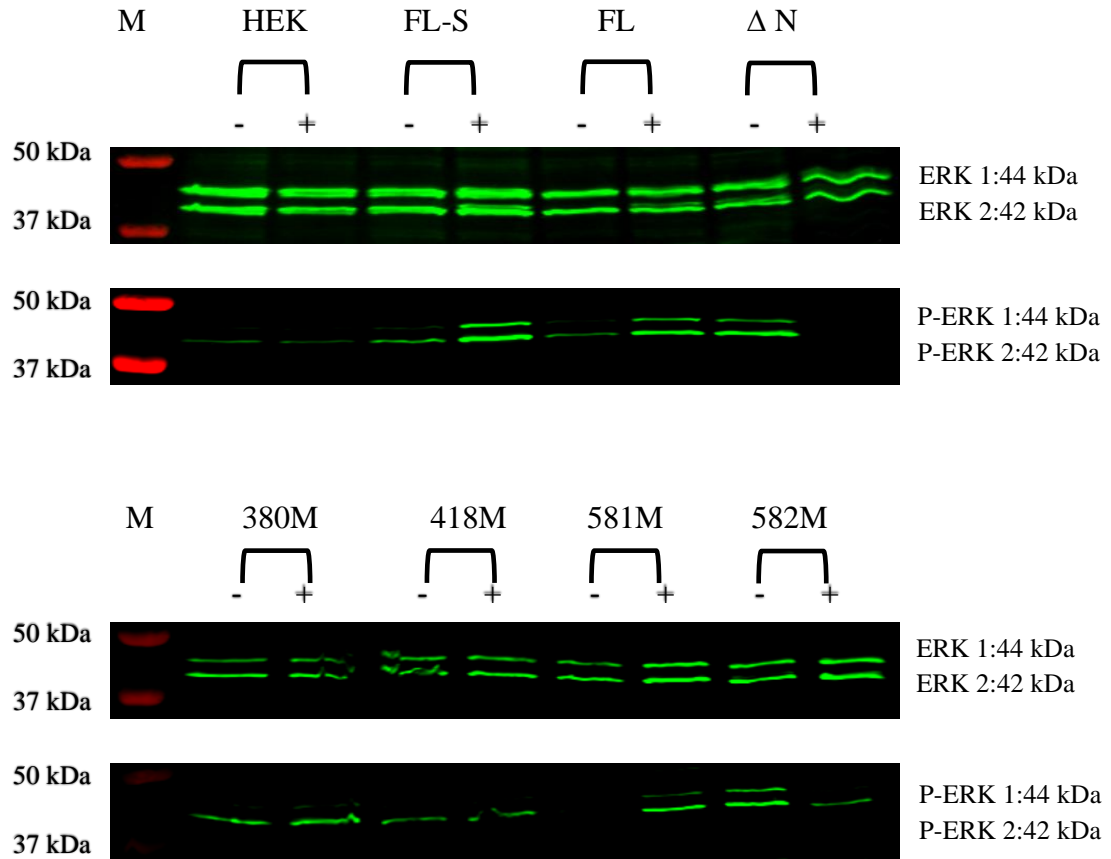


Figure 29: rP2X7-GFP-(His)₈ and truncation mutants ERK (1/2) phosphorylation

HEK: HEK-293 cells, FL-S: rP2X7-GFP-(His)₈ full-length stably transfected, FL: rP2X7-GFP-(His)₈ full-length transiently transfected. Each sample has two groups; (+) cells were stimulated with 1 mM of ATP for 2 minutes before lysis and (-) cells were not stimulated. ERK 1 is 44 kDa, and ERK 2 is 42 kDa. Representative blot from 3 independent experiments.

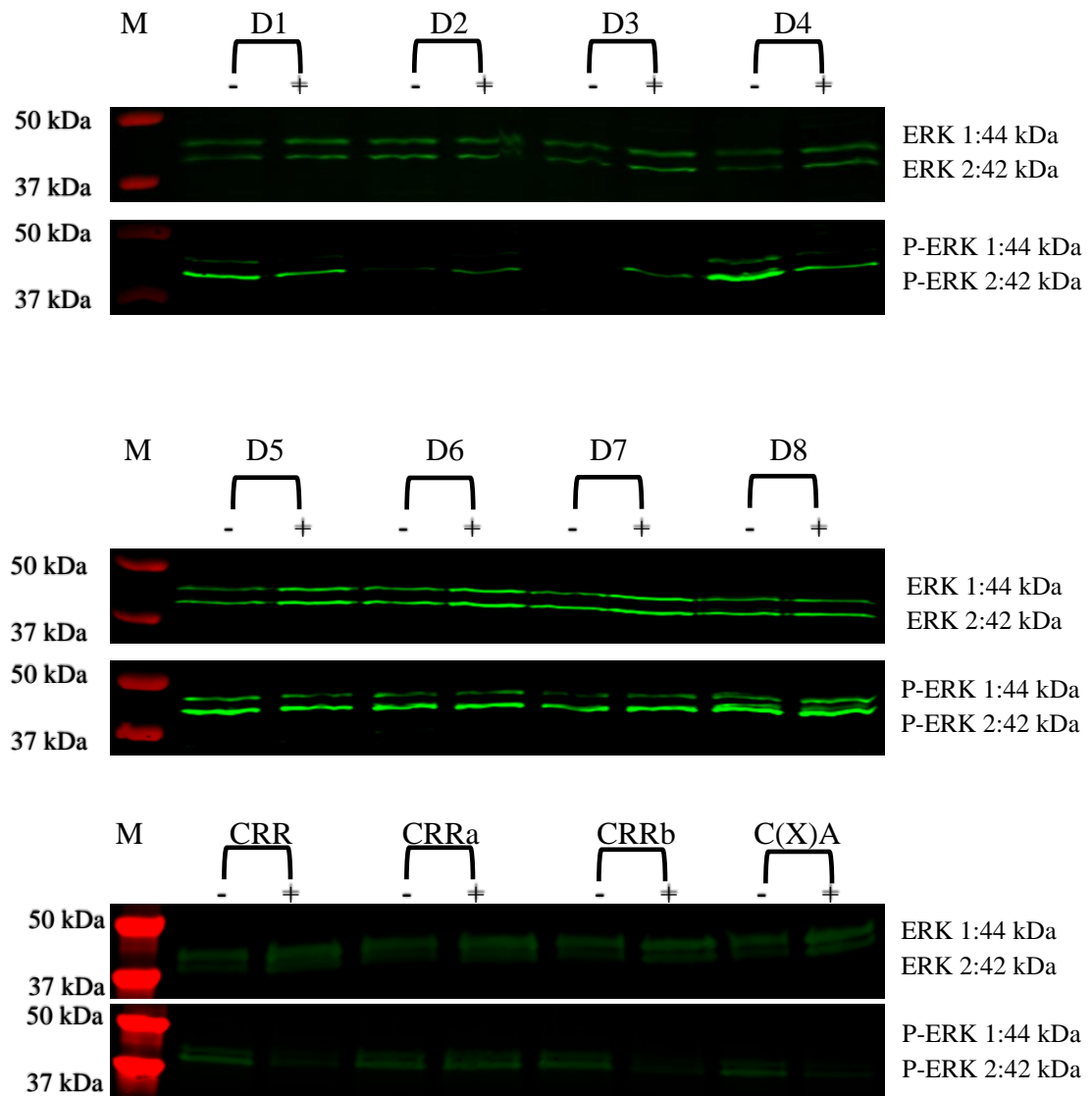
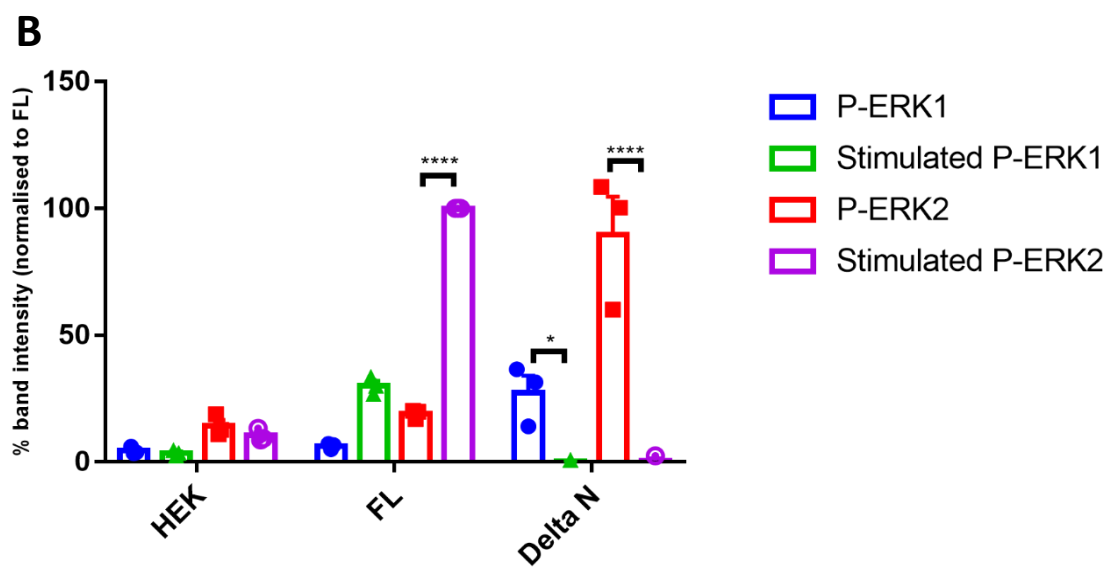
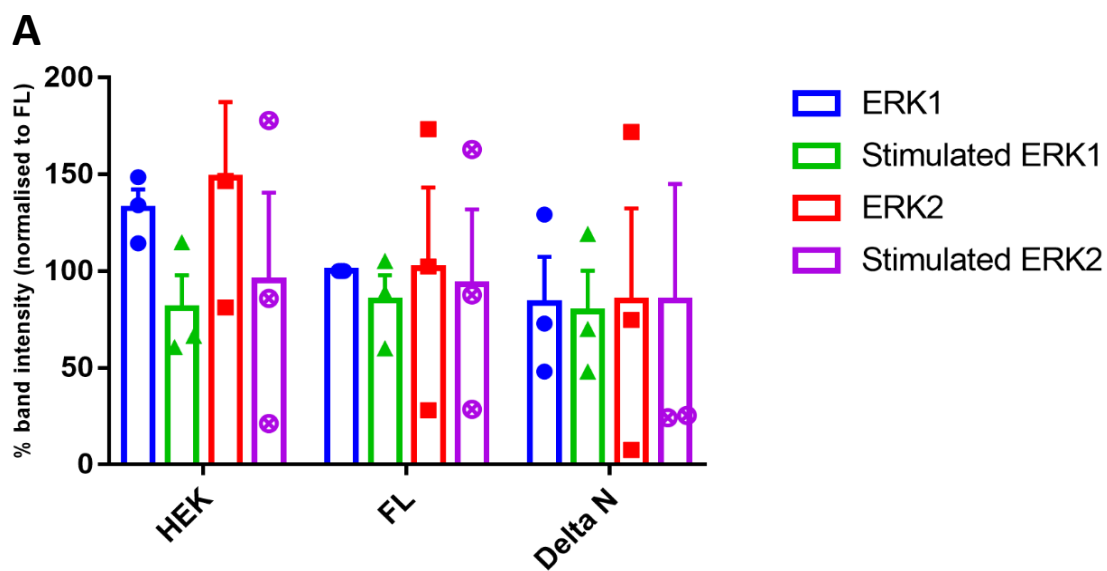
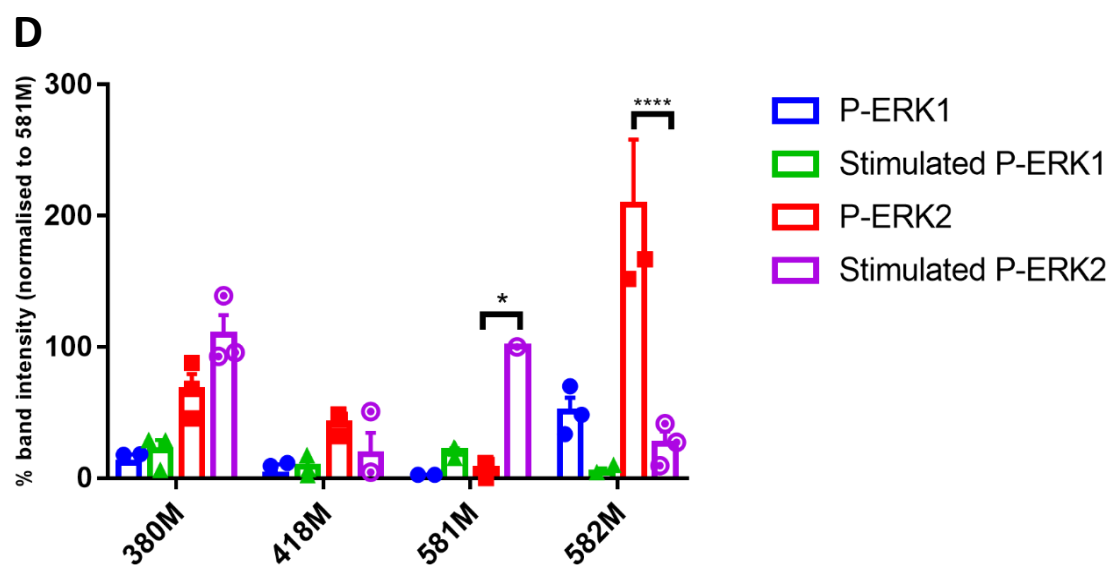
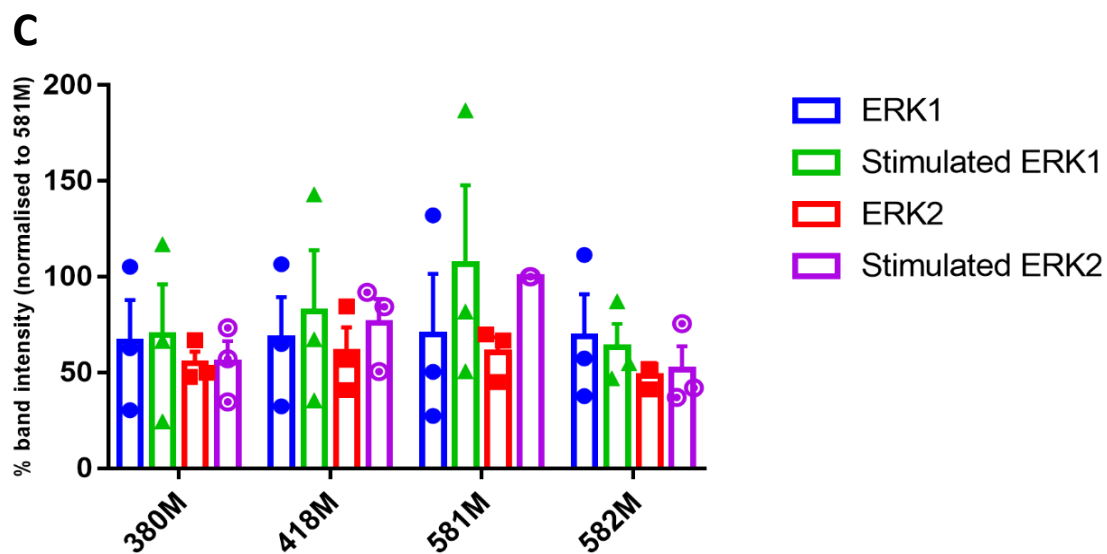


Figure 30: Internal deletions and C-Cys anchor mutants ERK (1/2) phosphorylation

Each sample has two groups; (+) cells were stimulated with 1 mM of ATP for 2 minutes before lysed and (-) cells were not stimulated. ERK 1 is 44 kDa, and ERK 2 is 42 kDa. Representative blot from 3 independent experiments.

In the representative blots (Figures 29 and 30) substantial variation in the band intensity for ERK1 and ERK2 signals can be seen, and we decided to quantify our data, performing 3 independent experiments and measuring the band density for ERK1, ERK2, P-ERK1 and P-ERK2 in non-stimulated and ATP-stimulated conditions (raw data in Appendix 7). Unfortunately, while all samples were processed simultaneously (transfection, cell lysis, and Bradford protein assay), and equal quantities of protein were loaded per lane, the appropriate control (e.g FL-S) was not included on each blot. Rather, the same samples were loaded in each blot across the 3 replicates, meaning that, while each blot can be normalized to one sample across the 3 experiments (so samples within a given blot can be compared), no statistical comparison could be performed on all samples. Band intensities from each individual blot were normalized to one sample on each blot, the means were calculated and data presented in histograms in Figures 31 and 32. Two-way ANOVA was used for statistical analysis of each blot group. First, we quantified the band intensities for ERK1 and ERK2 across each blot, finding that there was a high degree of variability, and no statistically significant difference for any of the mutants, FL (rP2X7-GFP-(His)₈), and HEK (HEK-293 un-transfected cells); Figure 31 (A, C, and E) and Appendix 8 (A and C). Second, we quantified the P-ERK1 and P-ERK2 levels in each mutant, finding that the majority of mutants showed no significant change in either P-ERK1 or P-ERK2 levels when stimulated by 1 mM ATP including 380M, 418M, D2, D5, D6, D7, D8, CRR, CRRa, CRRb, and C(X)A; Figure 31 (D and F) and Appendix 8 (B and D). In our blot-by-blot analysis, FL (rP2X7-GFP-(His)₈), ΔN, 581M, 582M, D1, D3, and D4 showed a significant difference in P-ERK1 and /or P-ERK2 levels when stimulated with ATP. FL, 581M, and D3 displayed a significant increase in ERK2 phosphorylation after ATP application (Figure 31; B, D, and F). 582M, D1, and D4 show a significant reduction in ERK2 phosphorylation after ATP application (Figure 31; D and F). Finally, ΔN shows a significant decrease in both ERK1 and ERK2 phosphorylation when stimulated with ATP (Figure 31; B).





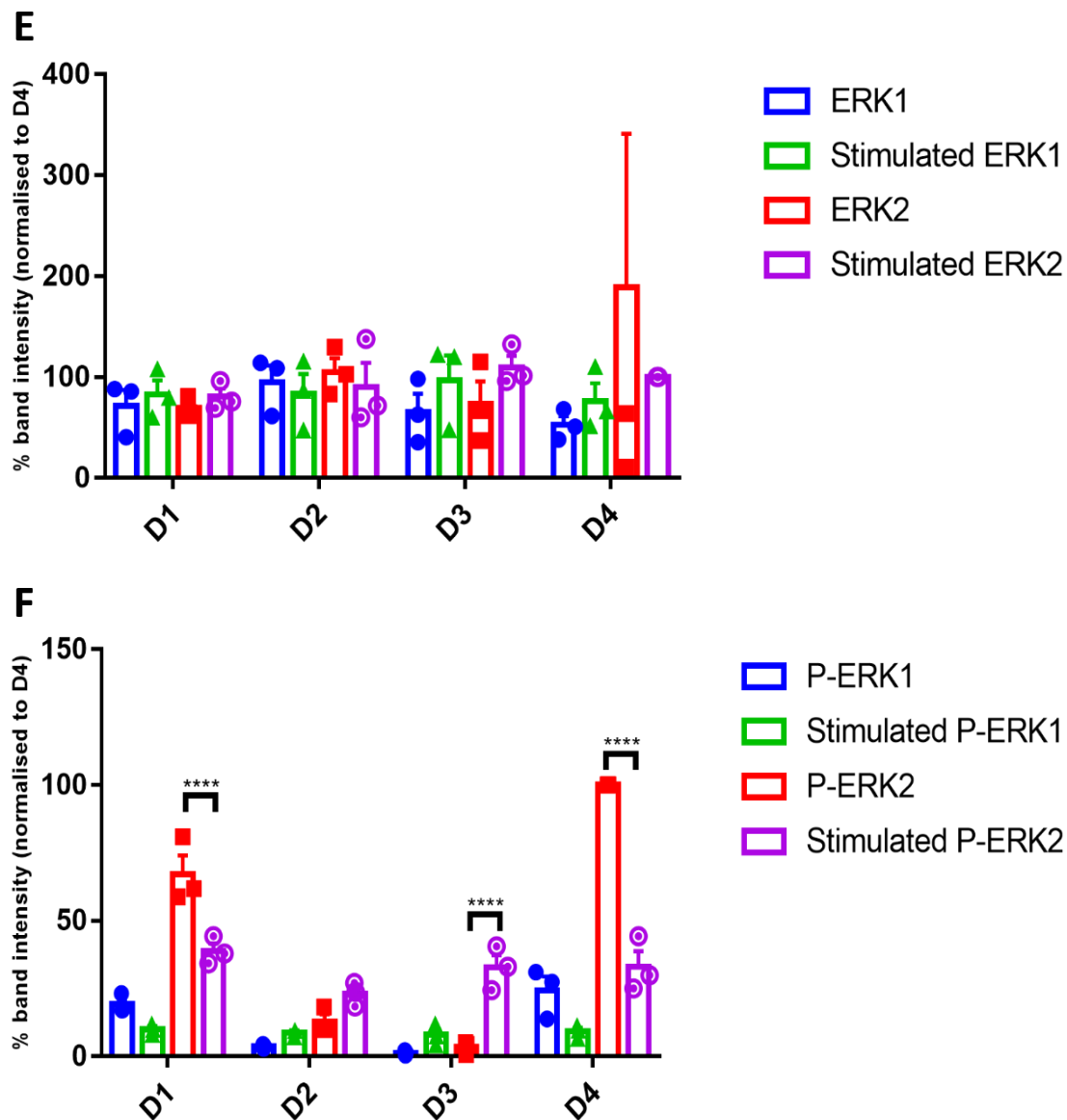
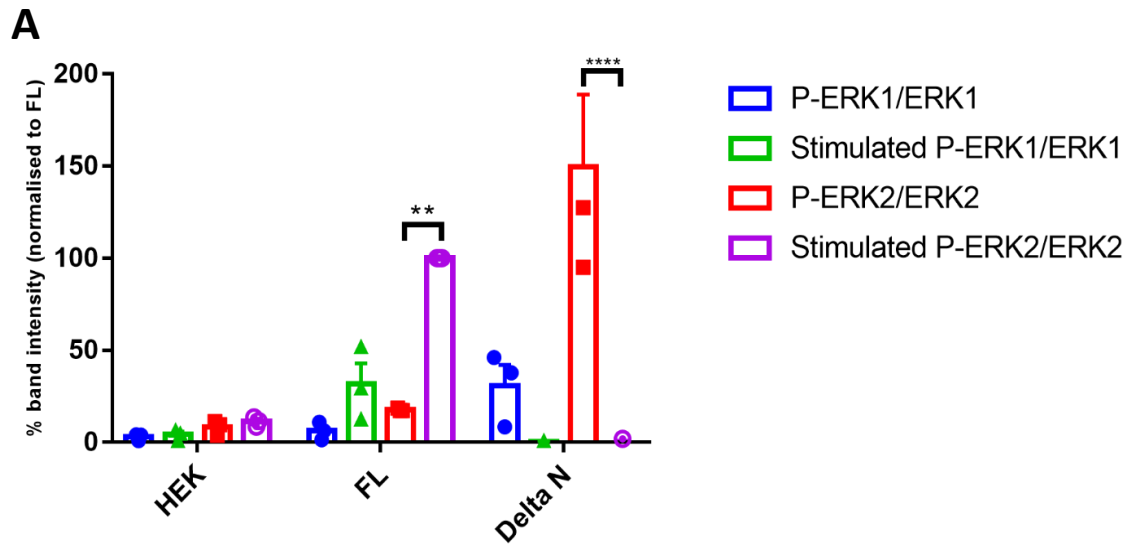


Figure 31: Effect of truncation and internal deletion mutants on basal and ATP-stimulated ERK (1/2) levels

(A): ERK (1/2) basal levels for stimulated and un-stimulated HEK, FL, and ΔN . (B): P-ERK (1/2) basal levels for stimulated and un-stimulated HEK, FL, and ΔN . (C): ERK (1/2) basal levels for stimulated and un-stimulated 380M, 418M, 581M, and 582M. (D): P-ERK (1/2) basal levels for stimulated and un-stimulated 380M, 418M, 581M, and 582M. (E): ERK (1/2) basal levels for stimulated and un-stimulated D1, D2, D3, and D4. (F): P-ERK (1/2) basal levels for stimulated and un-stimulated D1, D2, D3, and D4. Results are (\pm SEM). *P and ****P represent P-value ≤ 0.05 and ≤ 0.0001 respectively.

We measured the P-ERK induction (P-ERK intensity/ERK intensity) for basal ERK1 and ERK2 and ATP-stimulated ERK1 and ERK2 (Figure 32 and Appendix 9). Only FL (rP2X7-GFP-(His)₈) showed a significant increase in stimulated P-ERK2/ERK2 (Figure 32; A). However, ΔN and 582M both displayed a significant reduction in stimulated P-ERK2/ERK2 (Figure 32; A and B). Comparing the stimulated induction of ERK1 and ERK2 shows a significant difference only with FL. Taking all together, these results demonstrate the ability of rP2X7-GFP-(His)₈ full-length to phosphorylate ERK2, while none of our constructs were able to mediate ATP-stimulated ERK1/2 phosphorylation.



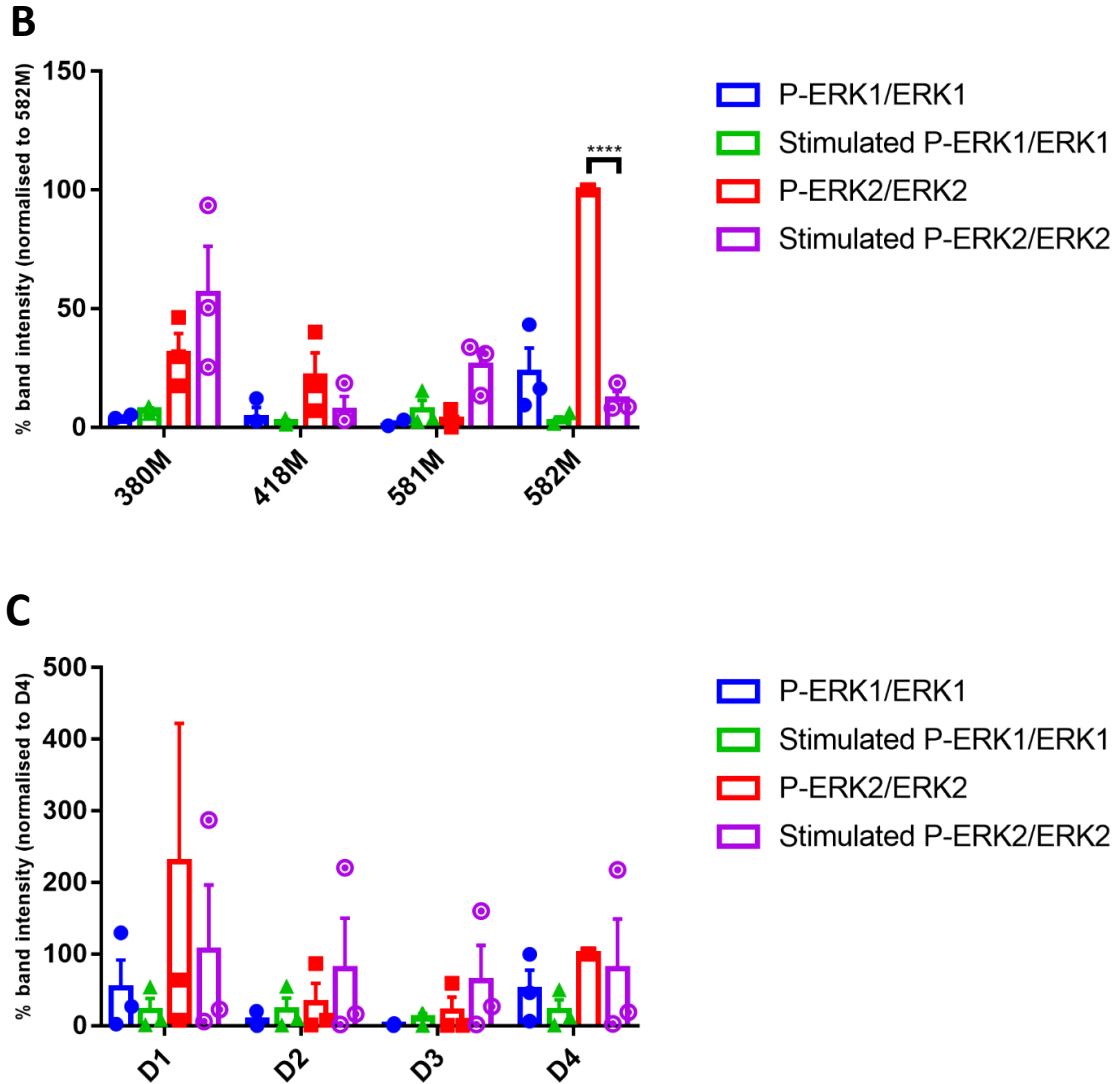
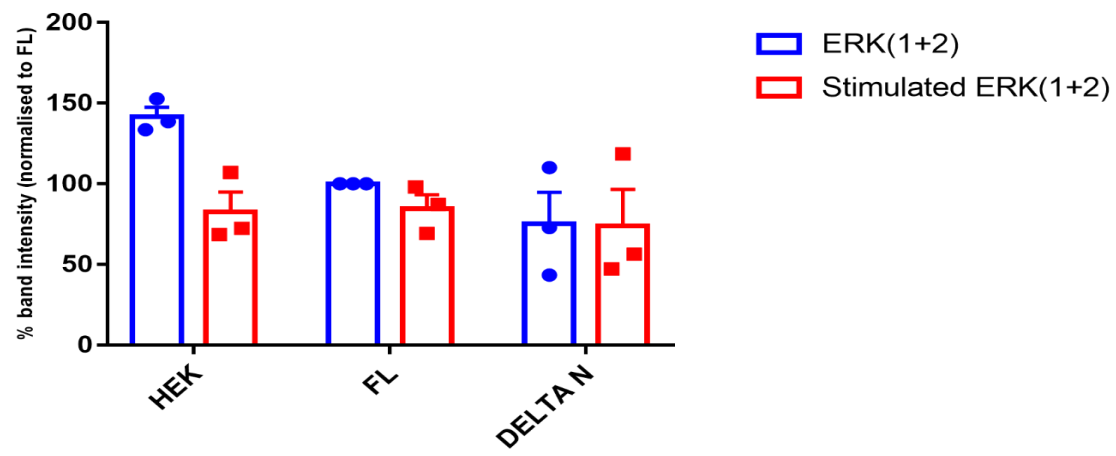
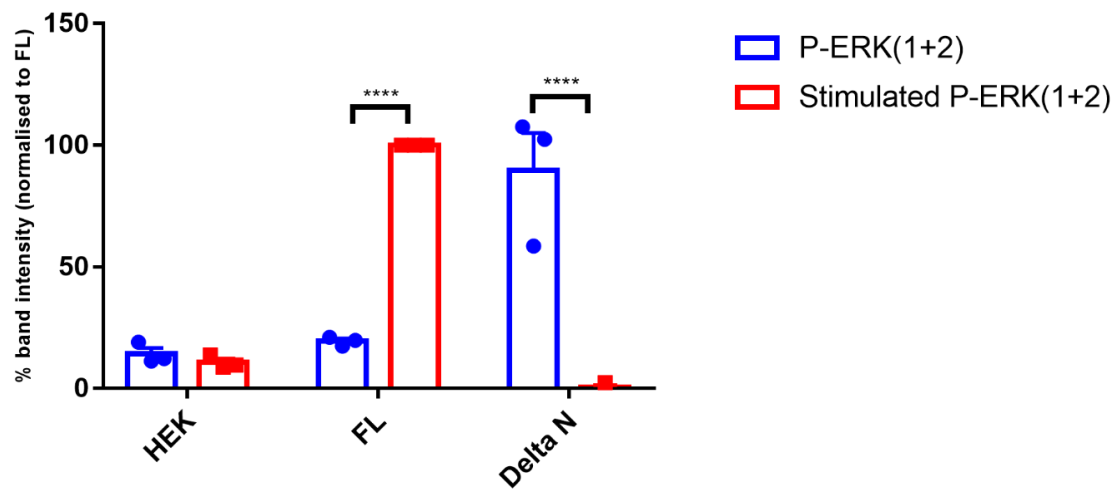


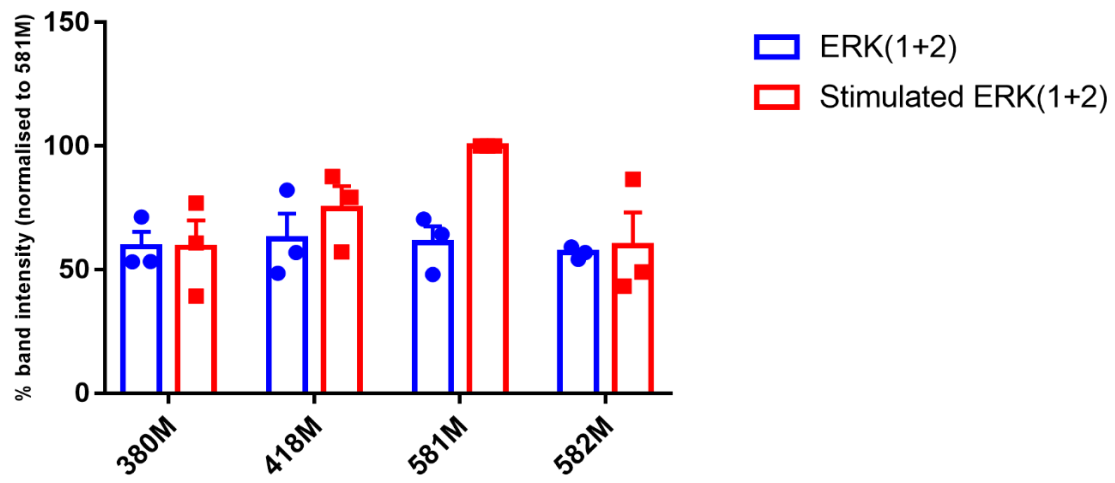
Figure 32: Effect of truncation and internal deletion mutants on P-ERK1 and P-ERK2 inductions

(A): P-ERK (1/2) inductions for stimulated and un-stimulated HEK, FL, and Δ N. (B): P-ERK (1/2) inductions for stimulated and un-stimulated 380M, 418M, 581M, and 582M. (C): P-ERK (1/2) inductions for stimulated and un-stimulated D1, D2, D3, and D4. Results are (\pm SEM). **P and ****P represent P-value ≤ 0.0021 and ≤ 0.0001 respectively.

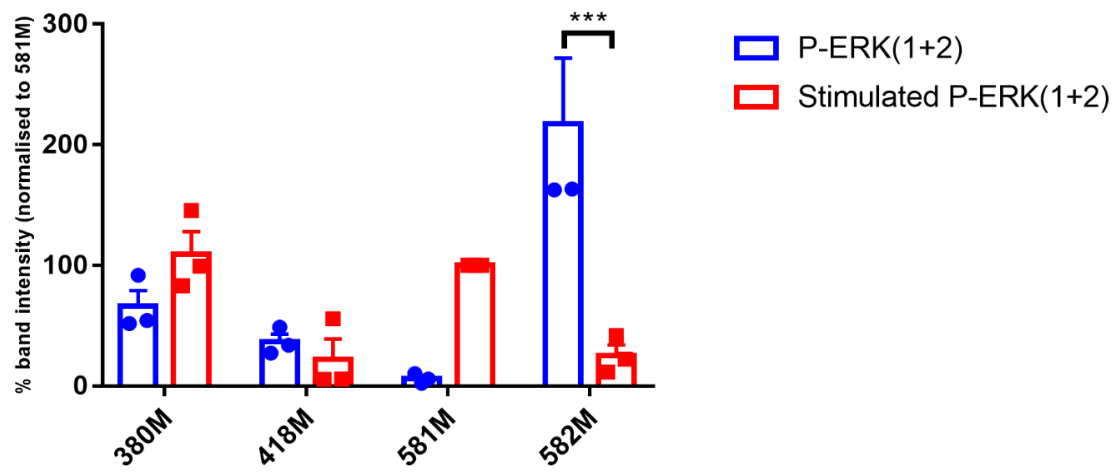
The ERK1 and ERK2 isoforms display the same subcellular localization and translocation from cytosol to the nucleus upon activation (Lenormand et al. 1993). Both isoforms display the same substrate specificities and they are activated by the same upstream kinases (Lefloch et al. 2008). For this reason, we decided to quantify ERK1 and ERK2 together, looking at the basal ERK (1+2), ATP-stimulated ERK (1+2), basal P-ERK (1+2), and ATP-stimulated P-ERK (1+2). There was no significant difference between mutants on the same blot for basal ERK (1+2) and ATP-stimulated ERK (1+2) (Figure 33 (A, C, and E); appendix 10 (A and B)). However, ATP-stimulated P-ERK (1+2) levels significantly increased in the case of FL (rP2X7-GFP-(His)₈) and significantly decreased for the receptor lacking the N-terminus (Figure 33; B). 582M, D1, and D4 mutants behaved like ΔN; stimulated P-ERK (1+2) levels were significantly reduced (Figure 33; D and F) while the D3 mutant behaved like FL; the ATP-stimulated P-ERK (1+2) level was significantly increased (Figure 33; F).

A**B**

C



D



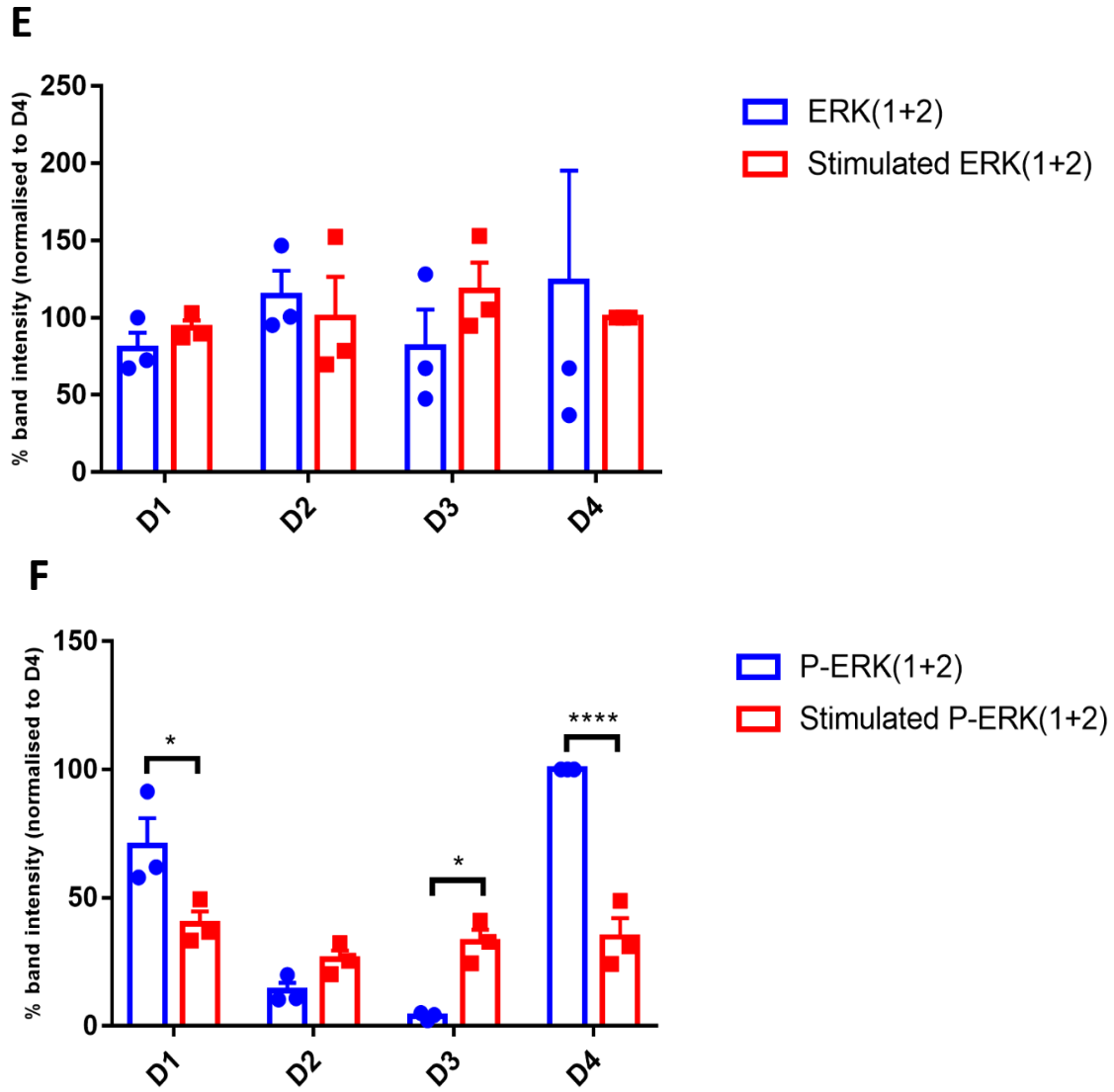


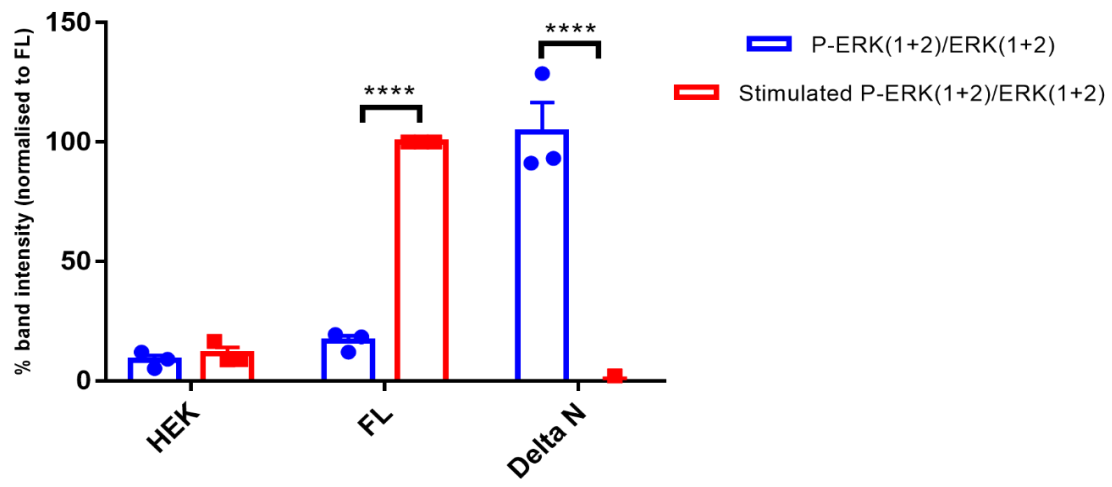
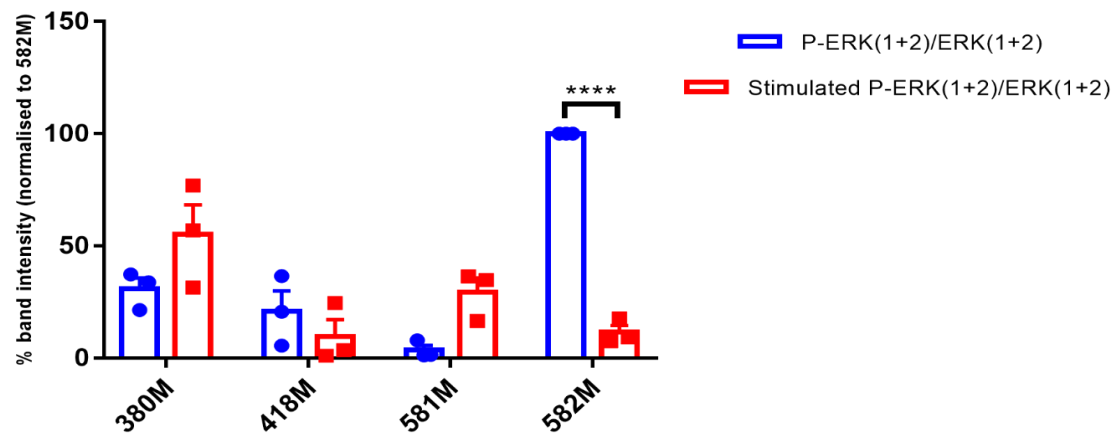
Figure 33: Effect of truncation and internal deletion mutants on basal and ATP-stimulated ERK (1+2) levels

(A): ERK (1+2) basal levels for stimulated and un-stimulated HEK, FL, and Δ N. (B): P-ERK (1+2) basal levels for stimulated and un-stimulated HEK, FL, and Δ N. (C): ERK (1+2) basal levels for stimulated and un-stimulated 380M, 418M, 581M, and 582M. (D): P-ERK (1+2) basal levels for stimulated and un-stimulated 380M, 418M, 581M, and 582M. (E): ERK (1+2) basal levels for stimulated and un-stimulated D1, D2, D3, and D4. (F): P-ERK (1+2) basal levels for stimulated and un-stimulated D1, D2, D3, and D4. Results are (\pm SEM). *P, ***P and ****P represent P-value ≤ 0.05 , ≤ 0.0002 and ≤ 0.0001 respectively.

We also measured the P-ERK (1+2) inductions for our mutants. Only FL (rP2X7-GFP-(His)₈) mediated a significant ERK (1+2) phosphorylation after ATP application. However, ΔN and 582M mutants significantly reduced ERK (1+2) phosphorylation (Figure 34, A and B). The remainder of our mutants show no significant difference between P-ERK (1+2) induction before and after ATP addition (Figure 34 and appendix 11).

It must be stated that our ERK1/2 analysis was severely limited due to the lack of controls loaded on each blot, meaning that our groups of mutants on each blot could only be analysed in isolation. However, with this caveat in mind, we did not observe a significant difference in the total expression levels of either ERK1 or ERK2 for any of the mutants. P-ERK2 levels were significantly increased upon stimulation of full-length receptor (rP2X7-GFP-(His)₈), 581M, and D3; however, only the full-length receptor showed a significant increase when measuring P-ERK2 induction. Perhaps our most surprising finding was that P-ERK2 levels were significantly *decreased* in ΔN (with P-ERK1 also reduced), 582M, D1, and D4. The only two constructs to show a significant decrease in P-ERK2 induction were ΔN and 582M.

Our data suggests that the P2X7 intracellular domains are required for ATP-stimulated ERK1/2 phosphorylation, because none of our mutant constructs were capable of increasing the levels of P-ERK1/2 on ATP treatment. However, our observation that ΔN and 582M mutant constructs appeared to have the opposite effect (high basal ERK phosphorylation which is reduced on ATP treatment) suggests that the interaction with P2X7 and the ERK pathway is not straightforward.

A**B**

C

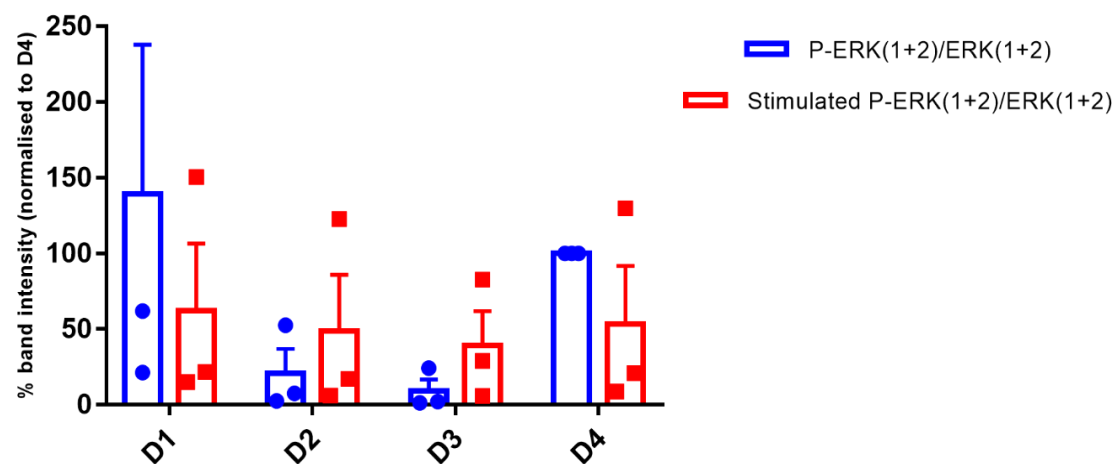


Figure 34: Effect of truncation and internal deletion mutants on P-ERK (1+2) inductions

(A): P-ERK (1+2) inductions for stimulated and un-stimulated HEK, FL, and ΔN . (B): P-ERK (1+2) inductions for stimulated and un-stimulated 380M, 418M, 581M, and 582M. (C): P-ERK (1+2) inductions for stimulated and un-stimulated D1, D2, D3, and D4. Results are (\pm SEM). ****P represents P-value ≤ 0.0001 .

Table 9 below summarizes mutant results for all pathways tested in this study.

Table 9: Summary of calcium influx, cell blebbing, P-ERK1/2, and pore formation results obtained for all mutants studied

P2X7-GFP construct	Deleted portion	Ca influx	Signalling pathways					
			Cell blebbing	P-ERK1/2				Pore formation
				Un-Stimulated		Stimulated		
				ERK1	ERK2	ERK1	ERK2	
Full length	No deletion	++++	Yes	-	+	+	++++	++++
380M	Δ (381-595)	-	Yes	-	+	+	+	+
418M	Δ (419-595)	++++	No	-	+	-	+	-
581M	Δ (582-595)	-	No	-	-	+	++	-
582M	Δ (583-595)	-	Yes	+	+	+	-	++++
D1	Δ (389-405)	-	No	+	+	-	++	-
D2	Δ (441-460)	++++	Yes	-	+	-	+	++++
D3	Δ (494-508)	-	No	-	-	-	++	-
D4	Δ (389-531)	-	No	+	+	+	-	-
D5	Δ (381-417)	-	No	+	+	+	+	-

P2X7-GFP construct	Deleted portion	Ca influx	Signalling pathways					
			Cell blebbing	P-ERK				Pore formation
				Un-Stimulated		Stimulated		
				ERK1	ERK2	ERK1	ERK2	
D6	Δ (441-493)	-	No	+	+	+	+	-
D7	Δ (418-460)	-	No	+	+	+	+	-
D8	Δ (583-595) & Δ (441-460)	-	No	+	+	+	+	-
ΔN	Δ (2-23)	-	No	+	+	-	-	-
CRR	Δ (362-379)	-	Yes	+	+	-	+	+
CRRa	Δ (362-370)	++++	Yes	+	+	+	+	++++
CRRb	Δ (371-379)	-	No	+	+	-	+	+
C(X)A	C371A C373A C374A C377A	-	Yes	+	+	-	+	+

Cell blebbing expressed as (yes or no), calcium influx and pore formation are expressed as (-) if the mutant does not induce the pathway and (+) if it causes it; the number of plus signs on the relative size of the response (one plus for a significant difference from negative control, more for a bigger response. ERK1/2 phosphorylation is expressed as (-) if the mutant does not induce ERK phosphorylation and (+) if it causes it; the number of plus signs on the relative level of ERK phosphorylation. Key results are highlighted in grey.

4.3. Discussion

4.3.1. P2X7 intracellular domains are essential for protein function and trafficking

We found that the deletions D4, D5, D6, D7, D8 and ΔN were unable to induce any of the pathways tested in this study. All these constructs showed a very low levels of protein cell-surface expression which suggest that receptor lacking these regions disrupts protein function and trafficking to the cell membrane. These deletions vary in length with deletion of 38 amino acids with D5: Δ (381-417) to 142 amino acids with D4: Δ (389-531), which disrupts the ballast domain. Only ΔN has been studied previously, where ATP-induced ERK phosphorylation as shown to be abolished (Amstrup and Novak 2003).

4.3.2. Cell blebbing and pore formation are intrinsically coupled

P2X7 has been stated to be a bifunctional receptor having a role in cell proliferation and death (De Marchi et al. 2016). P2X7 mediated cell blebbing and pore formation are events that may lead to cell death in conditions of long-term or repeated receptor activation; our data suggest that same regions of the receptor may regulate these pathways, and not depend on the ballast domain.

Our study demonstrates that any construct that is capable of ATP-induced cell blebbing, is also capable of ATP-induced pore formation (this includes 380M, 582M, D2, CRR, CRRa, and C(X)A). The only exception was our construct CRRb: Δ (371-379) which shows pore formation but no cell blebbing. Similarly to previous studies, 582M is capable of pore formation (Smart et al. 2003). However, in contrast to previous studies; (Smart et al. 2003) the 380M truncation (which lacks the entire ballast domain) was still capable of cell blebbing.

4.3.3. P2X7 receptor intracellular domains are essential for ERK1/2 phosphorylation

The ERK1 and ERK2 isoforms display the same substrate specificities (Yoon and Seger 2006) and both isoforms are activated by the same upstream kinases (Lefloch et al. 2008). However, ERK2 expression levels are higher than ERK1 in mammalian cells (Buscà et al. 2015; Frémin et al. 2015). Indeed, stoichiometry measurements indicate that ERK2 is four times more abundant than ERK1 in NIH 3T3 cells, and ERK2 activation is four times more abundant than ERK1 activation suggesting that ERK1 and ERK2 isoforms are activated equally by upstream kinases (Lefloch et al. 2008).

Our observations in this study show no significant difference between the basal expression levels of ERK1 and ERK2 either in ATP-stimulated and un-stimulated HEK-293 cells. However, ATP-stimulated ERK phosphorylation is impaired by nearly every mutation, suggesting that the whole protein integrity is important for ERK phosphorylation. All mutants in the C-Cys anchor domain (CRR, CRRa, CRRb, and C(X)A) and nearly all in the ballast domain abolished ATP-stimulated ERK1 and ERK2, suggesting that both these domains are required for this signalling phenomenon.

As expected, the rP2X7-GFP-(His)₈ full-length receptor is capable of ERK2 phosphorylation and the receptor lacking N-terminus is not (Amstrup and Novak 2003). Interestingly, 581M and D3 mutants also displayed significant ERK2 phosphorylation when stimulated by the extracellular ATP.

Our initial observations that deletion of the N-terminal domain abolished ATP-induced cell blebbing suggested a potential role for this domain (similar to what has previously been proposed for ERK (1/2) phosphorylation (Amstrup and Novak 2003)). However, our finding that N-terminal deletion led to undetectable levels of cell-surface expression mean that we can only conclude that this domain is required for receptor cell-surface expression. The N-terminal domain of P2X receptors contains a conserved protein kinase C site (TX(K/R)) (North 2002); the conserved threonine residue is important for protein function, and it has been suggested this may be due to phosphorylation as discussed previously in several mutagenesis studies (Boué-Grabot et al. 2000; North 2002).

Our results provide a limited comparison between mutants and rP2X7-GFP-(His)₈ full-length receptor because we did not load a control on each blot. However, despite this, our data suggest that ERK1/2 phosphorylation does not appear to be coupled to calcium influx, pore formation, and cell blebbing.

To enable firm conclusions to be drawn, this analysis needs to be repeated with the inclusion of the positive control (rP2X7-GFP-(His)₈ full-length) on every blot so that normalization can be done and compared for all mutants.

4.3.4. How might the intracellular domains of P2X7 couple to the ERK1/2 phosphorylation cascade?

Translation of the extracellular signal to a biological response is performed through activation of the multi-step MAPK cascade. This cascade starts from the interaction of the specific MAPKKK with GTPase, which transfers the phosphate group to MAPKK and ends with MAPK activation. The mechanism of P2X7-mediating ERK1/2 phosphorylation is poorly understood. However, Gendron *et al* describes the importance of proline-rich/Ca²⁺-activated tyrosine kinase (Pyk2), c-Src, and phosphatidylinositol 3'kinase (PI-3K) phosphorylation for P2X7 mediating ERK1/2 phosphorylation in astrocytes cells (Gendron et al. 2003). Activation of P2X7 receptor by BzATP mediates the phosphorylation of Pyk2, and the phosphorylated Pyk2 in turn serves as kinase and docking site for phosphorylated c-Src and PI-3K and subsequently activation of ERK1/2. While,

using c-Src, PI 3K inhibitors significantly reduce P2X7 mediating ERK1/2 activation (Lev et al. 1995; Sabri et al. 1998; Blaukat et al. 1999; Gendron et al. 2003).

Besides Gendron *et al's* findings, our results show that Δ N and 582M: Δ (583-595) are incapable of activation of ERK1/2. In contrast, rP2X7 receptors lacking D3: Δ (494-508) and 581M: Δ (582-595) are capable of ERK2 phosphorylation suggesting that P2X7 intracellular domains may serve as a docking site for the kinases and substrate to transfer the upstream signal to downstream ERK1/2 which may mediate the biological response.

Finally, the high degree of variability observed in our band intensities, particularly for basal ERK levels, shows the technical difficulties that we encountered in performing these experiments. Our findings provide a hint that P2X7 intracellular domains may be involved in the ERK1/2 phosphorylation but we cannot provide an explanation for our findings that ERK1/2 appeared to be constitutively phosphorylated in our delta N-expressing cells, and that phosphorylation was decreased upon ATP addition, especially given that we could detect no protein expressed at the cell surface.

Chapter 5: Investigating the mechanisms of
ATP-induced cell blebbing via P2X7
receptor activation

5.1. Introduction

5.1.1. The proposed molecular mechanism for P2X7-dependent cell blebbing - disruption of the interaction between P2X7 and the cytoskeleton *via* NMMHC-AII

Cell blebbing as a result of P2X7 activation has been proposed to depend on the disruption of an interaction between the receptor and the actomyosin cytoskeleton. Gu *et al* used immunoprecipitation and mass spectrometry to identify an interaction between the non-muscle myosins NMMHC-IIA or myosin V with the P2X7 membrane complex in human monocytic THP-1 and HEK-293 cells respectively, and P2X7 activation with ATP caused dissociation of the interaction (Gu et al. 2009). In the same study, fluorescence microscopy was used to observe co-localization of co-transfected P2X7-AcGFP and NMMHC-AII-DsRed in the plasma membrane of HEK-293 cells and cell blebbing following BzATP application (Gu et al. 2009). Further investigations using Fluorescence Resonance Energy Transfer (FRET) demonstrated the interaction of the P2X7-DsRed monomer and the NMMHC-IIA-AcGFP in HEK-293 cells, and fluorescence intensity was decreased following incubation of co-transfected cells with BzATP for 15 minutes (Gu et al. 2009). The authors propose that cell blebbing is enabled as a result of P2X7-NMMHC-AII dissociation, but the regions of the P2X7 receptor involved in the P2X7-myosin interactions were not determined, nor was the molecular mechanism of the dissociation.

The myosin protein family consists of at least 20 structurally and functionally distinct classes and constitutes major components of the cytoskeleton. Myosins are actin-dependent molecular motors that use ATP hydrolysis to move along the actin filament (Simons et al. 1991; Gu et al. 2009). The myosin II family includes muscle myosin, which causes the contraction of striated and smooth muscles, and non-muscle myosin which is expressed in eukaryotic cells and participates in processes requiring production of force and actin cytoskeleton translocation including cytokinesis, cell migration, polarization, cell adhesion, and signal transduction (Pecci et al. 2018).

Myosin II and V are the most common members of the myosin family in non-muscle cells (Mercer et al. 1991; Conti et al. 2004). Myosin II has at least three isoforms: IIA, IIB, and IIC which differ in their heavy chains and are encoded by distinct genes; *MYH9*, *MYH10*, and *MYH14* respectively (Marigo et al. 2004; Gu et al. 2009). Class II myosin is a hexameric protein consisting of homodimer heavy chains (230 kDa), two regulatory light chains (20 kDa) controlling myosin activity, and two essential light chains (17 kDa) stabilizing the heavy chain structure (Pecci et al. 2018). The heavy chains comprise the N-terminal head (motor domain) responsible for actin filament binding. A long C-terminal tail is responsible for cargo binding and heavy chains' dimerisation (Krendel and Mooseker 2005; Eddinger and Meer 2007).

Non-muscle myosin IIA heavy chain (NMMHC-IIA) is present in almost all non-muscle cells, and its expression is significantly greater than other two isoforms (IIB and IIC) (Simons et al. 1991; Golomb et al. 2004; Ma et al. 2010). NMMHC-IIA is involved in maintaining cell morphology, motility, membrane repair, cell adhesion and retraction (Wei and Adelstein 2000; Wylie and Chantler 2001,2003; Jacobelli et al. 2004; Togo and Steinhardt 2004; DePina et al. 2007; Takizawa et al. 2007).

Myosin V is a molecular motor that functions as an organelle transporter (Reck-Peterson et al. 2000). There are three myosin V isoforms in human, myosin Va is expressed mainly in brain and melanocytes, myosin Vb and Vc are expressed in epithelial cells (Mercer et al. 1991; Rodriguez and Cheney 2002; Swiatecka-Urban et al. 2007). Myosin V has four structural domains; the motor domain which contains the actin and nucleotide-binding sites, the lever (24 nm in length) which amplifies small nucleotide-dependent changes following ATP hydrolysis at the active site allowing large power stroke to occur, the rod domain which contains regions of α -helical coiled-coil responsible for dimerization of the molecule, and finally the C-terminal domain, which binds adapter proteins that link myosin V to cargo (Trybus 2008).

5.1.2. The role of cholesterol in P2X7 signalling

Cholesterol is an essential component of the plasma membrane (comprising up to 25% of membrane lipid) (Reboldi and Dang 2018). It is synthesized in the endoplasmic reticulum and transported to the cell membrane where its concentration is higher than in other cellular compartments (Yang et al. 2016). Cholesterol has a structure of four fused hydrocarbon rings with a polar hydroxyl group at one end and an eight-carbon branched aliphatic tail at the other end, cholesterol inserts into the bilayer of phospholipid with its polar hydroxyl group aligned with ester carbonyl groups of phospholipids (Yang et al. 2016). Cholesterol ordering within the lipid bilayer affects membrane fluidity and reduces the lateral and rotational diffusion of lipids and embedded proteins (Kahya et al. 2003; Crane and Tamm 2004).

In 2017, the Kawate group demonstrated that panda P2X7 receptors lacking N and C termini (P2X7 Δ CN) reconstituted into proteoliposomes were capable of ATP-induced pore formation, in contrast to when these truncated constructs were expressed in HEK-293 cells. Furthermore, they showed that the reason their construct was incapable of pore formation in cell-based systems was due to the lipid composition (primarily the high concentration of cholesterol) (Karasawa et al. 2017). The incapability of P2X7 Δ CN to induce pore formation in liposomes having the same cholesterol amount as HEK-293 cells supported these findings, and removal of cholesterol enhanced YO-PRO-1 uptake (Karasawa et al. 2017). The authors proposed that cholesterol is able to interact with the C-terminal domain of P2X7, and this interaction sequesters it from the channel, preventing it from inhibiting pore formation (Karasawa et al. 2017).

It is clear from the above that cholesterol plays a pivotal role in the cell membrane through the regulation of membrane fluidity and protein movement and plays a significant role in P2X7 signalling.

The aims of this study were to investigate mechanism of P2X7-dependent cell blebbing, in terms of the roles of both myosin and cholesterol. Using the DuolinkTM proximity ligation assay in conjunction with pull-down assays, we investigated the rP2X7-GFP-(His)₈-NMMHC-AII interaction in Hela and HEK-293 cells. Using the -cholesterol- depleting agent methyl- β -cyclodextrin (MCD), we investigated the effects of reducing plasma membrane cholesterol on ATP-induced cell blebbing.

5.2. Results

5.2.1. NMMHC-IIA expression in HEK-293 and HeLa cells

First, we confirmed the expression of NMMHC-IIA in HeLa and HEK-293 cells transfected with full-length rP2X7-GFP-(His)₈ and our constructs using Western blotting with an anti-NMMHC-IIA (Figure 35). As expected, we observed a single band at approximately 220 kDa in all samples-our initial observations suggest no variation in myosin expression levels when P2X7 mutants are expressed.

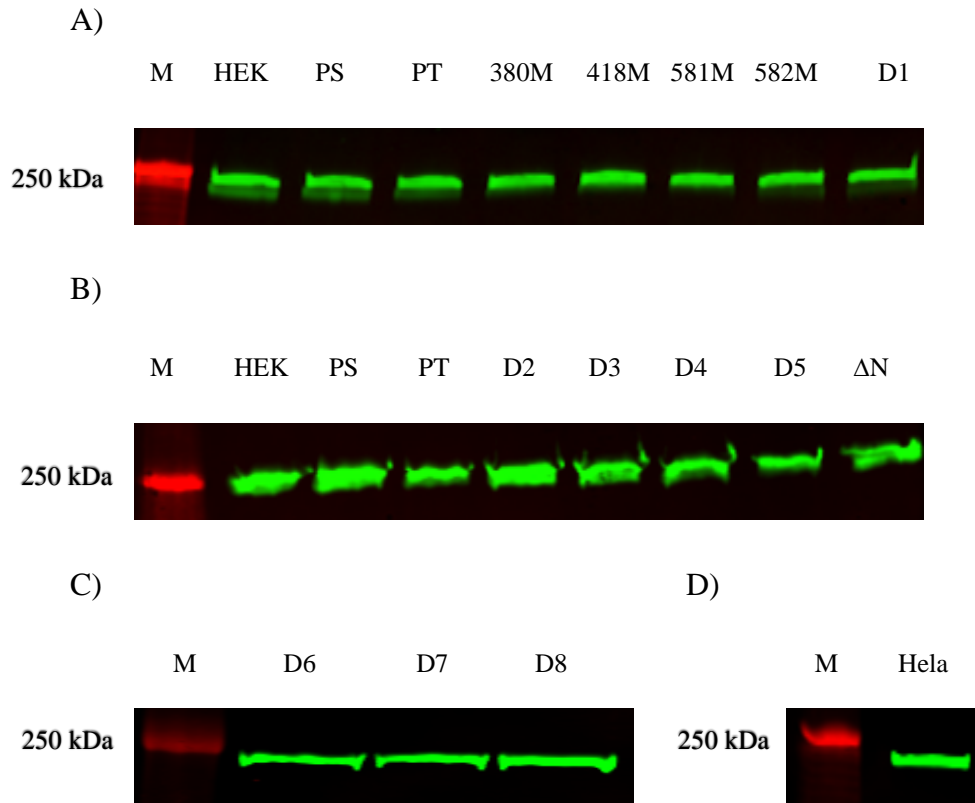


Figure 35: Non-Muscle Myosin (NMMHC-IIA) expression

PS: rP2X7-GFP-(His)₈ full-length stable line, PT: rP2X7-GFP-(His)₈ full-length transient transfected. NMMHC-IIA is 226 kDa.

5.2.2. Proximity Ligation Assay (PLA) indicates a potential interaction between P2X7 and NMMHC-IIA

PLA is an *in-situ* assay which measures the close proximity of two proteins. Compared to pull-down assays and immunoprecipitation, it has two advantages; first, it shows the interaction *in situ*, and second, it can capture weak or transient interactions that do not survive cell disruption or the conditions of the pull-down experiment. We hypothesized that, if ATP treatment disrupted a P2X7-myosin interaction we would observe a positive signal in non-treated cells, which would diminish upon ATP treatment. If the interaction (and its disruption) is important for P2X7-dependent cell blebbing, we should also either see no interaction or no change in the interaction in constructs that cannot bleb, because they may either not interact with the cytoskeleton at all, or they may not be able to dissociate from it.

First, we performed the Duolink™ PLA on HeLa cells transfected with full-length rP2X7-GFP-(His)₈ or our mutant constructs (Figure 36); note that this experiment was performed only once (n=1) due to the expense of the Duolink kit. We imaged cell nuclei (using DAPI, blue), GFP (green) and a positive PLA signal (orange dots (puncta)). In non-transfected control cells, we observe a very low level of positive signal, indicating that there is some non-specific signal, but that it is at low levels. In cells transfected with full-length rP2X7-GFP-(His)₈ (FL) we observed a much higher concentration of puncta indicating proximity in the cells with a positive GFP signal. Surprisingly, the blebbing mutant 380M shows weak interaction signals similar to the non-specific signal observed in the negative control. These observations may suggest the proximity of NMMHC-AII to the C-terminal of the P2X7 receptor within (381-595 amino acids residues) (Figure 36). We observed a positive proximity signal for every mutant construct tested, even those where we detected little or no cell-surface protein expression (e.g. ΔN). This may suggest that P2X7-NMMHC-IIA are in close proximity regardless of whether the receptor is at the cell surface.

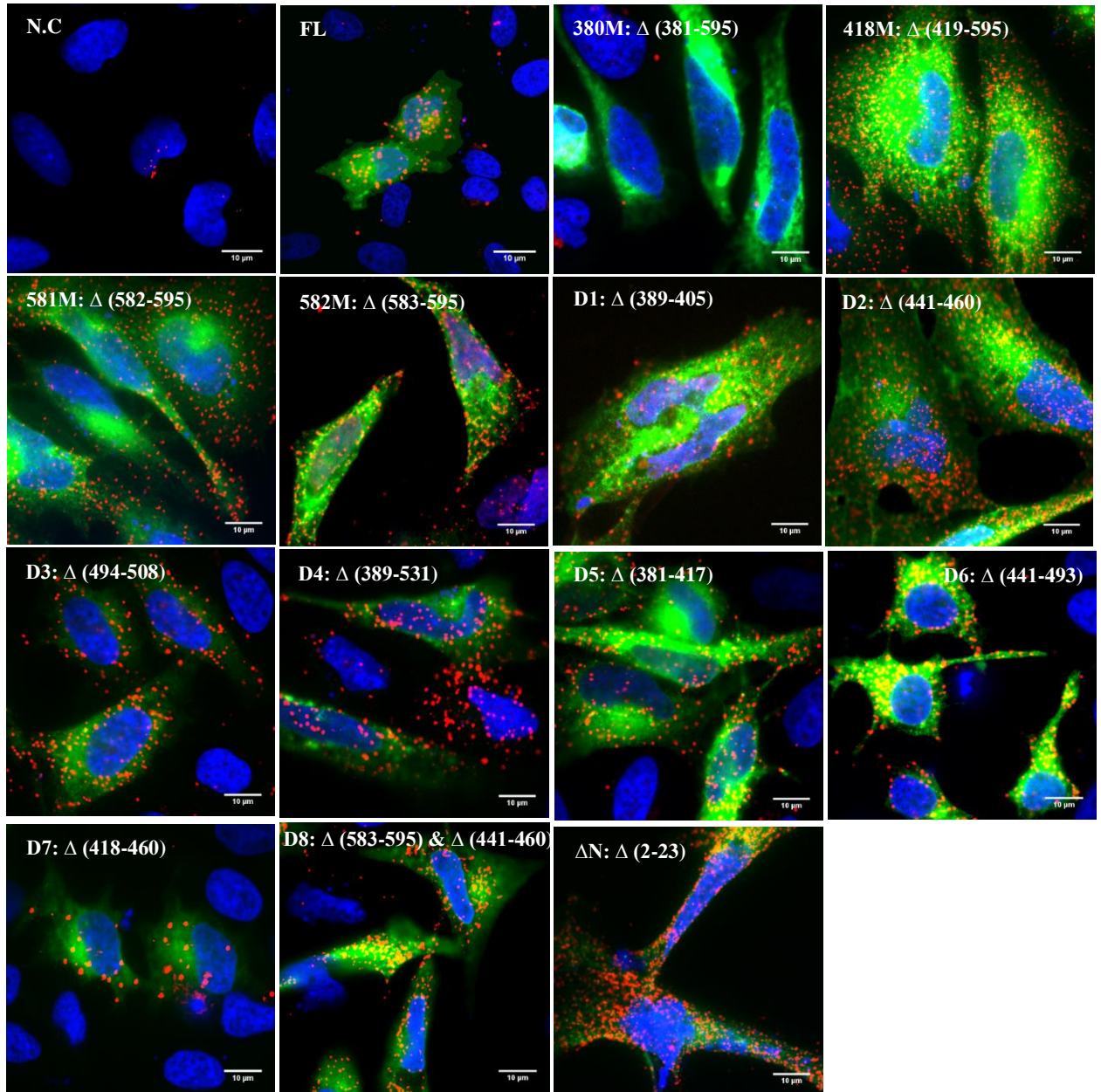


Figure 36: Proximity ligation assay to measure the rP2X7-GFP-(His)₈-NMMHC-IIA interaction

N.C: un-transfected Hela cells, FL: rP2X7-GFP-(His)₈ full-length receptor. Blue colour show nucleus stained with DAPI, green colour represents GFP, small orange dots represent rP2X7-GFP-(His)₈ and NMMHC-IIA interaction. Scale bar represents 10 μm.

For further investigations, cells transiently transfected with FL, 582M, D2, and D8 were incubated with 1 mM ATP for 5 minutes at room temperature before PLA analysis (Figure 37). A positive signal denoting the interaction was observed in all constructs tested, indicating that the proximity of the P2X7 receptor and NMMHC-IIA was maintained following receptor activation.

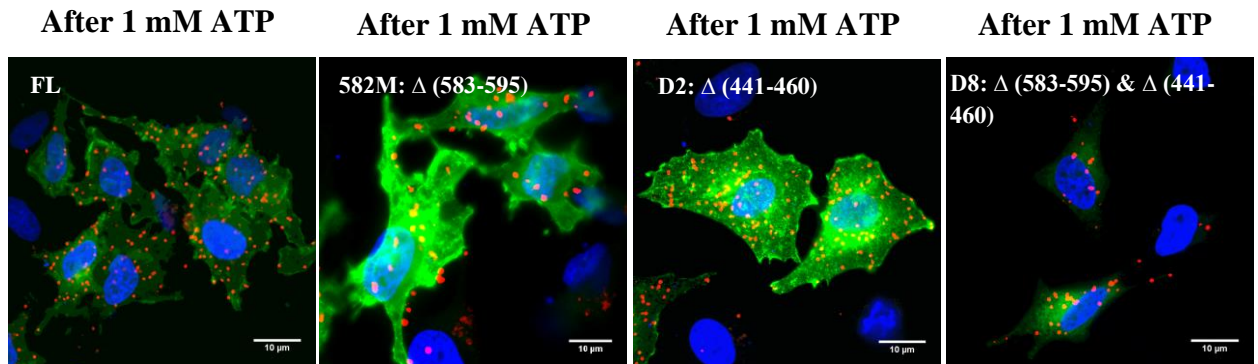


Figure 37: rP2X7-GFP-(His)₈-NMMHC-IIA interaction after ATP application

FL: rP2X7-GFP-(His)₈ full-length receptor. Blue colour show nucleus stained with DAPI, green colour represents GFP, small orange dots represent P2X7-NMMHC-IIA interaction. Scale bar represents 10 μm.

The signal interaction in terms of the number of puncta per cell was quantified using Image J software (n=10 cells) for each construct (Figure 38). Most constructs displayed a similar level of signal (approx. 100 puncta per cell), but the signals for 418M, 581M, D8, and ΔN were higher, albeit showing much more variability. These results suggest the interaction of the P2X7 receptor and NMMHC-AII is maintained following the ATP application, which potentially means that this interaction is not significant for cell blebbing. However, if proximity between P2X7 and myosin is maintained even when the receptor is not at the cell surface, this may have masked any change in signal due to dissociation at the cell membrane, and we cannot make a firm conclusion about the role of myosin in P2X7-dependent cell blebbing.

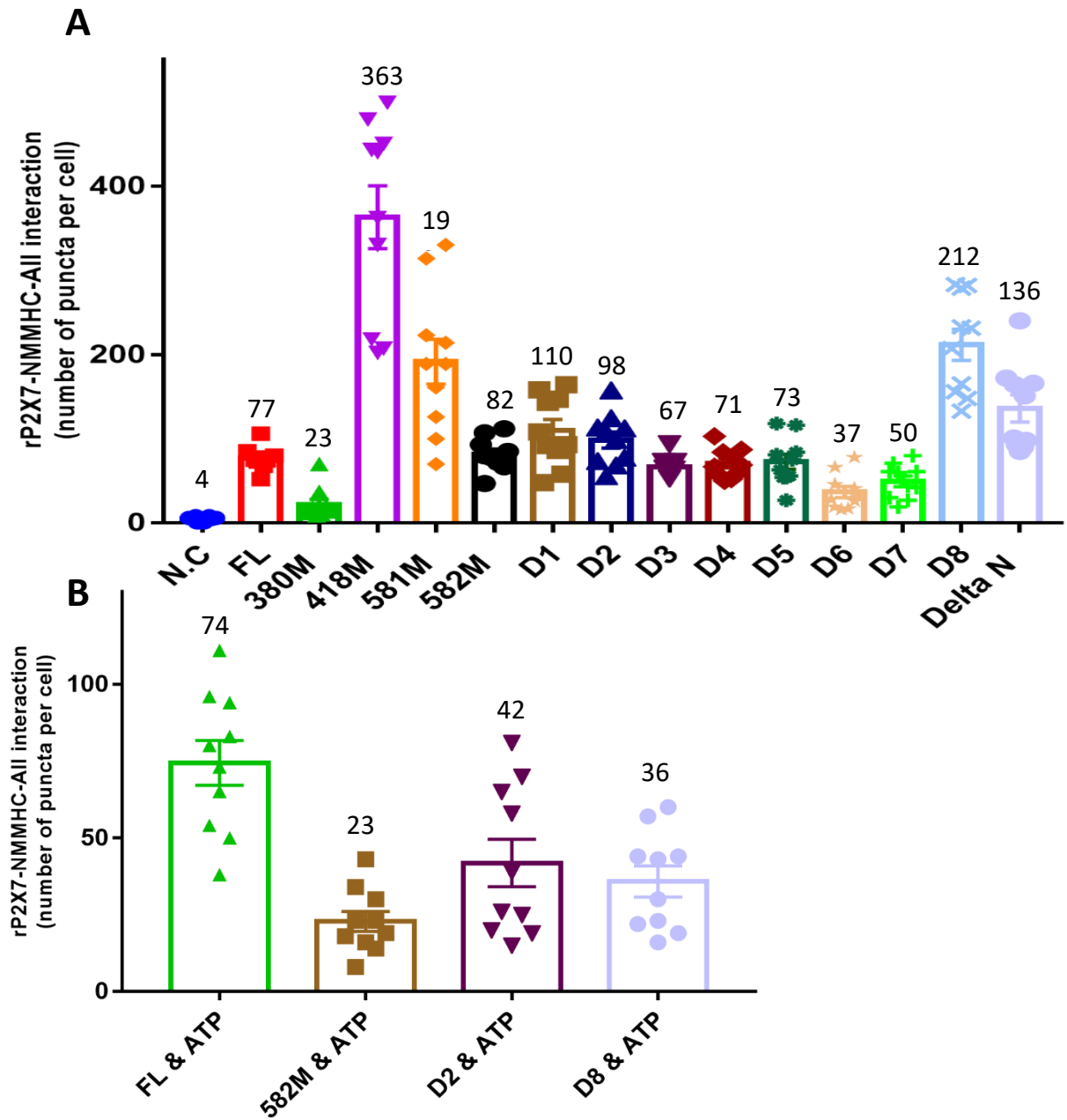


Figure 38: rP2X7-GFP-(His)₈-NMMHC-IIA interaction intensity

(A): rP2X7-GFP-(His)₈- NMMHC-IIA interaction intensity (number of puncta per cell).

(B): rP2X7-GFP-(His)₈- NMMHC-IIA interaction intensity (number of puncta per cell)

after ATP-treated and un-treated constructs. N.C: un-transfected Hela cells, FL: rP2X7-

GFP-(His)₈ full-length receptor. Average number of puncta is shown above each bar

(number of cells = 10).

5.2.3. No interaction between P2X7 and NMMHC-IIA is observed in pull-down assay

Our PLA data indicate that P2X7 and NMMHC-IIA are in close proximity, but we could not detect a change in the interaction upon ATP treatment. We therefore attempted to detect the interaction using the His-tag on our P2X7-GFP-(His)₈ construct as bait in pull-down assay using nickel beads. Total cellular protein was solubilized in either dodecyl maltoside (DDM; a relatively mild non-denaturing detergent) or fos-choline 12 (FC-12; a harsher detergent employed to reduce non-specific interactions) (Figure 39). HEK-293 cells not expressing the receptor were used as a negative control (labelled H), and HEK-293 cells stably expression P2X7 were used as experimental samples (P7). In DDM, NMMHC-IIA bound non-specifically to the pull-down assay beads (figure 39, top panel, elution and bead lanes), so it was not possible to determine whether or not there was an interaction. In FC-12, no non-specific binding was observed (figure 39, bottom panel, elution and bead lanes), but additionally there was no myosin present in the P2X7-containing elution or bead fractions. This data suggests that, under the conditions and timescale of our pull-down experiments, no specific interaction between NMMHC-IIA and P2X7 was maintained.

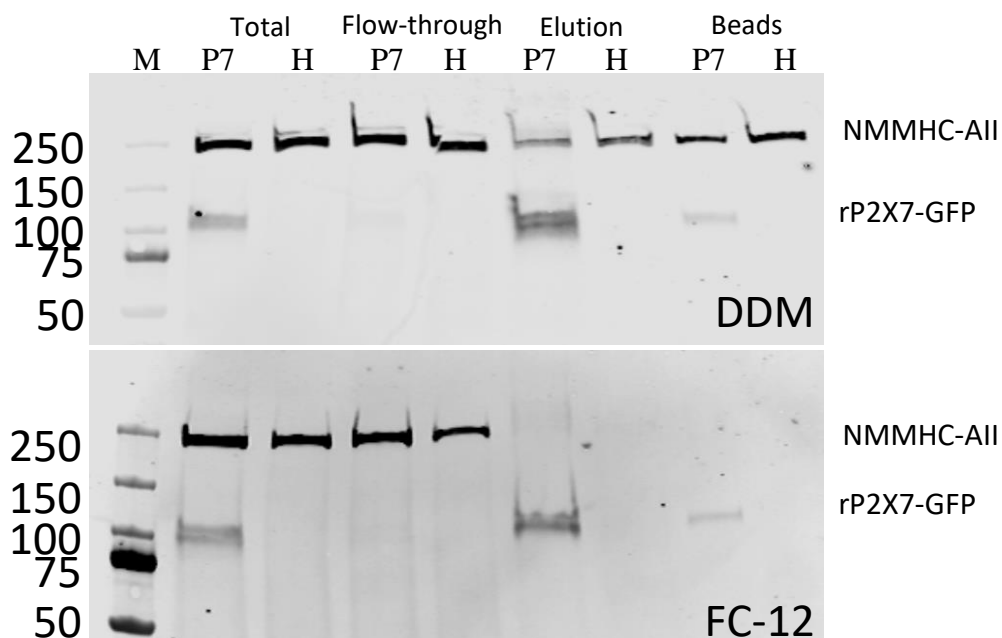


Figure 39: No interaction between rP2X7-GFP-(His)₈ and NMMHC-IIA was observed using pull-down assay

Top and bottom panels represent cell solubilized in DDM and FC-12, respectively. Total: total solubilized protein; flow-through: supernatant from bead pellet; Elution: supernatant from beads after elution addition. P7: HEK cells expressed rP2X7-GFP-(His)₈; H: HEK-293. This assay was performed by Joel Chubb (project student in Dr Young's lab) under my supervision.

5.2.4. Cell blebbing and pore formation in Cholesterol-depleted cells

The association of P2X7 receptors with cholesterol-rich lipid rafts has been reported in different cell-types such as peritoneal macrophages, osteoblasts, and lung alveolar cells. The cholesterol content of the membrane has also been shown to affect P2X7 plasma membrane expression and signalling phenomena such as pore formation (Robinson et al. 2014; Karasawa et al. 2017; Murrell-Lagnado 2017). For this reason, we wanted to investigate whether depletion of cellular cholesterol affected P2X7-dependent cell blebbing and pore formation, and if any of our mutants affected this.

5.2.4.1. Cholesterol depletion by Methyl- β -cyclodextrin (MCD)

To determine whether the incubation of HEK-293 cells with 5 mM MCD for 1 hour at 37°C depletes the plasma membrane cholesterol; we measured the cholesterol concentration (amplexTM red cholesterol assay; **section 2.2.3**) in HEK-293 and P2X7-stably transfected HEK-293 cells with and without MCD treatment, (Figure 40). The results show a significant reduction in cholesterol concentration following MCD treatment.

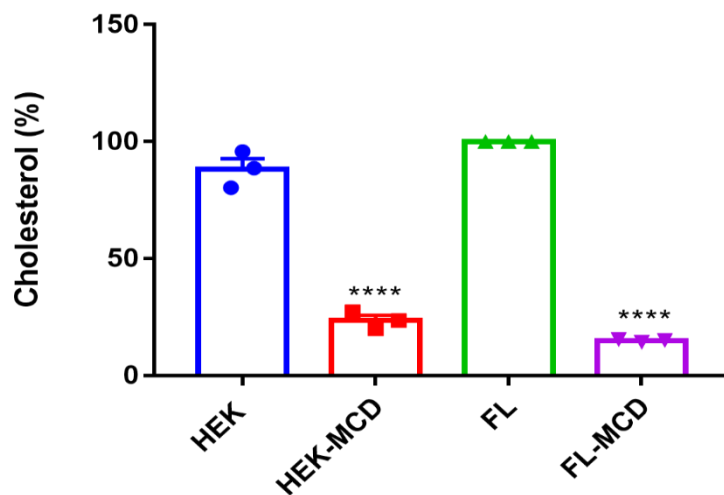


Figure 40: Quantification of cholesterol depletion in HEK-293 cells

HEK: HEK-293 MCD-untreated cells, HEK-MCD: HEK-293 MCD-treated cells, FL: rP2X7-GFP-(His)₈ MCD-untreated cells, and FL-MCD: rP2X7-GFP-(His)₈ MCD-treated cells. ****P represent P-value ≤ 0.0001 . representative mean \pm SEM from 3 independent experiments.

5.2.4.2. Cell blebbing in MCD pre-treated HEK-293 cells

HEK-293 cells transiently transfected with rP2X7-GFP-(His)₈ full-length receptor or mutant constructs were treated with 5 mM MCD for 1 hour at 37°C and then movies recorded for these cells in the same manner described in **section 2.4.1**. Unexpectedly, it was observed that cholesterol depletion completely abolished cell blebbing following 1 mM ATP application in all constructs, including rP2X7-GFP-(His)₈ full-length receptor (n=3; Figure 41; Appendix 12, 13, and 14).

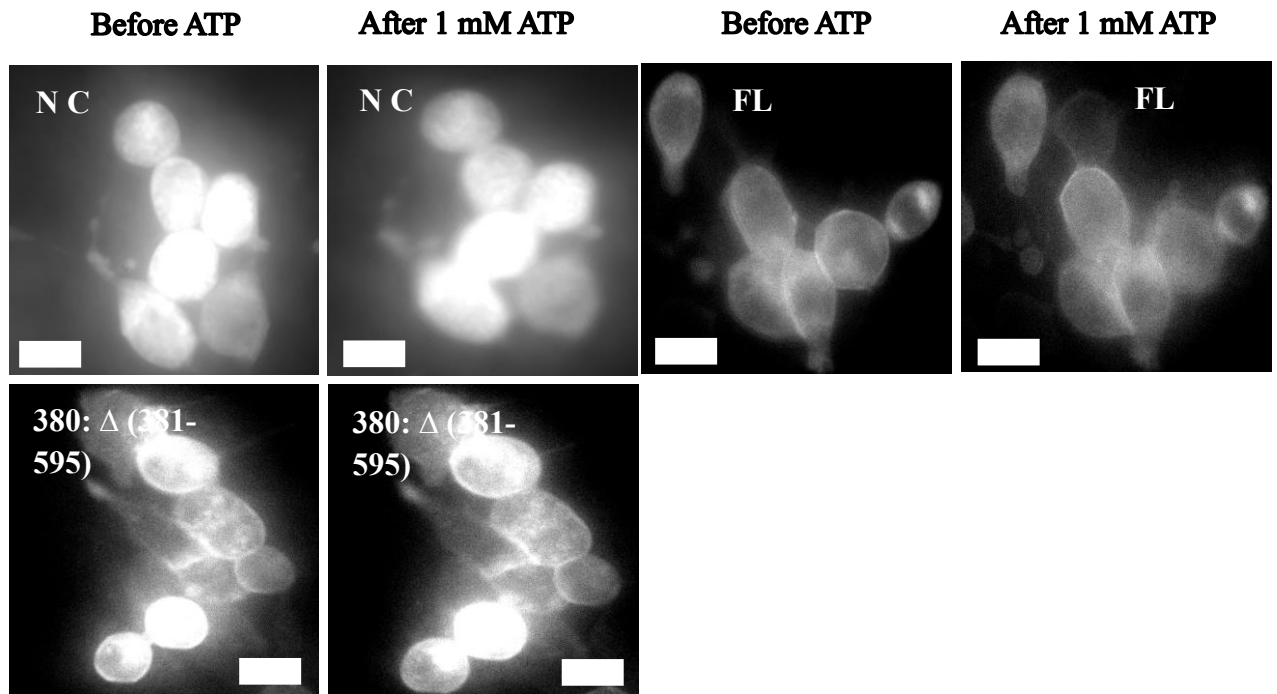


Figure 41: Cell blebbing in MCD-treated cells

N.C: HEK-293 cells transfected with GFP”, FL: rP2X7-GFP-(His)₈ full length. Scale bar represents 10 μ m. The figure shows representative images, the number of cells analysed per experiment varied between (2-8) from 3 independent experiments.

5.2.4.3. YO-PRO-1 dye uptake in MCD pre-treated HEK-293 cells

We measured YO-PRO-1 dye uptake for each construct in MCD pre-treated cells to determine the effect of cholesterol depletion on rP2X7-GFP-(His)₈ full-length and mutant construct-mediate pore formation (Figure 42; n=3). Interestingly, 380M and 418M (which were not capable of pore formation in MCD-untreated cells) exhibited a significantly increased dye uptake following cholesterol depletion. The same constructs that were capable of pore formation in MCD-untreated HEK-293 cells were also capable of pore formation in MCD-treated cells (rP2X7-GFP-(His)₈ full-length, 380M, 582M, D2, CRR, CRRa, CRRb, and C(X)A). We also found that dye uptake was significantly decreased with our CRRa construct. Our results are consistent with a role for cholesterol in inhibiting pore formation in the absence of the C-terminal domain, but potentially highlight a more subtle role for the C-Cys anchor region in this process.

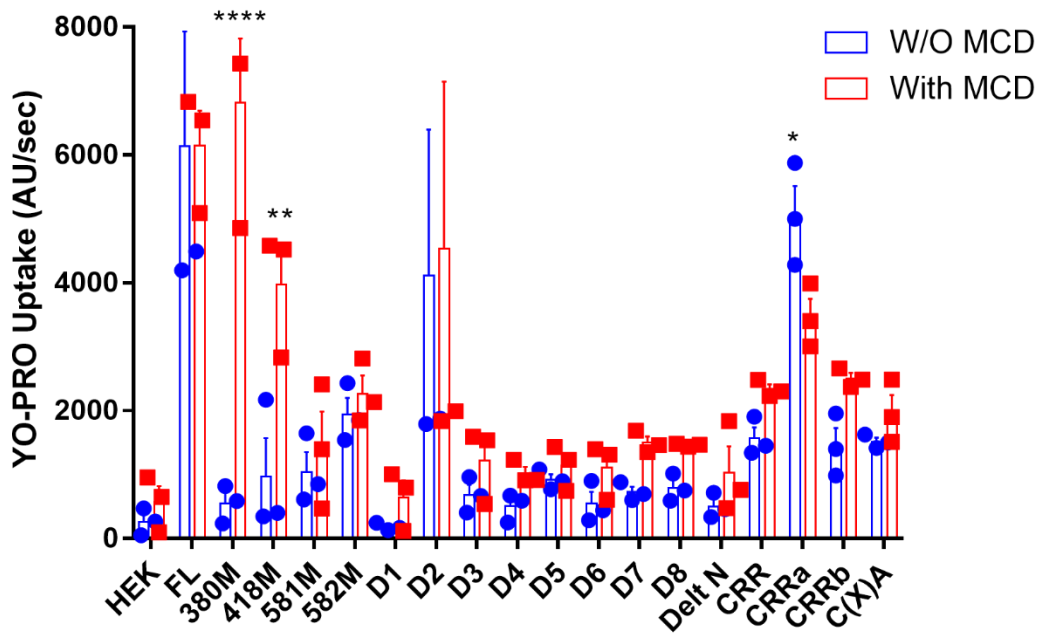


Figure 42: YO-PRO-1 dye uptake in MCD pre-treated and untreated HEK-293 cells

YO-PRO uptake \pm SEM; red columns show dye-uptake for constructs in MCD pre-treated cells, and blue columns show dye-uptake for constructs in MCD-untreated cells. *P, **P, and ****P represent P-value ≤ 0.05 , 0.0021 , and ≤ 0.0001 respectively.

5.3. Discussion

5.3.1. P2X7-NMMHC-AII dissociation and its role in cell blebbing

Further to a previous study that observed the localization and close proximity of P2X7 receptor and NMMHC-AII in HEK-293; a theory of ATP-induced cell blebbing resulting from P2X7-NMMHC-AII dissociation has been suggested (Gu et al. 2009). Here in this study, the similar *in-situ* experiment, PLA, confirmed the proximity of these two proteins in Hela cells. However, we did not observe a substantial change in proximity following 1 mM ATP application for 5 minutes; contrary to the previously reported FRET results which showed a decrease of P2X7- DsRed intensity in parallel with a slight increase of NMMHC-AIIAcGFP intensity over 15 minutes of ATP application (Gu et al. 2009). On potential confounding factor is that we observed proximity signals for P2X7 and myosin in constructs that we were unable to detect at the cell surface, potentially suggesting that proximity does not depend on cell-surface expression. If this is the case, any change in signal due to dissociation at the cell-surface would be masked by the intracellular interaction in our experiment. It may also be that myosin does not dissociate from P2X7, but rather from actin upon P2X7 receptor activation, allowing dissociation of P2X7 from cytoskeleton without disrupting the P2X7-myosin interaction. Further experiments looking at myosin phosphorylation (Qu et al. 2018) induced by P2X7 activation, and the proximity of P2X7 and actin before and after receptor activation may help to address this.

Because we could not confirm a role for myosin in the blebbing process, we performed a pull-down assay in an attempt to detect an interaction between the two proteins. We found that, using DDM as the solubilizing detergent, there was a non-specific interaction between P2X7 and the Ni-sepharose resin, so we used a slightly harsher detergent (FC-12) in the experiment. FC-12 eliminated the non-specific interaction, but surprisingly there was no interaction between P2X7 and NMMHC-AII. This result suggests that either the PLA data is a false-positive, or (perhaps more likely) that the two proteins are in close proximity at the membrane but do not physically interact in a way that can survive solubilization in FC-12.

5.3.2. P2X7 induced cell blebbing and pore formation are uncoupled by membrane cholesterol depletion

Several studies have observed the association of P2X7 receptor with cholesterol-rich lipid rafts. While P2X7 pore formation and channel activity are enhanced by cholesterol depletion using MCD, its reduction by loading of cholesterol confirms the inhibitory role of cholesterol on P2X7 signalling (Robinson et al. 2014; Karasawa et al. 2017; Murrell-Lagnado 2017).






This study assessed the behaviour of rP2X7-GFP-(His)₈ and our mutant constructs in cholesterol-depleted HEK-293 in terms of pore formation and cell blebbing. Following cholesterol depletion, YO-PRO-1 dye uptake was significantly enhanced with 380M and 418M, but it was significantly reduced with CRRa: Δ (362-370) construct. Interestingly, cholesterol depletion abolished cell blebbing in all constructs including full-length receptor; suggesting that blebbing has an absolute requirement for cholesterol. We cannot say whether this is due to a general effect on membrane fluidity induced by cholesterol depletion, or if it is due to a specific requirement for cholesterol by P2X7 (e.g. by changing the structure of the receptor, changing the downstream processes that result from activation, or changing the membrane localization (and potentially other interactions as a result)).

Chapter 6: General Discussion

Table 10 shows the results summary for all constructs studied in this thesis

Table 10: Results summary

P2X7-GFP construct	Deleted portion	Ca influx	Signalling pathways						
			Cell blebbing	P-ERK1/2				Pore formation	Cell-surface
				Un-Stimulated		Stimulated			
				ERK1	ERK2	ERK1	ERK2		
Full length	No deletion	++++	Yes	-	+	+	++++	++++	++++
380M	Δ (381-595)	-	Yes	-	+	+	+	+	++
418M	Δ (419-595)	++++	No	-	+	-	+	-	-
581M	Δ (582-595)	-	No	-	-	+	++	-	+
582M	Δ (583-595)	-	Yes	+	+	+	-	++++	++
D1	Δ (389-405)	-	No	+	+	-	++	-	+
D2	Δ (441-460)	++++	Yes	-	+	-	+	++++	++
D3	Δ (494-508)	-	No	-	-	-	++	-	+
D4	Δ (389-531)	-	No	+	+	+	-	-	+
D5	Δ (381-417)	-	No	+	+	+	+	-	-

P2X7- GFP construct	Deleted portion	Ca influx	Signalling pathways						
			Cell blebbing	P-ERK				Pore formation	Cell- surface
				Un-Stimulated		Stimulated			
				ERK1	ERK2	ERK1	ERK2		
D6	Δ (441-493)	-	No	+	+	+	+	-	+
D7	Δ (418-460)	-	No	+	+	+	+	-	+
D8	Δ (583-595) & Δ (441-460)	-	No	+	+	+	+	-	+
ΔN	Δ (2-23)	-	No	+	+			-	-
CRR	Δ (362-379)	-	Yes	+	+	-	+		++
CRRa	Δ (362-370)	++++	Yes	+	+	+	+	++++	++
CRRb	Δ (371-379)	-	No	+	+	-	+		+
C(X)A	C371A C373A C374A C377A	-	Yes	+	+	-	+		++

Cell blebbing expressed as (yes or no), calcium influx and pore formation are expressed as (-) if the mutant does not induce the pathway and (+) if it causes it; the number of plus signs on the relative size of the response (one plus for a significant difference from negative control, more for a bigger response). ERK1/2 phosphorylation is expressed as (-) if the mutant does not induce ERK phosphorylation and (+) if it causes it; the number of plus signs on the relative level of ERK phosphorylation. For cell-surface expression; (-) indicate no cell-surface or very low expression and (+) indicate cell-surface expression, more (+) indicate the relative level of cell-surface expression. Key results are highlighted in grey.

6.1. The C-terminal GFP-(His)₈ tag does not affect receptor function

Tagging receptors with fluorescent proteins might cause functional changes. Our receptor construct was fused with GFP-(His)₈ at the C-terminus of the receptor to enable us to visualise cell blebbing using fluorescence microscopy and performing pull-down assays using the (His)₈ tag. To confirm that this tag did not have a substantial effect on rP2X7 function, we compared it with the untagged receptor in terms of calcium influx, pore formation and ERK1/2 phosphorylation.

While our comparison demonstrated that the GFP-(His)₈ tag on the C-terminus of rP2X7 did not affect receptor function, it would be important to repeat some of our experiments using untagged receptors, particularly the D2 and Δ N mutants. We also cannot rule out a subtle effect on the pathway that mediates cell blebbing as we did not make this comparison in our experiments.

6.2. P2X7 intracellular domains are important for cell-surface protein expression

This study demonstrates the importance of the structural integrity of the P2X7 intracellular domains for cell-surface expression. We found that all our mutants constructs displayed reduced or absent cell-surface protein expression, indicating that disruption or removal of intracellular domains likely impaired the ability of the protein to get to the cell surface. In some cases our mutations removed known trafficking motifs (e.g. C-terminal truncations) (Chaumont et al. 2004), but in others they will have disrupted globular domains (e.g. the ballast domain), potentially leading to protein misfolding. For any mutant which was absent at the cell-surface, we cannot say whether or not this was due to altered trafficking or misfolding, and we cannot ascribe any signalling function to the domains which are absent in those mutants. In light of the rat P2X7 cryoEM structure (McCarthy et al. 2019b) it is clear that many of our constructs represent a substantial disruption to the ballast domain. It is therefore not surprising that receptor lacking D4: Δ (389-531), D5: Δ (381-

417), D6: Δ (441-493), and D7: Δ (418-460), and Δ N: Δ (2-23) severely affected cell-surface protein expression and receptor signalling pathways. This demonstrates the importance of the integrity of the ballast domain and N-terminus for correct protein trafficking to the cell membrane. Even though cell-surface protein expression was impaired in all our mutants, some constructs were still capable of mediating P2X7 signalling pathways and/or calcium channel activity, allowing us to draw some conclusions about the potential role of intracellular domains in these pathways.

6.3. Cell blebbing and pore formation may not require the intracellular domains, but are regulated by them

A role for P2X7 in both cell proliferation and death has been previously reported (De Marchi et al. 2016). This raises the question of whether P2X7 has distinct domains which mediate cell death or proliferation. It is known that activation of the P2X7 receptor by extracellular ATP for sustained duration (>30 min) causes irreversible cell blebbing which eventually leads to cell death (Mackenzie et al. 2005); it is the same with prolonged activation and pore formation, which would permit the prolonged opening of a pore for large molecules (900 kDa) in the plasma membrane; hinting that both blebbing and pore formation are early markers of cell death and the same domains of P2X7 receptor may regulate it.

Our findings demonstrate that nearly all our constructs capable of ATP-induced cell blebbing were also capable of ATP-induced YO-PRO-1 uptake. We were able to replicate the results of Smart *et al.* (Smart et al. 2003), showing that the truncation 582M was capable of YO-PRO-1 uptake, but the truncation 581M was not, and this was also the case for cell blebbing (with caveat that in our study the truncation 581M was not highly expressed at the cell surface). However, we also found that the truncation 380M, lacking nearly the entire ballast domain, was capable of cell blebbing and pore formation (in the cholesterol-depleted condition), and that the construct CRR, lacking the C-Cys anchor region, was also capable of blebbing and pore formation (albeit with very low calcium channel activity). This data suggests that the C-Cys anchor and ballast domain may not be required for either cell blebbing or YO-PRO-1 uptake.

6.4. Cell blebbing and pore formation in the light of recent cryoEM rat P2X7 structure-N-terminal domain, C-Cys anchor and ballast

Our construct lacking the N-terminal domain (Δ N lacking amino-acids 2-23) was not capable of calcium influx, cell blebbing, pore formation, or ERK phosphorylation, and indeed displayed very low levels of the cell-surface protein expression, suggesting that the N terminus is essential for cell-surface protein expression.

Within the C-Cys anchor domain, we constructed four mutants (CRR, CRRa, CRRb, C(X)A)); all of them were capable of cell blebbing and pore formation except CRRb which was only capable of pore formation. We did not observe enhanced YO-PRO-1 uptake in these constructs under conditions of cholesterol depletion, which is somewhat contrary to results obtained by the Kawate group, who demonstrated that panda P2X7 receptors lacking the N- and C- termini domains but extended to contain the cysteine-rich region (CRR) displayed significantly enhanced YO-PRO uptake in HEK-293 cells, potentially suggesting that the CRR region counteracts the inhibitory effect of membrane cholesterol (Karasawa et al. 2017). This comparison between our findings and their results is not strictly accurate because (as well as being from different species) our construct also contains the N-terminal domain and ballast, whereas their construct just contained the extracellular and transmembrane domains extended with the CRR. However, our findings suggest that C-Cys anchor domain may not be required for pore formation and cell blebbing. It could be (for example) that in our construct the N-terminal domain or ballast domain is also able to sequester cholesterol to prevent inhibition of pore formation.

The rest of our constructs are located within the P2X7 ballast domain. Surprisingly, receptors lacking the nearly entire ballast domain (380M: Δ (381-595)) were capable of cell blebbing and pore formation, potentially suggesting that the ballast domain is not required for P2X7-mediated cell blebbing and pore formation. Our results are contrary to those of Smart *et al* findings in terms of pore formation, which suggested the requirement of 95% of ballast domain for pore formation by the activated P2X7 receptor (Smart et al. 2003).

6.5. P2X7 lies in close proximity to NMMHC-IIA, but does not necessarily dissociate from it on activation

Investigation of the mechanism of P2X7-dependent cell blebbing found no evidence for uncoupling of non-muscle myosin from P2X7 following receptor activation but did demonstrate an absolute requirement for cholesterol. We detected the expression of NMMHC-IIA in HEK-293 and HeLa cells and demonstrated that P2X7 and NMMHC-IIA were in close proximity within HeLa cells, but did not observe a significant change in the degree of proximity when P2X7 receptors were activated by ATP. As a result, P2X7-mediated cell blebbing may occur independently of P2X7-myosin dissociation, contrary to what has been proposed by the Wiley group (Gu et al. 2009).

However, it is known that actin is associated with myosin in muscle and non-muscle cells and that the role of myosin is that of the molecular motor, converting chemical energy (ATP hydrolysis) to mechanical energy in the form of muscle contraction and cell motility in non-muscle cells (Qu et al. 2018). Activation of P2X7 receptor by extracellular ATP may lead to the dissociation of actin protein from the P2X7-myosin complex, generating the mechanical force to induce cell blebbing, a process that plays an essential role in cell migration and movement. Further experiments should include investigating the proximity of P2X7 to actin before and after receptor activation, in addition to measuring myosin phosphorylation which can lead to its dissociation from actin (Qu et al. 2018).

6.6. Cell blebbing and pore formation are uncoupled by depletion of membrane cholesterol

The molecular mechanism of P2X7-mediated cell blebbing remains unclear, but our results suggest that cell blebbing and pore formation are coupled, in the sense that nearly all our mutants that were capable of blebbing were also capable of pore formation. This may mean that P2X7-induced cell blebbing and pore formation proceed *via* similar mechanisms, or just they are both intrinsic to the ion channel (i.e. they do not require the intracellular domains). Karasawa *et al* demonstrated that membrane cholesterol depletion by MCD pre-treatment of HEK-293 cells potentiated PdP2X7-mediate YO-PRO-1 uptake (Karasawa *et al.* 2017) which gave rise to questions about the role of cholesterol in cell blebbing.

In contrast to Karasawa *et al*, we did not observe potentiation of wild-type P2X7 receptor YO-PRO-1 uptake following cholesterol depletion, but we did observe this for our 380M and 418M truncation mutants, hinting at a similar role for cholesterol in inhibition of pore formation in truncated channels. Most surprisingly, we found that cholesterol depletion completely abolished ATP-dependent cell blebbing. This could be a generalized effect on membrane fluidity from loss of the plasticizing effects of cholesterol (Kahya *et al.* 2003; Crane and Tamm 2004), but it is tempting to speculate that cholesterol depletion may have a specific impact on P2X7 function and/or localization in the membrane.

P2X7 receptors are known to associate with ‘lipid raft’ like plasma membrane microdomains (Barth *et al.* 2007), are heavily palmitoylated both in the C-Cys anchor region (Gonnord *et al.* 2009; Karasawa *et al.* 2017; McCarthy *et al.* 2019b) and N-terminal domain (Karasawa *et al.* 2017; McCarthy *et al.* 2019b), and a physical interaction with cholesterol has been proposed. It may be that cholesterol depletion either disrupts the raft localization of P2X7 or directly affects the receptor structure, organization or stability. P2X7 receptors have been shown to interact with epithelial membrane proteins (EMPs), overexpression of which leads to constitutive membrane blebbing (Wilson *et al.* 2002), and EMPs are known to recruit proteins to lipid rafts (Wadehra *et al.* 2003), so it may be that disruption of rafts by cholesterol depletion disrupts the physical coupling of P2X7 receptors and EMPs.

Our finding that the receptor lacking C-Cys anchor domain, was still capable of blebbing would seem to go against this speculation, but deletion of this region would not fully ‘de-palmitoylate’ the receptor, as the N-terminal domain which lies parallel to the membrane is also palmitoylated, and this might be sufficient to localize the receptor to a lipid raft.

6.7. The ‘hidden’ region in the recent P2X7 structure; D2: Δ (441-460)

One truncation capable of blebbing, YO-PRO-1 uptake and calcium influx was D2 (deletion of amino acid residues 441-460). This region corresponds to the region of missing density in the rat P2X7 cryoEM structure (McCarthy et al. 2019b). This region has 40% homology with human SH3 domain-binding protein 1. SH3 domains are known to mediate protein interactions and act as scaffolds (Denlinger et al. 2001; Kopp et al. 2019b).

Because density for this region is missing in the cryoEM structure, it is not possible to know for certain how it connects the N-terminal portion of the ballast domain to the C-terminal portion, meaning that domain-swapping (where each ballast domain is composed of protein sequence from 2 different subunits) is a possibility (McCarthy et al. 2019b). Deletion of the D2 region might be considered likely to prevent domain swapping. Our observation that the D2 truncation is functional may suggest that domain swapping is not a feature of the ballast domain (or at least not required for functional protein expression).

6.8. The P2X7 intracellular domains may mediate ERK1/2 phosphorylation

The conclusions that can be drawn from our experiments to determine which portions of the intracellular domains regulate ERK1/2 phosphorylation were limited due to lack of appropriate controls loaded on each Western blot, but we were able to show that the full-length receptor was capable of mediating ATP-induced ERK1/2 phosphorylation, whereas nearly all our truncation mutants were not. This finding suggests that P2X7-induced ERK1/2 phosphorylation is very sensitive to disruption of the intracellular domains, and in light of this, our mutations were too crude to enable us to draw specific conclusions about the domains involved. However, it is interesting that the ballast deletion mutations D2 (441-460) and 582M were both capable of blebbing and pore formation, but seemingly not capable of ERK phosphorylation. This finding may implicate the ballast domain as the site of coupling of P2X7 activation to ERK1/2 phosphorylation, but more careful experiments with less disrupting mutations need to be done before a strong conclusion can be drawn.

Strikingly, when we analysed ERK1/2 phosphorylation by the Δ N mutant (always loaded on the same blots as our full-length construct), we found that ERK1/2 were phosphorylated before stimulus with ATP, and dephosphorylated after stimulus. This was despite the fact that we saw no detectable protein at the cell surface, and no activity in any other assays. How could (a) the Δ N mutant seemingly constitutively activate ERK1/2, and (b) reduce this activation upon ATP treatment, if it is not at the cell-surface? The short answer is that we do not know. It may be that our cell-surface protein assay is not very sensitive, and channels can be present at the cell surface but we are unable to detect them. It may be that the Δ N mutant is overexpressed but misfolded, and that this causes stress to the cell which leads to ERK1/2 activation, but why then would ATP treatment reduce this? To address this question we need to make a series of less deleterious mutations in the N-terminal domain, which have detectable cell-surface expression and channel function, and analyse this phenomenon more carefully. These findings may suggest that the N-terminal domain (or lack of it) changes the way that P2X7 couples to the ERK1/2 cascade, but we cannot speculate on how.

We know that the MAPK family is very large, including ERKs, JNKs and p38/SAPKs, and it regulates several biological responses such as cell proliferation, cell differentiation, and cell death (Qi and Elion 2005; Raman et al. 2007; Keshet and Seger 2010). The essential steps in MAPK activation involve; (i) a specific extracellular signal received by a cell membrane receptor such as P2X7, (ii) interaction of a small GTPase with MAPKKK to provide the phosphate group which triggers MAPKKK, and (iii) a high-affinity docking site for the upstream kinase and downstream substrate (Morrison 2012).

The P2X7 intracellular domains may thus also serve as a docking site for kinases and/or their substrates to transfer the upstream signal to downstream ERK1/2 which in turn mediates the biological response. P2X7 has been reported to bind a large number of proteins (for a comprehensive review see (Kopp et al. 2019b)), but there are no clear targets (for example small G-proteins that are calcium-dependent) in this list. It is very interesting that the ballast domain is capable of binding both GDP and GTP, but no conformational or binding change was observed in the ATP-bound cryoEM structure (McCarthy et al. 2019b) to indicate that it could play a role in transduction of a channel activation signal to effector proteins.

Recommendations and future work

In this study, we have focused on just three signalling pathways mediated by P2X7 receptor in addition to channel activity, and all of them were measured in HEK-293 cell. We only investigated two potential factors essential for cell blebbing (membrane cholesterol and P2X7-NMMHC-AII interaction). While the study has provided some useful insights, work is still required in several areas to support and build on them.

Firstly, we suggest expanding this work by studying the other P2X7 receptor signalling pathways such as cytokines release and phospholipid flip in various cell lines, including those of more immediate physiological relevance, such as macrophages. Also, in the light of recently published rat P2X7 cryoEM structure, we would construct more targeted mutations in the ballast domain, including within the GDP and Zn^{+2} pockets to determine their importance for P2X7 function and stability.

Secondly, the molecular mechanism for cell blebbing remains unclear. While our findings suggest that blebbing is not due to P2X7-myosin dissociation, we have not conclusively ruled out an interaction between the two proteins. It may be that targeting the myosin-actin interaction may be more useful. Our data does show an absolute requirement for membrane cholesterol in the blebbing process, but whether or not this is due to a specific interaction between P2X7 and cholesterol, or a more generalized membrane effect is not clear. Either of these hypotheses could be tested using FRET (perhaps using fluorescent cholesterol derivatives) or PLA.

References

Adinolfi, E. et al. 2009. Expression of the P2X7 receptor increases the Ca²⁺ content of the endoplasmic reticulum, activates NFATc1, and protects from apoptosis. *J Biol Chem* 284(15), pp. 10120-10128. doi: 10.1074/jbc.M805805200

Adinolfi, E. et al. 2005. Basal activation of the P2X7 ATP receptor elevates mitochondrial calcium and potential, increases cellular ATP levels, and promotes serum-independent growth. *Mol Biol Cell* 16(7), pp. 3260-3272. doi: 10.1091/mbc.E04-11-1025

Adinolfi, E., Capece, M., Amoroso, F., De Marchi, E. and Franceschini, A. 2015. Emerging roles of P2X receptors in cancer. *Curr Med Chem* 22(7), pp. 878-890.

Adinolfi, E. et al. 2010. Trophic activity of a naturally occurring truncated isoform of the P2X7 receptor. *Faseb j* 24(9), pp. 3393-3404. doi: 10.1096/fj.09-153601

Adinolfi, E., Giuliani, A. L., De Marchi, E., Pegoraro, A., Orioli, E. and Di Virgilio, F. 2018. The P2X7 receptor: A main player in inflammation. *Biochem Pharmacol* 151, pp. 234-244. doi: 10.1016/j.bcp.2017.12.021

Adinolfi, E., Kim, M., Young, M. T., Di Virgilio, F. and Surprenant, A. 2003. Tyrosine phosphorylation of HSP90 within the P2X7 receptor complex negatively regulates P2X7 receptors. *J Biol Chem* 278(39), pp. 37344-37351. doi: 10.1074/jbc.M301508200

Adinolfi, E. et al. 2002. P2X7 receptor expression in evolutive and indolent forms of chronic B lymphocytic leukemia. *Blood* 99(2), pp. 706-708.

Adinolfi, E. et al. 2012. Expression of P2X7 receptor increases in vivo tumor growth. *Cancer Res* 72(12), pp. 2957-2969. doi: 10.1158/0008-5472.Can-11-1947

Aga, M., Watters, J. J., Pfeiffer, Z. A., Wiepz, G. J., Sommer, J. A. and Bertics, P. J. 2004. Evidence for nucleotide receptor modulation of cross talk between MAP kinase and NF-kappa B signaling pathways in murine RAW 264.7 macrophages. *Am J Physiol Cell Physiol* 286(4), pp. C923-930. doi: 10.1152/ajpcell.00417.2003

Al-Shukaili, A. et al. 2011. P2X7 receptor gene polymorphism analysis in rheumatoid arthritis. *Int J Immunogenet* 38(5), pp. 389-396. doi: 10.1111/j.1744-313X.2011.01019.x

- Alberto, A. V. et al. 2013. Is pannexin the pore associated with the P2X7 receptor? *Naunyn Schmiedeberg's Arch Pharmacol* 386(9), pp. 775-787. doi: 10.1007/s00210-013-0868-x
- Allsopp, R. C., Lalo, U. and Evans, R. J. 2010. Lipid raft association and cholesterol sensitivity of P2X1-4 receptors for ATP: chimeras and point mutants identify intracellular amino-terminal residues involved in lipid regulation of P2X1 receptors. *J Biol Chem* 285(43), pp. 32770-32777. doi: 10.1074/jbc.M110.148940
- Alves, L. A., de Melo Reis, R. A., de Souza, C. A., de Freitas, M. S., Teixeira, P. C., Neto Moreira Ferreira, D. and Xavier, R. F. 2014. The P2X7 receptor: shifting from a low- to a high-conductance channel - an enigmatic phenomenon? *Biochim Biophys Acta* 1838(10), pp. 2578-2587. doi: 10.1016/j.bbamem.2014.05.015
- Alves, M., Beamer, E. and Engel, T. 2018. The Metabotropic Purinergic P2Y Receptor Family as Novel Drug Target in Epilepsy. *Front Pharmacol* 9, p. 193. doi: 10.3389/fphar.2018.00193
- Amoroso, F. et al. 2015. The P2X7 receptor is a key modulator of the PI3K/GSK3 β /VEGF signaling network: evidence in experimental neuroblastoma. *Oncogene* 34(41), pp. 5240-5251. doi: 10.1038/onc.2014.444
- Amoroso, F., Falzoni, S., Adinolfi, E., Ferrari, D. and Di Virgilio, F. 2012. The P2X7 receptor is a key modulator of aerobic glycolysis. *Cell Death Dis* 3, p. e370. doi: 10.1038/cddis.2012.105
- Amstrup, J. and Novak, I. 2003. P2X7 receptor activates extracellular signal-regulated kinases ERK1 and ERK2 independently of Ca²⁺ influx. *Biochem J* 374(Pt 1), pp. 51-61. doi: 10.1042/bj20030585
- Babiychuk, E. B., Monastyrskaya, K., Potez, S. and Draeger, A. 2011. Blebbing confers resistance against cell lysis. *Cell Death Differ* 18(1), pp. 80-89. doi: 10.1038/cdd.2010.81
- Bang, S., Jeong, E. J., Kim, I. K., Jung, Y. K. and Kim, K. S. 2000. Fas- and tumor necrosis factor-mediated apoptosis uses the same binding surface of FADD to trigger signal transduction. A typical model for convergent signal transduction. *J Biol Chem* 275(46), pp. 36217-36222. doi: 10.1074/jbc.M006620200
- Bao, L., Locovei, S. and Dahl, G. 2004. Pannexin membrane channels are mechanosensitive conduits for ATP. *FEBS Lett* 572(1-3), pp. 65-68. doi: 10.1016/j.febslet.2004.07.009

- Bardwell, L. and Thorner, J. 1996. A conserved motif at the amino termini of MEKs might mediate high-affinity interaction with the cognate MAPKs. *Trends Biochem Sci* 21(10), pp. 373-374.
- Bargiotas, P. et al. 2011. Pannexins in ischemia-induced neurodegeneration. *Proc Natl Acad Sci U S A* 108(51), pp. 20772-20777. doi: 10.1073/pnas.1018262108
- Baricordi, O. R. et al. 1996. An ATP-activated channel is involved in mitogenic stimulation of human T lymphocytes. *Blood* 87(2), pp. 682-690.
- Barrera, N. P., Ormond, S. J., Henderson, R. M., Murrell-Lagnado, R. D. and Edwardson, J. M. 2005. Atomic force microscopy imaging demonstrates that P2X2 receptors are trimers but that P2X6 receptor subunits do not oligomerize. *J Biol Chem* 280(11), pp. 10759-10765. doi: 10.1074/jbc.M412265200
- Barth, K., Weinhold, K., Guenther, A., Linge, A., Gereke, M. and Kasper, M. 2008. Characterization of the molecular interaction between caveolin-1 and the P2X receptors 4 and 7 in E10 mouse lung alveolar epithelial cells. *Int J Biochem Cell Biol* 40(10), pp. 2230-2239. doi: 10.1016/j.biocel.2008.03.001
- Barth, K., Weinhold, K., Guenther, A., Young, M. T., Schnittler, H. and Kasper, M. 2007. Caveolin-1 influences P2X7 receptor expression and localization in mouse lung alveolar epithelial cells. *FEBS J* 274(12), pp. 3021-3033. doi: 10.1111/j.1742-4658.2007.05830.x
- Bartlett, R., Stokes, L. and Sluyter, R. 2014. The P2X7 receptor channel: recent developments and the use of P2X7 antagonists in models of disease. *Pharmacol Rev* 66(3), pp. 638-675. doi: 10.1124/pr.113.008003
- Bartlett, R., Yerbury, J. J. and Sluyter, R. 2013. P2X7 receptor activation induces reactive oxygen species formation and cell death in murine EOC13 microglia. *Mediators Inflamm* 2013, p. 271813. doi: 10.1155/2013/271813
- Becker, D., Woltersdorf, R., Boldt, W., Schmitz, S., Braam, U., Schmalzing, G. and Markwardt, F. 2008. The P2X7 carboxyl tail is a regulatory module of P2X7 receptor channel activity. *J Biol Chem* 283(37), pp. 25725-25734. doi: 10.1074/jbc.M803855200
- Belambri, S. A., Rolas, L., Raad, H., Hurtado-Nedelec, M., Dang, P. M. and El-Benna, J. 2018. NADPH oxidase activation in neutrophils: Role of the phosphorylation of its subunits. *Eur J Clin Invest* 48 Suppl 2, p. e12951. doi: 10.1111/eci.12951

- Benzaquen, J., Heeke, S., Janho Dit Hreich, S., Douguet, L., Marquette, C. H., Hofman, P. and Vouret-Craviari, V. 2019. Alternative splicing of P2RX7 pre-messenger RNA in health and diseases: Myth or reality? *Biomed J* 42(3), pp. 141-154. doi: 10.1016/j.bj.2019.05.007
- Bessonov, S. et al. 2010. Characterization of purified human Bact spliceosomal complexes reveals compositional and morphological changes during spliceosome activation and first step catalysis. *Rna* 16(12), pp. 2384-2403. doi: 10.1261/rna.2456210
- Bianchi, G. et al. 2014. ATP/P2X7 axis modulates myeloid-derived suppressor cell functions in neuroblastoma microenvironment. *Cell Death Dis* 5, p. e1135. doi: 10.1038/cddis.2014.109
- Blaukat, A., Ivankovic-Dikic, I., Grönroos, E., Dolfi, F., Tokiwa, G., Vuori, K. and Dikic, I. 1999. Adaptor proteins Grb2 and Crk couple Pyk2 with activation of specific mitogen-activated protein kinase cascades. *J Biol Chem* 274(21), pp. 14893-14901. doi: 10.1074/jbc.274.21.14893
- Bo, X., Jiang, L. H., Wilson, H. L., Kim, M., Burnstock, G., Surprenant, A. and North, R. A. 2003. Pharmacological and biophysical properties of the human P2X5 receptor. *Mol Pharmacol* 63(6), pp. 1407-1416. doi: 10.1124/mol.63.6.1407
- Bobanovic, L. K., Royle, S. J. and Murrell-Lagnado, R. D. 2002. P2X receptor trafficking in neurons is subunit specific. *J Neurosci* 22(12), pp. 4814-4824.
- Boldt, W., Klapperstück, M., Büttner, C., Sadtler, S., Schmalzing, G. and Markwardt, F. 2003. Glu496Ala polymorphism of human P2X7 receptor does not affect its electrophysiological phenotype. *Am J Physiol Cell Physiol* 284(3), pp. C749-756. doi: 10.1152/ajpcell.00042.2002
- Boué-Grabot, E., Archambault, V. and Séguéla, P. 2000. A protein kinase C site highly conserved in P2X subunits controls the desensitization kinetics of P2X(2) ATP-gated channels. *J Biol Chem* 275(14), pp. 10190-10195. doi: 10.1074/jbc.275.14.10190
- Boumechache, M., Masin, M., Edwardson, J. M., Gorecki, D. C. and Murrell-Lagnado, R. 2009. Analysis of assembly and trafficking of native P2X4 and P2X7 receptor complexes in rodent immune cells. *J Biol Chem* 284(20), pp. 13446-13454. doi: 10.1074/jbc.M901255200
- Boyce, A. K. J. and Swayne, L. A. 2017. P2X7 receptor cross-talk regulates ATP-induced pannexin 1 internalization. *Biochem J* 474(13), pp. 2133-2144. doi: 10.1042/bcj20170257
- Bradford, M. D. and Soltoff, S. P. 2002. P2X7 receptors activate protein kinase D and p42/p44 mitogen-activated protein kinase (MAPK) downstream of protein kinase C. *Biochem J* 366(Pt 3), pp. 745-755. doi: 10.1042/bj20020358

Brake, A. J., Wagenbach, M. J. and Julius, D. 1994. New structural motif for ligand-gated ion channels defined by an ionotropic ATP receptor. *Nature* 371(6497), pp. 519-523. doi: 10.1038/371519a0

Budagian, V., Bulanova, E., Brovko, L., Orinska, Z., Fayad, R., Paus, R. and Bulfone-Paus, S. 2003. Signaling through P2X7 receptor in human T cells involves p56lck, MAP kinases, and transcription factors AP-1 and NF-kappa B. *J Biol Chem* 278(3), pp. 1549-1560. doi: 10.1074/jbc.M206383200

Buell, G. N., Talabot, F., Gos, A., Lorenz, J., Lai, E., Morris, M. A. and Antonarakis, S. E. 1998. Gene structure and chromosomal localization of the human P2X7 receptor. *Recept Channels* 5(6), pp. 347-354.

Buratti, E., Baralle, M. and Baralle, F. E. 2006. Defective splicing, disease and therapy: searching for master checkpoints in exon definition. *Nucleic Acids Res* 34(12), pp. 3494-3510. doi: 10.1093/nar/gkl498

Burnstock, G. 2013. Introduction and perspective, historical note. *Front Cell Neurosci* 7, p. 227. doi: 10.3389/fncel.2013.00227

Burnstock, G. 2017. Purinergic Signalling: Therapeutic Developments. *Front Pharmacol* 8, p. 661. doi: 10.3389/fphar.2017.00661

Burnstock, G., Evans, L. C. and Bailey, M. A. 2014. Purinergic signalling in the kidney in health and disease. *Purinergic Signal* 10(1), pp. 71-101. doi: 10.1007/s11302-013-9400-5

Burnstock, G., Fredholm, B. B., North, R. A. and Verkhatsky, A. 2010. The birth and postnatal development of purinergic signalling. *Acta Physiol (Oxf)* 199(2), pp. 93-147. doi: 10.1111/j.1748-1716.2010.02114.x

Burnstock, G. and Knight, G. E. 2004. Cellular distribution and functions of P2 receptor subtypes in different systems. *Int Rev Cytol* 240, pp. 31-304. doi: 10.1016/s0074-7696(04)40002-3

Buscà, R. et al. 2015. ERK1 and ERK2 present functional redundancy in tetrapods despite higher evolution rate of ERK1. *BMC Evol Biol* 15, p. 179. doi: 10.1186/s12862-015-0450-x

Buscà, R., Pouyssegur, J. and Lenormand, P. 2016. ERK1 and ERK2 Map Kinases: Specific Roles or Functional Redundancy? *Front Cell Dev Biol* 4, p. 53. doi: 10.3389/fcell.2016.00053

Camps, M., Nichols, A. and Arkinstall, S. 2000. Dual specificity phosphatases: a gene family for control of MAP kinase function. *Faseb j* 14(1), pp. 6-16.

Chabot, B. and Shkreta, L. 2016. Defective control of pre-messenger RNA splicing in human disease. *J Cell Biol* 212(1), pp. 13-27. doi: 10.1083/jcb.201510032

Chambard, J. C., Lefloch, R., Pouyssegur, J. and Lenormand, P. 2007. ERK implication in cell cycle regulation. *Biochim Biophys Acta* 1773(8), pp. 1299-1310. doi: 10.1016/j.bbamcr.2006.11.010

Charras, G. and Paluch, E. 2008. Blebs lead the way: how to migrate without lamellipodia. *Nat Rev Mol Cell Biol* 9(9), pp. 730-736. doi: 10.1038/nrm2453

Charras, G. T. 2008. A short history of blebbing. *J Microsc* 231(3), pp. 466-478. doi: 10.1111/j.1365-2818.2008.02059.x

Charras, G. T., Yarrow, J. C., Horton, M. A., Mahadevan, L. and Mitchison, T. J. 2005. Non-equilibration of hydrostatic pressure in blebbing cells. *Nature* 435(7040), pp. 365-369. doi: 10.1038/nature03550

Chaumont, S., Compan, V., Toulme, E., Richler, E., Housley, G. D., Rassendren, F. and Khakh, B. S. 2008. Regulation of P2X2 receptors by the neuronal calcium sensor VILIP1. *Sci Signal* 1(41), p. ra8. doi: 10.1126/scisignal.1162329

Chaumont, S., Jiang, L. H., Penna, A., North, R. A. and Rassendren, F. 2004. Identification of a trafficking motif involved in the stabilization and polarization of P2X receptors. *J Biol Chem* 279(28), pp. 29628-29638. doi: 10.1074/jbc.M403940200

Cheewatrakoolpong, B., Gilchrest, H., Anthes, J. C. and Greenfeder, S. 2005. Identification and characterization of splice variants of the human P2X7 ATP channel. *Biochem Biophys Res Commun* 332(1), pp. 17-27. doi: 10.1016/j.bbrc.2005.04.087

Chekeni, F. B. et al. 2010. Pannexin 1 channels mediate 'find-me' signal release and membrane permeability during apoptosis. *Nature* 467(7317), pp. 863-867. doi: 10.1038/nature09413

Chessell, I. P., Michel, A. D. and Humphrey, P. P. 1997. Properties of the pore-forming P2X7 purinoceptor in mouse NTW8 microglial cells. *Br J Pharmacol* 121(7), pp. 1429-1437. doi: 10.1038/sj.bjp.0701278

Chhabra, E. S. and Higgs, H. N. 2007. The many faces of actin: matching assembly factors with cellular structures. *Nat Cell Biol* 9(10), pp. 1110-1121. doi: 10.1038/ncb1007-1110

Chong, J. H., Zheng, G. G., Ma, Y. Y., Zhang, H. Y., Nie, K., Lin, Y. M. and Wu, K. F. 2010. The hyposensitive N187D P2X7 mutant promotes malignant progression in nude mice. *J Biol Chem* 285(46), pp. 36179-36187. doi: 10.1074/jbc.M110.128488

Chow, L. T., Gelinas, R. E., Broker, T. R. and Roberts, R. J. 1977. An amazing sequence arrangement at the 5' ends of adenovirus 2 messenger RNA. *Cell* 12(1), pp. 1-8. doi: 10.1016/0092-8674(77)90180-5

Christian, F., Smith, E. L. and Carmody, R. J. 2016. The Regulation of NF-kappaB Subunits by Phosphorylation. *Cells* 5(1), doi: 10.3390/cells5010012

Cieslak, M., Wojtczak, A. and Komoszynski, M. 2017. Role of the purinergic signaling in epilepsy. *Pharmacol Rep* 69(1), pp. 130-138. doi: 10.1016/j.pharep.2016.09.018

Compan, V., Ulmann, L., Stelmashenko, O., Chemin, J., Chaumont, S. and Rassendren, F. 2012. P2X2 and P2X5 subunits define a new heteromeric receptor with P2X7-like properties. *J Neurosci* 32(12), pp. 4284-4296. doi: 10.1523/jneurosci.6332-11.2012

Constantinescu, P., Wang, B., Kovacevic, K., Jalilian, I., Bosman, G. J., Wiley, J. S. and Sluyter, R. 2010. P2X7 receptor activation induces cell death and microparticle release in murine erythroleukemia cells. *Biochim Biophys Acta* 1798(9), pp. 1797-1804. doi: 10.1016/j.bbamem.2010.06.002

Conti, M. A., Even-Ram, S., Liu, C., Yamada, K. M. and Adelstein, R. S. 2004. Defects in cell adhesion and the visceral endoderm following ablation of nonmuscle myosin heavy chain II-A in mice. *J Biol Chem* 279(40), pp. 41263-41266. doi: 10.1074/jbc.C400352200

Crane, J. M. and Tamm, L. K. 2004. Role of cholesterol in the formation and nature of lipid rafts in planar and spherical model membranes. *Biophys J* 86(5), pp. 2965-2979. doi: 10.1016/s0006-3495(04)74347-7

Cuadrado, A. and Nebreda, A. R. 2010. Mechanisms and functions of p38 MAPK signalling. *Biochem J* 429(3), pp. 403-417. doi: 10.1042/bj20100323

Cuenda, A. and Rousseau, S. 2007. p38 MAP-kinases pathway regulation, function and role in human diseases. *Biochim Biophys Acta* 1773(8), pp. 1358-1375. doi: 10.1016/j.bbamcr.2007.03.010

- Cuevas, B. D., Abell, A. N. and Johnson, G. L. 2007. Role of mitogen-activated protein kinase kinase kinases in signal integration. *Oncogene* 26(22), pp. 3159-3171. doi: 10.1038/sj.onc.1210409
- Cunningham, C. C. 1995. Actin polymerization and intracellular solvent flow in cell surface blebbing. *J Cell Biol* 129(6), pp. 1589-1599. doi: 10.1083/jcb.129.6.1589
- Dagvadorj, J. et al. 2015. Lipopolysaccharide Induces Alveolar Macrophage Necrosis via CD14 and the P2X7 Receptor Leading to Interleukin-1alpha Release. *Immunity* 42(4), pp. 640-653. doi: 10.1016/j.immuni.2015.03.007
- De Marchi, E., Orioli, E., Dal Ben, D. and Adinolfi, E. 2016. P2X7 Receptor as a Therapeutic Target. *Adv Protein Chem Struct Biol* 104, pp. 39-79. doi: 10.1016/bs.apcsb.2015.11.004
- Denlinger, L. C. et al. 2001. Cutting edge: the nucleotide receptor P2X7 contains multiple protein- and lipid-interaction motifs including a potential binding site for bacterial lipopolysaccharide. *J Immunol* 167(4), pp. 1871-1876. doi: 10.4049/jimmunol.167.4.1871
- Denlinger, L. C. et al. 2003. Mutation of a dibasic amino acid motif within the C terminus of the P2X7 nucleotide receptor results in trafficking defects and impaired function. *J Immunol* 171(3), pp. 1304-1311. doi: 10.4049/jimmunol.171.3.1304
- DePina, A. S., Wollert, T. and Langford, G. M. 2007. Membrane associated nonmuscle myosin II functions as a motor for actin-based vesicle transport in clam oocyte extracts. *Cell Motil Cytoskeleton* 64(10), pp. 739-755. doi: 10.1002/cm.20219
- Deschenes-Simard, X., Kottakis, F., Meloche, S. and Ferbeyre, G. 2014. ERKs in cancer: friends or foes? *Cancer Res* 74(2), pp. 412-419. doi: 10.1158/0008-5472.can-13-2381
- Di Virgilio, F. 1995. The P2Z purinoceptor: an intriguing role in immunity, inflammation and cell death. *Immunol Today* 16(11), pp. 524-528. doi: 10.1016/0167-5699(95)80045-x
- Di Virgilio, F. 2015. P2X receptors and inflammation. *Curr Med Chem* 22(7), pp. 866-877. doi: 10.2174/0929867322666141210155311
- Di Virgilio, F., Bronte, V., Collavo, D. and Zanovello, P. 1989. Responses of mouse lymphocytes to extracellular adenosine 5'-triphosphate (ATP). Lymphocytes with cytotoxic activity are resistant to the permeabilizing effects of ATP. *J Immunol* 143(6), pp. 1955-1960.

Di Virgilio, F., Chiozzi, P., Falzoni, S., Ferrari, D., Sanz, J. M., Venketaraman, V. and Baricordi, O. R. 1998. Cytolytic P2X purinoceptors. *Cell Death Differ* 5(3), pp. 191-199. doi: 10.1038/sj.cdd.4400341

Di Virgilio, F., Falzoni, S., Giuliani, A. L. and Adinolfi, E. 2016. P2 receptors in cancer progression and metastatic spreading. *Curr Opin Pharmacol* 29, pp. 17-25. doi: 10.1016/j.coph.2016.05.001

Dinarello, C. A. 2018. Introduction to the interleukin-1 family of cytokines and receptors: Drivers of innate inflammation and acquired immunity. *Immunol Rev* 281(1), pp. 5-7. doi: 10.1111/imr.12624

Dou, L., Chen, Y. F., Cowan, P. J. and Chen, X. P. 2018. Extracellular ATP signaling and clinical relevance. *Clin Immunol* 188, pp. 67-73. doi: 10.1016/j.clim.2017.12.006

Dreisig, K., Kristensen, N. P., Dommer, M. W., Jørgensen, N. R. and Kornum, B. R. 2018. N-terminal tagging of human P2X7 receptor disturbs calcium influx and dye uptake. *Purinergic Signal* 14(1), pp. 83-90. doi: 10.1007/s11302-017-9598-8

Eddinger, T. J. and Meer, D. P. 2007. Myosin II isoforms in smooth muscle: heterogeneity and function. *Am J Physiol Cell Physiol* 293(2), pp. C493-508. doi: 10.1152/ajpcell.00131.2007

Ennion, S. J. and Evans, R. J. 2001. Agonist-stimulated internalisation of the ligand-gated ion channel P2X(1) in rat vas deferens. *FEBS Lett* 489(2-3), pp. 154-158. doi: 10.1016/s0014-5793(01)02102-0

Erb, L., Liao, Z., Seye, C. I. and Weisman, G. A. 2006. P2 receptors: intracellular signaling. *Pflugers Arch* 452(5), pp. 552-562. doi: 10.1007/s00424-006-0069-2

Erb, L. and Weisman, G. A. 2012. Coupling of P2Y receptors to G proteins and other signaling pathways. *Wiley Interdiscip Rev Membr Transp Signal* 1(6), pp. 789-803. doi: 10.1002/wmts.62

Fackler, O. T. and Grosse, R. 2008. Cell motility through plasma membrane blebbing. *J Cell Biol* 181(6), pp. 879-884. doi: 10.1083/jcb.200802081

Faria, R. X., Defarias, F. P. and Alves, L. A. 2005. Are second messengers crucial for opening the pore associated with P2X7 receptor? *Am J Physiol Cell Physiol* 288(2), pp. C260-271. doi: 10.1152/ajpcell.00215.2004

Farooq, A. and Zhou, M. M. 2004. Structure and regulation of MAPK phosphatases. *Cell Signal* 16(7), pp. 769-779. doi: 10.1016/j.cellsig.2003.12.008

- Feinstein, E., Kimchi, A., Wallach, D., Boldin, M. and Varfolomeev, E. 1995. The death domain: a module shared by proteins with diverse cellular functions. *Trends Biochem Sci* 20(9), pp. 342-344. doi: 10.1016/s0968-0004(00)89070-2
- Feng, Y. H., Li, X., Wang, L., Zhou, L. and Gorodeski, G. I. 2006. A truncated P2X7 receptor variant (P2X7-j) endogenously expressed in cervical cancer cells antagonizes the full-length P2X7 receptor through hetero-oligomerization. *J Biol Chem* 281(25), pp. 17228-17237. doi: 10.1074/jbc.M602999200
- Ferrari, D., Los, M., Bauer, M. K., Vandenabeele, P., Wesselborg, S. and Schulze-Osthoff, K. 1999. P2Z purinoreceptor ligation induces activation of caspases with distinct roles in apoptotic and necrotic alterations of cell death. *FEBS Lett* 447(1), pp. 71-75. doi: 10.1016/s0014-5793(99)00270-7
- Ferrari, D., Wesselborg, S., Bauer, M. K. and Schulze-Osthoff, K. 1997. Extracellular ATP activates transcription factor NF-kappaB through the P2Z purinoreceptor by selectively targeting NF-kappaB p65. *J Cell Biol* 139(7), pp. 1635-1643. doi: 10.1083/jcb.139.7.1635
- Folkman, J. and Shing, Y. 1992. Angiogenesis. *J Biol Chem* 267(16), pp. 10931-10934.
- Franco, M., Bautista-Perez, R. and Perez-Mendez, O. 2015. Purinergic receptors in tubulointerstitial inflammatory cells: a pathophysiological mechanism of salt-sensitive hypertension. *Acta Physiol (Oxf)* 214(1), pp. 75-87. doi: 10.1111/apha.12471
- Franco, M. C. et al. 2013. Nitration of Hsp90 induces cell death. *Proc Natl Acad Sci U S A* 110(12), pp. E1102-1111. doi: 10.1073/pnas.1215177110
- Frémin, C., Saba-El-Leil, M. K., Lévesque, K., Ang, S. L. and Meloche, S. 2015. Functional Redundancy of ERK1 and ERK2 MAP Kinases during Development. *Cell Rep* 12(6), pp. 913-921. doi: 10.1016/j.celrep.2015.07.011
- Gangadharan, V., Nohe, A., Caplan, J., Czymmek, K. and Duncan, R. L. 2015. Caveolin-1 regulates P2X7 receptor signaling in osteoblasts. *Am J Physiol Cell Physiol* 308(1), pp. C41-50. doi: 10.1152/ajpcell.00037.2014
- Garcia-Marcos, M. et al. 2006a. Coupling of two pools of P2X7 receptors to distinct intracellular signaling pathways in rat submandibular gland. *J Lipid Res* 47(4), pp. 705-714. doi: 10.1194/jlr.M500408-JLR200

- Garcia-Marcos, M. et al. 2006b. Characterization and comparison of raft-like membranes isolated by two different methods from rat submandibular gland cells. *Biochim Biophys Acta* 1758(6), pp. 796-806. doi: 10.1016/j.bbamem.2006.05.008
- Gendron, F. P., Neary, J. T., Theiss, P. M., Sun, G. Y., Gonzalez, F. A. and Weisman, G. A. 2003. Mechanisms of P2X7 receptor-mediated ERK1/2 phosphorylation in human astrocytoma cells. *Am J Physiol Cell Physiol* 284(2), pp. C571-581. doi: 10.1152/ajpcell.00286.2002
- Genetos, D. C., Karin, N. J., Geist, D. J., Donahue, H. J. and Duncan, R. L. 2011. Purinergic signaling is required for fluid shear stress-induced NF-kappaB translocation in osteoblasts. *Exp Cell Res* 317(6), pp. 737-744. doi: 10.1016/j.yexcr.2011.01.007
- Gentile, D., Natale, M., Lazzerini, P. E., Capecchi, P. L. and Laghi-Pasini, F. 2015. The role of P2X7 receptors in tissue fibrosis: a brief review. *Purinergic Signal* 11(4), pp. 435-440. doi: 10.1007/s11302-015-9466-3
- Gidlof, O. et al. 2012. A common missense variant in the ATP receptor P2X7 is associated with reduced risk of cardiovascular events. *PLoS One* 7(5), p. e37491. doi: 10.1371/journal.pone.0037491
- Giuliani, A. L., Sarti, A. C., Falzoni, S. and Di Virgilio, F. 2017. The P2X7 Receptor-Interleukin-1 Liaison. *Front Pharmacol* 8, p. 123. doi: 10.3389/fphar.2017.00123
- Gnanasekaran, A., Sundukova, M., van den Maagdenberg, A. M., Fabbretti, E. and Nistri, A. 2011. Lipid rafts control P2X3 receptor distribution and function in trigeminal sensory neurons of a transgenic migraine mouse model. *Mol Pain* 7, p. 77. doi: 10.1186/1744-8069-7-77
- Golomb, E. et al. 2004. Identification and characterization of nonmuscle myosin II-C, a new member of the myosin II family. *J Biol Chem* 279(4), pp. 2800-2808. doi: 10.1074/jbc.M309981200
- Goncalves, R. G. et al. 2006. The role of purinergic P2X7 receptors in the inflammation and fibrosis of unilateral ureteral obstruction in mice. *Kidney Int* 70(9), pp. 1599-1606. doi: 10.1038/sj.ki.5001804
- Gonnord, P. et al. 2009. Palmitoylation of the P2X7 receptor, an ATP-gated channel, controls its expression and association with lipid rafts. *Faseb j* 23(3), pp. 795-805. doi: 10.1096/fj.08-114637

- Gu, B. J., Rathsam, C., Stokes, L., McGeachie, A. B. and Wiley, J. S. 2009. Extracellular ATP dissociates nonmuscle myosin from P2X(7) complex: this dissociation regulates P2X(7) pore formation. *Am J Physiol Cell Physiol* 297(2), pp. C430-439. doi: 10.1152/ajpcell.00079.2009
- Gu, B. J. and Wiley, J. S. 2006. Rapid ATP-induced release of matrix metalloproteinase 9 is mediated by the P2X7 receptor. *Blood* 107(12), pp. 4946-4953. doi: 10.1182/blood-2005-07-2994
- Gu, B. J. et al. 2001. A Glu-496 to Ala polymorphism leads to loss of function of the human P2X7 receptor. *J Biol Chem* 276(14), pp. 11135-11142. doi: 10.1074/jbc.M010353200
- Gu, B. J., Zhang, W. Y., Bendall, L. J., Chessell, I. P., Buell, G. N. and Wiley, J. S. 2000. Expression of P2X(7) purinoceptors on human lymphocytes and monocytes: evidence for nonfunctional P2X(7) receptors. *Am J Physiol Cell Physiol* 279(4), pp. C1189-1197. doi: 10.1152/ajpcell.2000.279.4.C1189
- Gudipaty, L., Humphreys, B. D., Buell, G. and Dubyak, G. R. 2001. Regulation of P2X(7) nucleotide receptor function in human monocytes by extracellular ions and receptor density. *Am J Physiol Cell Physiol* 280(4), pp. C943-953. doi: 10.1152/ajpcell.2001.280.4.C943
- Guzman-Aranguéz, A., Pérez de Lara, M. J. and Pintor, J. 2017. Hyperosmotic stress induces ATP release and changes in P2X7 receptor levels in human corneal and conjunctival epithelial cells. *Purinergic Signal* 13(2), pp. 249-258. doi: 10.1007/s11302-017-9556-5
- Haanes, K. A., Schwab, A. and Novak, I. 2012. The P2X7 receptor supports both life and death in fibrogenic pancreatic stellate cells. *PLoS One* 7(12), p. e51164. doi: 10.1371/journal.pone.0051164
- Hanahan, D. and Weinberg, R. A. 2011. Hallmarks of cancer: the next generation. *Cell* 144(5), pp. 646-674. doi: 10.1016/j.cell.2011.02.013
- Haslund-Vinding, J., McBean, G., Jaquet, V. and Vilhardt, F. 2017. NADPH oxidases in oxidant production by microglia: activating receptors, pharmacology and association with disease. *Br J Pharmacol* 174(12), pp. 1733-1749. doi: 10.1111/bph.13425
- Hattori, M. and Gouaux, E. 2012. Molecular mechanism of ATP binding and ion channel activation in P2X receptors. *Nature* 485(7397), pp. 207-212. doi: 10.1038/nature11010

Hickman, S. E., el Khoury, J., Greenberg, S., Schieren, I. and Silverstein, S. C. 1994. P2Z adenosine triphosphate receptor activity in cultured human monocyte-derived macrophages. *Blood* 84(8), pp. 2452-2456.

Hirayama, Y., Ikeda-Matsuo, Y., Notomi, S., Enaida, H., Kinouchi, H. and Koizumi, S. 2015. Astrocyte-mediated ischemic tolerance. *J Neurosci* 35(9), pp. 3794-3805. doi: 10.1523/jneurosci.4218-14.2015

Hirayama, Y. and Koizumi, S. 2017. Hypoxia-independent mechanisms of HIF-1alpha expression in astrocytes after ischemic preconditioning. *Glia* 65(3), pp. 523-530. doi: 10.1002/glia.23109

Holt, L. J., Tuch, B. B., Villen, J., Johnson, A. D., Gygi, S. P. and Morgan, D. O. 2009. Global analysis of Cdk1 substrate phosphorylation sites provides insights into evolution. *Science* 325(5948), pp. 1682-1686. doi: 10.1126/science.1172867

Huang, C., Yu, W., Cui, H., Wang, Y., Zhang, L., Han, F. and Huang, T. 2014. P2X7 blockade attenuates mouse liver fibrosis. *Mol Med Rep* 9(1), pp. 57-62. doi: 10.3892/mmr.2013.1807

Huang, G., Shi, L. Z. and Chi, H. 2009. Regulation of JNK and p38 MAPK in the immune system: signal integration, propagation and termination. *Cytokine* 48(3), pp. 161-169. doi: 10.1016/j.cyto.2009.08.002

Humphreys, B. D., Rice, J., Kertesz, S. B. and Dubyak, G. R. 2000. Stress-activated protein kinase/JNK activation and apoptotic induction by the macrophage P2X7 nucleotide receptor. *J Biol Chem* 275(35), pp. 26792-26798. doi: 10.1074/jbc.M002770200

Jacobelli, J., Chmura, S. A., Buxton, D. B., Davis, M. M. and Krummel, M. F. 2004. A single class II myosin modulates T cell motility and stopping, but not synapse formation. *Nat Immunol* 5(5), pp. 531-538. doi: 10.1038/ni1065

Jacques-Silva, M. C. et al. 2004. P2X7 receptors stimulate AKT phosphorylation in astrocytes. *Br J Pharmacol* 141(7), pp. 1106-1117. doi: 10.1038/sj.bjp.0705685

Jamieson, S. E. et al. 2010. Evidence for associations between the purinergic receptor P2X(7) (P2RX7) and toxoplasmosis. *Genes Immun* 11(5), pp. 374-383. doi: 10.1038/gene.2010.31

Jiang, L. H., Rassendren, F., Mackenzie, A., Zhang, Y. H., Surprenant, A. and North, R. A. 2005. N-methyl-D-glucamine and propidium dyes utilize different permeation pathways at rat P2X(7) receptors. *Am J Physiol Cell Physiol* 289(5), pp. C1295-1302. doi: 10.1152/ajpcell.00253.2005

- Johnson, G. L. and Lapadat, R. 2002. Mitogen-activated protein kinase pathways mediated by ERK, JNK, and p38 protein kinases. *Science* 298(5600), pp. 1911-1912. doi: 10.1126/science.1072682
- Johnson, G. L. and Nakamura, K. 2007. The c-jun kinase/stress-activated pathway: regulation, function and role in human disease. *Biochim Biophys Acta* 1773(8), pp. 1341-1348. doi: 10.1016/j.bbamcr.2006.12.009
- Kaczmarek-Hájek, K., Lörinczi, E., Hausmann, R. and Nicke, A. 2012. Molecular and functional properties of P2X receptors--recent progress and persisting challenges. *Purinergic Signal* 8(3), pp. 375-417. doi: 10.1007/s11302-012-9314-7
- Kahya, N., Scherfeld, D., Bacia, K., Poolman, B. and Schwille, P. 2003. Probing lipid mobility of raft-exhibiting model membranes by fluorescence correlation spectroscopy. *J Biol Chem* 278(30), pp. 28109-28115. doi: 10.1074/jbc.M302969200
- Kanjanamekanant, K., Luckprom, P. and Pavasant, P. 2014. P2X7 receptor-Pannexin1 interaction mediates stress-induced interleukin-1 beta expression in human periodontal ligament cells. *J Periodontal Res* 49(5), pp. 595-602. doi: 10.1111/jre.12139
- Karasawa, A. and Kawate, T. 2016. Structural basis for subtype-specific inhibition of the P2X7 receptor. *Elife* 5, doi: 10.7554/eLife.22153
- Karasawa, A., Michalski, K., Mikhelzon, P. and Kawate, T. 2017. The P2X7 receptor forms a dye-permeable pore independent of its intracellular domain but dependent on membrane lipid composition. *Elife* 6, doi: 10.7554/eLife.31186
- Kasuya, G. et al. 2016. Structural Insights into Divalent Cation Modulations of ATP-Gated P2X Receptor Channels. *Cell Rep* 14(4), pp. 932-944. doi: 10.1016/j.celrep.2015.12.087
- Kasuya, G. et al. 2017a. Structural insights into the nucleotide base specificity of P2X receptors. *Sci Rep* 7, p. 45208. doi: 10.1038/srep45208
- Kasuya, G. et al. 2017b. Structural insights into the competitive inhibition of the ATP-gated P2X receptor channel. *Nat Commun* 8(1), p. 876. doi: 10.1038/s41467-017-00887-9
- Kawate, T., Michel, J. C., Birdsong, W. T. and Gouaux, E. 2009. Crystal structure of the ATP-gated P2X(4) ion channel in the closed state. *Nature* 460(7255), pp. 592-598. doi: 10.1038/nature08198

Keren, H., Lev-Maor, G. and Ast, G. 2010. Alternative splicing and evolution: diversification, exon definition and function. *Nat Rev Genet* 11(5), pp. 345-355. doi: 10.1038/nrg2776

Keshet, Y. and Seger, R. 2010. The MAP kinase signaling cascades: a system of hundreds of components regulates a diverse array of physiological functions. *Methods Mol Biol* 661, pp. 3-38. doi: 10.1007/978-1-60761-795-2_1

Khajah, M. A. and Luqmani, Y. A. 2016. Involvement of Membrane Blebbing in Immunological Disorders and Cancer. *Med Princ Pract* 25 Suppl 2, pp. 18-27. doi: 10.1159/000441848

Kido, Y. et al. 2014. Regulation of activity of P2X7 receptor by its splice variants in cultured mouse astrocytes. *Glia* 62(3), pp. 440-451. doi: 10.1002/glia.22615

Kim, J. E. et al. 2013. The effect of P2X7 receptor activation on nuclear factor-kappaB phosphorylation induced by status epilepticus in the rat hippocampus. *Hippocampus* 23(6), pp. 500-514. doi: 10.1002/hipo.22109

Kim, M., Jiang, L. H., Wilson, H. L., North, R. A. and Surprenant, A. 2001. Proteomic and functional evidence for a P2X7 receptor signalling complex. *Embo j* 20(22), pp. 6347-6358. doi: 10.1093/emboj/20.22.6347

Koo, T. Y. et al. 2017. The P2X7 receptor antagonist, oxidized adenosine triphosphate, ameliorates renal ischemia-reperfusion injury by expansion of regulatory T cells. *Kidney Int* 92(2), pp. 415-431. doi: 10.1016/j.kint.2017.01.031

Kopp, R., Krautloher, A., Ramirez-Fernandez, A. and Nicke, A. 2019a. P2X7 Interactions and Signaling - Making Head or Tail of It. *Front Mol Neurosci* 12, p. 183. doi: 10.3389/fnmol.2019.00183

Kopp, R., Krautloher, A., Ramírez-Fernández, A. and Nicke, A. 2019b. P2X7 Interactions and Signaling - Making Head or Tail of It. *Front Mol Neurosci* 12, p. 183. doi: 10.3389/fnmol.2019.00183

Kotnis, S. et al. 2010. Genetic and functional analysis of human P2X5 reveals a distinct pattern of exon 10 polymorphism with predominant expression of the nonfunctional receptor isoform. *Mol Pharmacol* 77(6), pp. 953-960. doi: 10.1124/mol.110.063636

Krause, D. C. 1998. Mycoplasma pneumoniae cytodherence: organization and assembly of the attachment organelle. *Trends Microbiol* 6(1), pp. 15-18. doi: 10.1016/s0966-842x(97)01168-2

- Krendel, M. and Mooseker, M. S. 2005. Myosins: tails (and heads) of functional diversity. *Physiology (Bethesda)* 20, pp. 239-251. doi: 10.1152/physiol.00014.2005
- Kukulski, F., Levesque, S. A. and Sevigny, J. 2011. Impact of ectoenzymes on p2 and p1 receptor signaling. *Adv Pharmacol* 61, pp. 263-299. doi: 10.1016/b978-0-12-385526-8.00009-6
- Kuo, W. L., Duke, C. J., Abe, M. K., Kaplan, E. L., Gomes, S. and Rosner, M. R. 2004. ERK7 expression and kinase activity is regulated by the ubiquitin-proteasome pathway. *J Biol Chem* 279(22), pp. 23073-23081. doi: 10.1074/jbc.M313696200
- Kurochkina, N. and Guha, U. 2013. SH3 domains: modules of protein-protein interactions. *Biophys Rev* 5(1), pp. 29-39. doi: 10.1007/s12551-012-0081-z
- Lalo, U., Allsopp, R. C., Mahaut-Smith, M. P. and Evans, R. J. 2010. P2X1 receptor mobility and trafficking; regulation by receptor insertion and activation. *J Neurochem* 113(5), pp. 1177-1187. doi: 10.1111/j.1471-4159.2010.06730.x
- Lalo, U., Jones, S., Roberts, J. A., Mahaut-Smith, M. P. and Evans, R. J. 2012. Heat shock protein 90 inhibitors reduce trafficking of ATP-gated P2X1 receptors and human platelet responsiveness. *J Biol Chem* 287(39), pp. 32747-32754. doi: 10.1074/jbc.M112.376566
- Lamping, N. et al. 1996. Effects of site-directed mutagenesis of basic residues (Arg 94, Lys 95, Lys 99) of lipopolysaccharide (LPS)-binding protein on binding and transfer of LPS and subsequent immune cell activation. *J Immunol* 157(10), pp. 4648-4656.
- Langridge, P. D. and Kay, R. R. 2006. Blebbing of Dictyostelium cells in response to chemoattractant. *Exp Cell Res* 312(11), pp. 2009-2017. doi: 10.1016/j.yexcr.2006.03.007
- Lee, S. H., Meng, X. W., Flatten, K. S., Loegering, D. A. and Kaufmann, S. H. 2013. Phosphatidylserine exposure during apoptosis reflects bidirectional trafficking between plasma membrane and cytoplasm. *Cell Death Differ* 20(1), pp. 64-76. doi: 10.1038/cdd.2012.93
- Lefloch, R., Pouyssegur, J. and Lenormand, P. 2008. Single and combined silencing of ERK1 and ERK2 reveals their positive contribution to growth signaling depending on their expression levels. *Mol Cell Biol* 28(1), pp. 511-527. doi: 10.1128/mcb.00800-07
- Lenertz, L. Y., Gavala, M. L., Zhu, Y. and Bertics, P. J. 2011. Transcriptional control mechanisms associated with the nucleotide receptor P2X7, a critical regulator of immunologic, osteogenic, and neurologic functions. *Immunol Res* 50(1), pp. 22-38. doi: 10.1007/s12026-011-8203-4

Lenormand, P., Sardet, C., Pagès, G., L'Allemain, G., Brunet, A. and Pouyssegur, J. 1993. Growth factors induce nuclear translocation of MAP kinases (p42mapk and p44mapk) but not of their activator MAP kinase kinase (p45mapkk) in fibroblasts. *J Cell Biol* 122(5), pp. 1079-1088. doi: 10.1083/jcb.122.5.1079

Lev, S. et al. 1995. Protein tyrosine kinase PYK2 involved in Ca²⁺-induced regulation of ion channel and MAP kinase functions. *Nature* 376(6543), pp. 737-745. doi: 10.1038/376737a0

Li, J. and Fountain, S. J. 2012. Fluvastatin suppresses native and recombinant human P2X4 receptor function. *Purinergic Signal* 8(2), pp. 311-316. doi: 10.1007/s11302-011-9289-9

Li, M., Toombes, G. E., Silberberg, S. D. and Swartz, K. J. 2015. Physical basis of apparent pore dilation of ATP-activated P2X receptor channels. *Nat Neurosci* 18(11), pp. 1577-1583. doi: 10.1038/nn.4120

Li, S., Tomic, M. and Stojilkovic, S. S. 2011. Characterization of novel Pannexin 1 isoforms from rat pituitary cells and their association with ATP-gated P2X channels. *Gen Comp Endocrinol* 174(2), pp. 202-210. doi: 10.1016/j.ygcen.2011.08.019

Liu, Y., Xiao, Y. and Li, Z. 2011. P2X7 receptor positively regulates MyD88-dependent NF-kappaB activation. *Cytokine* 55(2), pp. 229-236. doi: 10.1016/j.cyto.2011.05.003

Locovei, S., Scemes, E., Qiu, F., Spray, D. C. and Dahl, G. 2007. Pannexin1 is part of the pore forming unit of the P2X(7) receptor death complex. *FEBS Lett* 581(3), pp. 483-488. doi: 10.1016/j.febslet.2006.12.056

Lucae, S. et al. 2006. P2RX7, a gene coding for a purinergic ligand-gated ion channel, is associated with major depressive disorder. *Hum Mol Genet* 15(16), pp. 2438-2445. doi: 10.1093/hmg/ddl166

Luo, L., Lucas, R. M., Liu, L. and Stow, J. L. 2019. Signalling, sorting and scaffolding adaptors for Toll-like receptors. *J Cell Sci* 133(5), doi: 10.1242/jcs.239194

Ma, X., Jana, S. S., Conti, M. A., Kawamoto, S., Claycomb, W. C. and Adelstein, R. S. 2010. Ablation of nonmuscle myosin II-B and II-C reveals a role for nonmuscle myosin II in cardiac myocyte karyokinesis. *Mol Biol Cell* 21(22), pp. 3952-3962. doi: 10.1091/mbc.E10-04-0293

Mackenzie, A. B., Young, M. T., Adinolfi, E. and Surprenant, A. 2005. Pseudoapoptosis induced by brief activation of ATP-gated P2X7 receptors. *J Biol Chem* 280(40), pp. 33968-33976. doi: 10.1074/jbc.M502705200

Mansoor, S. E., Lu, W., Oosterheert, W., Shekhar, M., Tajkhorshid, E. and Gouaux, E. 2016. X-ray structures define human P2X(3) receptor gating cycle and antagonist action. *Nature* 538(7623), pp. 66-71. doi: 10.1038/nature19367

Mariathasan, S. et al. 2006. Cryopyrin activates the inflammasome in response to toxins and ATP. *Nature* 440(7081), pp. 228-232. doi: 10.1038/nature04515

Marigo, V., Nigro, A., Pecci, A., Montanaro, D., Di Stazio, M., Balduini, C. L. and Savoia, A. 2004. Correlation between the clinical phenotype of MYH9-related disease and tissue distribution of class II nonmuscle myosin heavy chains. *Genomics* 83(6), pp. 1125-1133. doi: 10.1016/j.ygeno.2003.12.012

Marino, G. and Kroemer, G. 2013. Mechanisms of apoptotic phosphatidylserine exposure. *Cell Res* 23(11), pp. 1247-1248. doi: 10.1038/cr.2013.115

Martel-Gallegos, G. et al. 2013. Oxidative stress induced by P2X7 receptor stimulation in murine macrophages is mediated by c-Src/Pyk2 and ERK1/2. *Biochim Biophys Acta* 1830(10), pp. 4650-4659. doi: 10.1016/j.bbagen.2013.05.023

Masin, M., Kerschensteiner, D., Dumke, K., Rubio, M. E. and Soto, F. 2006. Fe65 interacts with P2X2 subunits at excitatory synapses and modulates receptor function. *J Biol Chem* 281(7), pp. 4100-4108. doi: 10.1074/jbc.M507735200

Masin, M. et al. 2012. Expression, assembly and function of novel C-terminal truncated variants of the mouse P2X7 receptor: re-evaluation of P2X7 knockouts. *Br J Pharmacol* 165(4), pp. 978-993. doi: 10.1111/j.1476-5381.2011.01624.x

McCarthy, A. E., Yoshioka, C. and Mansoor, S. E. 2019a. Full-Length P2X7 Structures Reveal How Palmitoylation Prevents Channel Desensitization. *Cell* 179(3), pp. 659-670.e613. doi: 10.1016/j.cell.2019.09.017

McCarthy, A. E., Yoshioka, C. and Mansoor, S. E. 2019b. Full-Length P2X(7) Structures Reveal How Palmitoylation Prevents Channel Desensitization. *Cell* 179(3), pp. 659-670.e613. doi: 10.1016/j.cell.2019.09.017

Mercer, J. A., Seperack, P. K., Strobel, M. C., Copeland, N. G. and Jenkins, N. A. 1991. Novel myosin heavy chain encoded by murine dilute coat colour locus. *Nature* 349(6311), pp. 709-713. doi: 10.1038/349709a0

Millan, J. L. 2006. Alkaline Phosphatases : Structure, substrate specificity and functional relatedness to other members of a large superfamily of enzymes. *Purinergic Signal* 2(2), pp. 335-341. doi: 10.1007/s11302-005-5435-6

Mishra, A., Chintagari, N. R., Guo, Y., Weng, T., Su, L. and Liu, L. 2011. Purinergic P2X7 receptor regulates lung surfactant secretion in a paracrine manner. *J Cell Sci* 124(Pt 4), pp. 657-668. doi: 10.1242/jcs.066977

Moore, S. F. and MacKenzie, A. B. 2009. NADPH oxidase NOX2 mediates rapid cellular oxidation following ATP stimulation of endotoxin-primed macrophages. *J Immunol* 183(5), pp. 3302-3308. doi: 10.4049/jimmunol.0900394

Morrison, D. K. 2012. MAP kinase pathways. *Cold Spring Harb Perspect Biol* 4(11), doi: 10.1101/cshperspect.a011254

Murrell-Lagnado, R. D. 2017. Regulation of P2X Purinergic Receptor Signaling by Cholesterol. *Curr Top Membr* 80, pp. 211-232. doi: 10.1016/bs.ctm.2017.05.004

Murrell-Lagnado, R. D. and Qureshi, O. S. 2008. Assembly and trafficking of P2X purinergic receptors (Review). *Mol Membr Biol* 25(4), pp. 321-331. doi: 10.1080/09687680802050385

Neves, S. R., Ram, P. T. and Iyengar, R. 2002. G protein pathways. *Science* 296(5573), pp. 1636-1639. doi: 10.1126/science.1071550

Nicke, A. et al. 2009. A functional P2X7 splice variant with an alternative transmembrane domain 1 escapes gene inactivation in P2X7 knock-out mice. *J Biol Chem* 284(38), pp. 25813-25822. doi: 10.1074/jbc.M109.033134

Norman, L., Sengupta, K. and Aranda-Espinoza, H. 2011. Blebbing dynamics during endothelial cell spreading. *Eur J Cell Biol* 90(1), pp. 37-48. doi: 10.1016/j.ejcb.2010.09.013

Norman, L. L., Brugues, J., Sengupta, K., Sens, P. and Aranda-Espinoza, H. 2010. Cell blebbing and membrane area homeostasis in spreading and retracting cells. *Biophys J* 99(6), pp. 1726-1733. doi: 10.1016/j.bpj.2010.07.031

North, R. A. 2002. Molecular physiology of P2X receptors. *Physiol Rev* 82(4), pp. 1013-1067. doi: 10.1152/physrev.00015.2002

- Nuttle, L. C. and Dubyak, G. R. 1994. Differential activation of cation channels and non-selective pores by macrophage P2z purinergic receptors expressed in *Xenopus* oocytes. *J Biol Chem* 269(19), pp. 13988-13996.
- Ormond, S. J., Barrera, N. P., Qureshi, O. S., Henderson, R. M., Edwardson, J. M. and Murrell-Lagnado, R. D. 2006. An uncharged region within the N terminus of the P2X6 receptor inhibits its assembly and exit from the endoplasmic reticulum. *Mol Pharmacol* 69(5), pp. 1692-1700. doi: 10.1124/mol.105.020404
- Ousingsawat, J., Wanitchakool, P., Kmit, A., Romao, A. M., Jantarajit, W., Schreiber, R. and Kunzelmann, K. 2015. Anoctamin 6 mediates effects essential for innate immunity downstream of P2X7 receptors in macrophages. *Nat Commun* 6, p. 6245. doi: 10.1038/ncomms7245
- Parvathenani, L. K., Tertyshnikova, S., Greco, C. R., Roberts, S. B., Robertson, B. and Posmantur, R. 2003. P2X7 mediates superoxide production in primary microglia and is up-regulated in a transgenic mouse model of Alzheimer's disease. *J Biol Chem* 278(15), pp. 13309-13317. doi: 10.1074/jbc.M209478200
- Pavlova, N. N. and Thompson, C. B. 2016. The Emerging Hallmarks of Cancer Metabolism. *Cell Metab* 23(1), pp. 27-47. doi: 10.1016/j.cmet.2015.12.006
- Pecci, A., Ma, X., Savoia, A. and Adelstein, R. S. 2018. MYH9: Structure, functions and role of non-muscle myosin IIA in human disease. *Gene* 664, pp. 152-167. doi: 10.1016/j.gene.2018.04.048
- Pelegrin, P. and Surprenant, A. 2006. Pannexin-1 mediates large pore formation and interleukin-1 β release by the ATP-gated P2X7 receptor. *Embo j* 25(21), pp. 5071-5082. doi: 10.1038/sj.emboj.7601378
- Pike, L. J. 2004. Lipid rafts: heterogeneity on the high seas. *Biochem J* 378(Pt 2), pp. 281-292. doi: 10.1042/bj20031672
- Pippel, A., Bessler, B., Klapperstuck, M. and Markwardt, F. 2015. Inhibition of antigen receptor-dependent Ca(2+) signals and NF-AT activation by P2X7 receptors in human B lymphocytes. *Cell Calcium* 57(4), pp. 275-289. doi: 10.1016/j.ceca.2015.01.010
- Poornima, V., Madhupriya, M., Kootar, S., Sujatha, G., Kumar, A. and Bera, A. K. 2012. P2X7 receptor-pannexin 1 hemichannel association: effect of extracellular calcium on membrane permeabilization. *J Mol Neurosci* 46(3), pp. 585-594. doi: 10.1007/s12031-011-9646-8

- Qj, M. and Elion, E. A. 2005. MAP kinase pathways. *J Cell Sci* 118(Pt 16), pp. 3569-3572. doi: 10.1242/jcs.02470
- Qiu, F. and Dahl, G. 2009. A permeant regulating its permeation pore: inhibition of pannexin 1 channels by ATP. *Am J Physiol Cell Physiol* 296(2), pp. C250-255. doi: 10.1152/ajpcell.00433.2008
- Qiu, Y., Li, W. H., Zhang, H. Q., Liu, Y., Tian, X. X. and Fang, W. G. 2014. P2X7 mediates ATP-driven invasiveness in prostate cancer cells. *PLoS One* 9(12), p. e114371. doi: 10.1371/journal.pone.0114371
- Qu, Y. et al. 2011. Pannexin-1 is required for ATP release during apoptosis but not for inflammasome activation. *J Immunol* 186(11), pp. 6553-6561. doi: 10.4049/jimmunol.1100478
- Qu, Z., Fujita-Becker, S., Ballweber, E., Ince, S., Herrmann, C., Schröder, R. R. and Mannherz, H. G. 2018. Interaction of isolated cross-linked short actin oligomers with the skeletal muscle myosin motor domain. *Febs j* 285(9), pp. 1715-1729. doi: 10.1111/febs.14442
- Qureshi, O. S., Paramasivam, A., Yu, J. C. and Murrell-Lagnado, R. D. 2007. Regulation of P2X4 receptors by lysosomal targeting, glycan protection and exocytosis. *J Cell Sci* 120(Pt 21), pp. 3838-3849. doi: 10.1242/jcs.010348
- Raffaghello, L., Chiozzi, P., Falzoni, S., Di Virgilio, F. and Pistoia, V. 2006. The P2X7 receptor sustains the growth of human neuroblastoma cells through a substance P-dependent mechanism. *Cancer Res* 66(2), pp. 907-914. doi: 10.1158/0008-5472.Can-05-3185
- Rak, J. 2010. Microparticles in cancer. *Semin Thromb Hemost* 36(8), pp. 888-906. doi: 10.1055/s-0030-1267043
- Ralevic, V. and Burnstock, G. 1998. Receptors for purines and pyrimidines. *Pharmacol Rev* 50(3), pp. 413-492.
- Raman, M., Chen, W. and Cobb, M. H. 2007. Differential regulation and properties of MAPKs. *Oncogene* 26(22), pp. 3100-3112. doi: 10.1038/sj.onc.1210392
- Rasola, A., Sciacovelli, M., Chiara, F., Pantic, B., Brusilow, W. S. and Bernardi, P. 2010. Activation of mitochondrial ERK protects cancer cells from death through inhibition of the permeability transition. *Proc Natl Acad Sci U S A* 107(2), pp. 726-731. doi: 10.1073/pnas.0912742107

- Rassendren, F., Buell, G. N., Virginio, C., Collo, G., North, R. A. and Surprenant, A. 1997. The permeabilizing ATP receptor, P2X7. Cloning and expression of a human cDNA. *J Biol Chem* 272(9), pp. 5482-5486. doi: 10.1074/jbc.272.9.5482
- Reboldi, A. and Dang, E. 2018. Cholesterol metabolism in innate and adaptive response. *F1000Res* 7, doi: 10.12688/f1000research.15500.1
- Reck-Peterson, S. L., Provance, D. W., Jr., Mooseker, M. S. and Mercer, J. A. 2000. Class V myosins. *Biochim Biophys Acta* 1496(1), pp. 36-51. doi: 10.1016/s0167-4889(00)00007-0
- Rincón, M. and Davis, R. J. 2009. Regulation of the immune response by stress-activated protein kinases. *Immunol Rev* 228(1), pp. 212-224. doi: 10.1111/j.1600-065X.2008.00744.x
- Risau, W. 1997. Mechanisms of angiogenesis. *Nature* 386(6626), pp. 671-674. doi: 10.1038/386671a0
- Robinson, L. E. and Murrell-Lagnado, R. D. 2013. The trafficking and targeting of P2X receptors. *Front Cell Neurosci* 7, p. 233. doi: 10.3389/fncel.2013.00233
- Robinson, L. E., Shridar, M., Smith, P. and Murrell-Lagnado, R. D. 2014. Plasma membrane cholesterol as a regulator of human and rodent P2X7 receptor activation and sensitization. *J Biol Chem* 289(46), pp. 31983-31994. doi: 10.1074/jbc.M114.574699
- Robinson, M. J. and Cobb, M. H. 1997. Mitogen-activated protein kinase pathways. *Curr Opin Cell Biol* 9(2), pp. 180-186.
- Rodrigues, A. M. et al. 2014. P2X(7) receptor in the kidneys of diabetic rats submitted to aerobic training or to N-acetylcysteine supplementation [corrected]. *PLoS One* 9(6), p. e97452. doi: 10.1371/journal.pone.0097452
- Rodriguez, O. C. and Cheney, R. E. 2002. Human myosin-Vc is a novel class V myosin expressed in epithelial cells. *J Cell Sci* 115(Pt 5), pp. 991-1004.
- Roger, S., Pelegrin, P. and Surprenant, A. 2008. Facilitation of P2X7 receptor currents and membrane blebbing via constitutive and dynamic calmodulin binding. *J Neurosci* 28(25), pp. 6393-6401. doi: 10.1523/jneurosci.0696-08.2008
- Sabri, A., Govindarajan, G., Griffin, T. M., Byron, K. L., Samarel, A. M. and Lucchesi, P. A. 1998. Calcium- and protein kinase C-dependent activation of the tyrosine kinase PYK2 by angiotensin II in vascular smooth muscle. *Circ Res* 83(8), pp. 841-851. doi: 10.1161/01.res.83.8.841

- Savio, L. E. B., de Andrade Mello, P., da Silva, C. G. and Coutinho-Silva, R. 2018. The P2X7 Receptor in Inflammatory Diseases: Angel or Demon? *Front Pharmacol* 9, p. 52. doi: 10.3389/fphar.2018.00052
- Savio, L. E. B. et al. 2017. CD39 limits P2X7 receptor inflammatory signaling and attenuates sepsis-induced liver injury. *J Hepatol* 67(4), pp. 716-726. doi: 10.1016/j.jhep.2017.05.021
- Schopf, F. H., Biebl, M. M. and Buchner, J. 2017. The HSP90 chaperone machinery. *Nat Rev Mol Cell Biol* 18(6), pp. 345-360. doi: 10.1038/nrm.2017.20
- Schubbert, S., Shannon, K. and Bollag, G. 2007. Hyperactive Ras in developmental disorders and cancer. *Nat Rev Cancer* 7(4), pp. 295-308. doi: 10.1038/nrc2109
- Schumann, R. R., Lamping, N. and Hoess, A. 1997. Interchangeable endotoxin-binding domains in proteins with opposite lipopolysaccharide-dependent activities. *J Immunol* 159(11), pp. 5599-5605.
- Schwarz, N. et al. 2012. Alternative splicing of the N-terminal cytosolic and transmembrane domains of P2X7 controls gating of the ion channel by ADP-ribosylation. *PLoS One* 7(7), p. e41269. doi: 10.1371/journal.pone.0041269
- Schwarz, N., Fliegert, R., Adriouch, S., Seman, M., Guse, A. H., Haag, F. and Koch-Nolte, F. 2009. Activation of the P2X7 ion channel by soluble and covalently bound ligands. *Purinergic Signal* 5(2), pp. 139-149. doi: 10.1007/s11302-009-9135-5
- Sebolt-Leopold, J. S. 2008. Advances in the development of cancer therapeutics directed against the RAS-mitogen-activated protein kinase pathway. *Clin Cancer Res* 14(12), pp. 3651-3656. doi: 10.1158/1078-0432.ccr-08-0333
- Sedgwick, S. G. and Smerdon, S. J. 1999. The ankyrin repeat: a diversity of interactions on a common structural framework. *Trends Biochem Sci* 24(8), pp. 311-316. doi: 10.1016/s0968-0004(99)01426-7
- Segawa, K. and Nagata, S. 2015a. An Apoptotic 'Eat Me' Signal: Phosphatidylserine Exposure. *Trends Cell Biol* 25(11), pp. 639-650. doi: 10.1016/j.tcb.2015.08.003
- Segawa, K. and Nagata, S. 2015b. An Apoptotic 'Eat Me' Signal: Phosphatidylserine Exposure. *Trends Cell Biol* 25(11), pp. 639-650. doi: 10.1016/j.tcb.2015.08.003

Serber, Z. and Ferrell, J. E., Jr. 2007. Tuning bulk electrostatics to regulate protein function. *Cell* 128(3), pp. 441-444. doi: 10.1016/j.cell.2007.01.018

Serfling, E., Avots, A., Klein-Hessling, S., Rudolf, R., Vaeth, M. and Berberich-Siebelt, F. 2012. NFATc1/alphaA: The other Face of NFAT Factors in Lymphocytes. *Cell Commun Signal* 10(1), p. 16. doi: 10.1186/1478-811x-10-16

Seror, C. et al. 2011. Extracellular ATP acts on P2Y2 purinergic receptors to facilitate HIV-1 infection. *J Exp Med* 208(9), pp. 1823-1834. doi: 10.1084/jem.20101805

Shiozaki, Y., Sato, M., Kimura, M., Sato, T., Tazaki, M. and Shibukawa, Y. 2017. Ionotropic P2X ATP Receptor Channels Mediate Purinergic Signaling in Mouse Odontoblasts. *Front Physiol* 8, p. 3. doi: 10.3389/fphys.2017.00003

Shrivastava, A. N., Triller, A., Sieghart, W. and Sarto-Jackson, I. 2011. Regulation of GABA(A) receptor dynamics by interaction with purinergic P2X(2) receptors. *J Biol Chem* 286(16), pp. 14455-14468. doi: 10.1074/jbc.M110.165282

Silverman, W. R. et al. 2009. The pannexin 1 channel activates the inflammasome in neurons and astrocytes. *J Biol Chem* 284(27), pp. 18143-18151. doi: 10.1074/jbc.M109.004804

Simons, M. et al. 1991. Human nonmuscle myosin heavy chains are encoded by two genes located on different chromosomes. *Circ Res* 69(2), pp. 530-539.

Sluyter, R. 2017. The P2X7 Receptor. *Adv Exp Med Biol* 1051, pp. 17-53. doi: 10.1007/5584_2017_59

Smart, M. L., Gu, B., Panchal, R. G., Wiley, J., Cromer, B., Williams, D. A. and Petrou, S. 2003. P2X7 receptor cell surface expression and cytolytic pore formation are regulated by a distal C-terminal region. *J Biol Chem* 278(10), pp. 8853-8860. doi: 10.1074/jbc.M211094200

Smart, M. L., Panchal, R. G., Bowser, D. N., Williams, D. A. and Petrou, S. 2002. Pore formation is not associated with macroscopic redistribution of P2X7 receptors. *Am J Physiol Cell Physiol* 283(1), pp. C77-84. doi: 10.1152/ajpcell.00456.2001

Solini, A. et al. 2008. Increased P2X7 receptor expression and function in thyroid papillary cancer: a new potential marker of the disease? *Endocrinology* 149(1), pp. 389-396. doi: 10.1210/en.2007-1223

- Solini, A. et al. 2013. The purinergic 2X7 receptor participates in renal inflammation and injury induced by high-fat diet: possible role of NLRP3 inflammasome activation. *J Pathol* 231(3), pp. 342-353. doi: 10.1002/path.4237
- Solle, M. et al. 2001. Altered cytokine production in mice lacking P2X(7) receptors. *J Biol Chem* 276(1), pp. 125-132. doi: 10.1074/jbc.M006781200
- Sperlagh, B., Vizi, E. S., Wirkner, K. and Illes, P. 2006. P2X7 receptors in the nervous system. *Prog Neurobiol* 78(6), pp. 327-346. doi: 10.1016/j.pneurobio.2006.03.007
- Spooner, R. and Yilmaz, O. 2011. The role of reactive-oxygen-species in microbial persistence and inflammation. *Int J Mol Sci* 12(1), pp. 334-352. doi: 10.3390/ijms12010334
- Steinberg, T. H., Newman, A. S., Swanson, J. A. and Silverstein, S. C. 1987. ATP4- permeabilizes the plasma membrane of mouse macrophages to fluorescent dyes. *J Biol Chem* 262(18), pp. 8884-8888.
- Surprenant, A. and North, R. A. 2009. Signaling at purinergic P2X receptors. *Annu Rev Physiol* 71, pp. 333-359. doi: 10.1146/annurev.physiol.70.113006.100630
- Surprenant, A., Rassendren, F., Kawashima, E., North, R. A. and Buell, G. 1996. The cytolytic P2Z receptor for extracellular ATP identified as a P2X receptor (P2X7). *Science* 272(5262), pp. 735-738. doi: 10.1126/science.272.5262.735
- Suzuki, J., Denning, D. P., Imanishi, E., Horvitz, H. R. and Nagata, S. 2013. Xk-related protein 8 and CED-8 promote phosphatidylserine exposure in apoptotic cells. *Science* 341(6144), pp. 403-406. doi: 10.1126/science.1236758
- Suzuki, J., Umeda, M., Sims, P. J. and Nagata, S. 2010. Calcium-dependent phospholipid scrambling by TMEM16F. *Nature* 468(7325), pp. 834-838. doi: 10.1038/nature09583
- Swiatecka-Urban, A. et al. 2007. Myosin Vb is required for trafficking of the cystic fibrosis transmembrane conductance regulator in Rab11a-specific apical recycling endosomes in polarized human airway epithelial cells. *J Biol Chem* 282(32), pp. 23725-23736. doi: 10.1074/jbc.M608531200
- Tafari, M. et al. 2011. Hypoxia-increased RAGE and P2X7R expression regulates tumor cell invasion through phosphorylation of Erk1/2 and Akt and nuclear translocation of NF- κ B. *Carcinogenesis* 32(8), pp. 1167-1175. doi: 10.1093/carcin/bgr101

Takai, E., Tsukimoto, M., Harada, H. and Kojima, S. 2014. Autocrine signaling via release of ATP and activation of P2X7 receptor influences motile activity of human lung cancer cells. *Purinergic Signal* 10(3), pp. 487-497. doi: 10.1007/s11302-014-9411-x

Takizawa, N., Ikebe, R., Ikebe, M. and Luna, E. J. 2007. Supervillin slows cell spreading by facilitating myosin II activation at the cell periphery. *J Cell Sci* 120(Pt 21), pp. 3792-3803. doi: 10.1242/jcs.008219

Tanoue, T. and Nishida, E. 2003. Molecular recognitions in the MAP kinase cascades. *Cell Signal* 15(5), pp. 455-462. doi: 10.1016/s0898-6568(02)00112-2

Tazi, J., Bakkour, N. and Stamm, S. 2009. Alternative splicing and disease. *Biochim Biophys Acta* 1792(1), pp. 14-26. doi: 10.1016/j.bbadis.2008.09.017

Theodosiou, A. and Ashworth, A. 2002. MAP kinase phosphatases. *Genome Biol* 3(7), p. Reviews3009. doi: 10.1186/gb-2002-3-7-reviews3009

Togo, T. and Steinhardt, R. A. 2004. Nonmuscle myosin IIA and IIB have distinct functions in the exocytosis-dependent process of cell membrane repair. *Mol Biol Cell* 15(2), pp. 688-695. doi: 10.1091/mbc.E03-06-0430

Tournaviti, S. et al. 2007. SH4-domain-induced plasma membrane dynamization promotes bleb-associated cell motility. *J Cell Sci* 120(Pt 21), pp. 3820-3829. doi: 10.1242/jcs.011130

Trybus, K. M. 2008. Myosin V from head to tail. *Cell Mol Life Sci* 65(9), pp. 1378-1389. doi: 10.1007/s00018-008-7507-6

Vacca, F., Amadio, S., Sancesario, G., Bernardi, G. and Volonte, C. 2004. P2X3 receptor localizes into lipid rafts in neuronal cells. *J Neurosci Res* 76(5), pp. 653-661. doi: 10.1002/jnr.20069

Vacca, F., Giustizieri, M., Ciotti, M. T., Mercuri, N. B. and Volonte, C. 2009. Rapid constitutive and ligand-activated endocytic trafficking of P2X receptor. *J Neurochem* 109(4), pp. 1031-1041. doi: 10.1111/j.1471-4159.2009.06029.x

Valera, S., Hussy, N., Evans, R. J., Adami, N., North, R. A., Surprenant, A. and Buell, G. 1994. A new class of ligand-gated ion channel defined by P2x receptor for extracellular ATP. *Nature* 371(6497), pp. 516-519. doi: 10.1038/371516a0

Vaughn, B. P., Robson, S. C. and Burnstock, G. 2012. Pathological roles of purinergic signaling in the liver. *J Hepatol* 57(4), pp. 916-920. doi: 10.1016/j.jhep.2012.06.008

Verkhatsky, A. and Burnstock, G. 2014. Biology of purinergic signalling: its ancient evolutionary roots, its omnipresence and its multiple functional significance. *Bioessays* 36(7), pp. 697-705. doi: 10.1002/bies.201400024

Vial, C. and Evans, R. J. 2005. Disruption of lipid rafts inhibits P2X1 receptor-mediated currents and arterial vasoconstriction. *J Biol Chem* 280(35), pp. 30705-30711. doi: 10.1074/jbc.M504256200

Vial, C., Fung, C. Y., Goodall, A. H., Mahaut-Smith, M. P. and Evans, R. J. 2006. Differential sensitivity of human platelet P2X1 and P2Y1 receptors to disruption of lipid rafts. *Biochem Biophys Res Commun* 343(2), pp. 415-419. doi: 10.1016/j.bbrc.2006.02.174

Virginio, C., Church, D., North, R. A. and Surprenant, A. 1997. Effects of divalent cations, protons and calmidazolium at the rat P2X7 receptor. *Neuropharmacology* 36(9), pp. 1285-1294.

Virginio, C., MacKenzie, A., North, R. A. and Surprenant, A. 1999. Kinetics of cell lysis, dye uptake and permeability changes in cells expressing the rat P2X7 receptor. *J Physiol* 519 Pt 2, pp. 335-346.

Wadehra, M., Sulur, G. G., Braun, J., Gordon, L. K. and Goodglick, L. 2003. Epithelial membrane protein-2 is expressed in discrete anatomical regions of the eye. *Exp Mol Pathol* 74(2), pp. 106-112. doi: 10.1016/s0014-4800(03)00009-1

Wang, B. and Sluyter, R. 2013. P2X7 receptor activation induces reactive oxygen species formation in erythroid cells. *Purinergic Signal* 9(1), pp. 101-112. doi: 10.1007/s11302-012-9335-2

Wei, Q. and Adelstein, R. S. 2000. Conditional expression of a truncated fragment of nonmuscle myosin II-A alters cell shape but not cytokinesis in HeLa cells. *Mol Biol Cell* 11(10), pp. 3617-3627.

Wei, W., Ryu, J. K., Choi, H. B. and McLarnon, J. G. 2008. Expression and function of the P2X(7) receptor in rat C6 glioma cells. *Cancer Lett* 260(1-2), pp. 79-87. doi: 10.1016/j.canlet.2007.10.025

Weinhold, K., Krause-Buchholz, U., Rodel, G., Kasper, M. and Barth, K. 2010. Interaction and interrelation of P2X7 and P2X4 receptor complexes in mouse lung epithelial cells. *Cell Mol Life Sci* 67(15), pp. 2631-2642. doi: 10.1007/s00018-010-0355-1

- Wiley, J. S., Sluyter, R., Gu, B. J., Stokes, L. and Fuller, S. J. 2011. The human P2X7 receptor and its role in innate immunity. *Tissue Antigens* 78(5), pp. 321-332. doi: 10.1111/j.1399-0039.2011.01780.x
- Wilson, H. L., Wilson, S. A., Surprenant, A. and North, R. A. 2002. Epithelial membrane proteins induce membrane blebbing and interact with the P2X7 receptor C terminus. *J Biol Chem* 277(37), pp. 34017-34023. doi: 10.1074/jbc.M205120200
- Worthington, R. A., Smart, M. L., Gu, B. J., Williams, D. A., Petrou, S., Wiley, J. S. and Barden, J. A. 2002. Point mutations confer loss of ATP-induced human P2X(7) receptor function. *FEBS Lett* 512(1-3), pp. 43-46. doi: 10.1016/s0014-5793(01)03311-7
- Wylie, S. R. and Chantler, P. D. 2001. Separate but linked functions of conventional myosins modulate adhesion and neurite outgrowth. *Nat Cell Biol* 3(1), pp. 88-92. doi: 10.1038/35050613
- Wylie, S. R. and Chantler, P. D. 2003. Myosin IIA drives neurite retraction. *Mol Biol Cell* 14(11), pp. 4654-4666. doi: 10.1091/mbc.E03-03-0187
- Xia, J., Yu, X., Tang, L., Li, G. and He, T. 2015. P2X7 receptor stimulates breast cancer cell invasion and migration via the AKT pathway. *Oncol Rep* 34(1), pp. 103-110. doi: 10.3892/or.2015.3979
- Xu, X. J., Boumechache, M., Robinson, L. E., Marschall, V., Gorecki, D. C., Masin, M. and Murrell-Lagnado, R. D. 2012. Splice variants of the P2X7 receptor reveal differential agonist dependence and functional coupling with pannexin-1. *J Cell Sci* 125(Pt 16), pp. 3776-3789. doi: 10.1242/jcs.099374
- Yang, S. T., Kreutzberger, A. J. B., Lee, J., Kiessling, V. and Tamm, L. K. 2016. The role of cholesterol in membrane fusion. *Chem Phys Lipids* 199, pp. 136-143. doi: 10.1016/j.chemphyslip.2016.05.003
- Yegutkin, G. G. 2008. Nucleotide- and nucleoside-converting ectoenzymes: Important modulators of purinergic signalling cascade. *Biochim Biophys Acta* 1783(5), pp. 673-694. doi: 10.1016/j.bbamcr.2008.01.024
- Ying, H. et al. 2012. Oncogenic Kras maintains pancreatic tumors through regulation of anabolic glucose metabolism. *Cell* 149(3), pp. 656-670. doi: 10.1016/j.cell.2012.01.058
- Yip, L. et al. 2009. Autocrine regulation of T-cell activation by ATP release and P2X7 receptors. *Faseb j* 23(6), pp. 1685-1693. doi: 10.1096/fj.08-126458

- Yoon, S. and Seger, R. 2006. The extracellular signal-regulated kinase: multiple substrates regulate diverse cellular functions. *Growth Factors* 24(1), pp. 21-44. doi: 10.1080/02699050500284218
- Young, C. N., Sinadinos, A., Lefebvre, A., Chan, P., Arkle, S., Vaudry, D. and Gorecki, D. C. 2015. A novel mechanism of autophagic cell death in dystrophic muscle regulated by P2RX7 receptor large-pore formation and HSP90. *Autophagy* 11(1), pp. 113-130. doi: 10.4161/15548627.2014.994402
- Young, M. T. 2010. P2X receptors: dawn of the post-structure era. *Trends Biochem Sci* 35(2), pp. 83-90. doi: 10.1016/j.tibs.2009.09.006
- Young, M. T., Fisher, J. A., Fountain, S. J., Ford, R. C., North, R. A. and Khakh, B. S. 2008. Molecular shape, architecture, and size of P2X4 receptors determined using fluorescence resonance energy transfer and electron microscopy. *J Biol Chem* 283(38), pp. 26241-26251. doi: 10.1074/jbc.M804458200
- Young, M. T., Pelegrin, P. and Surprenant, A. 2007. Amino acid residues in the P2X7 receptor that mediate differential sensitivity to ATP and BzATP. *Mol Pharmacol* 71(1), pp. 92-100. doi: 10.1124/mol.106.030163
- Zanoni, I. and Granucci, F. 2013. Role of CD14 in host protection against infections and in metabolism regulation. *Front Cell Infect Microbiol* 3, p. 32. doi: 10.3389/fcimb.2013.00032
- Zhang, Q., Lenardo, M. J. and Baltimore, D. 2017. 30 Years of NF-kappaB: A Blossoming of Relevance to Human Pathobiology. *Cell* 168(1-2), pp. 37-57. doi: 10.1016/j.cell.2016.12.012
- Zhang, X. J. et al. 2004. Expression of P2X7 in human hematopoietic cell lines and leukemia patients. *Leuk Res* 28(12), pp. 1313-1322. doi: 10.1016/j.leukres.2004.04.001
- Zhang, Y. and Dong, C. 2007. Regulatory mechanisms of mitogen-activated kinase signaling. *Cell Mol Life Sci* 64(21), pp. 2771-2789. doi: 10.1007/s00018-007-7012-3
- Zimmermann, H. 2006. Ectonucleotidases in the nervous system. *Novartis Found Symp* 276, pp. 113-128; discussion 128-130, 233-117, 275-181.
- Zimmermann, H. 2016. Extracellular ATP and other nucleotides-ubiquitous triggers of intercellular messenger release. *Purinergic Signal* 12(1), pp. 25-57. doi: 10.1007/s11302-015-9483-2

Zuo, Y., Wang, J., Liao, F., Yan, X., Li, J., Huang, L. and Liu, F. 2018. Inhibition of Heat Shock Protein 90 by 17-AAG Reduces Inflammation via P2X7 Receptor/NLRP3 Inflammasome Pathway and Increases Neurogenesis After Subarachnoid Hemorrhage in Mice. *Front Mol Neurosci* 11, p. 401. doi: 10.3389/fnmol.2018.00401

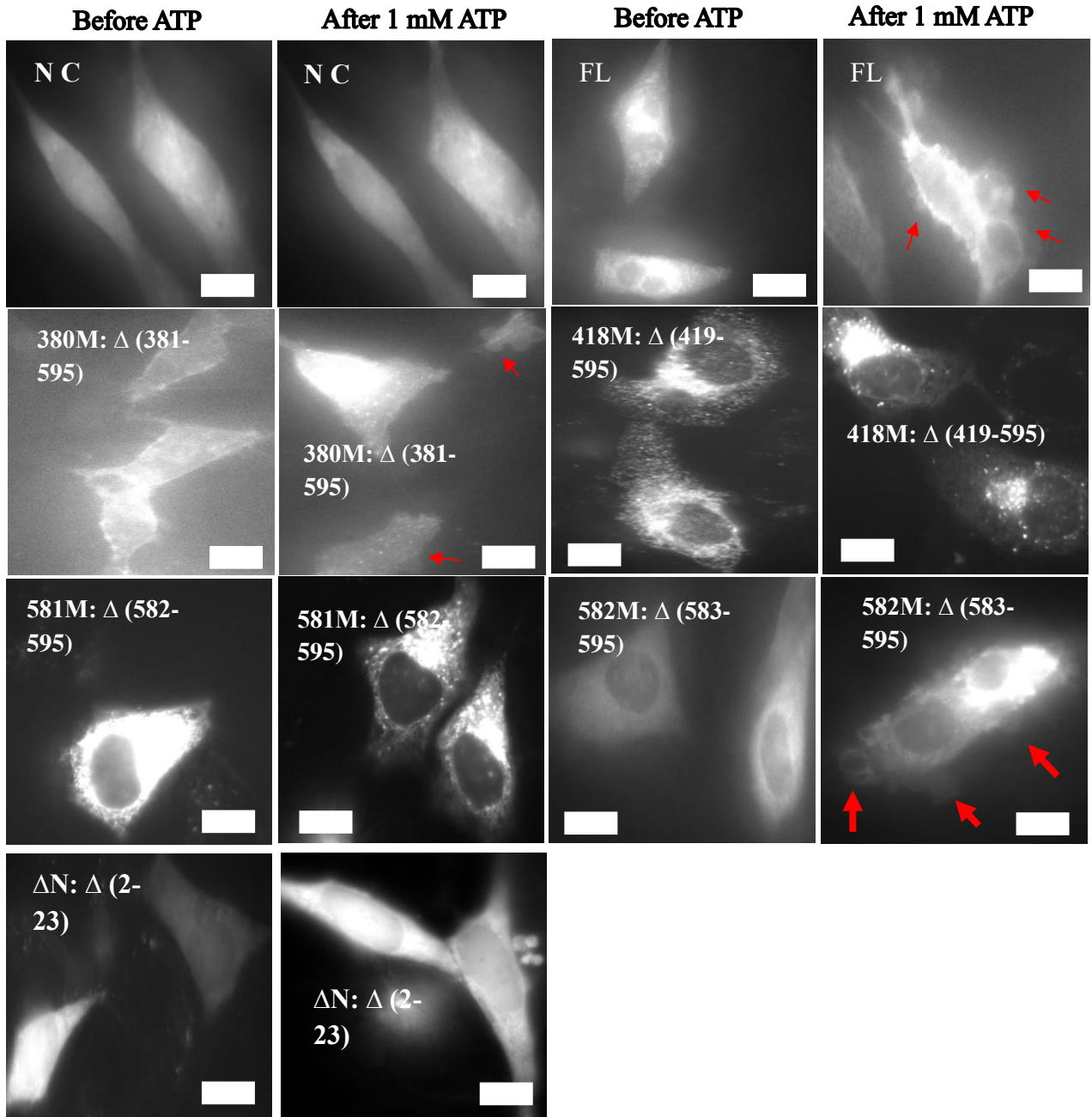
Appendix 1: PCR Conditions

Conditions	Guidelines
Denaturation	Temp: 98°C. Time: 10 sec on initial cycle; 30 sec on the rest
Annealing	Temp: 52°C. Time: 30 sec
Extension	Temp: 72°C. Time: 210 sec; 10 min on last cycle
Number of cycles	30 cycles

Appendix 2: Oligonucleotide sequences

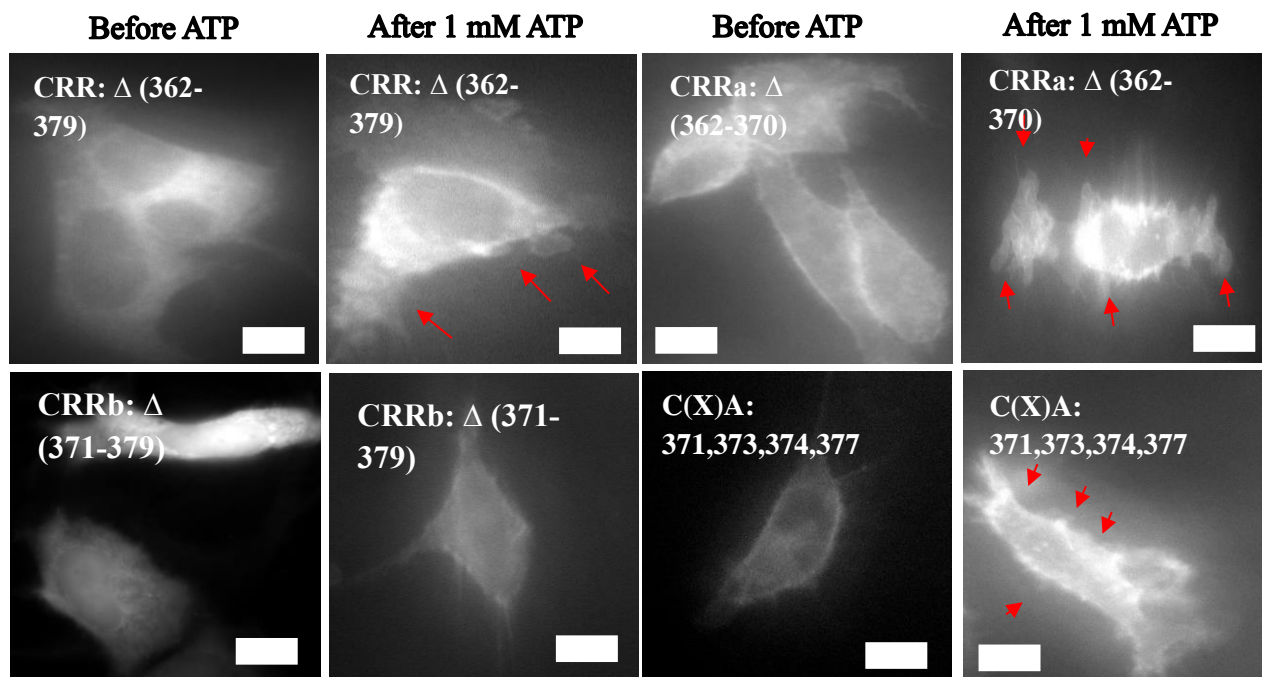
Mutants	Deleted portion	Primers	
		Sense	Anti-sense
1-380	Δ (381-595)	5'-GCGAATTCTGCAGTCGA-3'	5'-ATT CAC TGC ACA GGG C-3'
1-418	Δ (419-595)	5'-GCGAATTCTGCAGTCGA-3'	5'-CCCAAGCAGCTGCTGG-3'
1-581	Δ (582-595)	5'-GCGAATTCTGCAGTCGA-3'	5'-GAA CTC CTT CCG GAT CT-3'
1-582	Δ (583-595)	5'-GCGAATTCTGCAGTCGA-3'	5'-GGG GAA CTC CTT CCG-3'
D1	Δ (389-405)	5'- GAG CCC CAC ATT TGG ATG-3'	5'- ACA CTT CTT TCT GTA GTA GTA CTC-3'
D2	Δ (441-460)	5'- CTG CTC CAG ATA GAA GCG-3'	5'- AGA CAG TTC CAA GAA GTC C-3'
D3	Δ (494-508)	5'- ACC TCT GAG CTC TTC AGT-3'	5'- GGC CCT GCG GTT CTC-3'
D4	Δ (389-531)	5'- CCC TTG CTG GCG CTG-3'	5'- ACA CTT CTT TCT GTA GTA GTA CTC-3'
D5	Δ (381-417)	5'- GGG AAA AGT CTG CAA GAT G-3'	5'-ATT CAC TGC ACA GGG C-3'
ΔN	Δ (2-23)	5'-GTG AAT TAC GGC ACC ATC-3'	5'-CAT GGT GGC TCG AGA G -3'
D6	Δ (441-493)	5'-CTG GAG GAG CTG TGC-3'	5'- AGA CAG TTC CAA GAA GTC C-3'
D7	Δ (418-460)	5'- CTG CTC CAG ATA GAA GCG-3'	5'- AAG CAG CTG CTG GTC-3'
D8	Δ (583-595) & Δ (441-460)	It is 1-582 and D2 combination mutation; use D2 primers with 1-582 DNA template or 1-582 primers with D2 DNA template to produce D8.	
CRR	Δ (362-379)	5'- AAT GAG TAC TAC TAC AGA AAG AAG TG-3'	5'-GGT ACT GGC ATA CGT G-3'
CE	Δ (362-370)	5'-TGT AAG TGC TGC GAG C-3'	5'-GGT ACT GGC ATA CGT G-3'
CNE	Δ (371-379)	5'- AAT GAG TAC TAC TAC AGA AAG AAG TG-3'	5'-GGA GGG GTA AAC ACG T-3'
C(X)A	371, 373 374, 377	5'- GCA GAG CCC GCA GCA GTG AAT GAG TAC TAC TAC AGA AAG AAG TGT-3'	5'- TGC CTT TGC GGA GGG GTA AAC ACG TGA CCT GCA G-3'

Appendix 3: Cell blebbing of truncation mutants in Hela cells



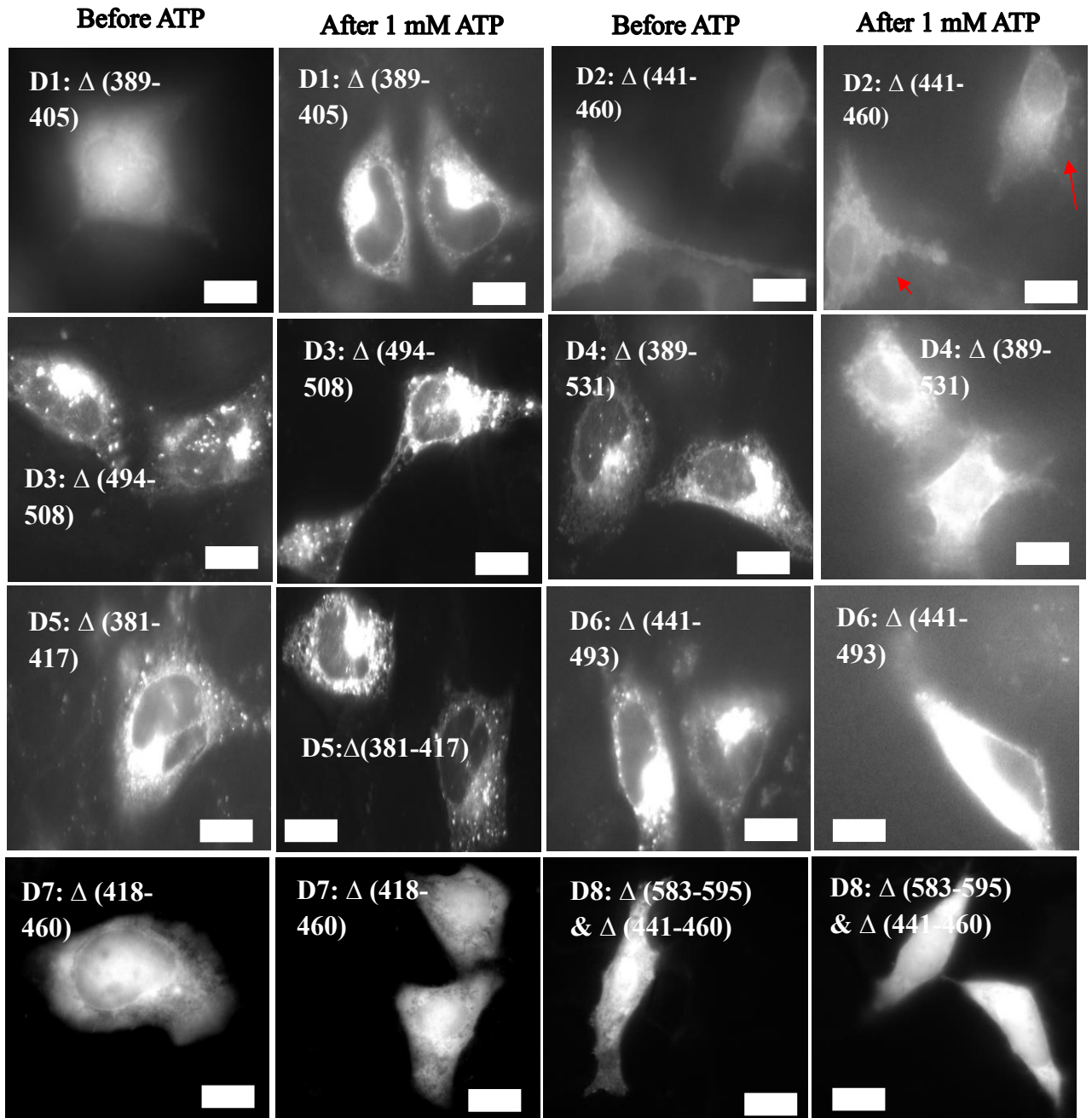
N.C: HeLa cells transfected with GFP⁺, FL: rP2X7-GFP-(His)₈ full length. Red arrows show cell blebbing, scale bar represents 10 μ m. The figure shows representative images, the number of cells analysed per experiment varied between (2-8) from 3 independent experiments.

Appendix 4: Cell blebbing of C-cys anchor mutants in Hela cells



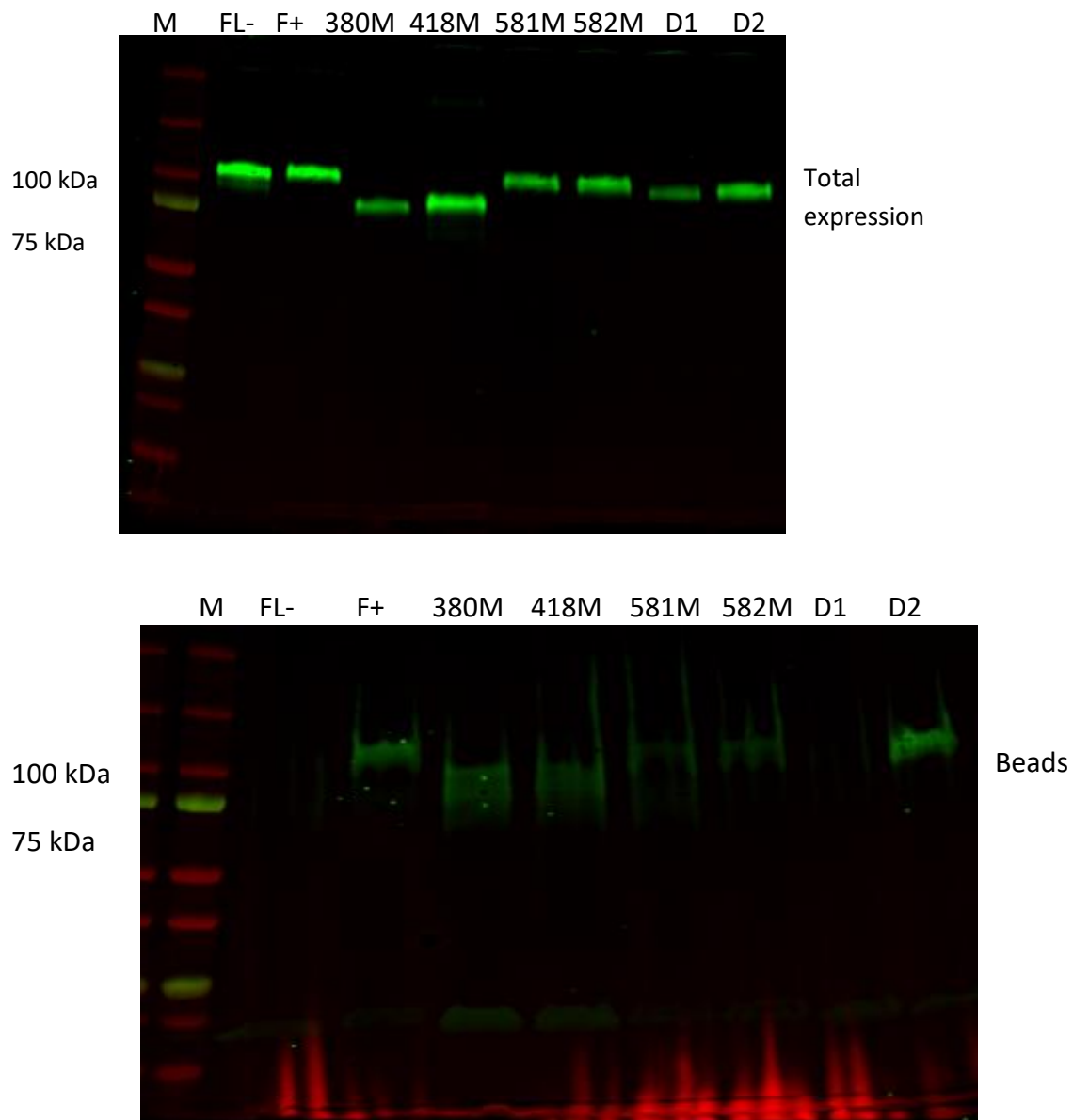
Red arrows show cell blebbing, scale bar represents 10 μm . The figure shows representative images, the number of cells analysed per experiment varied between (2-8) from 3 independent experiments.

Appendix 5: Cell blebbing of the internal deletions in Hela cells

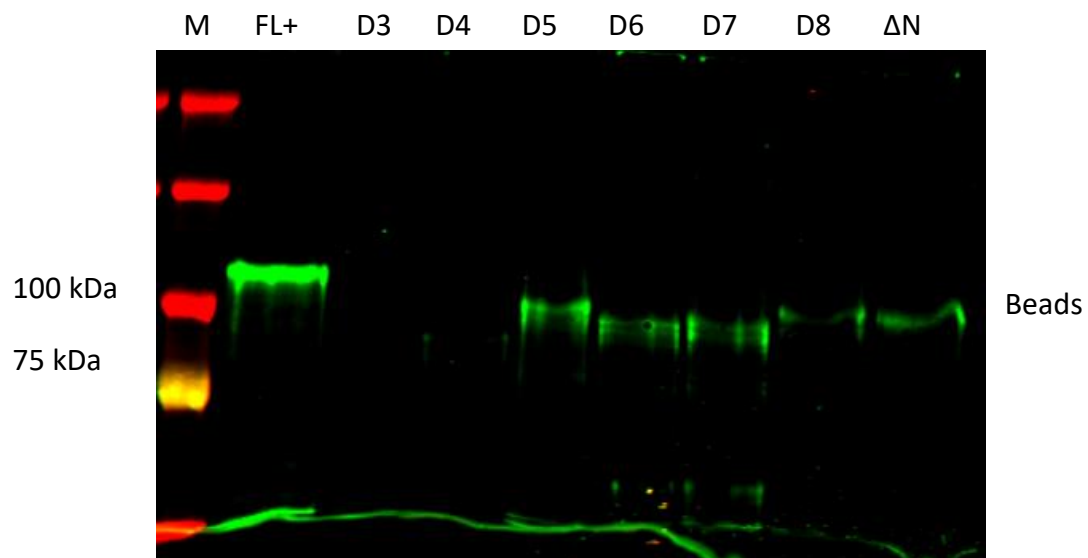
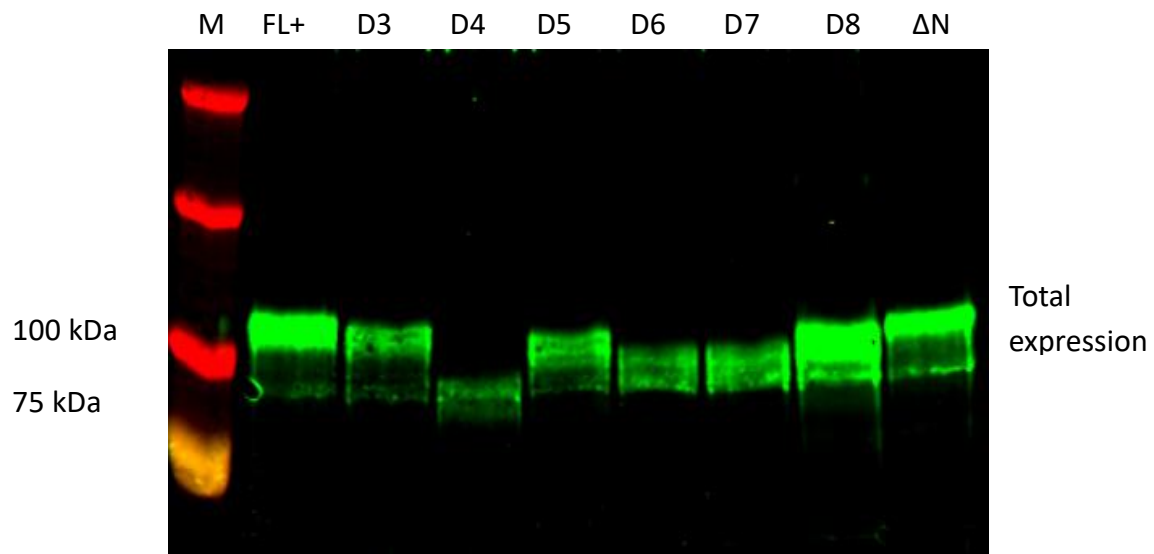


Red arrows show cell blebbing, scale bar represents 10 μ m. The figure shows representative images, the number of cells analysed per experiment varied between (2-8) from 3 independent experiments.

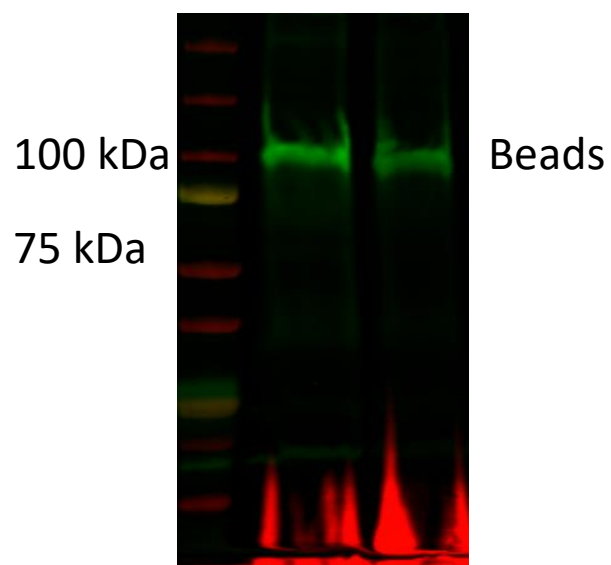
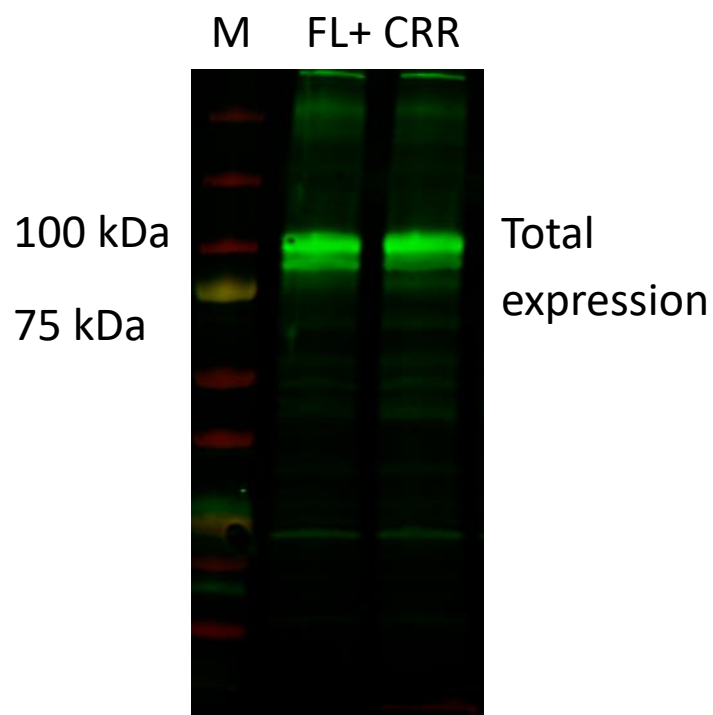
Appendix 6: Cell surface expression blots



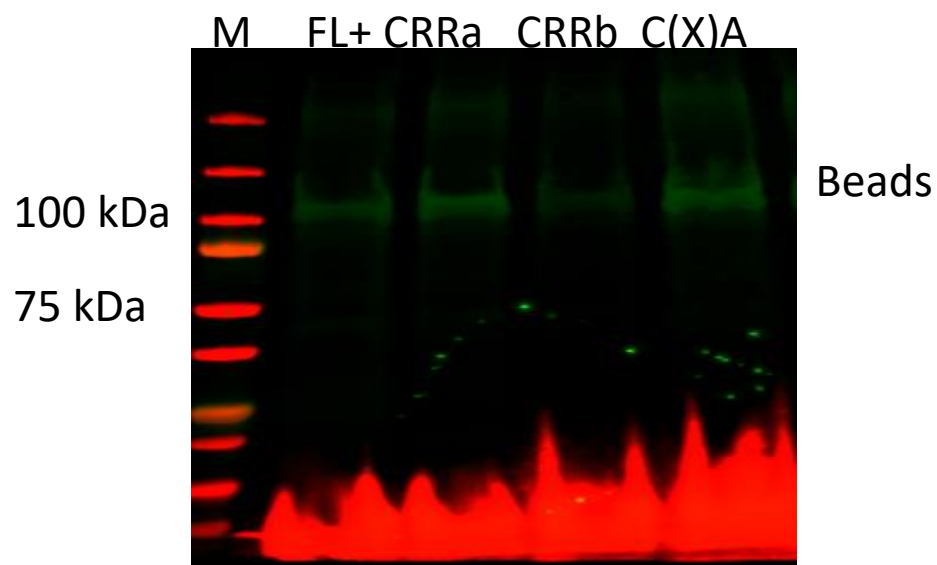
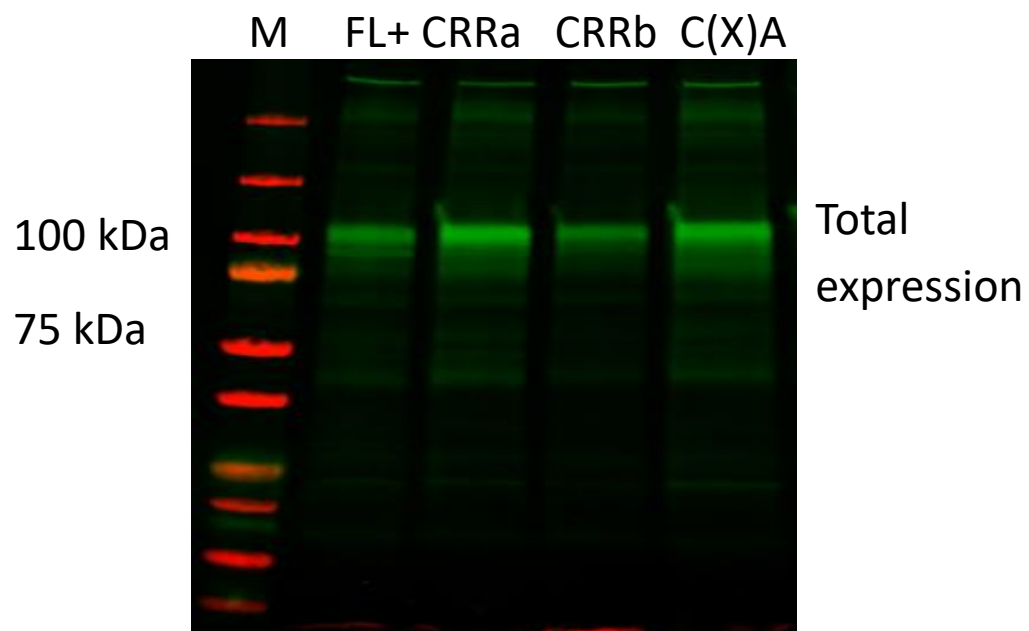
FL-: rP2X7-GFP-(His)₈ transient transfected full-length (negative control, cells were not incubated with biotin), FL+: rP2X7-GFP-(His)₈ transient transfected full-length (positive control, cells were incubated with biotin).



FL+: rP2X7-GFP-(His)₈ transient transfected full-length (positive control, cells were incubated with biotin).

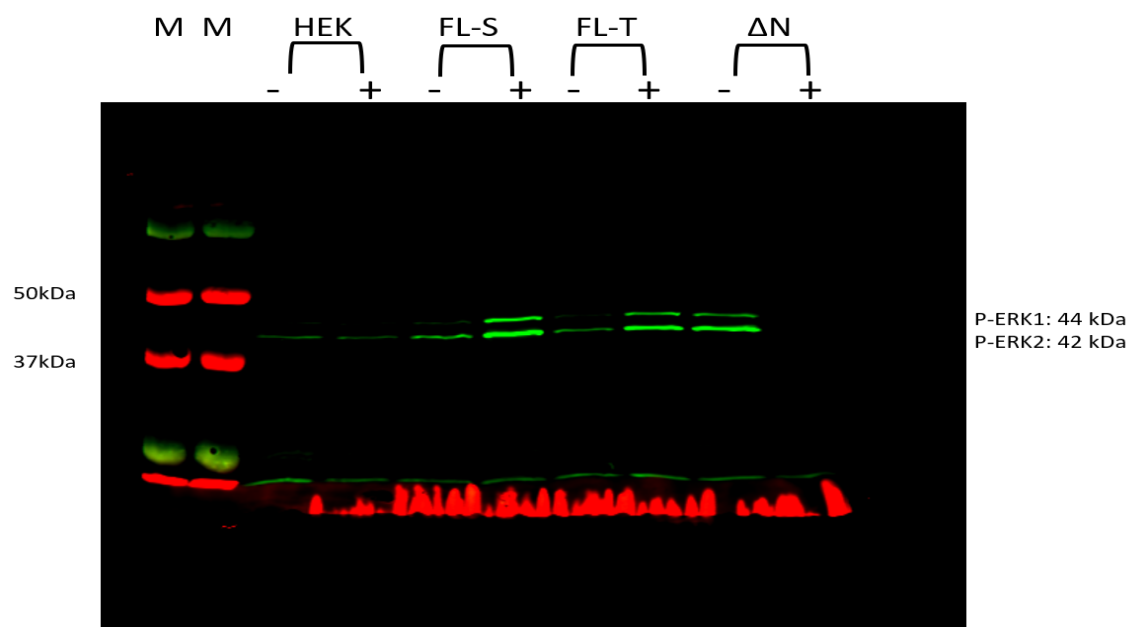
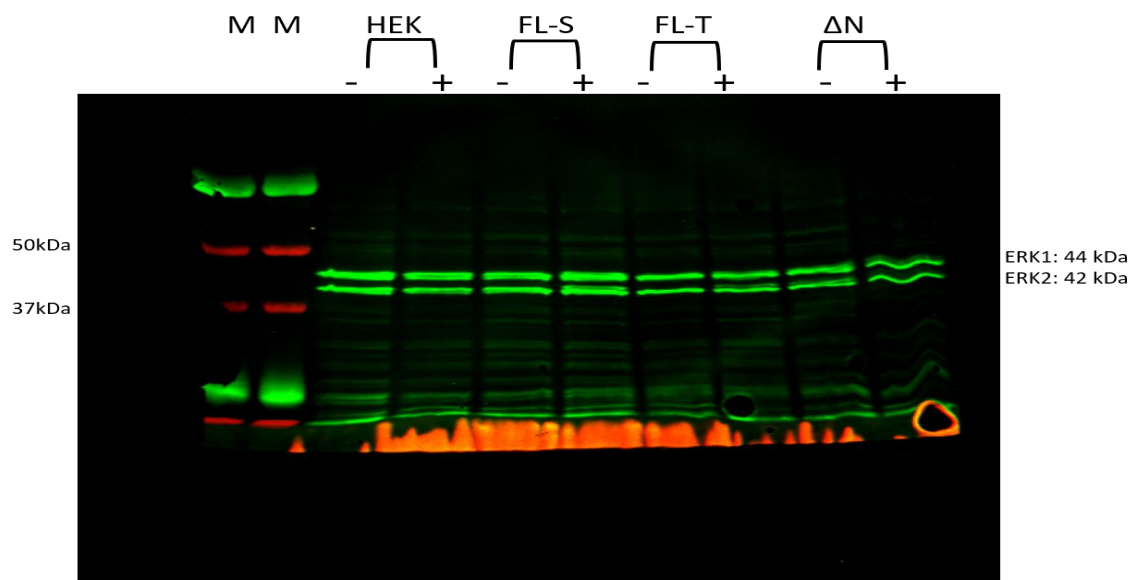


FL+: rP2X7-GFP-(His)₈ transient transfected full-length (positive control, cells were incubated with biotin).

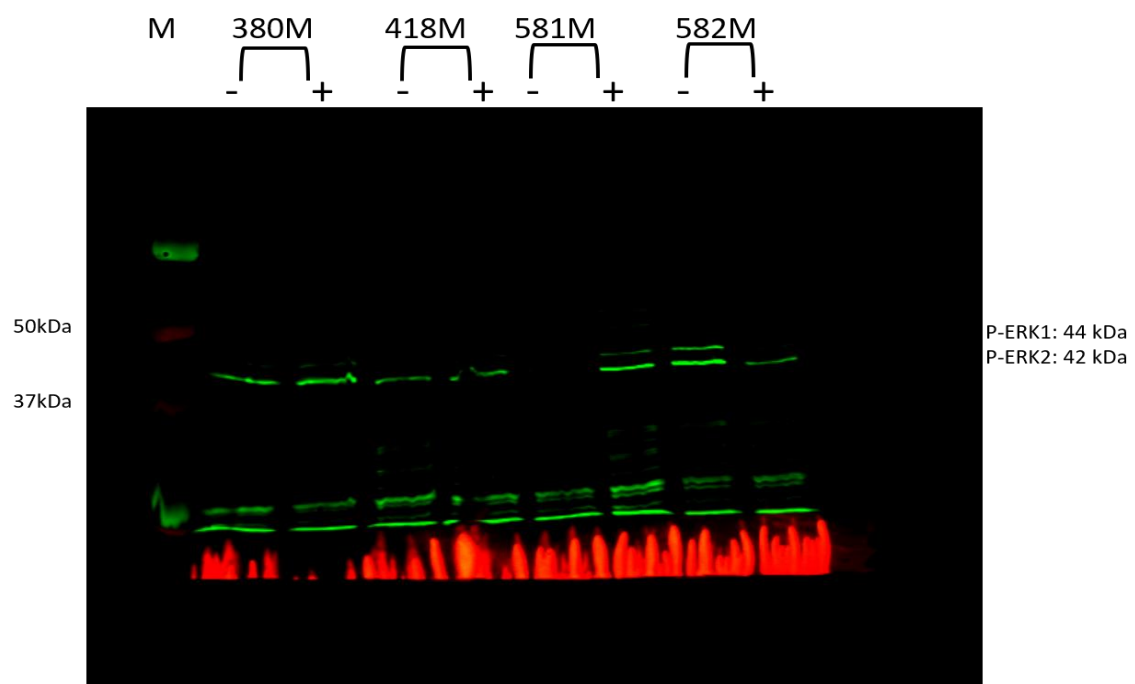
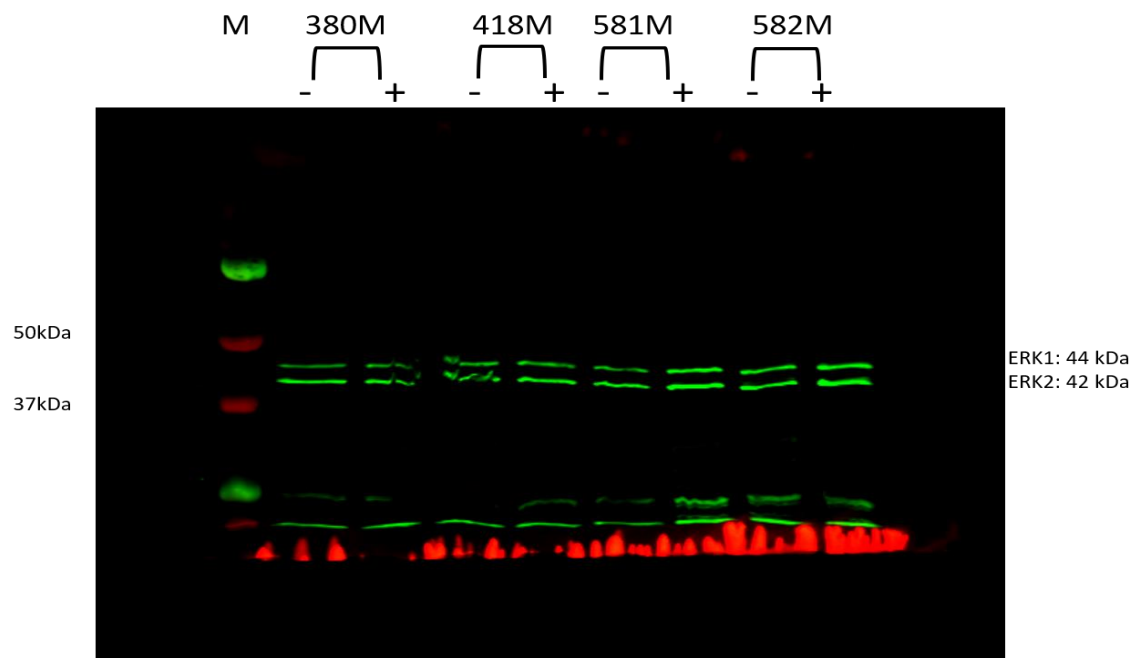


FL+: rP2X7-GFP-(His)₈ transient transfected full-length (positive control, cells were incubated with biotin.

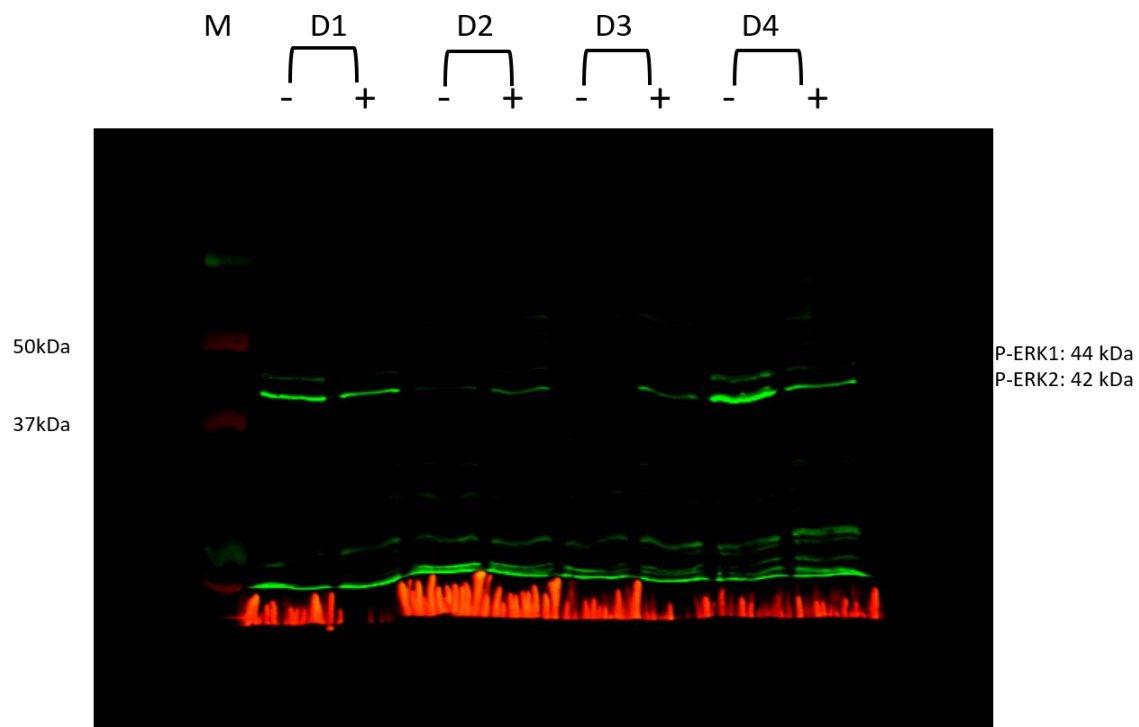
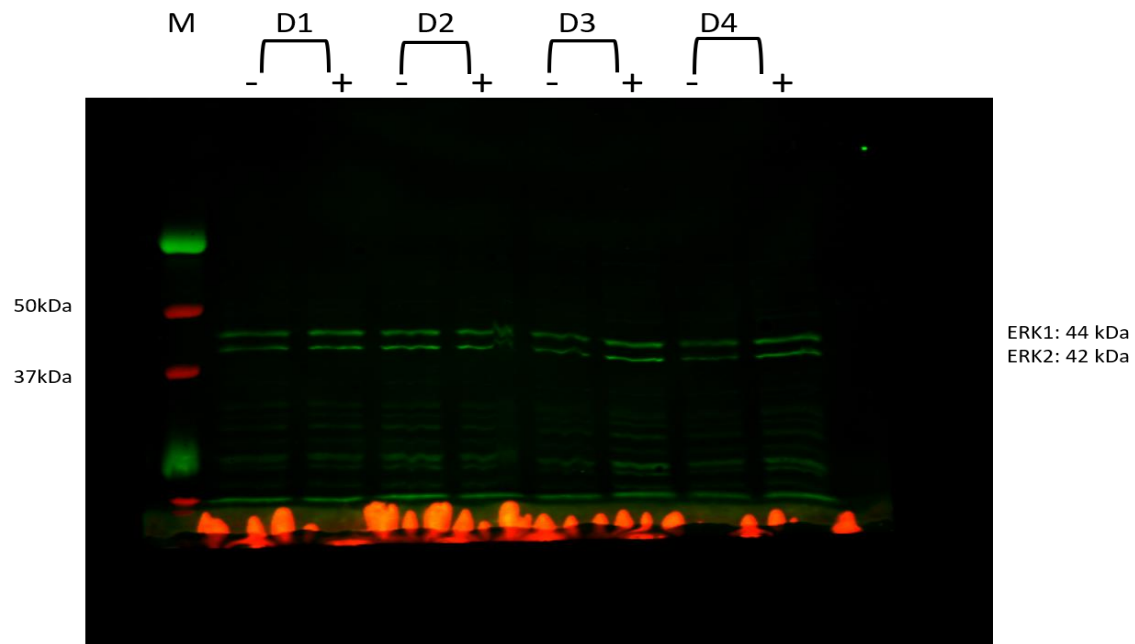
Appendix 7: ERK1/2 phosphorylation blots



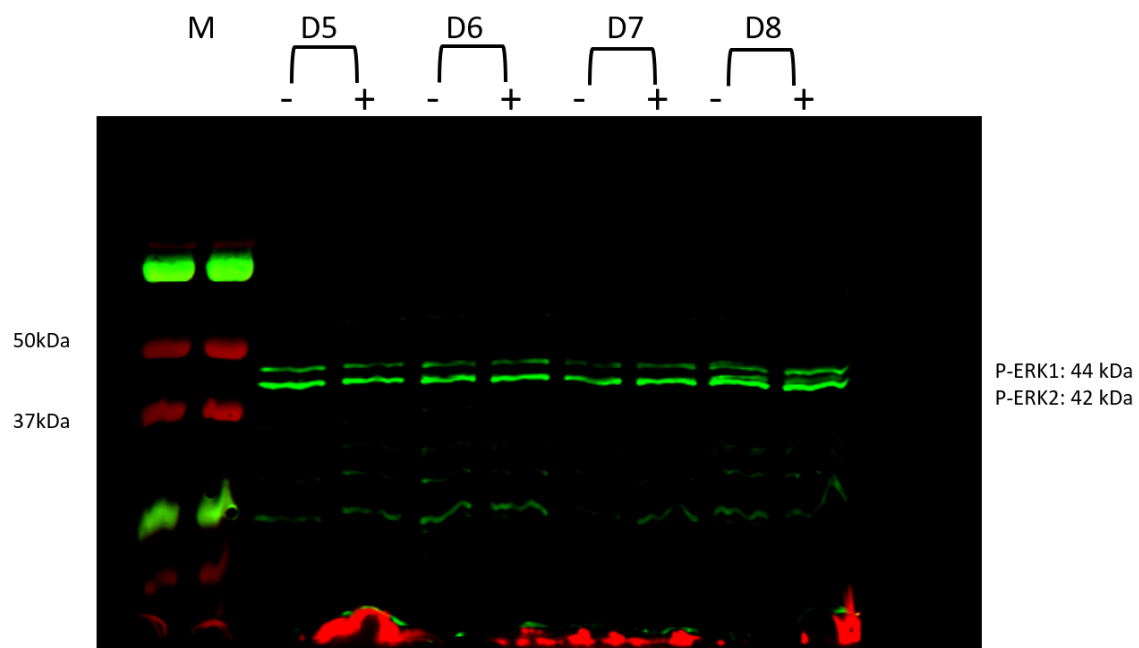
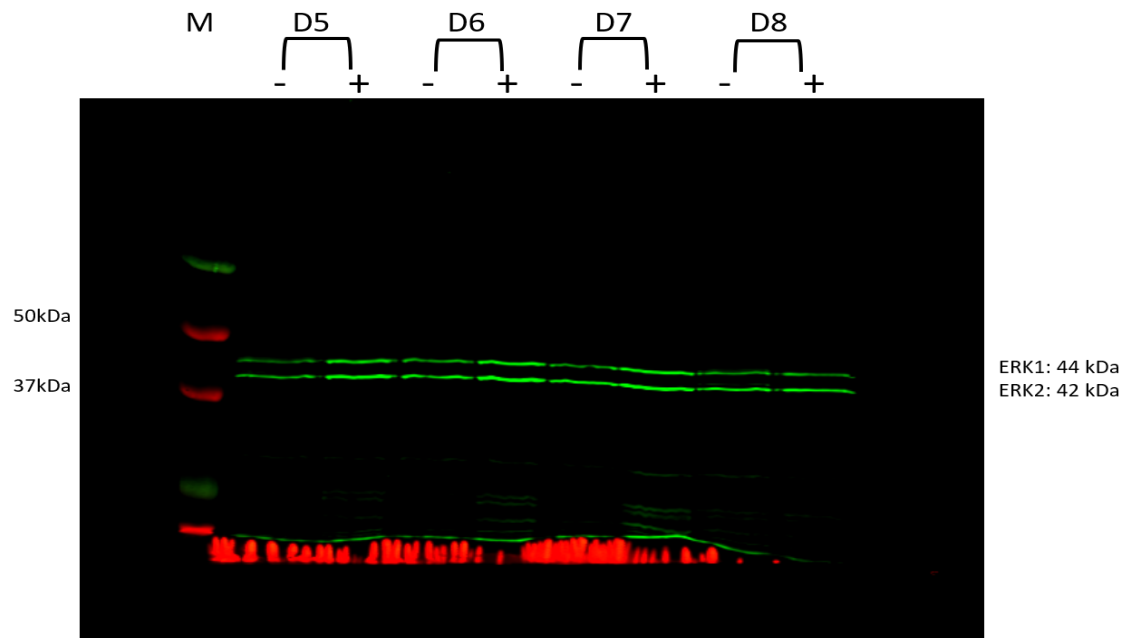
HEK: HEK-293 cells, FL-S: rP2X7-GFP-(His)₈ full-length stably transfected, FL-T: rP2X7-GFP-(His)₈ full-length transiently transfected. Each sample has two groups; (+) cells were stimulated with 1 mM of ATP for 2 minutes before lysis and (-) cells were not stimulated. ERK 1 is 44 kDa, and ERK 2 is 42 kDa. Representative blot from 3 independent experiments.



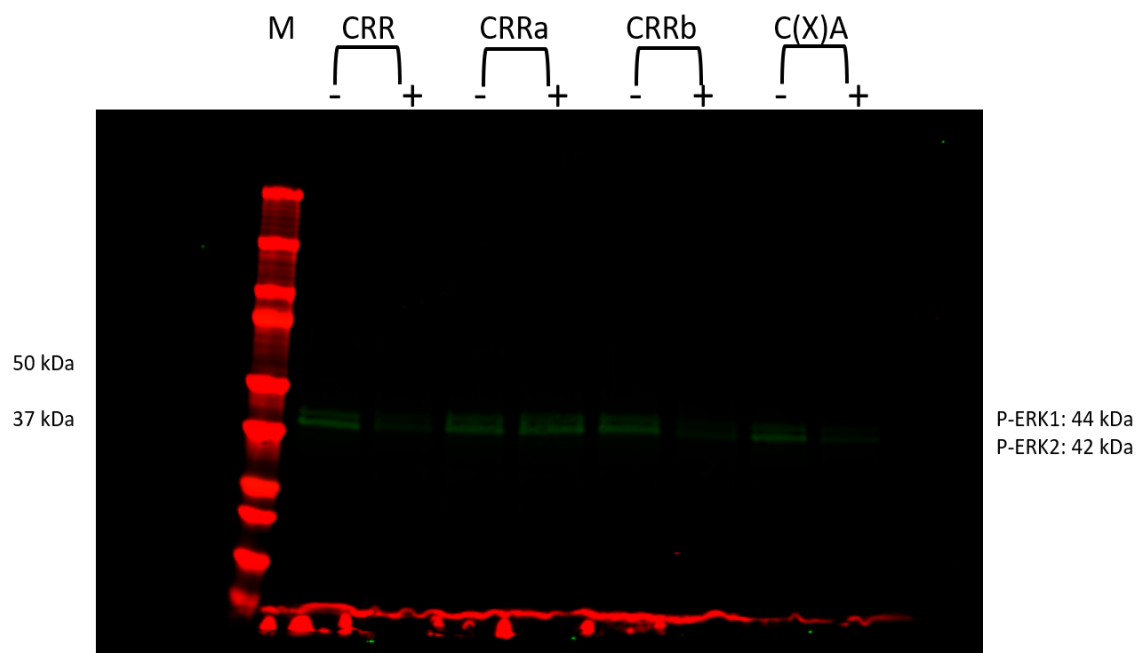
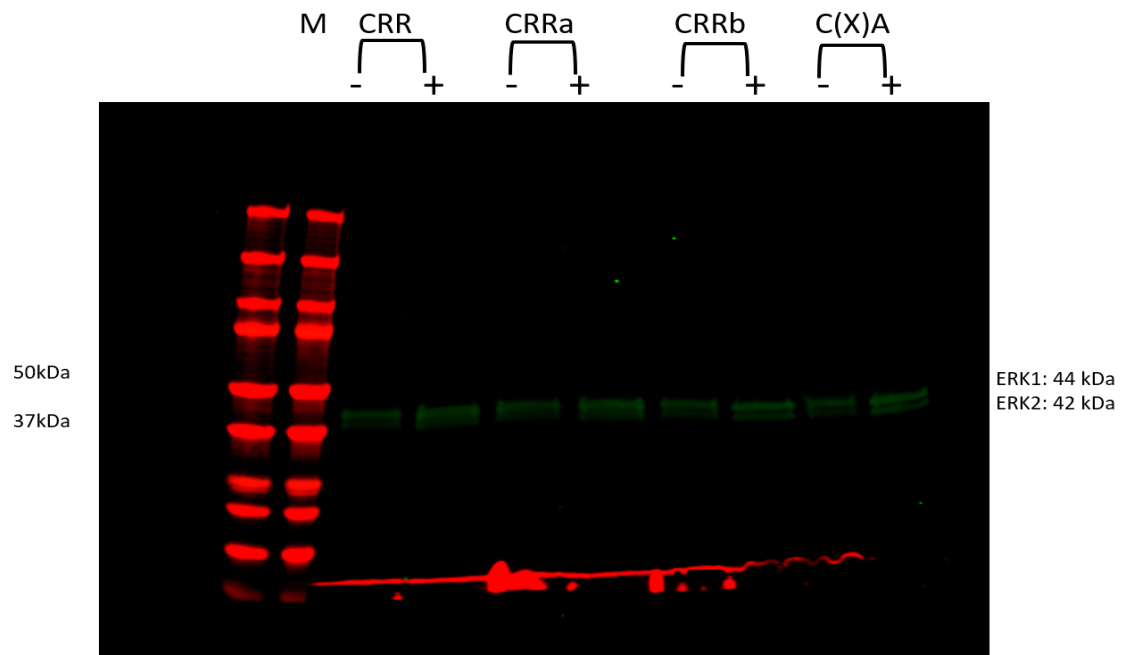
Each sample has two groups; (+) cells were stimulated with 1 mM of ATP for 2 minutes before lysis and (-) cells were not stimulated. ERK 1 is 44 kDa, and ERK 2 is 42 kDa. Representative blot from 3 independent experiments.



Each sample has two groups; (+) cells were stimulated with 1 mM of ATP for 2 minutes before lysis and (-) cells were not stimulated. ERK 1 is 44 kDa, and ERK 2 is 42 kDa. Representative blot from 3 independent experiments.

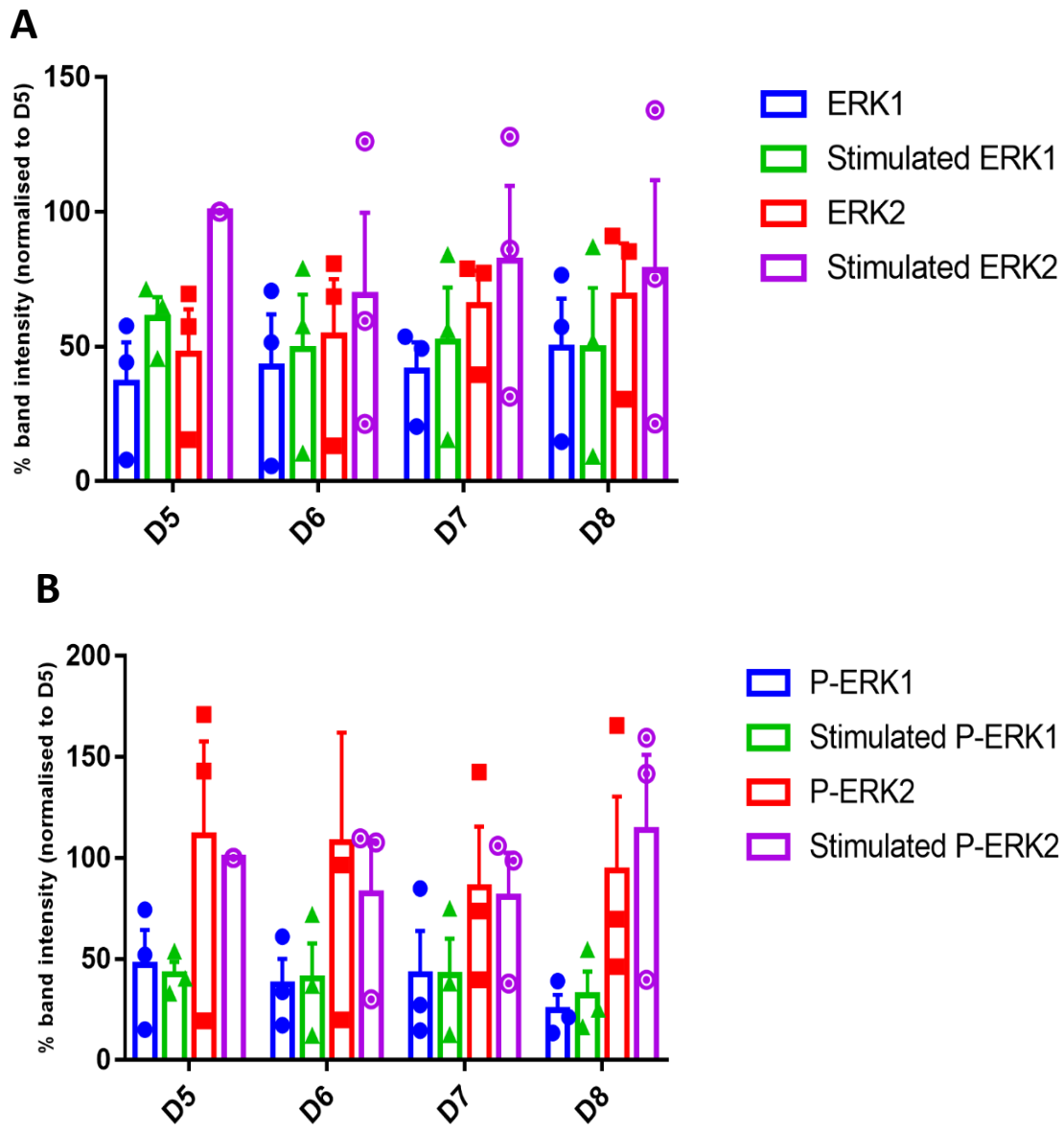


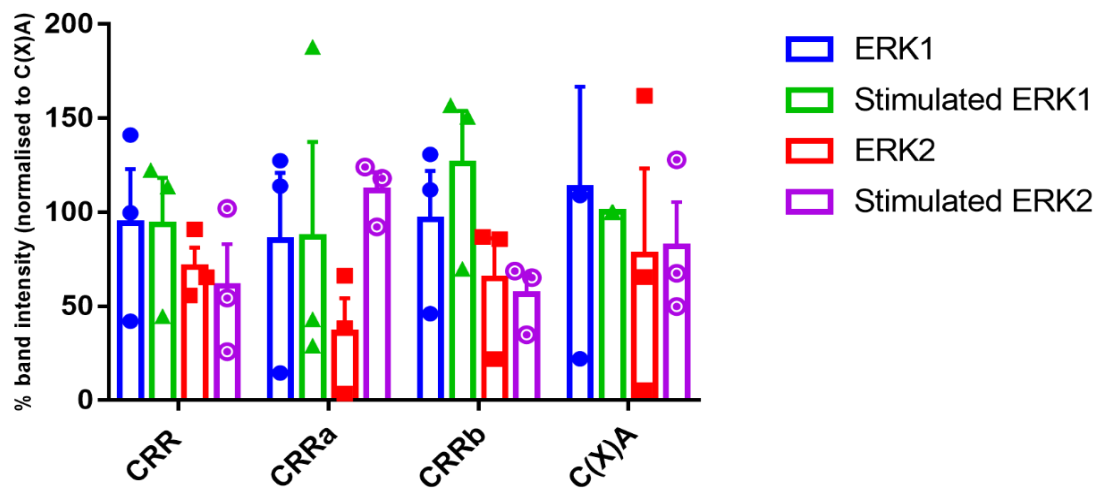
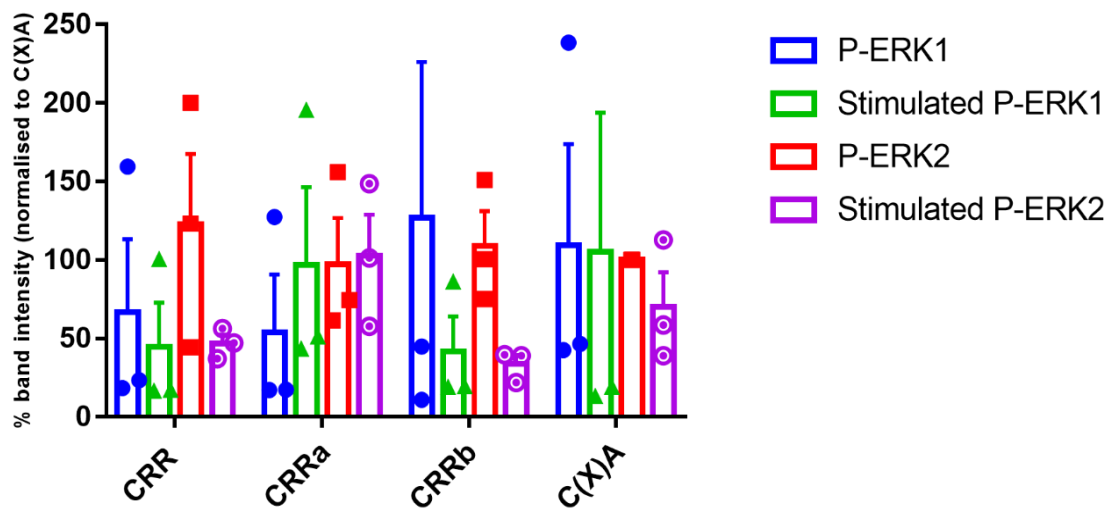
Each sample has two groups; (+) cells were stimulated with 1 mM of ATP for 2 minutes before lysis and (-) cells were not stimulated. ERK 1 is 44 kDa, and ERK 2 is 42 kDa. Representative blot from 3 independent experiments.



Each sample has two groups; (+) cells were stimulated with 1 mM of ATP for 2 minutes before lysis and (-) cells were not stimulated. ERK 1 is 44 kDa, and ERK 2 is 42 kDa. Representative blot from 3 independent experiments.

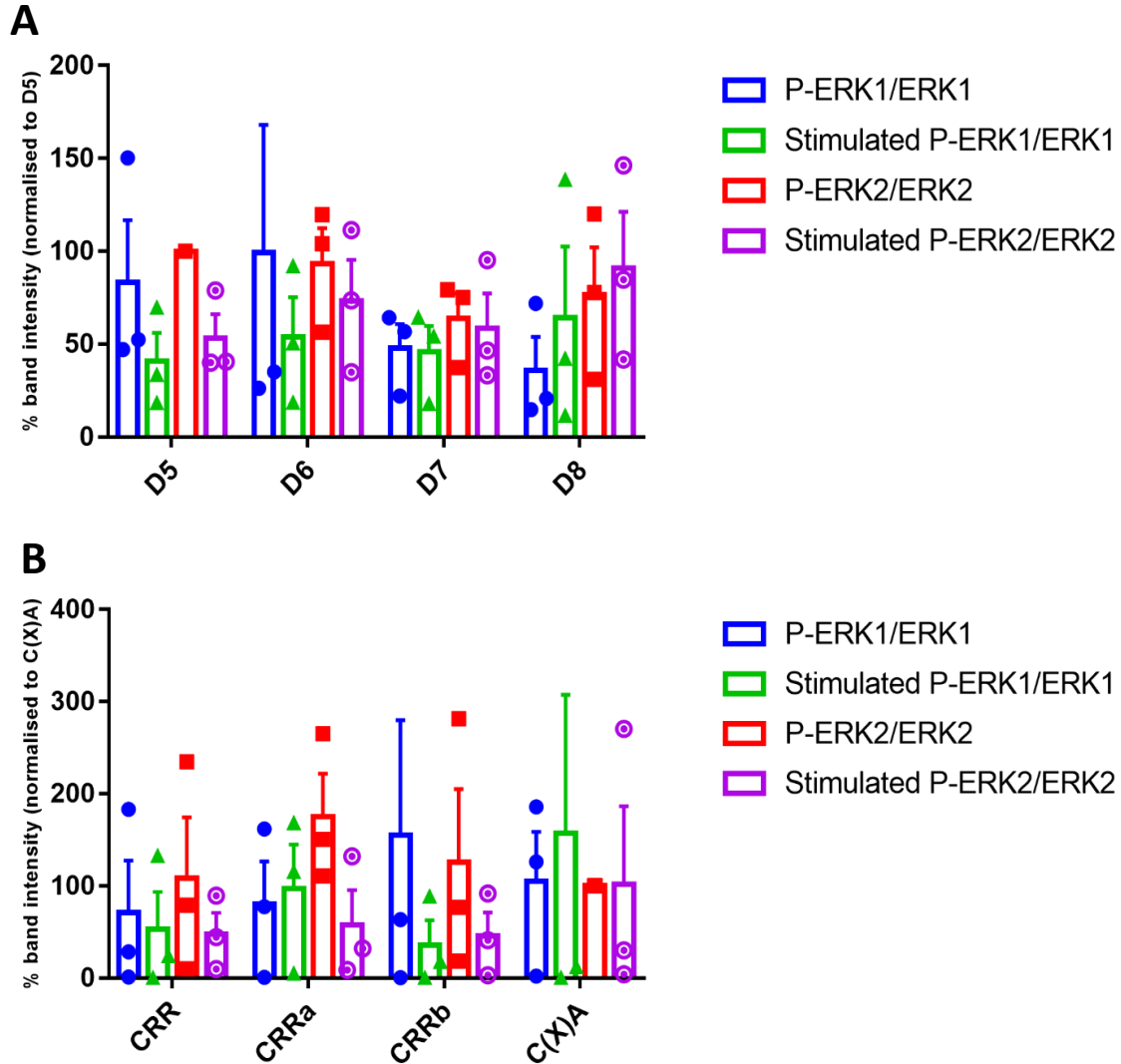
Appendix 8: ERK(1/2) and P-ERK(1/2) levels



C**D**

(A): ERK (1/2) basal levels for stimulated and un-stimulated D5, D6, D7 and D8. (B): P-ERK (1/2) basal levels for stimulated and un-stimulated D5, D6, D7 and D8. (C): ERK (1/2) basal levels for stimulated and un-stimulated CRR, CRRa, CRRb, and C(X)A. (D): P-ERK (1/2) basal levels for stimulated and un-stimulated CRR, CRRa, CRRb, and C(X)A. Results are (\pm SEM).

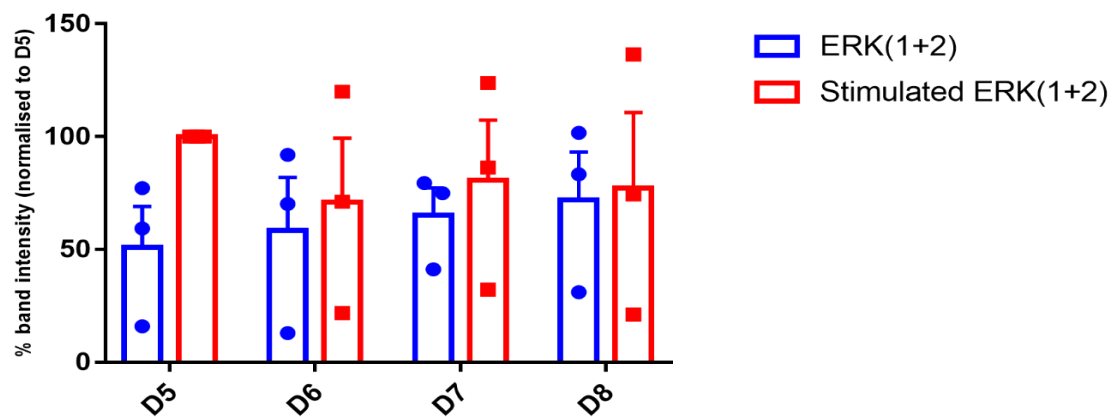
Appendix 9: P-ERK1 and P-ERK2 inductions



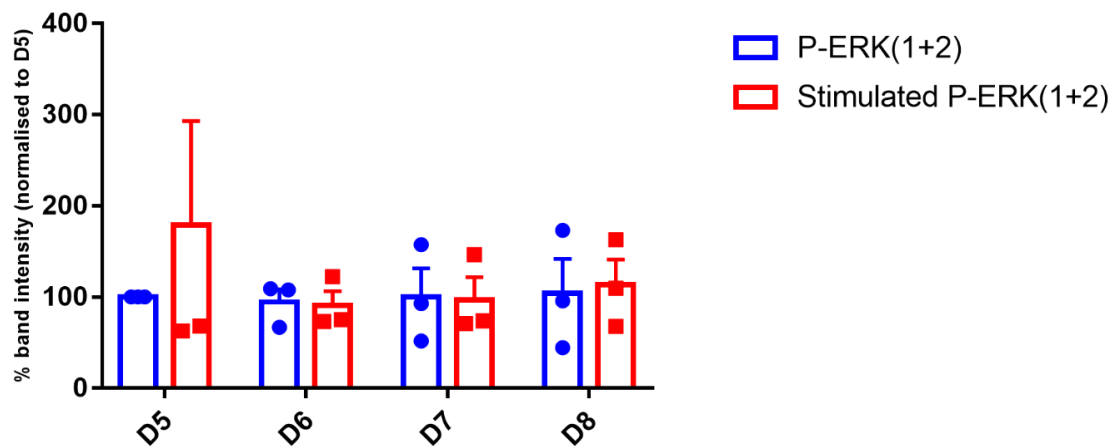
(A): P-ERK (1/2) inductions for stimulated and un-stimulated D5, D6, D7 and D8. (B): P-ERK (1/2) inductions for stimulated and un-stimulated CRR, CRRa, CRRb, and C(X)A. Results are (\pm SEM).

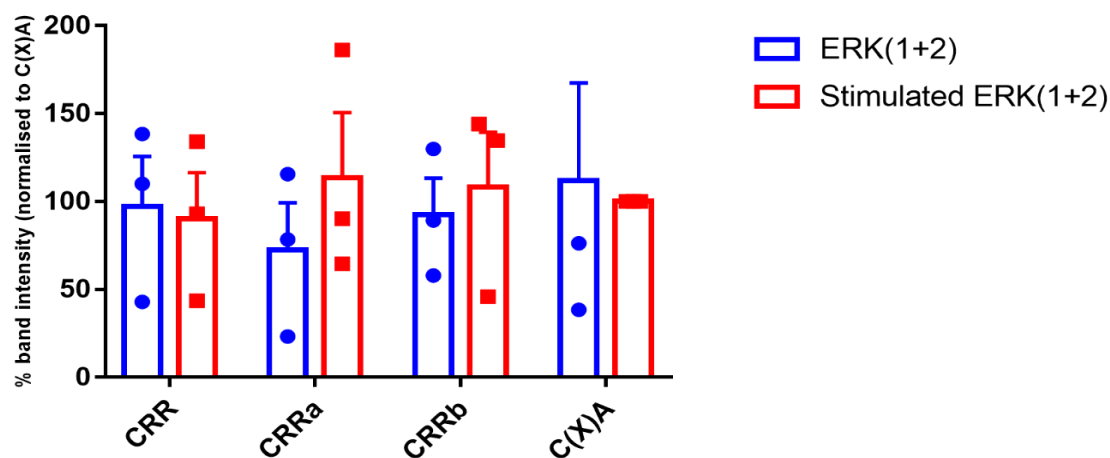
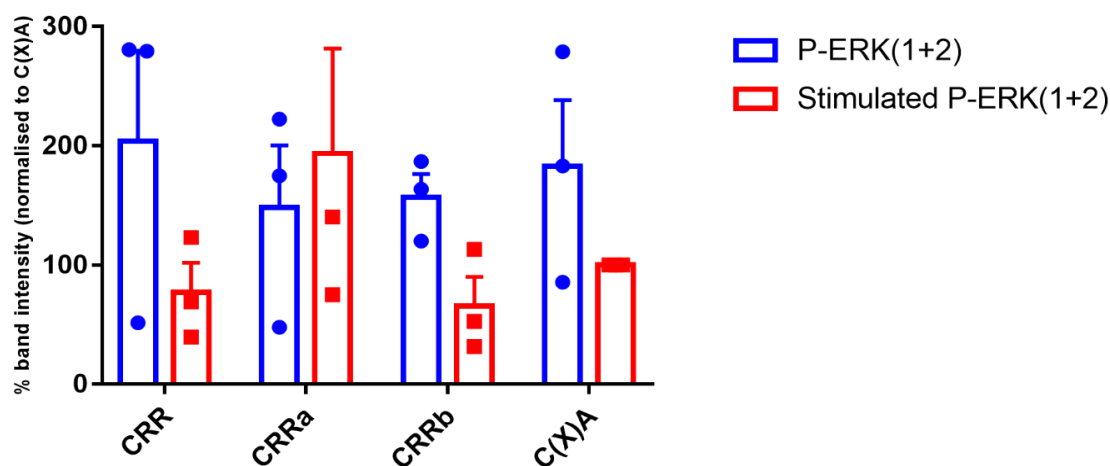
Appendix 10: ERK (1+2) and P-ERK (1+2) levels

A



B

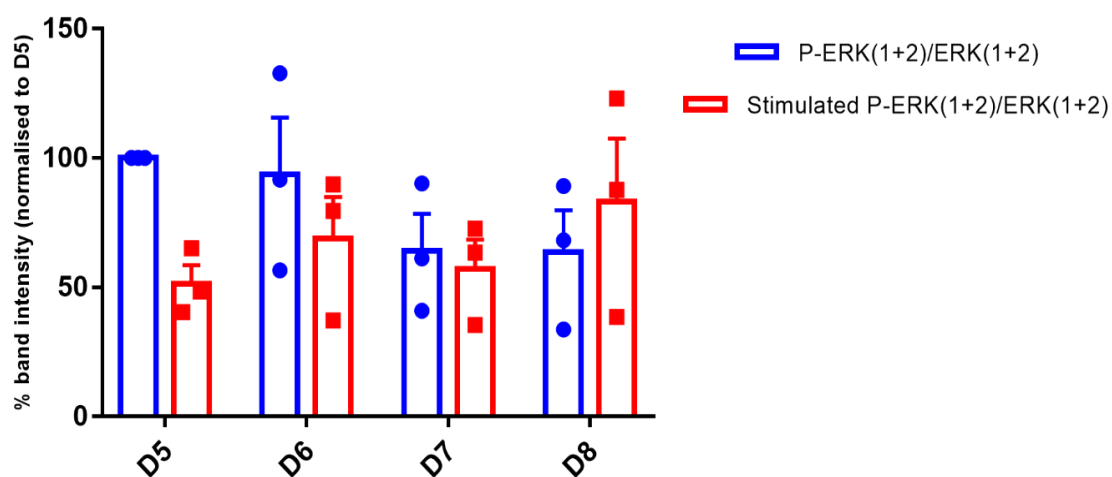


C**D**

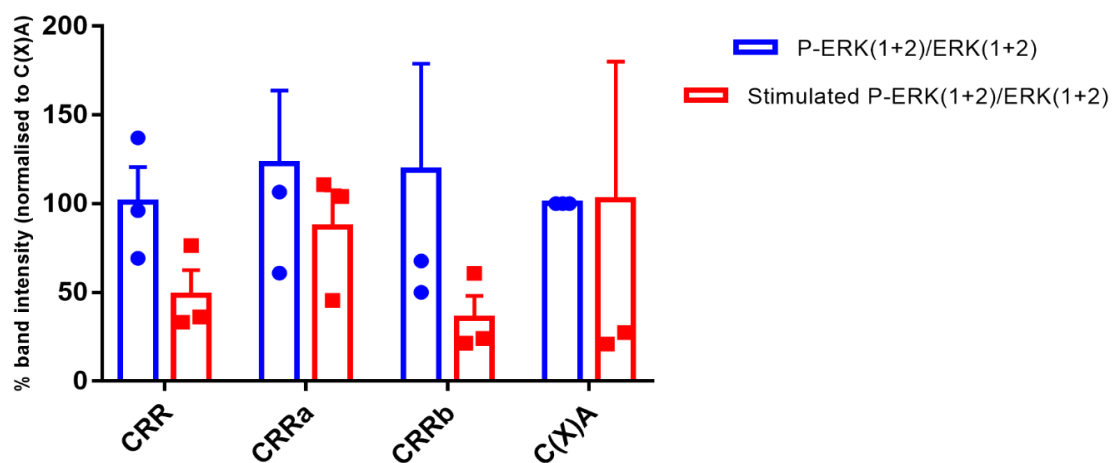
(A): ERK (1+2) basal levels for stimulated and un-stimulated D5, D6, D7 and D8. (B): P-ERK (1+2) basal levels for stimulated and un-stimulated D5, D6, D7 and D8. (C): ERK (1+2) basal levels for stimulated and un-stimulated CRR, CRRa, CRRb, and C(X)A. (D): P-ERK (1+2) basal levels for stimulated and un-stimulated CRR, CRRa, CRRb, and C(X)A. Results are (\pm SEM).

Appendix 11: P-ERK (1+2) inductions

A

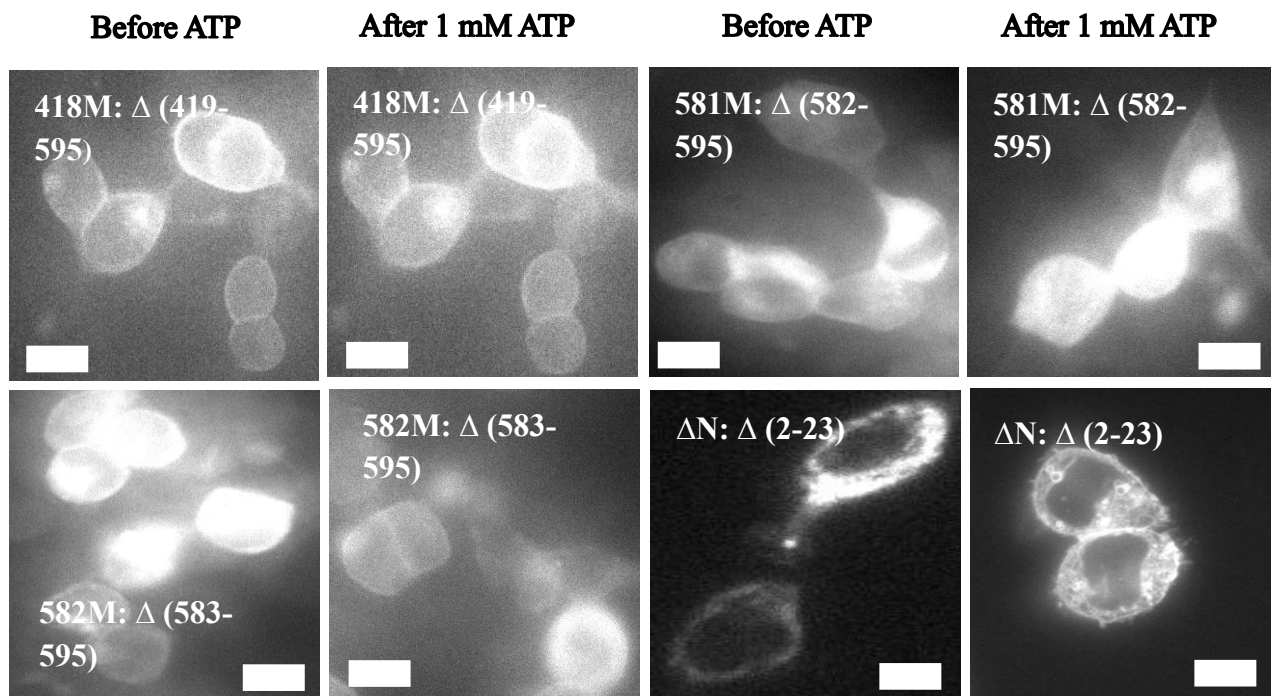


B



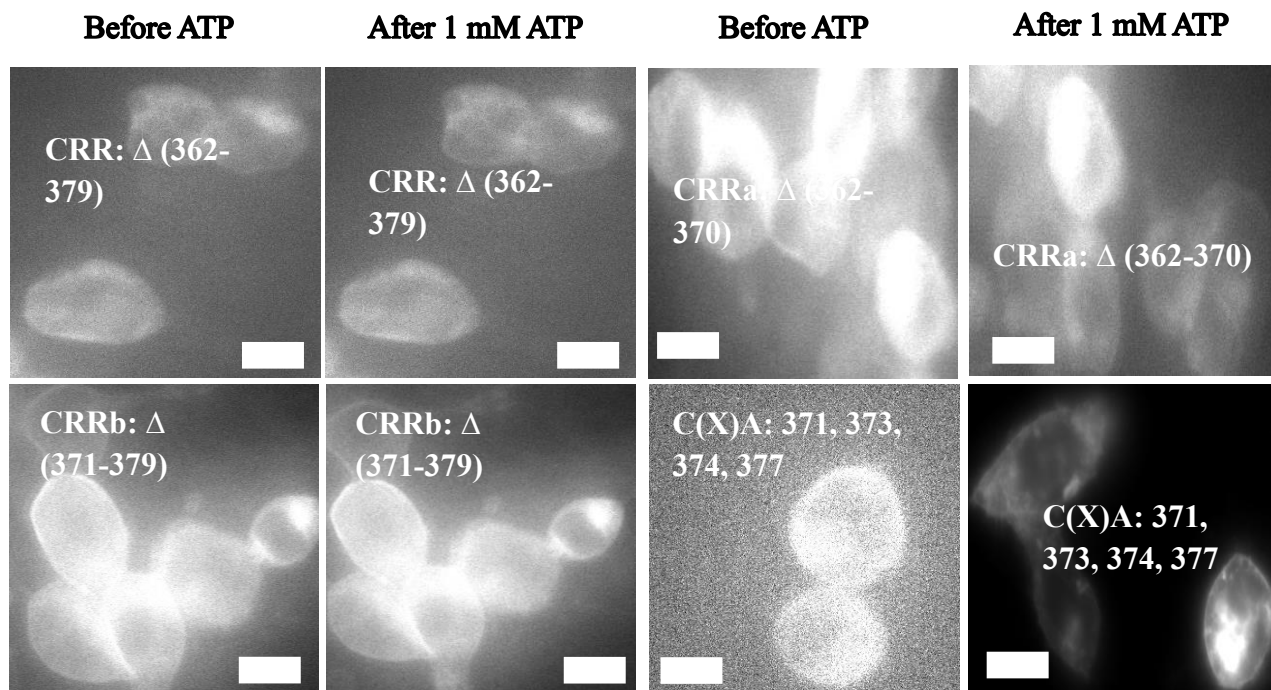
(A): P-ERK (1+2) inductions for stimulated and un-stimulated D5, D6, D7 and D8. (B): P-ERK (1+2) inductions for stimulated and un-stimulated CRR, CRRa, CRRb, and C(X)A. Results are (\pm SEM).

Appendix 12: Cell blebbing of truncation mutants in MCD-treated cells



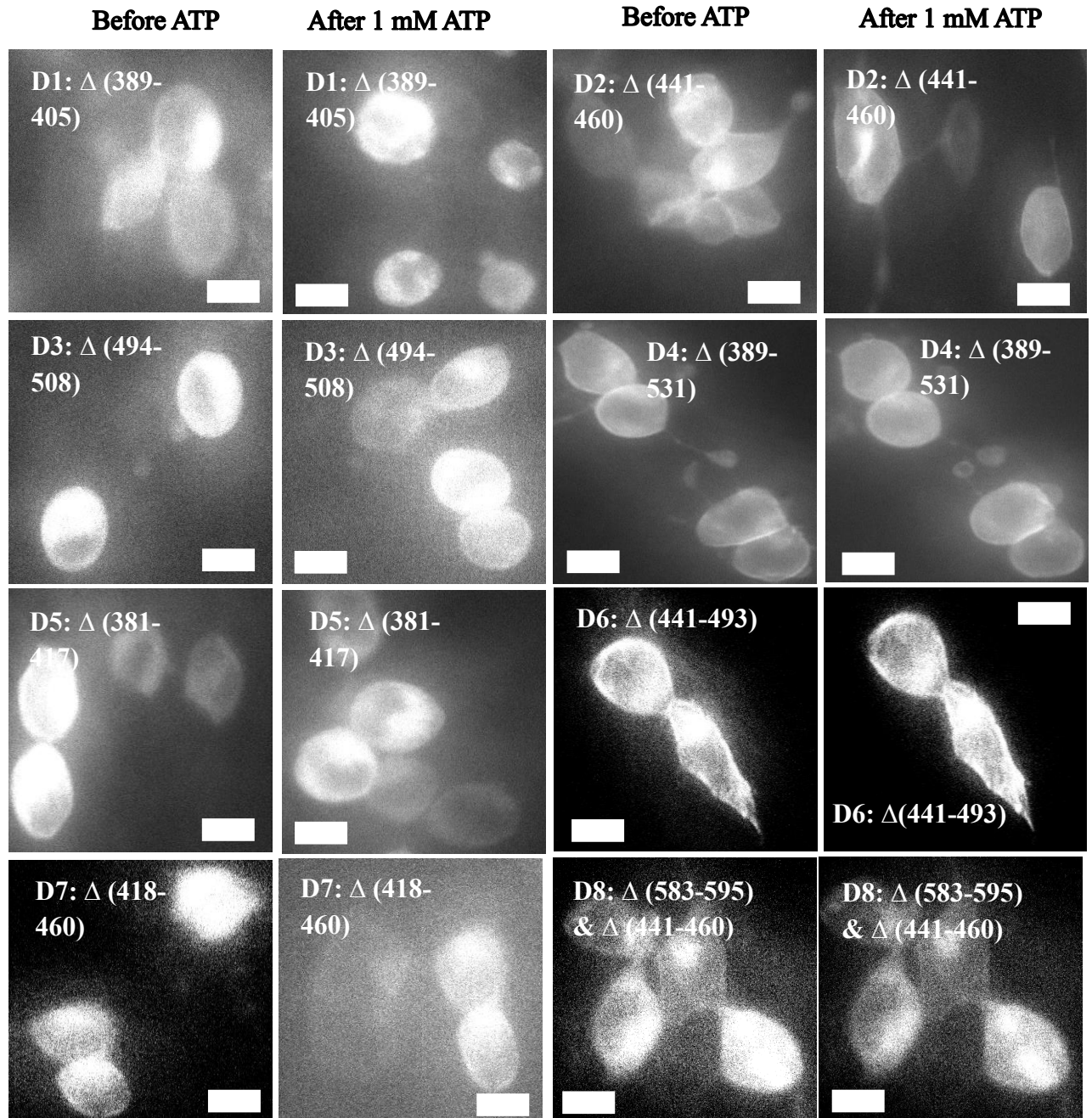
Scale bar represents 10 μ m. The figure shows representative images, the number of cells analysed per experiment varied between (2-8) from 3 independent experiments.

Appendix 13: Cell blebbing of C-cys anchor mutants in MCD-treated cells



Scale bar represents 10 μ m. The figure shows representative images, the number of cells analysed per experiment varied between (2-8) from 3 independent experiments.

Appendix 14: Cell blebbing of internal deletions in MCD-treated cells



Scale bar represents 10 μ m. The figure shows representative images, the number of cells analysed per experiment varied between (2-8) from 3 independent experiments.